Organophosphates in Aircraft Cabin Air

by

Tracy Bradford

A thesis submitted in partial fulfilment for the requirements for the degree of Doctor of Philosophy at the University of Central Lancashire

September 2023

RESEARCH STUDENT DECLARATION FORM

Type of Award __PhD_____

School __School of Engineering and Computing_____

*Sections marked * delete as appropriate*

1. Concurrent registration for two or more academic awards

I declare that while registered as a candidate for the research degree, I have not been a registered candidate or enrolled student for another award of the University or other academic or professional institution

2. Material submitted for another award

I declare that no material contained in the thesis has been used in any other submission for an academic award and is solely my own work

3. Collaboration

Where a candidate's research programme is part of a collaborative project, the thesis must indicate in addition clearly the candidate's individual contribution and the extent of the collaboration. Please state below:

___

4. Use of a Proof-reader

No proof-reading service was used in the compilation of this thesis.

Signature of Candidate ____ Tracy Bradford _____

Print name: _____**Tracy Bradford**_____

Declaration

The writing of this thesis and the research discussed was carried out solely by Tracy Bradford under the supervision of Dr Tony Lee Graham (Director of Studies), Dr Eleni Asimakopoulou (Supervisor) and Dr Andrei Chamchine (Supervisor). Where other sources are quoted full references are given.

Abstract

The quality of aircraft cabin air on commercial aircraft has been the subject of adverse press reports for several years. One of the current issues is the potential for aircraft cabin air to become contaminated with organophosphate compounds. The primary compound causing concern is tricresyl phosphate (TCP) and the related decomposition products. It is believed that the contamination is occurring through the bleed air system supplying air to aircraft cabin. Both military and commercial pilots and cabin crew have reported symptoms such as nausea and blurred vision following smoke and fumes leaking from the jet engines and entering into the aircraft cabin. A number of investigations have suggested that the cause of these symptoms was due to the presence of additives in the engine lubricating oils, but as yet no consensus in the conclusions has been reached. The motivation for this research was to understand the problem, to determine if there was potential for air to become contaminated with organophosphate compounds and if the air was to become contaminated, was there sufficient contaminant to cause adverse health issues for cabin crew and passengers.

This research determines the potential levels of organophosphates present in aircraft cabin air. This work aims to experimentally and numerically investigate particle dispersion in aircraft cabins and the associated health risks. Firstly, experimental analysis was undertaken to determine the concentration of organophosphate, in particular TCP in aircraft engine oil and the levels present after pyrolysis. Secondly, mathematical analysis has been conducted to determine the levels of TCP in an aircraft cabin and the potential levels after several hours flight. Thirdly, numerical simulation has been performed to determine the flow paths of particles of within the aircraft cabin.

Chemical analysis has shown that TCP is present in aircraft engine oil in significant levels which would be available to be absorbed into the human body. The mathematical analysis has shown that high levels of TCP will enter the cabin and that short haul and long-haul flights presented a hazard to health. Numerical simulation has shown there would be significant levels of particles within the aircraft cabin, that could be inhaled by occupants or deposited on surfaces which would then accumulate over time.

This research has shown that there are sufficient levels of TCP contaminating aircraft cabin air to cause health issues and that particles will deposit on surfaces in sufficient quantities to cause health issues.

There are a number of recommendations which could reduce the incidences of fume event occurring such as incorporating filters or changing the type of oil used in engines.

Acknowledgements

There are several people who have contributed to my development and enabling me to complete this thesis, to whom I am extremely grateful.

I would like to thank all my supervisors for donating their time and giving their expertise and assistance with this research. It has been a particularly challenging task and I would particularly like to thanks the members of the supervisory team Dr Tony Graham, Dr Eleni Asimakopoulou and Dr Andrei Chamchine.

There have been some difficult personal times during the period of this research, and I would like to thank my partner, Ian for his love and support, my mother Ellen, and my sister Karen whose continued support and constant motivation have helped me complete this research. I would also like to acknowledge my late father Thomas, who was there when this research commenced but sadly is not here to see its conclusion.

Contents

List of Figures

List of Tables

Abbreviations

ABS/PC	Acrylonitrile-butadiene-styrene terpolymer/ polycarbonate
Ach	Acetylcholine
AchE	Acetylcholinesterase
AchR	Acetylcholine receptors
ALoSP	Acceptance Level of Safety Performance
APU	Auxiliary power unit
ATP	Adenosine Triphosphate
BALPA	British Airline Pilots Association
BDP	Bisphenol A diphosphate
CAA	Civil Aviation Authority
CASA	Civil Aviation Safety Authority
CAQ	Cabin Air Quality
ChAT	Choline acetyltransferase
ChT	Choline transporter
CFD	Computational fluid dynamics
COPIND	Chronic Organophosphate Induced Neuropsychological Disorder
COT	Committee of Toxicology
COVID	Coronavirus
DfT	Department for Transport
DG-MOVE	Directorate-General for Mobility and Transport
DOCP	Diorthocresyl Phosphate
DOE	Department of Energy
EASA	European Aviation Safety Agency
EPAAQ	Expert Panel on Aircraft Air Quality
FAA	Federal Aviation Administration
FACTS	FreshAirCraft

FDS	Fire Dynamic Simulator
GABA	Gamma-aminobutyric acid
GCAQE	Global Cabin Air Quality Executive
GC-MS	Gas chromatography and Mass spectrophotometry
GCxGC-ToF-MS	Two-dimensional gas chromatography coupled with time-of-flight mass spectrometry
HAChT	High-affinity choline transport
IATA	International Air Transport Association
ICAO	International Civil Aviation Organisation
ICPMS	Inductively coupled plasma mass spectrometry
LC_{50}	Lethal concentration 50
LCt_{50}	Lethal dose from exposure
LD_{50}	Lethal dose 50
MOCP	Mono orthocresyl Phosphate
MORs	Mandatory Occurrence Report
NIST	National Institute of Standards and Technology
NTE	Neurotoxic esterase
ODE	Ordinary differential equation
OP	Organophosphate
OPIDN	Organophosphate induced delayed neuropathy
OPIDP	Organophosphate Induced Delayed Peripheral Neuropathy
PACTS	Parliamentary Advisory Council for Transport Safety
PPO	Polyphenylene oxide
PVC	Polyvinyl chloride
RDP	Resorcinol diphosphate
SARS	Severe acute respiratory syndrome
TBP	Tributyl phosphate
TCP	Tricresyl Phosphate

TCEP	Tris(2-chloroethyl) phosphate
TCPP	Tris-(2-chloro-, 1-methyl-ethyl)-phosphate
TDCPP	Tris (1,3-dichloro-2-propyl) phosphate
TEELs	Temporary Emergency Exposure Limits
TiBP	Tri iso butyl phosphate
TmCP	Tri-m-cresyl phosphate
TMPP	Trimethylol Propane Phosphate
TnBP	Tri -n-butyl phosphate
TOCP	Tricresyl *ortho* Phosphate
TpCP	Tri-p-cresyl phosphate
TWA	Time weighted average
VAChT	Vesicular acetylcholine transporter
VOCs	Volatile organic chemicals
WHO	World Health Organisation

Nomenclature

Symbol	Quantity	Units
A_i	Cross sectional area	m^2
A	Matrix label	-
C_p	Specific heat	J/kg/K
C	Constant 1	-
D	Droplet/ particle diameter	µm
f	Flow rate	m^3/min
g	Acceleration due to gravity	9.81 m/s^s
h_s	Sensible enthalpy per unit mass	J/kgK
h	Height of fluid	m
I	Identity matrix	-
m	Mass	kg
$\dot{m}$	Mass flow	kg/min
$\dot{m}_a^{''\prime}$	Reaction source term	-
$\bar{p}$	Pressure perturbation	-
ρ_∞	Ambient density	kg/m^3
Q	Flow rate	l/min
$\dot{q}_m$	Heat release rate per unit volume	J/Km^3
R	Ideal gas constant	J/Kmol
S	Sulphur	-
t	Time	minutes
T_∞	Ambient temperature	°C or K
u	Velocity	m/s
v	Vector	-
$\overline{W}$	Mixture molecular weight	g/mol
X	Constant	-

X'	Rate of change	kg/s
Y	Constant	-
Y_a	Mass fraction of species a	-

Greek letters

Symbol	Quantity	Units
α	Alpha	-
γ	Empirical constant	2.4
λ	Eigen Values	-
ρ	Density	kg/m^3
σ	Empirical constant	0.48
τ	Time factor	Minutes

Subscripts

$in1$	Into tank 1	m^3/min
12	From tank 1 to tank 2	m^3/min
out	Out of tank 2	m^3/min
$cabin$	In cabin	kg
$engine$	In engine	kg
h	Homogeneous solution	-
in	In	m^3/min
0	Initial state	kg
out	Out	m^3/min
p	Inhomogeneous solution	-

Terminology

Chain stripping	As a result of overheating, the polymer is thermally degraded, causing molecular deterioration. At high temperatures components of the long chain backbone of the polymer, begin to break and react with each other causing the polymer to change its properties
Cresols	Natural organic compounds which are methylphenols.
Ester	An organic compound made by replacing the hydrogen of an acid with an alkyl group.
Free radical	A radical is an atom that has an unpaired valence electron and is highly reactive.
Insecticides	Type of pesticide which is used to kill specific types of insects.
Isomer	Molecules with the same chemical formula but have different chemical structures.
LD_{50}	Lethal dose of material when given at all at once will cause death of 50% of the group.
LC_{50}	Lethal concentration of a chemical in air (or water) that kills 50% of the group, during a specified observation period (4 hours).
LCt_{50}	This is the measure of the amount of vapour or aerosol lethality and is the product of concentration and exposure time, that is lethal to 50% of the group.
Muscarinic	This is a type of acetylcholine receptor within the nervous system (controls activities such as heart rate).
Nicotinic	This receptor controls voluntary muscle action.
Pesticide	Chemicals used to kill fungus, bacteria, insects, plant diseases, snails, slugs and weeds.

Synapses	Structure that allows chemical and electrical signals to be transferred from one neuron to another, eventually reaching the target cell.
TEEL	Estimates of concentrations at which most of the people exposed, will begin to experience health effects (over a particular length of time)
TEEL – 3	Airborne concentrations above which it is predicted that the general population when exposed for more than 1 hour will experience life threatening effects or death.
TEEL - 2	Airborne concentrations above which it is predicted that the general population when exposed for more than 1 hour will experience irreversible, serious long term health effect.
TEEL – 1	Airborne concentrations above which it is predicted that the general population when exposed for more than 1 hour will experience notable discomfort or irritation, the effects of which are usually reversible.

Chapter 1: Introduction

Air travel is a large and ever-expanding industry. It enables economic growth, international trade, and investment. It facilitates the rapid expansion of tourism and is therefore crucial to the globalization of many businesses. Air travel is more accessible to more people. In 2018 a record number of cities were connected (IATA 2019). In the past decade alone air travel has increased on average by 7% per year with more people travelling for business and pleasure (IATA 2019). The cost of seats has halved in the last two decades (IATA 2019).

In 2018, there were more than 4.3 billion passengers on scheduled flights (IATA 2019). Given the hundred-fold growth of the aviation industry during the last 60 years, aviation safety has improved much more than one hundred times. Higher safety standards have been implemented through the development of newer technologies within the aircraft, and in air traffic control and runway management. The airline industry has seen a massive increase in the safety of aircraft although fatal incidents do still occur. In 2018 there were 11 fatal accidents that resulted in 523 fatalities of passengers and crew. This was an increase on the average of 234 fatalities over the previous five years (IATA 2019).

The number of people travelling by air for both short and long-haul flights has increased dramatically in the last decade. The first scheduled non-stop flight between Australia and the United Kingdom took place in 2018, this was a distance of 14,498 km (BBC 2019). In 2019 a flight from New York to Sydney flew 16,200 km non-stop (BBC 2019). Approximately 100,000 planes take off around the world each day carrying 5,500,000 passengers to their destinations (Flight Delayed 2019). Domestic and international travel decreased dramatically during the COVID pandemic, but numbers have started to increase, to levels similar to those pre-COVID as can be seen in Figure 1, the global number of passengers has increased (IATA 2022).

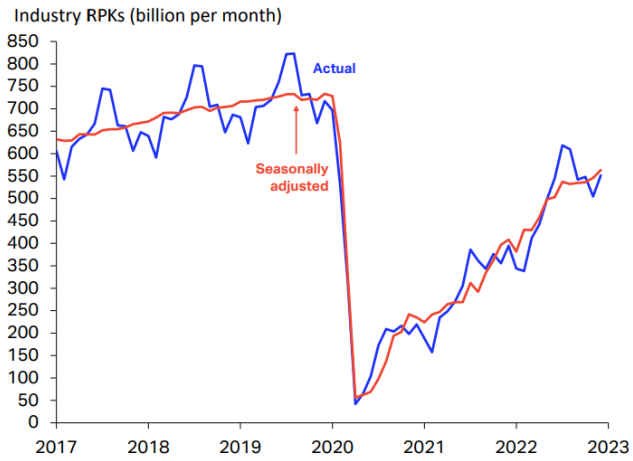

Figure 1: Global air passengers (IATA 2022)

With developments in aircraft technology modern aircraft can fly for longer without the need for refuelling and can hold a larger number of passengers per flight. With the rise of cheaper flights, people are also increasing the number of times they fly per year. It is expected that this number will rise by 3.5 % annually until 2037 (IATA 2019) as a result previously non-recurrent incidents may re-occur while incidents with a one in a million probability could occur at a higher rate.

The quality of aircraft cabin air during normal operations, is considered to be of a higher quality than most indoor environments (IATA 2020). The European Aviation Safety Agency (EASA 2015) conducted a study on the quality of aircraft cabin air, they found that no occupational exposure limits or guidelines were violated during flights conducted to assess air quality (EASA 2015). Transmission of diseases by biological contaminants within aircraft cabins has recently received a high level of media attention (IATA 2020). As the number of people undertaking air travel annually increases, the potential for the transmission of respiratory infections does increase. A large proportion of the travelling population experience a health problem, related to overseas travel (Leder et al. 2005). It was generally assumed that if people became ill on flights, several factors may have been involved, including travel to exotic destinations, exposure to different micro-organisms,

disrupted sleep and jet-lag, as well as aircraft specific factors, such as the reduced cabin air pressure, travelling in different environments or by being in a confined space with re-circulating air for extended periods, possibly allowing greater exposure to bacteria or viruses (Leder et al. 2005). It has been recognized that people with pre-existing health conditions are at greater risk when flying (Michaelis 2007). The main transmission routes for pathogens to infect the occupants of an aircraft cabin are by droplets and airborne particles (Leder et al. 2005). A study showed that a person infected with severe acute respiratory syndrome (SARS) who travelled on an aircraft spread the disease to 16 other travellers (Olsen et al. 2003). During the first months of 2020, the COVID pandemic highlighted the potential for the spread of respiratory disease within aircraft. Studies by Guo et al. (2022) have shown that the main routes of transmission of pathogens such as COVID are respiratory droplets, aerosols and close contact transmission. A study of 3 different flights found that 7.5%, 1.6% and 1.5% of passengers were infected even though at this time passengers were wearing face masks. Guo et al. (2022) found no evidence associated between the prevalence of infection and being seated in the window, aisle or centre seat location. Whilst a study by Foxwell et al. (2009) looking at the transmission of Influenza on international flights, did find a correlation between seating position and rate of transmission. Foxwell et al. (2009) studied 738 passengers on 2 flights. From the first flight, an Airbus A380 from Los Angeles to Sydney carrying 445 passengers, twenty of the twenty-four passengers who developed Influenza-like illness were sat in the aisle seat, indicating that seat location did increase the risk of exposure (Foxwell et al. 2009).
The issue of air quality within aircraft cabins initially came to the fore when smoking was banned on board aircraft in 1990. Cigarette smoke could mask smells, incident-related fumes and mists, so although crew members would not have been less likely to get sick, they would have been less likely to make the connection between their illness and possible fume events within the aircraft. It was also assumed at the time, that as smoking was no longer permitted on flights, the rate of air exchange would be reduced and therefore the quality of the air within the cabin would be reduced (Michaelis 2007).

There have been a number of incidents which have highlighted the possibility that cabin air may have become contaminated with chemical species which could have adverse health consequences. One such chemical species is thought to be an organophosphate. Organophosphates are a diverse group of chemicals used in both domestic and industrial settings. Examples of organophosphates include insecticides, nerve gases and herbicides (Katz et al. 2023). Whilst these incidents do not provide conclusive evidence of a problem, they have raised the question which now requires resolving through a thorough investigation (Winder 2005).

Safety concerns are generally taken very seriously by the aviation industry, but concerns raised by commercial airline pilots and flight crews across the world have gone unanswered. Aircraft cabin air quality has the potential to affect significant numbers of people and as such this issue requires investigation. A number of studies have been conducted over the last decade to try to provide an answer (National Research Council 2002). Various governments and regulatory authorities have commissioned research into this issue, but as yet have failed to demonstrate a link between contaminated cabin air and health problems, although numerous independent studies claim to have demonstrated this link. They suggest that corporate profit, conflicts of interests and ineffective control by Government and regulating authorities means that the industry as a whole remains in denial of this problem (Muir 2009).

Due to concerns about the possible negative health effects on cabin crew of contaminated cabin air, the UKs' Department for Transport asked the Committee on Toxicity (COT) to undertake an independent scientific review of the data submitted to the British Airline Pilots Association (BALPA). The report was concluded by COT in 2007, finding that the evidence available at that time, did not establish a link between contamination of cabin air and the ill health of pilots and crew. However, COT and indeed the House of Lords Select Committee on Science and Technology have recommended that further research into the components of cabin air is required (COT 1999).

It is estimated that there are over 300 aircraft are impacted by contamination events each year, worldwide, resulting in over 40, 000 passengers and crew being exposed (Winder et al. 2001). A study by Winder et al. (2001) collated data on the symptoms of crew, including pilots, first officers, pursers and flight attendants, who had been exposed to a potential contamination event, a leak of oil mist to the flight deck or passenger cabin. Symptoms were reported from single exposures to elevated exposures, and from long-term low-level exposures to low level oil leaks or residual problems from previous contamination. Combined exposures (that is, short term intense exposures combined with low-level long-term exposures) were also prevalent. Symptoms from single or short-term exposures are shown in Figure 2. Symptoms such as irritation of the eyes, nose and throat or respiratory effects could occur immediately or soon after exposure. Other issues such as nervous system impairment and chemical sensitivity developed later, after exposure had stopped. Symptoms from repeated low-level exposure include memory loss and lack of coordination. Winder et al. (2001) determined that the symptoms, such as those indicated in Figure 2, were sufficiently consistent to indicate the development of a discrete occupational health condition, and the term aerotoxic syndrome was introduced to describe it.

Symptom	Imme-diate	Post-flight	Short term	Medium term	Long term
Seizures, "gray outs", unconsciousness	✓✓	✓			
Disorientation	✓✓	✓✓	✓		
Loss of balance	✓✓	✓✓	✓	✓	
Problems with coordination	✓✓	✓✓	✓✓	✓	
Headache, lightheaded, dizziness	✓✓	✓✓	✓✓	✓✓	✓✓
Weakness, fatigue, exhaustion	✓✓	✓	✓	✓	✓
Chronic fatigue			✓	✓✓	✓✓
Cognitive problems	✓	✓	✓✓	✓✓	✓✓
Numbness, hot flashes	✓✓	✓✓	✓	✓	
Shaking/tremors, fasciculations, nystagmus	✓✓	✓✓	✓	✓	✓
Irritation of eyes, nose and throat	✓✓	✓			
Nausea, vomiting	✓✓	✓✓			
Blurred vision, tunnel vision	✓✓	✓	✓		
Respiratory problems	✓✓	✓			
Chest pain	✓✓	✓			
Increased heart rate, palpitations	✓	✓			
Joint pain, muscle weakness, salivation	✓	✓			
Rashes, blisters (uncovered body parts)	✓	✓✓	✓		
Loosing hair (2 cases of severe exposure)		✓	✓		
Immunodepression			✓	✓	
Acquired Multiple Chemical Sensitivity				✓	✓✓

Key to Exposure Intensity:
✓ Mild intensity and/or symptoms occur occasionally
✓✓ Severe intensity and/or symptoms present continuously

Key to Column headings:
Immediate: minutes to hour, during or soon after exposure
Post-flight: hours to days **Short term:** days to weeks
Medium term: weeks to months **Long term:** months to years

Figure 2: Aerotoxic Syndrome – Symptoms, Intensity and Chronological Sequence (Winder et al. 2001)

Organophosphate compounds are chemical agents in widespread use throughout the world in household chemicals, fire retardants, and medical treatments, but their main use is within the agricultural industry as pesticides. Several thousand organophosphate compounds have been synthesized since World War II (Muir 2009). Organophosphates are chemical substances that can be produced by reacting alcohols, amines or thiols with phosphoric acid forming esters, amides or thiol derivatives respectively.

Many organophosphates are biologically active. Some aid health while others have detrimental effects. Effects of organophosphates on the human body can be long term or short term. Signs and symptoms of organophosphate poisoning can be divided into three broad categories muscarinic effects, nicotinic effects, and central nervous system effects as seen in Table 1 (Traumagency 2015).

Table 1: Signs and symptoms of organophosphate poisoning (Traumagency 2015)

Cholinergic Toxidrome		
Muscarinic symptoms	**Nicotinic Symptoms**	**Central Nervous System Symptoms**
Salivation	Muscle cramps	Anxiety
Lacrimation	Tachycardia	Confusion
Urination	Weakness	Seizures
Defecation	Twitching	Coma
GI cramping	Fasciculations	Impaired memory
Emesis		Irritability
		Lethargy
		Psychosis

Physostigmine was the first organophosphate to be commercialised. It was discovered in the Calabar bean found in West Africa and brought to the UK in the 1840s. Fraser and Argyll Robertson examined its properties and found it was useful for the treatment of glaucoma (Gupta 2006). By the 1900s several organophosphate compounds had been synthesized, although it was not until the 1930s that their potential toxicity was fully understood. The German chemist Lange was one of the first to comprehend the toxicity of the organophosphate compounds (Bardin et al.1994) by noticing the effects such as a choking sensation and a dimming of vision after exposure to an organophosphate compound. This led to the introduction of organophosphates being used as insecticides. The first wide-spread exposure to the organophosphate tricresyl phosphate (TCP) has been associated with the “Ginger Jake” paralysis. This occurred in the United States in 1930 when up to 50,000 people were affected when an adulterated alcohol based Jamaican Ginger, a ginger extract, used to medicate stomach problems, was consumed. Prohibition was in force during this time, and as the Jamaican Ginger was alcohol based, it was also widely taken as an illicit source of alcohol which increased the number of people affected (Schopfer et al. 2010). An additive, tri-ortho-cresyl phosphate was shown to be present at a 2% concentration. Tri-ortho-cresyl phosphate was and is widely used as a liquid plasticizer and is valuable in glues and fuels because of its heat resistance. It

was suspected that it was used as a substitute for the oleoresin (essential oils) of ginger in the particular batch that produced clinical toxicity. It is soluble in alcohol and miscible with the true oleoresin. It was also very cheap, selling at 30 cents per gallon, and was apparently used to enable the seller to undercut competitors, who were using castor oil to adulterate their version of Ginger Jake (Morgan et al. 1976). The people affected suffered from muscle pain, weakness of upper and lower extremities, and minimal sensory impairment. The additive tri-ortho-cresyl phosphate was thought to have caused severe, only partially reversible damage to the spinal cord and peripheral nervous tissue. Victims were also associated with a gait impairment, sometimes permanent and were said to have the "Jake Leg" or "Jake Walk."

1.1 Aim and Objectives

The aim of this study is to determine if sufficient quantities of contamination (TCP) are present in jet engine oils which could then potentially contaminate aircraft cabin air, and if contamination did occur, how would the particles be distributed throughout the aircraft cabin and therefore potentially affect occupants' health.
The objectives of this research are:

1. To provide an overview of organophosphate compounds, their toxicity and their uses, including use in the aircraft industry, through a literature review.
2. To determine the compounds, present within commercial samples of tricresyl phosphate and aircraft engine oils and their decomposition products using gas chromatography and mass spectrometry.
3. To mathematically determine the quantities of organophosphate that could contaminate the aircraft cabin air and formulate a mathematical model to describe the organophosphate mass flow into the aircraft cabin.
4. To develop a numerical model to determine the flow paths of particles throughout the aircraft cabin

The study intends to experimentally analyse the components of the aircraft cabin oil and determine the potential levels of organophosphates that could enter the aircraft cabin. Available data in the literature will be used to validate laboratory decomposition and predicted data with published concentrations in aircraft cabins, this knowledge will then be used to identify those critical conditions in aircraft engines which allow for the production of organophosphates in order to facilitate the development of a suitable preventative measures. Data from the experimental analysis will then support the calculation by the mathematical model in determining the quantities of contaminant present which would then enter the aircraft cabin. A numerical model will be developed to describe the dispersal patterns of the vapour contaminants from the oil products,

around the cabin. Analyses of the flow paths will be undertaken to determine where organophosphate will flow and determine the areas of the aircraft cabin where occupants' exposure to organophosphates could be increased.

The study will identify how the organophosphates enter the recycled air used for ventilation, then how this will get into the aircraft cabin, onto the surfaces within the aircraft cabin, and discuss how this could enter the human body and the effect it could have on the cabin crew and passengers.

1.2 Outline of thesis chapters

The current thesis consists of seven chapters and one appendix as depicted in detail in Figure 3.

Chapter 1 - Introduction – this chapter contains a brief discussion of the background to the research, outlining the issue of aircraft cabin air contamination, the potential scale of events where contamination can occur and the potential impact of these event. The aims and objectives of the research are provided.

Chapter 2 – Literature Review - Organophosphates – this part of the literature review discusses organophosphates, what they are, their uses and their chemistry.

Chapter 3 – Literature Review – Air supply, Oil and lubricants, Contamination events – there are three parts to this chapter. Part 1 discusses the contamination pathways and air supply. Part 2 discusses the types of jet oil and lubricants used within the aircraft industry. Part 3 discusses the toxicity and routes of exposure of organophosphates.

Chapter 4 – Experimental investigation to determine chemical properties – this chapter discusses the gas chromatography and mass spectrometry (GC-MS) analysis of commercial grade tricresyl phosphate and a commercially available jet engine oil as well as decomposition samples.

Chapter 5 – Development of a mathematical model – discussion of the mathematical model developed to determine the amount of organophosphates that could enter the aircraft cabin.

Chapter 6 - Development of a fluid dynamic model - discussion of the computational model used to determine the flow paths of particles within the aircraft cabin.

Input from the experimental analysis (Chapter 4) was used to determine the presence of tricresyl phosphate in engine oils which would then contaminate the aircraft cabin. Calculation by the mathematical model (Chapter 5) determined the quantities of contaminant present which would then enter the aircraft cabin. The numerical analysis determined the flow paths of the particles once they enter the cabin, determining the effect of particle size and seat location (Chapter 6).

Chapter 7 – Conclusions and Recommendations – this chapter gives a summary of the conclusions in respect to the experimental aspects, the mathematical analysis and the computer modelling and the within this area of research. This research has found that TCP isomers were present in pyrolysed and non-pyrolysed engine jet oil and that it was possible for small amounts to get into the aircraft cabin. The numerical modelling identified the locations within the aircraft cabin at greatest risk of exposure, this being the aisle seat.

It was recommended that further investigation is undertaken to determine the number of contaminations events taking place, this would then lead to further studies to determine the flow paths of particles and the concentrations present.

Advancements in engine design and developments in engine oils have provided solutions to the contamination problem, it is recommended that these advancements and new technologies are implemented in a wider range of aircraft.

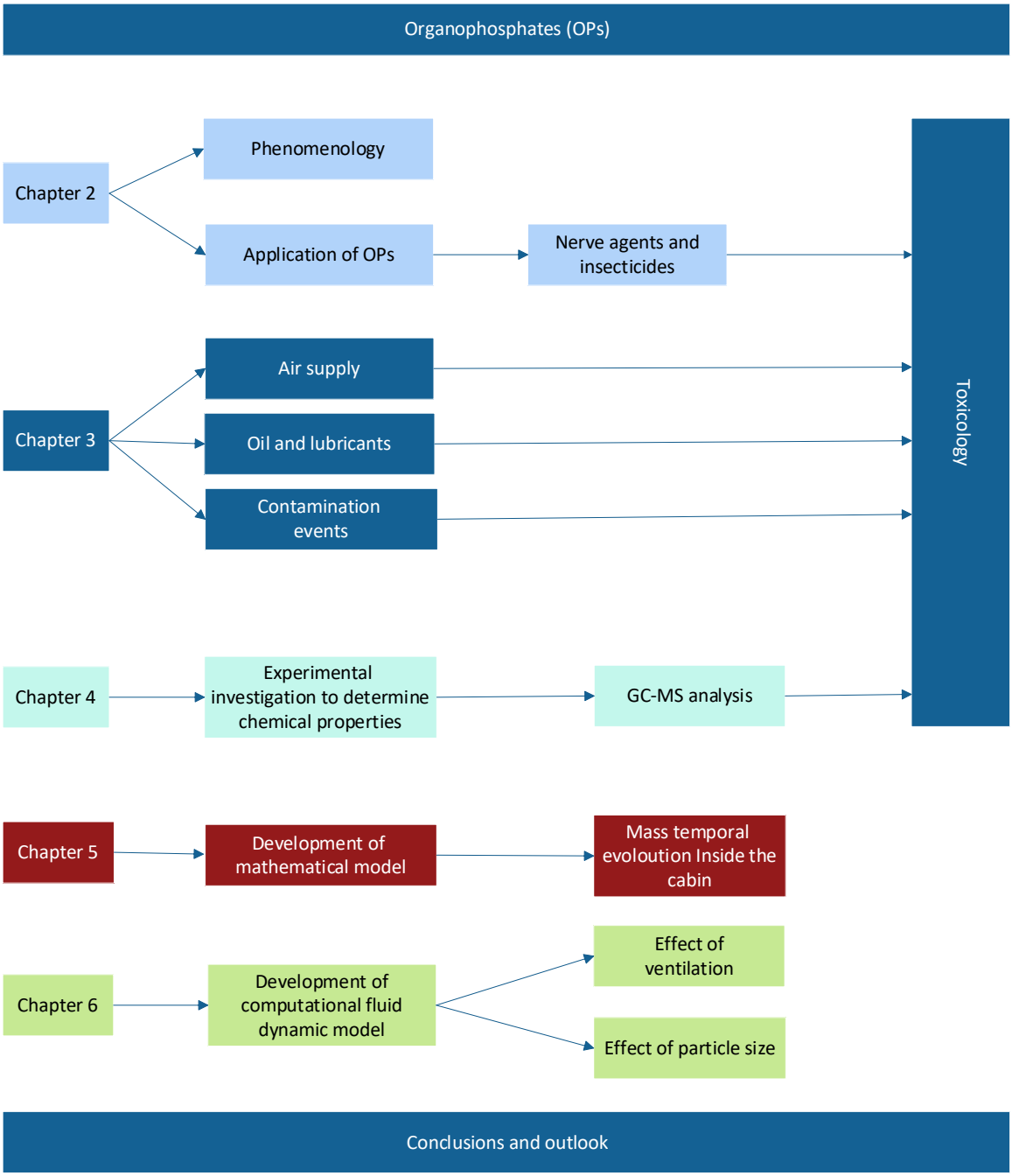

Figure 3: Structure of thesis

1.3 Main findings

This research has provided an overview of several organophosphate compounds, their uses and their effects on the human body.

A review of the available oils used within aircraft is undertaken determining that the amount of organophosphates in these oils was up to 5%. The literature review showed that contamination of aircraft cabin air was possible as a number of studies had been conducted. Impacts of organophosphates on human health was determined through a literature review.

GC-MS analysis of TCP and jet engine oil confirmed the presence of TCP and a number of its isomers. Isomers of TCP was also found to be present within the decomposition products.

Mathematical analysis showed that over a short flight, contaminated particles would enter the aircraft cabin. This was at a level that would cause health issues to some occupants.

A numerical model was developed to determine the flow path of the particles within the aircraft cabin. A parametric analysis was conducted to determine the appropriate parameters to be used. The numerical analysis showed the flow of the particles and level of exposure occupants would be subjected to in different location within the aircraft.

Chapter 2: Literature Review - Organophosphates

2.1 Introduction

This literature review is divided into sections which outline what organophosphates are, their use, the chemistry of organophosphates, pathways for contamination, jet engine oils how they can get into the human body and the effects on the human body. The order of Chapter 2 and 3 is illustrated in Figure 4, mirroring the path of the potential contaminants from source to destination within the occupants of the aircraft.

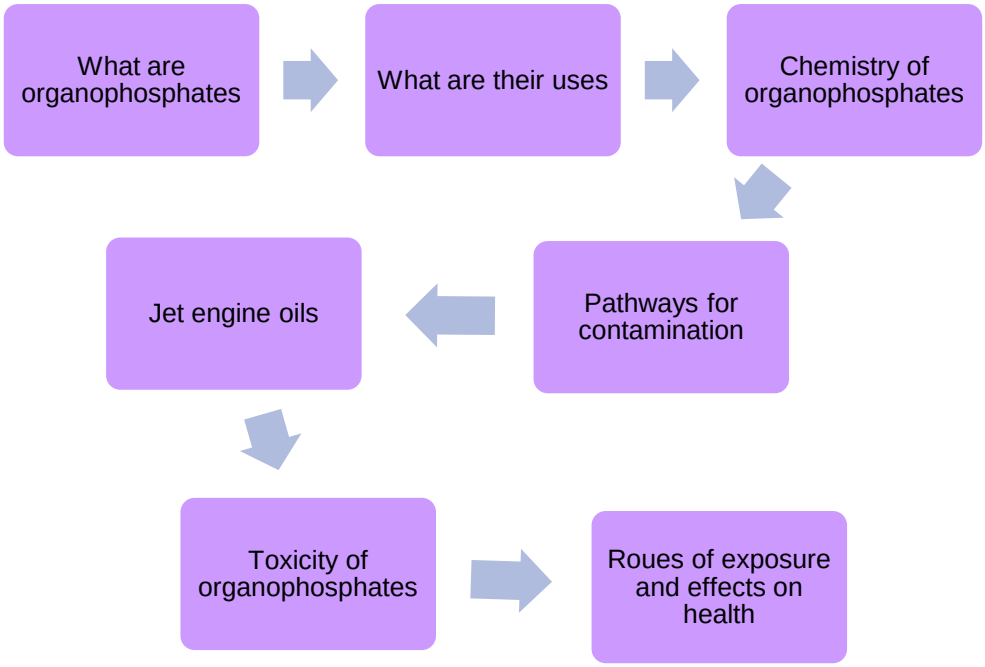

Figure 4: Illustration of literature review

.

2.2 What are the uses of organophosphate compounds?

Organophosphate compounds have a wide range of uses in domestic, industrial and military applications, including insecticides (e.g., Malathion and Parathion), nerve gases (e.g. Soman and Sarin), ophthalmic agents and herbicides (e.g. Tribufos and Merphos)

(Kamanyire et al. 2004). Organophosphates make up approximately 40% of the market for insecticides (Trump 2012).

Although the cholinesterase inhibition by the organophosphate compounds makes them very effective pesticides and nerve agents, they are also being used therapeutically for the treatment of dementia.

Reducing flammability is the main justification for using organophosphate fire retardants. However, there are potential health risks from the toxicity of organophosphate flame retardants. In recent times the use of polymeric and plastic materials has increased dramatically, and they are present in all parts of society. As plastics are synthetic materials composed of hydrocarbons, they are subsequently highly combustible. When plastics are used in various industries, they have to comply to flame retardancy requirements, and these can be achieved by the addition of a chemical in the manufacturing process which will aid as a flame retardant an example of one of these types of chemicals would be an organophosphate compound. These organophosphate compounds are additive flame retardants; they do not bond with the plastic hydrocarbons but diffuse throughout the material. This migration throughout the material may eventually lead to leaching out to the surrounding environment (Sjogren et al. 2009). Phosphorus containing fire retardants are the most diverse groups of such products. They can be divided into two groups condensed phase fire retardants, which act as char promoters and gas phase flame quenchers, which interfere with the free radical processes of flaming combustion (Sjogren et al. 2009). Inorganic phosphorus compounds can lead to the formation of a glassy layer which can aid to the protection of the substrate from the combustion process and/or promote char formation by the formation of phosphoric acid, which promotes chain stripping.

Organophosphates act in the gas phase by the evolution of a free radical quenching agents during the flaming process. The most prolific type of gas phase organophosphorus retardants is the phosphate ester, triaryl phosphates, and flame products like resorcinol diphosphate (RDP) and bisphenol A diphosphate (BDP). These type of flame retardants

are widely used in PVC, acrylonitrile-butadiene-styrene terpolymer / polycarbonate (ABS/PC) and polyphenylene oxide (PPO) applications (Sjogren et al. 2009).

Although thousands of organophosphate compounds have been synthesised, only those that are mono-, di-, or tri-substituted esters have been incorporated into commercial use as lubricant additives. Studies in the 1940s examined the anti-wear properties of the organophosphate compounds. As aircraft were being developed and modified, changing from mechanical to hydraulic control systems, there was also a developing need for safe, non-flammable hydraulic fluids and lubricants. In 1946 W.F Hamilton from the Lockheed Aircraft Corporation was awarded the patent on a hydraulic fluid which was and still is the basis for many of the fluids in use today (Michaelis 2007).

2.3 Organophosphates as nerve agents

In the 1930s further exploration of the damaging effects of organophosphate compounds on health was carried out which led to them being developed as chemical warfare agents. The first class of nerve agents were discovered accidentally in 1936, in Germany by Dr Schrader (US military 2010). He was developing a pesticide for the chemical manufacturer IG Farbenindustrie (Sparks et al. 1990) and began with the development of diisopropyl phosphorofluoridate. Schrader continued his experimental studies with fluorine compounds, eventually discovering Tabun. Initially the high toxicity of Tabun on insects was known, but it was not until 1937 that he observed the effects on humans, following an accident in the laboratory (Wiener et al. 2004). He continued working with organophosphorus compounds and in 1938 went on to discover Sarin, a chemical which was ten times more potent than Tabun (Wiener et al. 2004). In 1944 Dr Kuhn discovered another nerve agent Soman. The United States renamed these nerve agents when they discovered the work of the Germans, Tabun became GA (German agent A), Sarin became GB and Soman became GD (Wiener et al. 2004).

Long term neurological and cognitive health issues have been reported by those manufacturing nerve agents during World War II up to 10 years after their last exposure (Wiener et al. 2004). In 1949 a chemist in England working on the synthesis of insecticides discovered an extremely potent nerve agent which became known as VX (Wiener et al. 2004). Two accidental exposures of VX occurred in the 1960s. One was at Utah's Dugway Proving Ground on March 13, 1968, where approximately 9 kg of VX was released and contaminated adjacent grazing land, resulting in the death of 6,000 sheep. The second accidental release was at a storage facility in Okinawa, Japan, this resulted in 23 military personnel and 1 civilian being hospitalized (US military Dictionary 2010). The UK was soon to abandon research into nerve agents and traded all their technology with the United States in 1958. The United States continued research into nerve agents and produced four agents VE, VG, VM and VX (the V-Series) (Muir et al. 2009). Although many countries had signed the Geneva Convention in 1925, the United States had not ratified this agreement. When President Nixon came to office, he agreed to a "no first" use policy of nerve agents but reserved the right to retaliate should chemical weapons be used against them. Allegations have been made that this agreement was broken in 1970, during the Vietnam War, when it is claimed that the use of Sarin was ordered (Wiener et al. 2004). Sarin is still used in chemical warfare. The latest reported use was in 2017 in Syria (Brooks et al. 2018). Although nerve agents were developed over 60 years ago for military use, they continue to be a threat not only on the battlefields but also as terrorist weapons. VX was used in Japan by a cult leader – Aum Shinrinkyo – to kill several of his opponents and dissident members of his own cult, who were opposed his views. More recently two terrorist attacks occurred in Japan in 1994 and 1995. In the first incident pond water was intentionally contaminated with Sarin, causing 600 people to become ill and 7 deaths. In the second incident was an intentional release of Sarin gas on a subway train. A cup of Sarin was left under a seat and was left to evaporate. This led to the injury of 5,000 people and 12 deaths (Muir et al. 2009).

It has been found that the G series nerve agents are most hazardous when delivered through inhalation of vapours or aerosols but can be absorbed through the eyes or sores. They are less of a percutaneous threat (absorbed through the skin) than the V series nerve agents. A new group of nerve agents has been developed combining the properties of both the G series and V series, posing a hazardous threat through inhalation and percutaneous absorption (Wiener et al. 2004).

Modern classification of military nerve agents are G-agents (formerly G-Series) and V-agents (formerly V-Series). The G-agents are non-persistent and cause death principally by inhalation. V-agents are persistent and cause death by inhalation, or absorption via skin, eyes or mucosal routes (US Military Dictionary 2010). Nerve agents are absorbed within minutes of exposure and can cause death in 15-30 minutes.

Chemical warfare agents or nerve agents which are used by the military are often from the organophosphate group and are among the most toxic synthetic compounds ever made. There are four main ones: Tabun (GA), Sarin (GB), Soman (GD), VX. These compounds exist as colourless, low odour liquids which are meant for use in chemical warfare and are designed to be dispersed as aerosols. Example structures of Tabun, Sarin, Soman and VX are shown below in Figure 5.

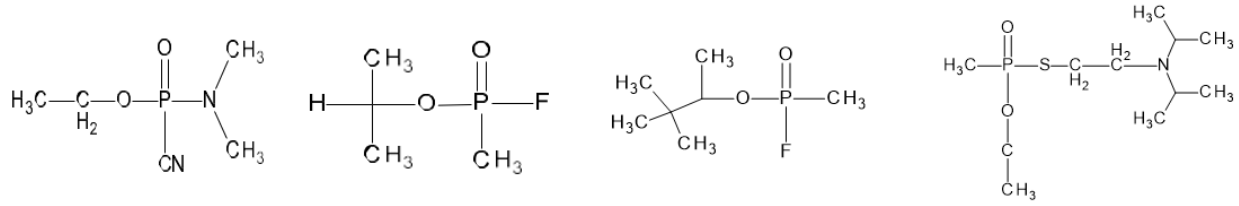

a) b) c) d)

Figure 5: Structures of a) Tabun b) Sarin c) Soman, and d) VX

The action of the nerve agent Sarin is typical of the organophosphorus military poisons. Its lethal dose to humans may be as low as 0.01 mg/kg. Sarin is an irreversible inhibitor of acetylcholinesterase (AChE). The physical characteristics of the nerve agents Tabun,

Sarin, Soman and VX are shown in Table 2 below. This illustrates that the volatility of the agents is low and less volatile agents will take longer to evaporate and will remain active within the environment for longer. V series agents will have a greater persistency than the G series. As nerve agents are lipid soluble, when they are inhaled as vapour or aerosols, they will immediately enter the systemic circulation, resulting in toxic manifestations at muscarinic, nicotinic and central nervous system cholinergic sites.

Table 2: Physical Properties of Nerve Agents (Wiener et al. 2004)

Nerve Agent	Vapour Pressure mmHg (25°C)	Volatility Mg/m3 (25°C)	Odour -	Solubility 100g (25°C)	Persistency hours
Tabun (GA)	0.037	576-610	Fruity	9.8	24-36
Sarin (GB)	2.1	16,400-22,000	Odourless	Miscible	2-24
Soman (GD)	0.40	3,060-3,900	Fruity	2.1	-
VX	0.0007	3-30	Odourless	Slightly	48-144

The acute cholinergic symptoms are due to the inhibition of acetyl cholinesterase at central, peripheral, and autonomic synapses, resulting in the accumulation of acetylcholine at synaptic junctions. The route of exposure will affect the time it takes for the nerve agents to react and the symptoms it will produce. Inhalation is usually the fastest practical method of exposure. The lungs have numerous capillaries through which the nerve agent can diffuse and be incorporated into the circulatory system and reach target organs in seconds. All nerve agents are lipophilic and readily penetrate the central nervous system. People exposed to nerve agents usually die due to peripheral and central effects which lead to respiratory failure. A single acute exposure to a nerve agent could result in death within 5 minutes or 24 hours, dependant on the dose, route of exposure and the particular type of nerve agent (Wiener et al. 2004). An review was conducted by the National Research Council (1997) of the toxicity estimates of chemical warfare agents. The reviewed toxicity values are provided for Tabun, Sarin, Soman and

VX nerve agents in Table 3. As can be seen from the data VX has the greater toxicity of these four nerve agents.

Table 3: Toxicity of Nerve Agents to Humans (National Research Council 1997)

Nerve Agent	LCt_{50} Inhalation mg.min/m^3	LD_{50} Skin mg/individual
Tabun	70	1500
Sarin	35	1700
Soman	35	350
VX	15	5

Nerve agents are still being used today. As recently as 2018 an incident involving the release of a Novichok nerve agent in Salisbury in the UK affected a number of people resulting in one death. Novichoks are the fourth generation of chemical weapons developed in the former Soviet Union during the late 1980s early 1990s. There are a number of varieties of Novichok agents with different structures and characteristics. All Novichok agents are extremely toxic, 10 times more toxic than VX. They are difficult to treat those who have been poisoned as a result of coming into contact with it. Novichok inhibits cholinesterase, as do other nerve agents, but it is thought this is not its main mechanisms of action. It is also believed to cause permanent neuropathy (Gupta 2006). Novichok reagents are extremely robust and have a potency lifetime of up to 12 months. The chemical structure of Novichok agents is still relatively unknown, but it is known that they are all organophosphorus compounds. Each agent has a different side group which alters its potency and half-life (May 2018).

2.4 Organophosphates as insecticides and pesticides

During the 1960s most pesticides were organo-chlorine based, but when their toxicity became apparent, this led to their eventual ban, leading to an increase in the use of organophosphate pesticides, as a safer alternative. Over a hundred organophosphate

compounds are used as insecticides worldwide, although due to their lack of target selectivity and severe toxicity to animals and humans they do not make ideal insecticides. Worldwide there are between 750,000 and 3,000,000 human organophosphate poisonings annually (Chemical Terrorism 2003). Organophosphate insecticides are used to kill all developmental forms of insects, but mainly mature adults of the species. Common organophosphate compounds used are parathion, malathion, chlorpyrofos and dichlorvos. Most organophosphate insecticides are lipophilic and not ionised, they are absorbed rapidly following inhalation or ingestion. Dermal absorption is slower but may still result in lethal poisoning. Organophosphate insecticide toxicity occurs from inhalation, ingestion or through skin contamination. Organophosphate pesticides and insecticides irreversibly inactivate acetyl cholinesterase, which is essential to nerve function in insects, humans, and many other animals. The organophosphates interrupt the electrochemical communication process between nerves and muscles. The rate of poisoning is dependent on the rate of absorption as breakdown of the organophosphate occurs by hydrolysis in the liver.

Pesticides and insecticides are not species specific; in the correct quantities they will have detrimental effects on insects, mammals, and humans alike. Long term use or exposures to organophosphate pesticides are well known, including damage to the nervous system. Numerous studies have been conducted into the long-term effect of low-level exposure. One such study looked at 146 sheep farmers, who had been exposed to organophosphates whilst performing annual sheep dipping. The farmers were set tasks to test sustained attention and speed of information processing, the results showed that they performed significantly worse than the control groups. It was also noted that the farmers showed an increased sensitivity to psychiatric disorders. No effects on short term memory performance or learning were found, however it was found that repeated exposure to organophosphates did affect the nervous system (Stephens et al. 1995). There is limited data on the effects of organophosphates on humans, but some animal

studies have been conducted. Table 4 below presents toxicity data from 2016 based on rat studies, by ingestion, skin absorption, and inhalation.

Table 4: Lethal Dose of Organophosphate Pesticides to Rats (DOE 2016)

Pesticide	Oral LD_{50} mg/kg	Dermal LD_{50} mg/kg	Inhalation IC_{50} mg/m^3 in hours
Dichlorvos	25-80	70.4-250	>200 (1 hour)
Malathion	1000-10000+	>4000	-
Parathion	2-30	6.8-50	84 (4 hours)
Phorate	1.1-3.7	2.5-6.2	60 (4 hours)

Extrapolation of this data to indicate human exposure can be performed. The oral and dermal lethal dose (LD_{50}) animal values in units of mg of chemical per 1 kg of body weight can be multiplied by 70 to estimate the dose for a 70 kg human. For inhalation LD_{50} the accumulated dose up to 1 hour in time is assumed to be linear, e.g., Dose = (concentration)x(time), x denotes multiplication. The accumulative dose drops of after 1 hour of exposure and tends to become proportional to the square root of the exposure time. This means that to convert the 4-hour test to a 1-hour equivalent test, the 4-hour concentrations (mg/m^3) should be multiplied by 2. To get units of $mg\text{-}min/m^{3\cdot}$, the 1-hour test equivalent should be multiplied by 60. For example, phorate is one of the most toxic organophosphate pesticides listed with a 4-hour LC_{50} for rats of 60 mg/m^3. The 1-hour equivalent LC_{50} calculates out to be 120 mg/m^3. This number is multiplied by 60 to get 72,000 $mg\text{-}min/m^3$ (or 72 $grams\text{-}min/m^3$). The major conclusion is that the lethal dose required to kill is several orders of magnitude higher for pesticides than for any of the nerve agents (DOE 2016). The U.S. Department of Energy has published Temporary Emergency Exposure Limits (TEELs) for inhaling many of the organophosphate (Table 5).

Table 5: DOE-recommended Temporary Emergency Exposure Limits for Inhalation of Organophosphate Pesticides (DOE 2016)

Pesticide	TEEL-1 mg/m^3	TEEL-2 mg/m^3	TEEL-3 mg/m^3
Dichlorvos	2.5	20	750
Malathion	30	250	250
Parathion	0.3	2	10
Phorate	0.1	0.6	0.6

The TEEL concentrations for pesticides are almost always several orders of magnitude greater than for nerve agents. However, the TEEL-3 values for a few of the most toxic pesticides do indeed approach the TEEL-3 value for Sarin 0.126 mg/m^3 (Centres for Disease Control and Prevention 2023). A study conducted in China, examined pesticide poisoning of children. The study focused on children poisoned between 2006 and 2015. During this period 2952 children were poisoned, resulting in 66 deaths (Yimaer et al. 2015). Accidental pesticide poisoning of humans is a worldwide issue with approximately 300,000 deaths worldwide every year (Robb et al. 2023). With the World Health Organization reporting about 1 million serious unintentional poisonings per year (Boedeker 2020).

2.5 Organophosphates as fire retardants

Organophosphate compounds have been used as flame retardants for a number of years, but their use has increased over the last decade as they have increasingly been used as a replacement for polybrominated diphenyl ethers. It is estimated that of all the flame retardants in use, organophosphorus flame retardants account for approximately 15% (Marklund 2005). A vast array of products within homes and workplaces now contain organophosphates as fire retardants, products such as furniture, electronics, paint and plastics. For use as flame retardants the organophosphate compounds are used as

additives rather than being chemically bound into the material. A fire retardant is a substance that is used within the material to either stop or slow the spread of fire by supressing the chemical reactions within the flame, or by forming a protective layer on the surface of the material. Fire is a gas phase reaction and for materials to burn they must be transformed from solid or liquids into a gas. Fire retardants are used try to deter or slow down this process. Fire retardants can either involve physical or chemical actions to retard the combustion process. Numerous studies have highlighted the potential issue of large amounts of organophosphates being found in dust, air, products of combustion after a fire as well as leaching out from materials (Marklund 2005). Which potentially could affect human health as well as the environment. Figure 6 illustrates the vast variety of products that incorporate organophosphate flame retardants and the potential routes they can take to cause contamination.

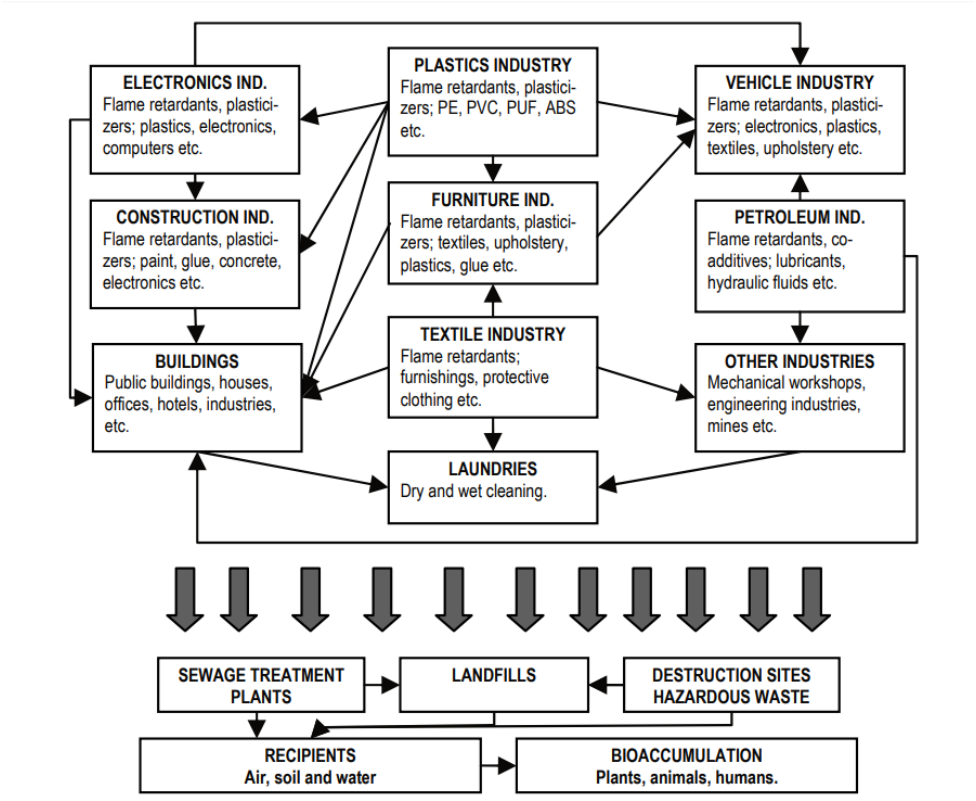

Figure 6: Chart illustrating the flow of organophosphorus flame retardants and plasticizers (Marklund 2005)

A study in Sweden (Marklund 2005) identified a number of different organophosphate fire retardants found in common items, these included TCEP, TCPP, TDCPP, TBP as well as TCP. There is a vast array of different organophosphates used as fire retardants depending of the materials they are protecting and the desired properties, e.g. trialkyl phosphates are stable at 200-300°C whereas triaryl phosphates are thermally stable up to 600°C (Marklund 2005). The Swedish study (Marklund 2005) tested indoor and outdoor environments to determine the levels of organophosphates. The study found that organophosphate proliferated throughout indoor environments whether they be domestic or industrial as can be seen in Table 6 below.

Table 6: Potent concentrations of organophosphate (Marklund 2005)

Sample site	TCPP (mg/kg) (Dust samples)	Total OPs (mg/kg) (Dust samples)
Home 1	0.47	27
University lobby	50	110
Aircraft	18	34

2.6 Other uses of organophosphates

As well as being used in agricultural products, organophosphates can be used in head lice treatments, pet shampoos, other household products, lubricants, and plasticizers.
In Morocco 1959, cooking oil became contaminated with aircraft hydraulic oil. Hydraulic oils contained additives to prevent wear during extreme conditions, one such additive was TCP. 10,000 people suffered various symptoms following consumption of the cooking oil, these included paralysis and were exhibited one to two weeks after consumption (Schopfer 2010). One of the first organophosphates, physostigmine developed in 1850, was used to treat glaucoma and has since been used to treat Alzheimer's disease.

2.7 Chemistry of organophosphates

Organophosphate is the umbrella term for a wide range of chemicals which have a broad spectrum of physical and chemical properties. They have been widely used for a number of years in both domestic and industrial settings. Several thousand organophosphorus compounds have been synthesised for various purposes (COT 1999). They include all chemicals which contain both carbon and phosphorus. Originally produced from the reaction of alcohols and phosphoric acid, organophosphate is the general name for esters of phosphoric acid with varying combinations of oxygen (O), carbon (C), sulphur (S), halogens or nitrogen. All organophosphate compounds contain a phosphorus (P) atom and a characteristic phosphoryl bond (P=O) or thiophosphoryl bond (P=S). Phosphates are the most pervasive of the organophosphorus compounds; this is why they are widely

used in pesticides, herbicides and as nerve gases as they can travel throughout the body. All organophosphate compounds share a similar chemical structure, and this is represented in Figure 7.

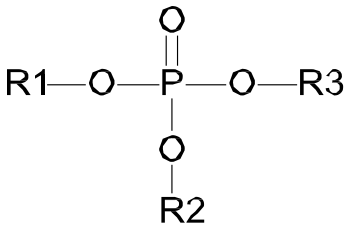

Figure 7: General structure of organophosphate (Balali-Mood et al. 2008)

Where P is the phosphorus atom, O is an oxygen atom and R^1-R^3 represents any organic structures giving the class of compounds a wide range of properties.

In nearly all cases organophosphates have a central phosphorus atom surrounded by three substituent groups, usually two alkyl groups, but can be almost any aliphatic or aromatic hydrocarbon. These groups will also differ between organophosphorus compounds and will have some influence on the toxicokinetics. Compounds with a sulphur atom are known as *phosphorothioates or organothiophosphorus* compounds. On their own these compounds will generally have a lower toxicity. The third group can be described as the leaving group. It will determine the chemical properties of the compound as it is more liable to hydrolysis than the alkyl groups (Winder et al. 2002). One classification identifies fourteen types of organophosphates.

2.8 Tricresyl Phosphate (TCP)

Tricresyl Phosphate (TCP) is a lubricating oil additive used in aircraft engines. It is of interest to this study because of this use. TCP is produced by reacting cresols with phosphorus oxychloride see Figure 8, commercial TCP contains a heterogeneous mixture

of isomers. Each molecule has a phosphate group linked to three cresyl (methylphenyl) groups.

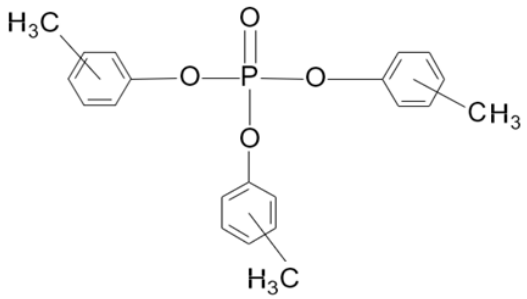

Figure 8: Structure of the TCP with ortho-, meta- and para- isomers (Balali-Mood et al. 2008)

Cresol is an aryl structure comprising of a hydroxyl (OH) and methyl (CH_3) group attached to the benzene molecule. Industrial cresol is a mixture of three positional isomers, ortho- para- and meta- cresol molecules (Balali-Mood et al. 2008). The ortho-, meta- or para- prefixes denote how far apart the hydroxyl and methyl groups are on the
Cresol molecule as shown in Figure 9.

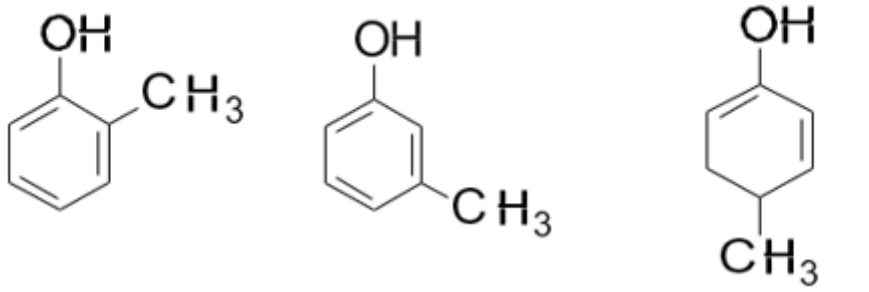

a) ortho- b) meta- c) para-

Figure 9: Structure of Tricresyl Phosphate isomers (Bali-Mood et al. 2008)

As can be seen for the ortho isomer the OH and CH_3 groups are situated adjacent to each other (Figure 9a), whilst in the meta isomer they are separated by one position on the

aromatic compound (Figure 9b) and the para isomer they are directly opposite each other (Figure 9c).

Commercial TCP is a complex mixture of isomers (*ortho-, meta-, and para-isomers)* as well as a mixture of tricresyl and dicresyl phosphate esters. Theoretically the number of tri-cresyl phosphate isomers (symmetrical and mixed) is ten. The synthesis and composition of commercial TCP has changed over the years. Tri-ortho-cresyl phosphate (TOCP) concentrations have been greatly reduced to below 0.1%. Analysis of the TCP used in aircraft engine oils such as Mobil Jet II oil, revealed that there was a higher concentration of meta cresyl isomers, with ortho cresyl phosphate isomers present almost exclusively as mono-ortho tricresyl phosphate isomer. Mono-ortho and di-ortho cresyl isomers are thought to be more neurotoxic than TOCP. TCP is an almost colourless liquid with a slightly aromatic odour. The properties of TCP are given in Table 7 below.

Table 7: Tricresyl Phosphate (TCP) data (Environment Agency 2009)

Property		Value
Molecular weight		368.4 g/mol
Density (liquid)		1.160 g/ml
Specific heat		578 J/mol K
Boiling point		266 - 272°C (at 1.3 kPa)
Heat of vaporisation		$1.86 * 10^5$ J/kg
Viscosity		12 mpa
Vapour pressure		0.03 mm Hg (25°C)
Flashpoint		225 °C
Autoignition temperature		410 °C
Particle size		100nm (0.1µm (from BS 16897)
Exposure limits	**OSHA**	0.1 mg/m^3 (0.0066ppm)
	NIOSH	0.1 mg/m^3 (0.0066ppm)

Due to the great variability of TCP products, there are no conventional workplace exposure standards. The properties identified in Table 7, give rise to TCP characteristics as use as a lubricant in oils. It is uncertain of the exact mechanism by which TCP forms the lubricant film. The main ones are: (i) TCP acts as a reservoir for acidic phosphate

(which is the active ingredient), with the film being formed by corrosion, (ii) thermally decomposed TCP forms the deposited film, and (iii) TCP decomposes by oxidation/hydrolysis (Guan 2015).

Chapter 3: Literature Review – Air supply, oil and lubricants, contamination events

3.1 Cabin air contaminants: pathways for organophosphate additives in lubricating oils

Initial concerns for the aircraft cabin environment were related to fire safety, cabin pressure and thermal comfort. In the 1960s air pollutants were beginning to cause concern, including environmental tobacco smoke and the effects this would have on passengers and crew. Following the ban on smoking the focus shifted to chemical contamination which could be present within the aircraft environment.

To enable safe air travel, aircraft must have an environmental control system to protect the occupants from extreme external conditions. Atmospheric conditions at cruising altitudes are dramatically different to those found at sea level. The system needs to maintain a comfortable constant pressure and temperature. At 12,000 m external pressures are reduced by 65%, the cabin needs to be at a pressure equivalent of an altitude of roughly 2500 m. External temperatures can fall to -60 °C, internal temperatures of around 20 °C need to be maintained (Hoffman et al. 2004). The air distribution system is an important part of this environmental control as it is used to distribute the air the occupants need around the cabin. In commercial and military aircraft there is a universal practice used to control the environment within the aircraft cabin. This practice utilises the hot compressed air from the jet engines known as bleed air to provide the comfortable environment that passengers and crew expect (NRC 2002).

Commercial aircraft also have an auxiliary power unit (APU), a small jet engine, located in the tail of the aircraft. This operates during boarding before the main engine start up particularly in extreme climates. This can also provide bleed air for the ventilation system. The APU also uses the same lubricating oil as the main engines. Pressurized air for the cabin comes from the compressor stages in the aircraft's jet engines, but before the fuel injection and combustion stages shown in Figure 10. Moving through the compressor, the

air is heated to approximately 500 °C as it becomes pressurized. It is here that the air may come into contact with lubricating oil and its additives keeping the bearings running smoothly. The oil is separated from the compressed air with labyrinth seals (a series of concentric ridges providing a pressure differential between the oil and the air zones). Over the lifetime of the engine the labyrinth seals may begin to wear and instead of preventing the oil mixing with the air supply, they begin to allow the vaporised jet engine oil and air to mix.

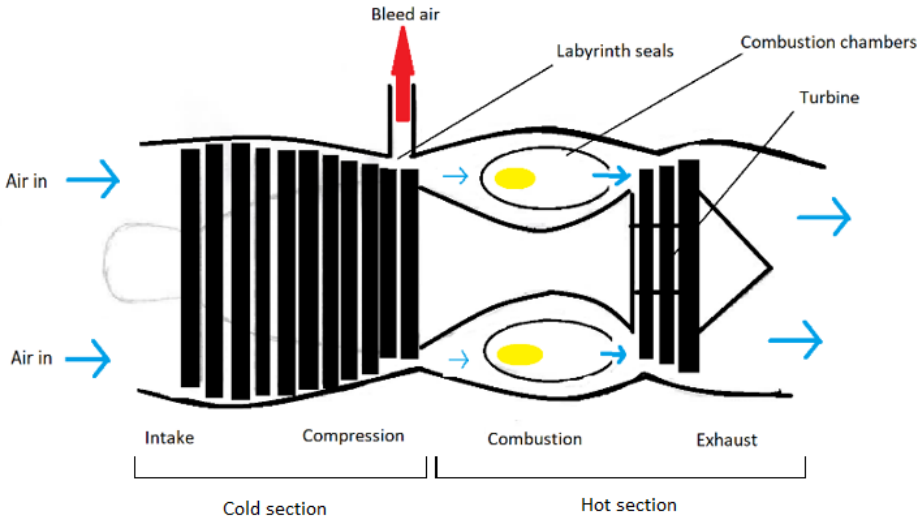

Figure 10: Typical aircraft engine

The major components of a jet engine are similar across the major different types of engines, although not all engine types have all components. The major parts include:

Cold section:

- **Air intake (Inlet)** —for subsonic aircraft, the air intake consists of an opening which is designed to minimize drag. The air reaching the compressor must be travelling below the speed of sound.
- **Compressor or fan** — the compressor is made up of stages each creating higher pressure than the one before. Each stage consists of vanes which

rotate, and stators which remain stationary. As air is drawn deeper through the compressor, its heat and pressure increase.

- **Shaft** — the shaft connects the turbine to the compressor and runs most of the length of the engine. There may be as many as three concentric shafts, rotating at independent speeds, with as many sets of turbines and compressors. Other services, like a bleed of cool air, may also run down the shaft (Baviskar 2015).

Hot section:

- **Combustion chamber** — this is where fuel is continuously burned in the compressed air.
- **Turbine** — the turbine is a series of bladed discs that act like a windmill, gaining energy from the hot gases leaving the combustor. Some of this energy is used to drive the compressor, and in some turbine engines (i.e. turboprop, turbo shaft or turbofan engines), energy is extracted by additional turbine discs and used to drive devices such as propellers, bypass fans or helicopter rotors. One type, a free turbine, is configured such that the turbine disc driving the compressor rotates independently of the discs that power the external components. Relatively cool air, bled from the compressor, may be used to cool the turbine blades and vanes, to prevent them from melting.
- **Exhaust or nozzle** — hot gases leaving the engine exhaust to atmospheric pressure via a nozzle, the objective being to produce a high velocity jet. In most cases, the nozzle is convergent and of fixed flow area (Baviskar 2015).

The portion drawn off for the passenger cabin from the cool section is first cooled by heat exchangers in the engine struts and then, after flowing through ducting in the wing, is further cooled by the main air conditioning units as shown in Figure 11. It is unclear at the moment at what stage potential contamination occurs, but it may be from one of two sources, the cooling system, or the engine itself (Michaelis 2007).

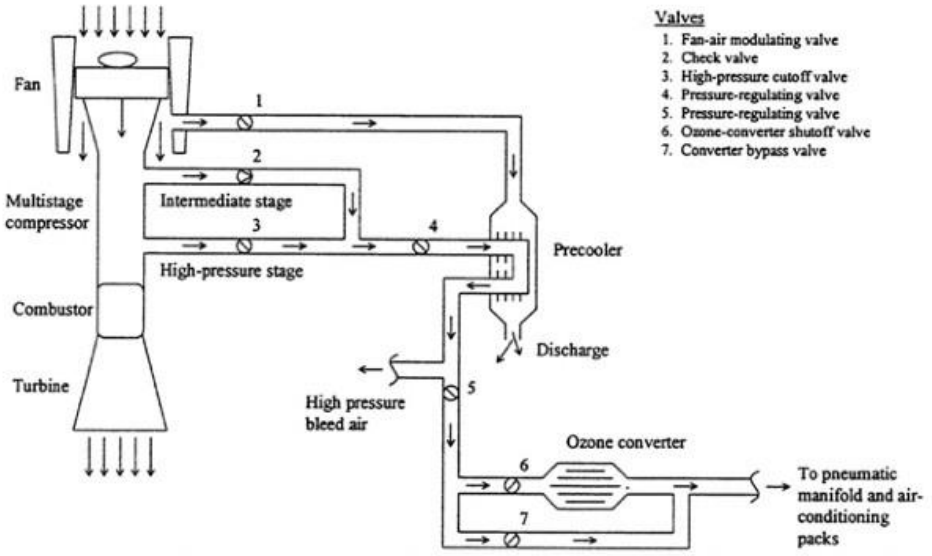

Figure 11: Bleed air supply (Winder 2006)

The cooled air then flows to a chamber where it is mixed with an approximately equal amount (50:50) of filtered air from the passenger cabin. The combined outside and filtered air is ducted to the cabin and distributed through overhead outlets. Complete exchanges of aircraft cabin air occur every 2-3 minutes (van Netten 2009).

3.2 Bleed air

Air which is extracted from the engine compressor is termed – bleed air. Most bleed-air systems have at least two extraction ports. One near the end of the compressor (high pressure stage) to get the highest possible pressure when the engine is operating at low speed and one at the intermediate stage where the pressure is adequate during the normal cruise and high-power conditions (Figure 10). When the pressure at the intermediate stage is sufficient, the bleed-air extraction from the high-pressure stage is turned off but is automatically turned on when the pressure at the intermediate stage is

low. The high-pressure port is used only during descent and taxiing. Bleed air is at high temperatures and pressures. The typical temperatures and pressures of bleed air are shown in Table 8 (Winder 2006).

Table 8: Typical conditions of bleed air (Winder 2006)

Mode of operation	Temperature (°C)	Absolute pressure (psi)	Extraction stage
Take off	660	170	Low pressure
Top of the ascent	590	100	Low pressure
Cruising	480	50	Low pressure
Start of descent	365	29	High pressure
End of descent	445	67	High pressure
Ground operations	340	-	APU

As a result of compression, the bleed air attains high temperatures, this is usually hotter than required and would be unsafe to distribute throughout the aircraft cabin. Therefore, it is necessary to pass it through a pre-cooler immediately after extraction form the engine. Air from the fan stage of the engine is used to cool the bleed air. The temperature and pressure need to be regulated, the temperature is controlled to about 175 °C and the pressure to 60 - 70 psi. Not all bleed air is used by the environmental control system; some will be used to control ice formation on the leading edge of the wing and for engine start up. The supply for these operations will be tapped off before the remaining bleed air is supplied to the environmental control systems (Winder 2006).

Mixing air distribution systems are used to circulate air in an aircraft cabin as shown in Figure 12. The ventilation system does more than simply supply breathable air into the cabin; it also distributes this air effectively around the cabin, creating circular airflow patterns. Conditioned air is supplied at the ceiling level with a high velocity and then mixes with the air already present in the cabin. Air is supplied and exhausted along the full length of the cabin rather than just in certain areas, this helps maintain a constant temperature and pressure throughout the cabin. This will also dilute any contaminant within the air.

The mixing air distribution system could also spread not only airborne infections but also particulates, droplets and vapours such as organophosphate compounds. A proportion of the exhausted air is then re-circulated, sometimes without effective filtration.

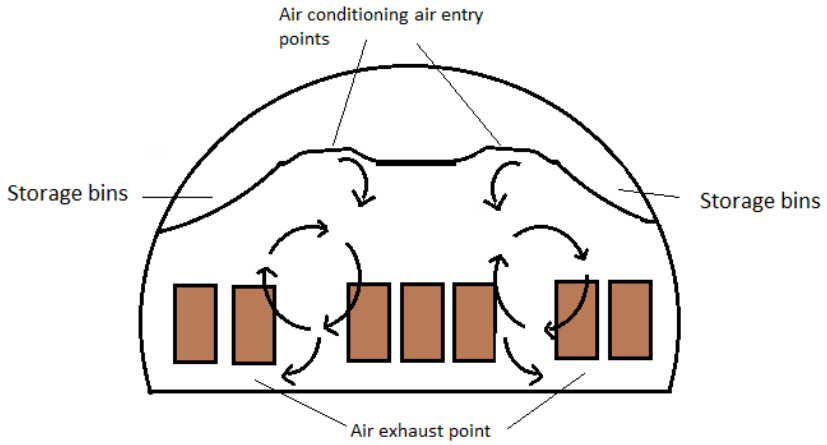

Figure 12: Air distribution in aircraft (Winder 2006)

Aircraft cabins have a higher occupant density, a more complex geometry, and a lower outside air supply rate per person when compared to buildings. Inside the cabin, the air flows from the top of the cabin, flowing downwards in a circular pattern and exits through floor grilles on either side of the cabin or, on some aeroplanes, through overhead intakes. The exiting air goes below the cabin floor into the lower lobe of the fuselage, baggage area etc. The airflow is continuous and is used for maintaining a comfortable cabin temperature. About half of the air exiting the cabin is exhausted through an outflow valve in the lower lobe, which also controls the cabin pressure. The other half is drawn by fans through special filters under the cabin floor, and then is mixed with the outside air coming in from the engine compressors. Minor oil contamination is assumed to occur, therefore the air intended for the cabin will pass through catalytic converters, which will oxidise

sporadic contaminants, but when abnormal amounts of oil contaminate the air, the catalytic converters will become overloaded and ineffective (Hunt et al. 1994).

There are high efficiency filters which have similar performance to those filters used to keep the air clean in hospitals. Such filters are very effective at trapping microscopic particles such as bacteria and viruses (Hunt et al. 1994). Studies such as the European Cabin Air (Zhang et al. 2009), project have shown that normally the levels of chemical and biological contaminants in aircraft are less than in many work environments such as office buildings. However, contaminated air can result in exposure to a mixture of chemicals, some of which are believed to have neurotoxic effects on humans. After years of use, oil seals within the engine can begin to wear, losing the ability to prevent oil leaks. This can then allow vaporised jet lubricating oil to enter the ventilation system of the aircraft. The effects of air contamination can be slow acting and have long term rather than immediate effects on health. However, if there are any incidents where the aircraft has been damaged or the hull has been breached, these would be investigated immediately. The seriousness of air contamination may have been played down for a number of years. Cabin crew have been continually informed that these events are not serious and that they do not pose a threat to health. Air crew who notice unusual odours may simply attribute this to the regular flying environment.

In the UK the independent Committee on Toxicity (COT 2010) estimated in 2007 that fume events occur on roughly 0.05% of flights overall (1 in 2000). The most recent figures show that in 2008 there were 97 contaminated air events reported to the CAA via the mandatory reporting scheme (MORS) out of 1.2 million passenger and cargo flights by UK carriers about 20% of COTs' estimates, not all fume events are reported, but even if the number was doubled or tripled this would still be a very small proportion.

The UK Department for Transport commissioned Cranfield University to undertake functionality tests to identify equipment capable of capturing fume events in real time (Muir et al. 2008).

- The DfT commissioned a data analysis study of fume events and operational parameters – especially whether there is any link between —full power take-off and fume events.
- The DfT is currently undertaking a second and more substantive phase of in-flight functionality tests to assemble data on substances in cabin air during fume events. This work builds on the equipment and methodology tested in the first phase. Several airlines have volunteered to take part by allowing an independent scientist to come on board with sampling equipment. Testing began in 2008 and continues (Muir et al. 2008).

It is assumed that air contamination events occur by oil leaking from a hot engine, into the compressed air pathway; the oil is then pyrolysed, taken up into the air flow and then dispersed around the cabin. The type of chemicals used, the type and age of the engine, temperatures reached, and point of origin for the bleed air, maintenance procedures and stage of the flight can all influence the composition and concentration of the contaminants present. Engine seals should keep the lubricating oils out of the air supply, but their failure could result in contamination. The problem of air contamination can be compounded as wear increases, carrying excessive heating, and increasing vapour pressure while the seals age, become brittle, wear and become less efficient.

3.3 Labyrinth seals

Jet engines work at extreme temperatures and pressures and to prevent the loss of gases and vapours a specific type of seal, the labyrinth seal, was developed and is now widely in use. The labyrinth seal is a non-contacting mechanical seal separating areas of low and high pressures used to reduce leakage. The labyrinth seal is composed of interlocking teeth and grooves as illustrated in the Figure 13, making the escape path for a fluid difficult.

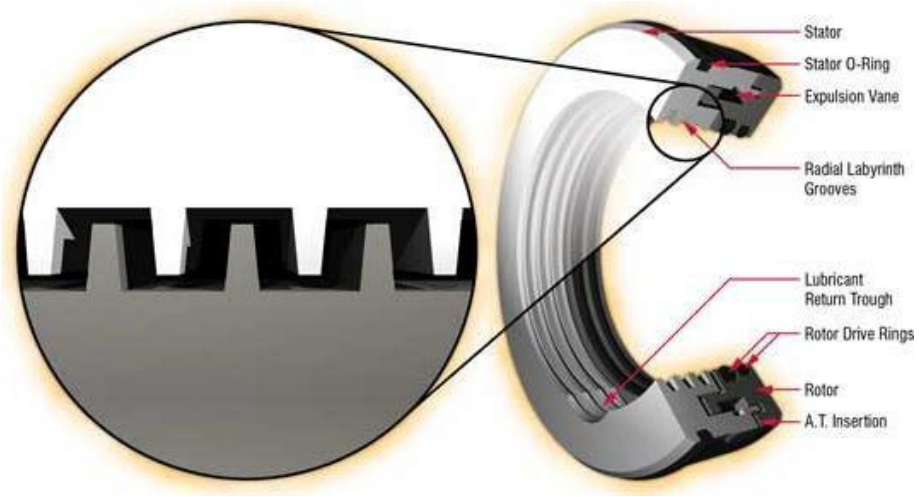

Figure 13: Labyrinth Seals (CBS 2011)

Labyrinth seals are made up of rotating and stationary parts. The rotating part is characterized by a number of grooves (the labyrinth) separated by ridges. Seal systems are used in jet engines in order to reduce the gas path leakage between the rotor (sator) parts at tips of the blades (vanes) to control air streams for cooling and pressurization as well as to avoid oil leakage at bearing chambers (CBS 2011). The gas flow through a labyrinth seal may be briefly described as follows and seen in Figure 14.

Swirling gas at high pressure enters through the clearance between the first tooth of the labyrinth seal and wall opposite to it to first cavity of labyrinth seal, expanding somewhat and altering its rotational momentum by the first friction of cavity walls which may rotate at speeds quite different from the inlet swirl. This rotation is in general non-axisymmetric and time dependent due to small but nevertheless important vibration of the rotor. Once the gas crosses several such cavities it emerges at the other end of the labyrinth seal at significantly reduced pressure. A significant assumption which facilities the semi analytic treatment of this very complex three-dimensional unsteady flow is that the gas pressure in each labyrinth cavity as well as the circumferential velocity in each cavity are

independent of the radial and axial coordinates within the cavity. Of course, appropriate boundary layers are utilized in estimating the circumferential momentum transfer from the walls to the gas. When the zeroth order approximation to this flow is considered, the one for a perfectly centric rotor rotation, the flow can be taken to be axisymmetric and of steady state.

Labyrinth seals on rotating shafts provide non-contact sealing action by controlling the passage of fluid through a variety of chambers by centrifugal motion, as well as by the formation of controlled fluid vortices. At higher speeds, centrifugal motion forces the liquid towards the outside and therefore away from any passages. Similarly, if the labyrinth chambers are correctly designed, any liquid that has escaped the main chamber, becomes entrapped in a labyrinth chamber, where it is forced into a vortex-like motion. This acts to prevent its escape, and also acts to repel any other fluid. Because these labyrinth seals are non-contact, they should not wear out (Gopal 2011).

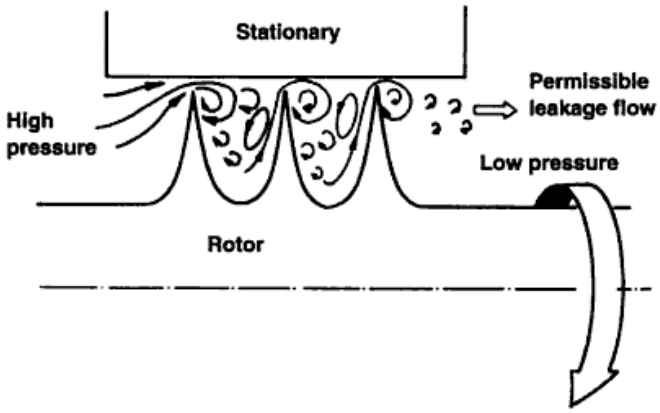

Figure 14: Gas flow through a labyrinth seal (Gopal 2011)

Wear and tear on labyrinth seals can reduce their effectiveness. The teeth on the labyrinth seals are thin and sharp to limit heat generation and lower leakage rates. Solid particles such as dust, sand and volcanic ash can enter aircraft engines from a number of different

sources. These solid particles can cause erosion of the labyrinth seal teeth which in turn can then allow leakage to occur.

3.4 What is a contamination event?

A contamination air event will occur when an engine seal fails, allowing jet oil to leak into the hot compressed air, pyrolyzing, then passing through the compressor stage of the engine and into the bleed air supply, taking it to the aircraft cabin. This manifest itself as an oil vapour or mist with an odour. The high working temperatures and pressures within the engine cause pyrolysis of the oil into a range of substances, such as volatile organic compounds, low molecular weight organic acids, esters, ketones and the additive are localized as tri-cresyl phosphate and its isomers and decomposition products (Somani et al. 2000). Several different aircraft types have reported occasional bad smells or fume events during flights. It was estimated by the Committee on Toxicity that in 2007 that fume events occur on roughly 0.05% of flights overall (1 in 2000). In 2008 there were 97 contaminated air events reported to the Civil Aviation Authority (CAA) mandatory reporting scheme (MORS) out of 1.2 million passenger and cargo flights by UK carriers. Not all fume events are reported, but even if the number was doubled or tripled this would still be a very small proportion (PACTS 2010). Fume events can be caused by substances other than organophosphates or oil. In September 2007 a fume event occurred on a flight from Belfast. The origin of the fumes was traced to the forward toilet and was probably due to a chemical in the toilet. The fumes may have been as a result formaldehyde, released as a degradation product of a toilet chemical added during maintenance at Exeter. It was not possible positively to determine to what extent the symptoms of the crew were a result of the fumes or of the stress associated with the in-flight fumes emergency, or a combination of both (PACTS 2010).

3.5 Aircraft engine lubrication oils and their composition

Jet oils are specialised synthetic oils used under extreme conditions such as those encountered by high-performance jet engines. All manufacturers of aircraft engine oils confirm that their products contain 1-5% TCP (Hanel et al. 2005). Many commercial jet oils have been in use for a number of years. One of these is called Mobil Jet Oil II, developed in the 1960s (Hanel et al. 2005), Its chemical composition has undergone little change since that time. Mobile Jet Oil II contains approximately 3% tricresyl phosphate (TCP). There are 10 isomers of TCP within the oil, but the total present is 3% (Balali-Mood et al. 2008). The isomer tricresyl-*o*-cresyl phosphate (TOCP) is present at 0.1 – 1.0% (Balali-Mood et al. 2008). Industrially TCP is made by the controlled reaction of phosphorus oxychloride ($POCl_3$) with industrial cresol. The TCP used in 95% of all synthetic Jet Engine Oils comes from only two suppliers Chemtura and Supresta. Tricresyl phosphate is added to the oil to prevent metal wear and aid as a fire retardant (Balali-Mood et al. 2008).

3.6 Decomposition products of oils and organophosphates

When oil leaks from the engine into bleed air crew and passengers could be exposed to the thermal breakdown products of engine oils. Previous work by van Netten et al. (2009) has investigated the thermal breakdown products of two commercially available oils at 525 °C. The two oils used were Castrol 5000 and Exxon 280 both of which contained 3% TCP. Each sample was heated to 250 °C at a rate of 10 °C/min and 525 °C at a faster rate until the liquid vapourised and only char residue remained. Sampling for volatiles was done using a midget impinge filled with a 10ml ethanol and isopropyl alcohol mixture (95/5%) kept at 0°C and using an air sampling pump running at 1 l/min. GC-MS was used to detect the presence of tricresyl phosphate isomers (TCP) and trimethylol propane phosphate (TMPP) another contaminant. Although TMPP was not found in these experiments the presence of TCP was found in the bulk oils and volatiles, but TCP was

not found in cabin air. It was believed that this could have been caused by localized condensation within the ventilation ducts and filters in the air- conditioning units (Michaelis 2008).

3.7 What makes organophosphates toxic?

Different organophosphates have different chemical composition and therefore have varying degrees of toxicity. All nerve gases function by inhibiting the action of the acetyl cholinesterase (AChE) in the nerve cells. Toxicity is not limited to the acute phase and chronic effects have been noted. Neurotransmitters such as acetylcholine (which are affected by organophosphate pesticides) are profoundly important in the brain's development, and many organophosphates have neurotoxic effects on developing organisms at even lower levels of exposure.

3.8 What is acetylcholine?

Acetylcholine is an ester of choline which affects people's movement and cognitive process. An imbalance of acetylcholine can cause mental problems that involve cognition processes such as thinking, learning, memory, understanding. Areas of the human body that utilize or are affected by acetylcholine are called cholinergic.

Organophosphates can have both rapid and chronic toxicity; this is mainly due to their action on specific esterase's and lipases. The main esterase's and lipases affected are acetyl cholinesterase (AChE) and neuropathic target esterase (NTE) (Kim et al. 2010).

Anticholinesterase inhibiting organophosphates are derivatives of phosphoric acids or phosphonic acids, or their sulphur containing analogues. These organophosphates possess anticholinesterase activity, unlike those that are derivatives of phosphinic acid.

The organophosphates which are derivatives of phosphoric or phosphonic acid possess anticholinesterase activity, whilst those that are derivatives of phosphinic acid do not

(Gupta 2006). Some organophosphates have anticholinesterase activity but have no well-defined leaving group, S,S,S-tributyl phosphorotrithioate is an example (Winder et al. 2002). This has very low mammalian toxicity. Organophosphates which are derivatives of phosphorothioic acid have little inhibitory action on cholinesterase until they have been activated by oxidative desulphuration within the body. Malathion is an example that becomes toxic in this way (Winder et al. 2002).

Organophosphates work by inhibiting an enzyme of the nervous system which plays a vital role in the transmission of nerve impulses. Nerve impulses travel along neurons (nerve cells) as electrical signals. However, at a junction between two neurons, (the synapse), or between a neuron and a muscle, (the neuromuscular junction), the impulse is transmitted from one side to the other in the form of a chemical substance, (the neurotransmitter). Acetylcholine (Ach) is the excitatory neurotransmitter working within the autonomic nervous system; it is released by cholinergic neurons. It is released in response to nerve simulations and binds to post synaptic acetylcholine receptors, resulting in muscle contraction or gland secretions. It can be rapidly broken down and made inactive by the enzyme acetyl cholinesterase (AChE), allowing the muscle or organ to relax (Goldberg 1976).

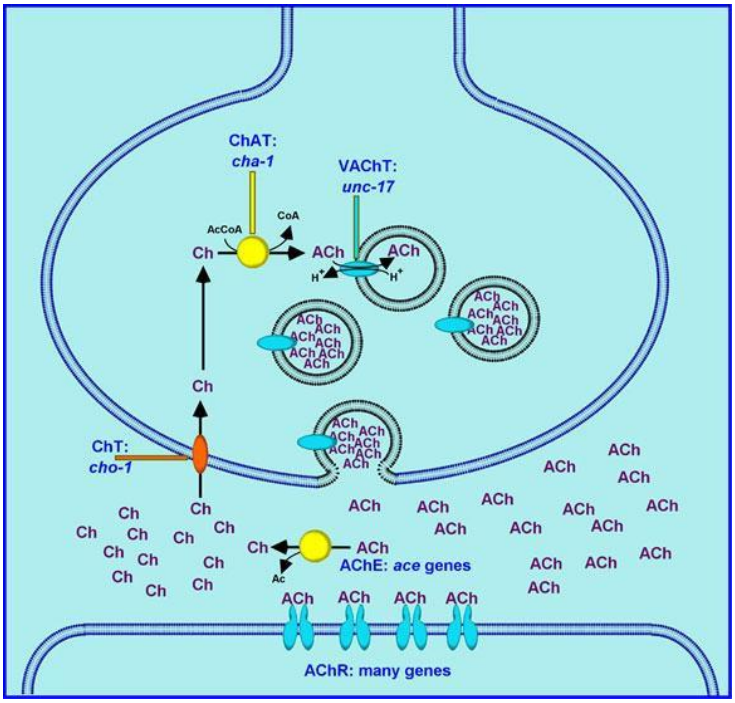

Figure 15: Cholinergic enzymes and transporters (Goldberg 1976)

As shown in Figure 15 ACh is synthesized by choline acetyltransferase (ChAT) and is loaded into synaptic vesicles by the vesicular acetylcholine transporter (VAChT). The synaptic vesicle lumen is acidified by the action of an ATP-dependent proton pump located in the synaptic vesicle membrane. The pH gradient between the vesicle lumen and the cytoplasm provides the driving force for ACh transport; the VAChT essentially exchanges ACh for protons. The docking and priming of synaptic vesicles, and their calcium-stimulated fusion with the cell membrane are all general processes that are independent of the neurotransmitter contained in the vesicles. Following synaptic vesicle fusion and transmitter release, the ACh diffuses within the synaptic cleft and activates acetylcholine receptors (AChRs), usually located on post-synaptic cells. For most other neurotransmitters (e.g., GABA, dopamine, serotonin), the action of the transmitter is terminated by transporter- mediated removal of the transmitter from the synaptic cleft. The action of acetylcholine, however, is terminated by direct enzymatic hydrolysis of the

neurotransmitter in the synaptic cleft by acetylcholinesterase (AChE). The resulting choline is then transported back into the presynaptic neuron by a high affinity choline transporter (HAChT, or ChT); this choline is then available for the synthesis of additional ACh (Goldberg 1976).

Certain chemicals such as organophosphates can throw this out of balance by interfering with the enzyme that breaks down the acetylcholine and excessive acetylcholine will build up at the receptors. Organophosphates inactivate the AChE enzyme by phosphorylating the serine hydroxyl group located at the active site of AChE. The phosphorylation occurs by loss of the leaving group on the organophosphate and establishment of a covalent bond with AChE. Exposure to organophosphate compounds with anti-acetyl cholinesterase activity prevents the enzyme from functioning allowing a build-up of acetylcholine to occur. This results in repeated nerve impulse transmissions continually telling the affected muscle to tighten, disrupting the normal functions. Normal functioning of the synapse action; degradation of the neurotransmitter ACh is illustrated in Figure 16b. Organophosphate activity and the reduced ability of the enzyme is illustrated in Figure 16c. In humans, symptoms of poisoning by AChE inhibition include dimming or tunnel vision, excessive sweating, salivation and lacrimation, nausea, vomiting, diarrhoea, abdominal cramps, weakness, headaches, deteriorating concentration and tremors. In serious cases respiratory failure will occur and eventual death (University of Washington 2007).

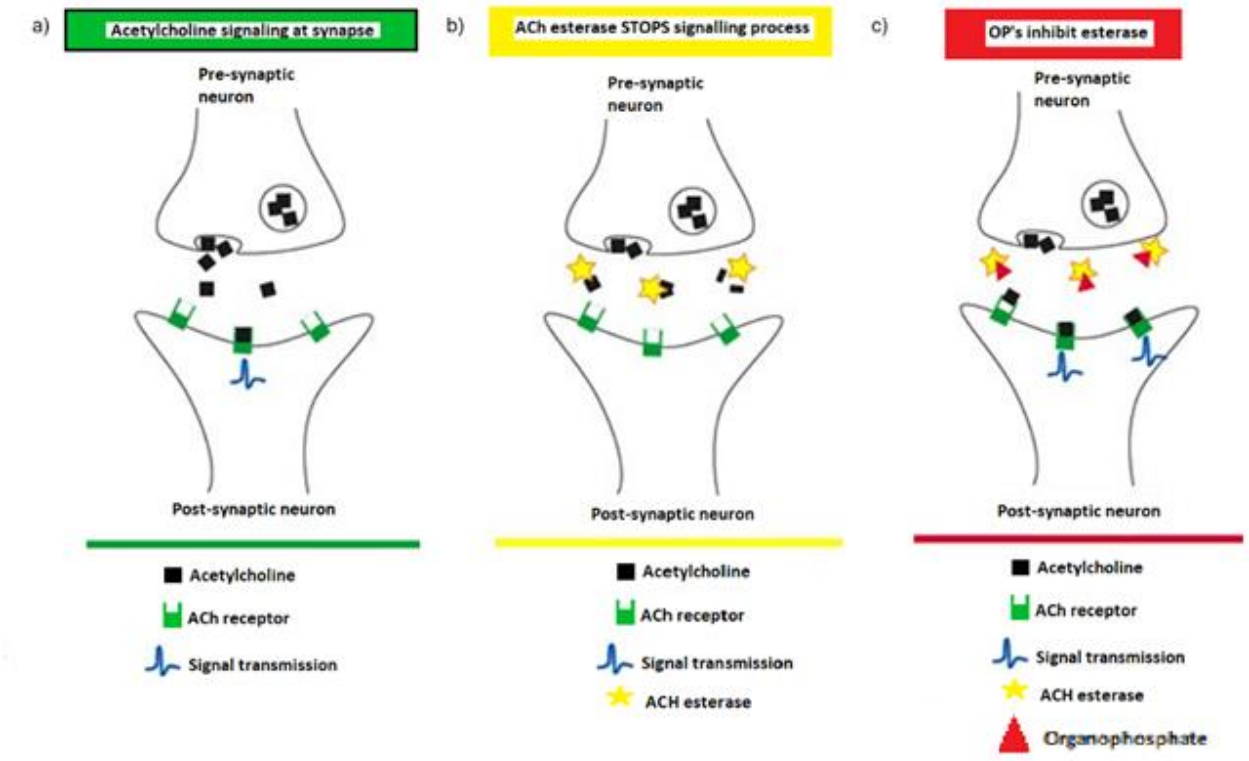

Figure 16: Acetylcholine signalling and inhibition (University of Washington 2007)

Once AChE has been inactivated, ACh accumulates throughout the nervous system, resulting in overstimulation of muscarinic and nicotinic receptors. The duration of this depends on the type of organophosphate compound involved. Clinical effects are manifested via activation of the autonomic and central nervous systems and at nicotinic receptors on skeletal muscle (Goldberg 1976). Once an organophosphate has bound to the AChE, the enzyme will undergo one of the following: hydrolysis of the phosphorylated enzyme by esterase or paraoxonases, reactivation by a strong nucleophile such as pralidoxime and irreversible binding and permanent enzyme inactivation, this is known as ageing (Goldberg 1976).

3.9 Routes of exposure and toxicity

Most organophosphates are highly lipid soluble and can be absorbed through the skin, they can be ingested; absorbed through oral mucous membranes and gastrointestinal routes, inhaled and absorbed through respiratory routes, through conjunctiva or injected as can be seen in Figure 17. The onset, severity and duration of the poisoning is determined not only by dose, by route of exposure, physicochemical properties of the organophosphate themselves (such as lipid solubility), rate of metabolism (whether transformation in the liver is required before the compound becomes toxic) and whether the organophosphorylated cholinesterase ages rapidly (Kenneth et al. 2010).

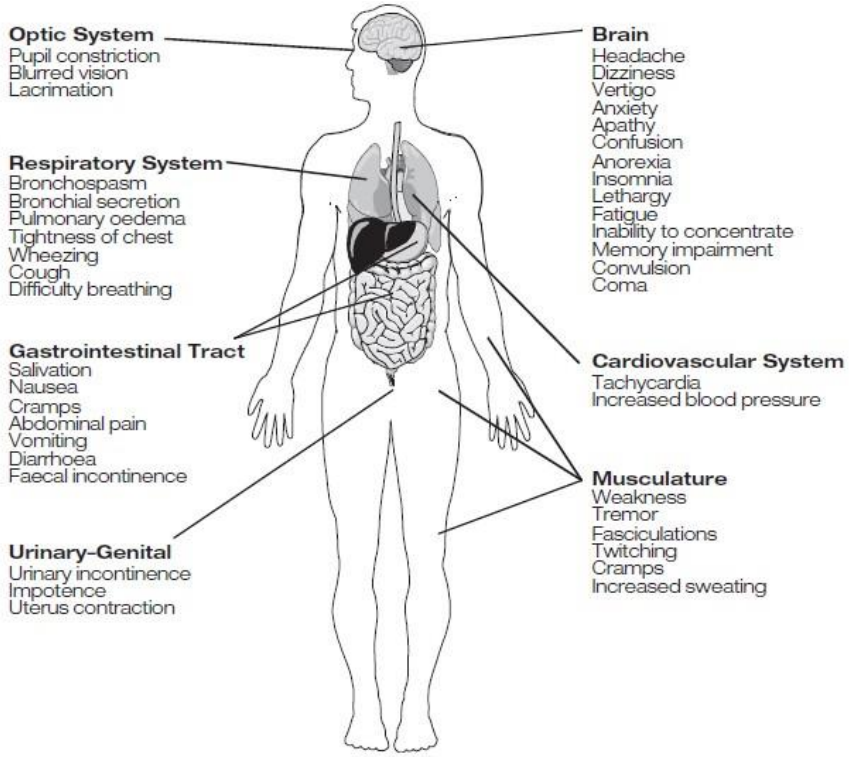

Figure 17: Organophosphate poisoning – Target systems and organs and their effects (Kamanyire et al. 2004)

3.10 Exposure rates

The severity and time to onset of the symptoms is dependent on the specific compound and the route of exposure. Exposure to organophosphates can result in four clinical syndromes:

1. Acute toxicity from acute high or intermediate level exposures or repetitive low-level exposure of significant magnitude (acute cholinergic phase),
2. Delayed neuromuscular effects which will become evident days or weeks after acute exposure (*intermediate syndrome*),
3. Delayed peripheral neuropathy developing weeks or months after acute exposure (*organophosphate induced delayed peripheral neuropathy* OPIDN).

The acute cholinergic phase and the intermediate syndrome are associated with high risk of mortality. Risk of death through OPIDN exposure is negligible. OPIDN may not necessarily be preceded by either the acute cholinergic phase or the intermediate phase. In approximately 20% of subjects the cholinergic phase will progress to the intermediate syndrome (Kenneth et al. 2010). OPIDP is not related to AChE inhibition. TOCP is a very poor AChE inhibitor. Extensive studies over the last three decades have identified the target in another esterase, neurotoxic esterase's (NTE). NTE can be inhibited by a number of organophosphates. Phosphorylation of NTE by organophosphates is similar to that observed for AChE. Only organophosphates whose chemical structure leads to ageing of phosphorylated NTE can cause OPIDN (Abou-Donia 2003).

3.11 Acute toxicity.

Organophosphates are acutely toxic. Their primary action is the irreversible inhibition of acetylcholinesterase AChE, resulting in the accumulation of acetylcholine and subsequent over stimulation of the nicotinic and muscarinic acetylcholine receptors leading to cholinergic effects, effecting blocking the action of motor neurones, and hence

all muscular control. Although some organophosphate chemicals may have similar structures, they have widely varying degrees of toxicity. Most organophosphates may be translocated and readily transported, in living organisms. Many have the ability to travel to every cell within the body, which is why they have been extensively used as pesticides and nerve agents. Some organophosphates have a greater residual effect than others (Gupta 2005).

Some are lipophilic and are thus attracted to and may be temporarily stored in lipids, which are found more in some cells, such as brain cells and fatty tissue, than others.

Low level exposure to organophosphates has been implicated as the causal factor in a variety of different forms of human ill health involving the nervous and immune systems.

Acute toxicity usually follows a single exposure when a threshold level of cholinesterase inhibition has been reached. This is typically when 30-50% of AChE has been inhibited (although this value can vary widely between individuals) (Costa 2006).

Following single exposure some of these compounds produce a delayed onset of ataxia, (lack of muscle co-ordination) accompanied by a chemical transaction, cutting or crushing of the axon known as Wallerian type degeneration see Figure 18. Followed by myelin degeneration in the most distal portion of the largest tracts in both the central and the peripheral systems that is known as organophosphorus ester induced delayed neurotoxicity (OPIDN) (Balali-Mood et al. 2008).

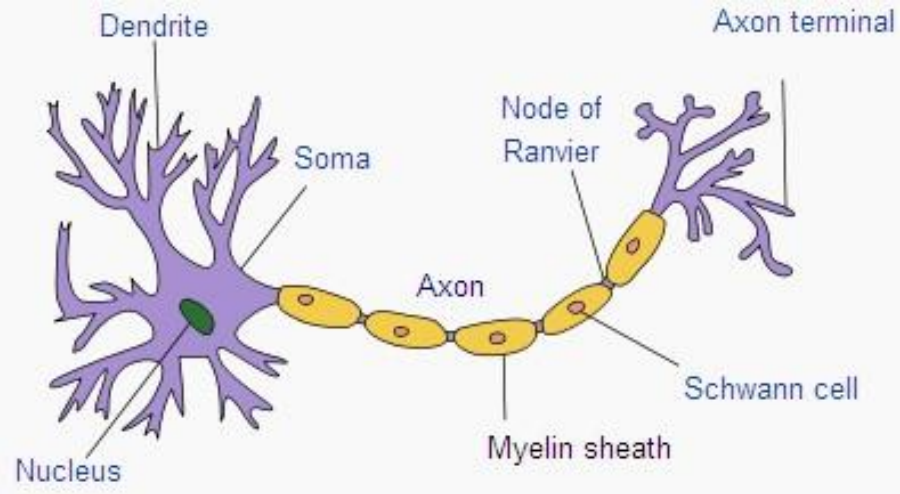

Figure 18: Structure of a typical neuron (Science ABC 2022)

All the organophosphate molecules will react with any –OH groups present on the active site of the enzyme, Figure 19.

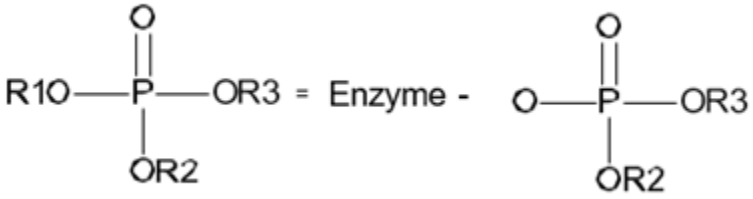

Figure 19: Reaction of –OH with enzyme (Balali-Mood et al. 2008)

The resultant neurotoxic esterase's (NTE) are initially phosphorylated, this is followed by a second reaction of enzyme — ageing, where the enzyme structure is modified and irreversibly bound, stopping it from functioning correctly. Phosphorylation of these enzymes results in localised disruption of axonal transport (transport of the axoplasm to the terminal of the axon). The basic mechanism is the breaking of the P-O-R bond, which results in the P-O group becoming negatively charged and creating a free –R group. A determinant of toxicity is the extent of inhibition of these enzymes. Inhibition of more than 50% leads to acute toxicity (Chambers et al. 2004). This ageing process is

highly dependent upon the type of organophosphate such that significant ageing varies between, 2-36 hours after initial binding. The molecular structure of the organophosphate compound will affect the probability of the above reaction occurring. OPIDN can occur if either of the R^1 or R^2 groups, or both, is linked to the phosphorus with a P-O-R and not a P-R bond (Balali-Mood et al. 2008). The organophosphate structures which allow OPIDN to occur are shown in Figure 20.

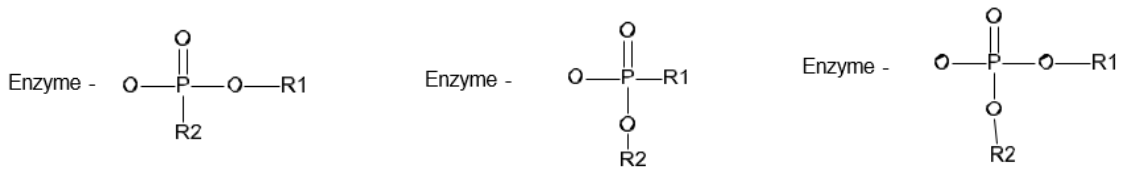

Figure 20: Structure of organophosphates which allow the occurrence of OPIDN (Balali-Mood et al. 2008)

Three groups of organophosphates the phosphates, phosphonates and phosphoroamidates are the molecules most likely to cause OPIDN. The structural features which contribute to OPIDN are esters having one or more rings substituted in the ortho position are neurotoxic provided that the ortho-alkyl group has at least one hydrogen atom on the carbon (the carbon attached to the phenyl ring). Further substitution in the phenyl ring containing the ortho-substituent greatly reduces the neurotoxicity by providing alternative degrading pathways. Thus, methyl groups in the meta or para positions, in addition to the ortho position, reduce neurotoxicity by opening a route to inactive excretable products. Further substitution in the other two rings of an ortho-substituted phosphate ester reduces neurotoxicity only slightly. The delayed neurotoxicity is greater in isomers having only one ortho-substituent, compared to the symmetrical tri-ortho-ester. The delayed neurotoxicity also decreases as the substituent in the ortho position becomes larger and more branched. The tert-butyl group is unable to undergo the activation to the neurotoxic metabolite. Furthermore, triaryl phosphate esters having no neurotoxic substituent. A substituent in the *para* position requires two hydrogen atoms on the α-carbon to produce neurotoxicity. Substituent in the *meta* position do not generally

produce neurotoxicity. Mixed esters with some substituents in both *meta* and *para* positions are less active than the symmetrical tri-*para*esters (Stephens et al. 2004).

The focus of this study is on the toxicology of organophosphate compounds and has mainly been concerned with TCP and its isomers. Commercial TCP is a mixture of various positional cresyl isomers (*ortho-, meta-,* and *para-*) as shown in Figure 21 below. It has been shown that TCP produces acute poisoning based on cholinesterase inhibition, and a well-defined syndrome of neurological degeneration. As well as affecting the nervous system, TCP has also been found to have toxic effects on the adrenal gland, ovaries and testes (Chambers et al. 2004).

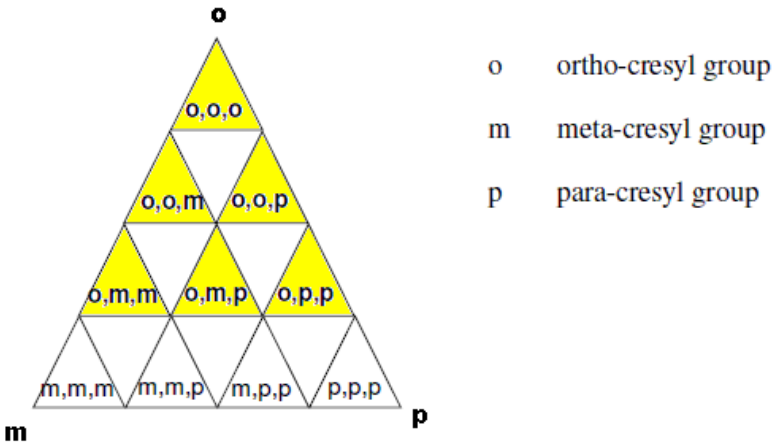

Figure 21: Isomers of TCP

The toxicity of tri-ortho-cresyl phosphate has been recognized for decades and the presence of this isomer in products containing TCP will contribute to health problems. Six of the TCP isomers (highlighted in yellow in Figure 21) contain -ortho chemical bonds. Of these TOCP has historically been identified as the most toxic. Recent studies have shown that other isomers of TCP also exhibit the ability to induce OPIDN (Hausherr et al. 2017). The mono- and di- ortho- tricresyl phosphates are reported to have toxicities like the neurotoxicity of TOCP. It should be noted that the three-dimensional structure of a phosphate is tetragonal, not square planar as it appears on paper. This means that all three –OR positions are identical. Commercial TCP will also contain mixed esters of

orthophosphoric acid with different cresyl groups, of the mono- and di-cresyl types. Other contaminants, such as mono-ortho di-cresyl phosphates also have the potential to be toxic. The mono-ortho-cresyl-diphenyl phosphate (that is, an organophosphate molecule with one cresyl group only (see Figure 22) appears to be the most toxic molecule of all (Balali-Mood et al. 2008).

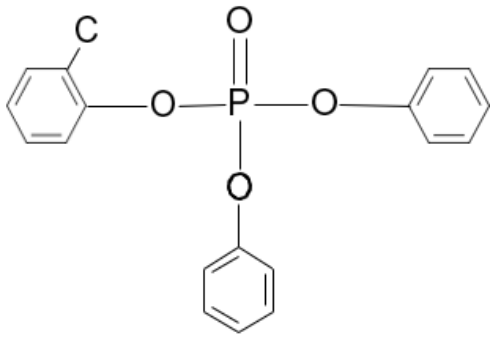

Figure 22: Mono-ortho-cresyl-diphenyl phosphate (Balali-Mood et al. 2008)

The toxic syndromes described above are well documented and are clearly linked to organophosphate exposure. The chronic effects are much less well publicised and characterised.

3.12 Chronic toxicity

Occasional or prolonged, repetitive exposure to organophosphates can produce toxic effects. The effects of this type of exposure are infrequently as severe or as fast in onset as with acute exposure. The difference in these effects is due to the extensive tissue accumulation of some of these agents and also the time required to synthesize new cholinesterase. If the rate of accumulation and AChE binding exceeds the body's rate of detoxification and fresh enzyme production, cholinesterase activity levels will start to fall, and symptoms will begin to develop. Chronic exposure to organophosphates has recently been associated with a range of neurological and neuropsychological effects. A distinct

condition, chronic organophosphate induced neuropsychological disorder (COPIND) has also been described, with both neurological and neuropsychological symptoms.
These include: headaches, mental fatigue, depression, anxiety, irritability, reduction in concentration and vigilance, reduction in information processing and psychomotor speed and memory deficiency and speech impairments.
COPIND can be seen in individuals who have been exposed in one event, short term exposures or long-time low-level repeated exposure. The basic mechanisms of the effect have not yet been identified, although it is not believed to be related to the esterase inhibition properties of organophosphate compounds, it is also unknown if the symptoms are permanent or not. It is evident that these symptoms are not desirable attributes in airplane pilots or cabin crew.

3.13 Aerotoxic Syndrome: short- and long-term symptoms.

Several incidents have been reported where flight and cabin crews have experienced a variety of symptoms possibly caused by exposure to TCP and its isomers. The earliest reported case of exposure to jet oil was in 1977 (Hanel et al. 2005). In this report it states that a healthy military aircraft flight crew was incapacitated during a routine flight. The crew suffered neurological and gastrointestinal distress (nausea and vomiting). Other studies have highlighted the possibility of fume events, including a 1983 study of 89 cases of smoke or fumes within the cockpits of US Airforce aircraft (Hanel et al. 2005) and more recently a 1998 study of BAe 146 flight crews in Canada (Raymen et al. 1983). Many of these reports include similar symptoms suffered by the crew such as headaches, dizziness, confusion and disorientation. These symptoms have been grouped together in some studies and have been termed aero toxic syndrome (Sparks et al. 1990). It is claimed that this syndrome can be reversible after brief exposures, but prolonged and frequent exposure is thought to be linked with more chronic symptoms which have long term health effects. The symptoms of aerotoxic syndrome have been classified into two

groups: single, or short- term exposure and long-term low-level exposure (Balali-Mood et al. 2008). After short-term exposure, patients may complain of (Michaelis 2007):

- Neurotoxic symptoms: blurred or tunnel vision, disorientation, shaking and tremors, loss of balance and vertigo, seizures, loss of consciousness,
- Neuropsychological symptoms: memory impairment, headache, light-headedness, dizziness, confusion and feeling intoxicated,
- Gastro-intestinal symptoms: nausea, vomiting,
- Respiratory symptoms: cough, breathing difficulties (shortness of breath), tightness in chest, respiratory failure requiring oxygen,
- Cardiovascular symptoms: increased heart rate and palpitations,
- Irritation: of eyes, nose and upper airways.

After long-term exposure, patients may complain of (Michaelis 2007):

- Neurotoxic symptoms: numbness (fingers, lips and limbs),
- Neuropsychological symptoms: memory impairment, forgetfulness, lack of co-ordination, severe headaches, dizziness, depression, sleep disorders,
- Gastro-intestinal symptoms: salivation, nausea, vomiting, diarrhoea,
- Respiratory symptoms: breathing difficulties (shortness of breath), tightness in chest, respiratory failure, susceptibility to upper respiratory tract infections,
- Cardiovascular symptoms: chest pain, increased heart rate and palpitations,
- Skin symptoms: skin itching and rashes, skin blisters (on uncovered body parts), hair loss,
- Irritation: of eyes, nose and upper airways,
- Sensitivity: signs of immunosuppressant, chemical sensitivity leading to acquired or multiple chemical sensitivity,
- General: weakness and fatigue (leading to chronic fatigue), exhaustion, hot flushes, joint pain, muscle weakness and pain.

Research by Freudenthal et al. (1993) has focused on identifying a dose response relationship for TOCP. Results of a short term 10 week repeated daily oral dose study in hens of aviation engine oil containing various amounts of commercial TCP suggest that oil containing 1% TCP (a TCP equivalent of 20 mg $kg^{-1}day^{-1}$) was considered a no observable effect level. Whilst hens which received oil containing 3% TCP showed significant neurotoxicity in the form of lack of muscle control, 77% neurotoxic esterase (NTE) inhibition, and abnormal growths in the tissues of the nervous system. It is generally assumed that most exposure in aircraft cabins to TOCP is by the inhalational route. Absorption through skin exposure cannot be discarded, as significant exposure (maximally estimated at a trans-dermal flux rate of 0.01 $mgcm^{-2}hr^{-1}$) through this route is possible.

The isomers that make up commercial TCP are toxicologically different, but the *ortho* containing isomers are the most toxic. The location of the methyl group is critical in the toxicity. TCP has been shown to be related to OPIDN and manufacturers have reduced the levels of TOCP in commercial grades of TCP, which have then been included on lists of hazardous chemicals. The other *ortho* containing isomers in TCP, three *mono-ortho* (MOCP) isomers and two *di-ortho* (DOCP) isomers have not been specified in lists of hazardous chemicals, and this may be one reason why they are not disclosed on labels and material safety data sheets (MSDS).

These compounds have been found to be more neurotoxic than TOCP; DOCPs are five times more toxic, and the MOCPs ten times more toxic, than TOCP (Balali-Mood et al. 2008) as can be seen in Table 9. The total toxicity of a particular mixture is therefore dependent on concentration of the proportion of each isomer, their relative toxicities and the effect of any interaction between the isomers.

Table 9: Toxicity of isomers in commercial TCP (Balali-Mood et al. 2008)

Isomer	Concentration (ppm)	Relative Toxicity	Equivalent Toxicity
TOCP	0.005	1	1x
DOCP	6	5	30x
MOCP	3070	10	30700x
		Total	30731x

The above discussion is limited to the toxicity of the TCP, as added to the lubricant. On thermal decomposition, changes such as isomerisation or bond cleavage may widen the range of organophosphates present or change their concentrations.

3.14 Timeline of previous studies

Several investigations have been conducted by various organisations including governmental bodies since the first realization of the potential problem of air contamination. A timeline of some of these studies is shown below in Figure 23. The timeline illustrates when the bleed air system was first introduced into commercial aircraft, studies on aircraft cabin air quality in 1986. This led to the banning of smoking on commercial aircraft in 1998. Not long after this ban, there was an increase in the reporting of foul smells in the cabin and cockpit. In 1999 the term “Aerotoxic Syndrome” was first coined, indicating the impact on health from potential cabin contamination events. A number of high-profile studies was then conducted: BALPA 2002, CAA 2004 and UK House of Commons 2006. These studies are discussed further in the following sections. Numerous independent studies have also been conducted to determine if there was a significant problem (Michaelis 2007, Winder 2005). A number of cabin crew were reporting significant health impairments and one pilot died allegedly as a result of repeated exposure to aircraft cabin air contamination events. Legal action was brought against UK airlines in 2019 relating to these issues.

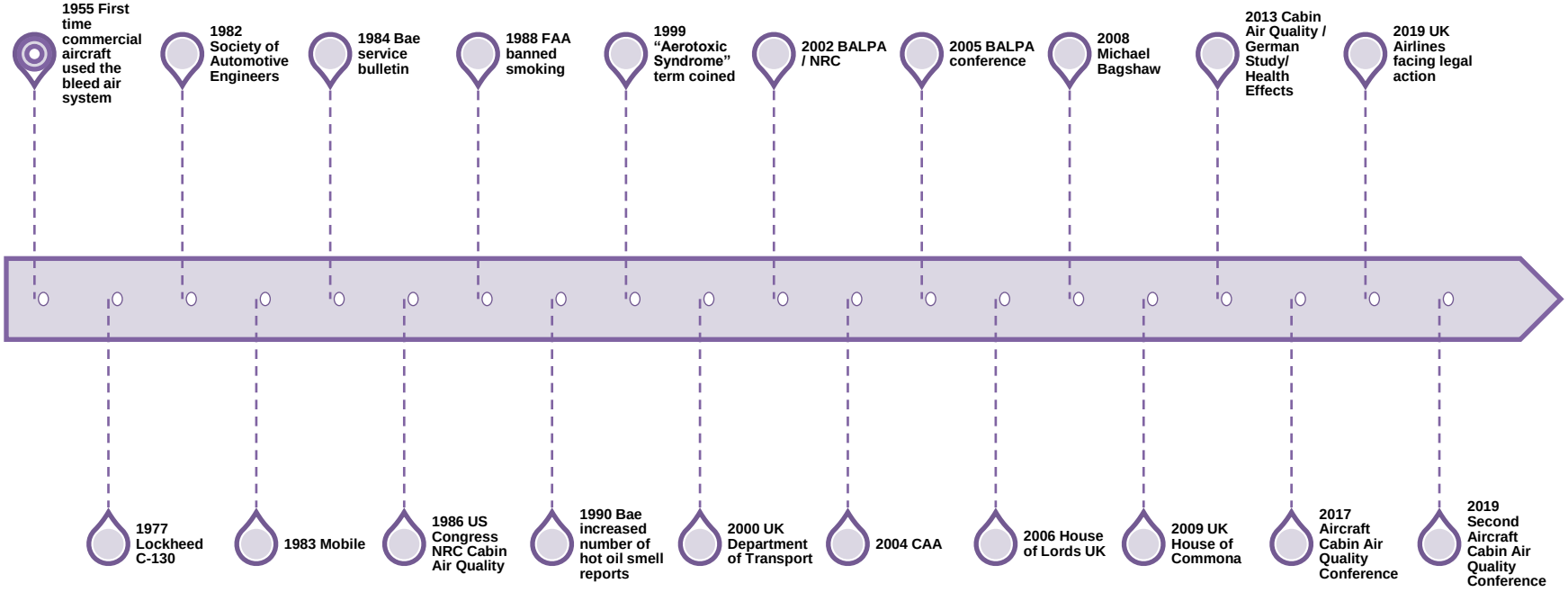

Figure 23: Timeline of studies on aircraft cabin air contamination

3.15 Committee of Toxicology (COT) 2007

In 2007 the United Kingdom's Department of Transport commissioned the Committee of Toxicology (COT) to undertake an independent scientific review into the possible adverse health effects of hydraulic oils and fluids contaminating aircraft cabin air (COT 2009). Data relating to contaminated air had been submitted by BALPA highlighting pilots and crew concerns over the potential impact on their health. COT was asked to evaluate the information submitted by BALPA as well as assess the risk of exposure of aircraft crews and passengers to contaminated air, in particular to air contaminated with organophosphate compounds. They were also asked to determine any correlation between this potential exposure and ill health exhibited by aircraft crew (COT 2009).

COT concluded that there was no direct link of exposure to oil contaminated air to cabin crew ill health. Several researchers have heavily criticised the COT report stating misleading statements and errors were included within the report. COT is accused of dismissing reports from experts such as physicians and engineers as well as statements from cabin crew. The report was criticised for presenting misleading information regarding the chemicals that were of concern, playing down the potential role of the organophosphate compounds found within engine oils. COT reviewed incidents presented to them by BALPA but failed to recognise that BALPA is not the reporting organisation. This report also criticised the fact that COT did not find evidence to support the link between exposure to oil contaminated air and ill health but stated it would be "prudent to prevent exposure to oil contaminated air".

Following the publication of the COT report, the Department of Transport commissioned further research. In 2008, the UK Government also commissioned a functionality study conducted by Cranfield University (Muir 2008). They study tried to determine the best equipment capable of capturing fume events. A second study was conducted in 2009 by Cranfield University to determine if there was a link between stages of flight and fume events – in particular when the aircraft was initiating "full power take offs" (Cot 2009)

A third study, again by Cranfield University, in 2011 involved in-flight testing to determine if potential hazardous substances could be found within the aircraft cabin.

Two types of aircraft were identified for the study – BAe 146 and the Boeing 757 (Crump et al. 2011), these were chosen based on the COT report. Samples were taken while the aircraft was stationary, on the ground with and without the engines running. Several methods of sampling were used: solid phase micro extract fibres and photoionization detectors. It was determined that these methods were suitable for background monitoring of cabin air in normal flight conditions. The study recommends that cabin crew complete questionnaires and that flight data recorders and maintenance reports should be analysed. This would then allow identification of substances which are within the cabin aircraft air. This functionality test was conducted to determine the methods and equipment that would be utilised in future studies (COT 2013). The Aircraft Cabin Air Sampling Study: Part 1 (Crump et al. March2011) and Part 2 (Aircraft Cabin Sampling Study April 2011) study analysed the cabins of five different aircraft and during a total of 100 flights for particular compounds during all phases of flight. The equipment used was a photo-ionisation detector tasking sample which would then be analysed using thermal desorption, gas chromatograph and mass spectrometry. The aircraft studied were a Boeing 757 (passenger and cargo), an Airbus A320/1, a BAe 146 and an Airbus 319. No fume events were observed during the test. The compounds that the study was trying to determine, the minimum and maximum concentrations found and the stage of flight that the highest concentration was found are presented in Table 10 below (Crump et al. 2011).

Table 10: Compounds identified, concentrations and stage of flight showing highest concentration

Compound	Concentration µg/m^3	Stage of flight during which highest concentration was found
TOCP	22.8	Climb
TCP	28.5	Climb
TBP	21.8	First engine start
Toluene	170.2	Take off
Xylenes	52.3	First engine start
Limonene	540.3	First engine start
TCE	20.1	Immediate
Undecane	87.3	First engine start

This study based its findings on guidelines (where available) for domestic and working environment exposure limits and concluded that there was "no evidence for target pollutants occurring in the cabin air at levels exceeding available health and safety standards and guidelines" (COT 2013).

The German Federal Bureau of Aircraft Accident Investigation commissioned research in to fume events due to an increased number of crew reporting the occurrence of fume events. The study investigated 663 reported incidents (between 2006 and 2013) which were related to smoke or abnormal smells within the aircraft cabin or specific symptoms identified by aircraft occupants. This study determined that fume events did occur and there was therefore contaminated air. The study did not determine however, if the contaminant was tricresyl phosphate or tri-ortho cresyl phosphate (Bagshaw 2013).

A number of studies have been conducted in Australia. In 2000 The Senate Rural and Regional Affairs and Transport published a report on the issues of organophosphates contaminating air in BAe 146 aircraft. The report does identify that the issue may be present on other aircraft and not just the BAe 146, but they did identify that there was a long history of events within this specific aircraft and suggested this would have an effect on health. Further research was recommended as it was difficult to pinpoint the exact cause / location of the contamination (Bagshaw 2013). Due to a number of reports from

Australian pilots and cabin crew concerning contaminated air events and the possible detrimental effects on health, the Australian Civil Aviation Safety Authority (CASA) established an Expert Panel on Aircraft Air Quality (EPAAQ) in 2007. This panel reviewed scientific data from international reports. Although the panel did acknowledge that it was possible that air contamination events could occur and that the pyrolyzed products of engine oils could be the source of the contaminants, this was not proven, there could be a potential number of sources. The panel determined that the occurrence of fume events would be rare, but this could be due to the non-standard reporting system that different airlines use. The panel determined that there was still many unanswered question and further research would be required (Bagshaw 2013).

The Final Report EASA Research Project: CAQ Preliminary cabin air quality measurement campaign 2014 covered the period June 2015 to June 2016 (Schuchardt et al. 2014). Looking at eight types of aircraft: the main part of the study analysed aircraft which utilized the bleed air system, and the second part of the study analysed the Boeing 787. The compounds that the study determined that were present, the minimum and maximum concentrations found are presented in Table 11 below. The study determined that the quantities identified, were similar to those found in normal residential and working environments.

Table 11: Compounds identified and concentration range (Schuchardt et al. 2014)

Compound	Main Study µg/m^3	Boeing 787 µg/m^3
Formaldehyde	0.03-48	0.02 -17
TCP	Mean 0.009 Max 1.515	Mean 0.020 Max 0.403
TBP	0.037 to 2.484	0.037 to 1.482
tris(chloro-isopropyl)phosphate	0.023 to 9.977	0.041 to 2.633

The Global Cabin Air Quality Executive (GCAQE) was established in 2006. This is a non-profit global organisation that representing air crew. This organisation was set up in relation to one issue of aviation safety – aircraft cabin air contamination. This organisation

was set up by a number of aircraft pilots and cabin crew due to what they saw as a direct failure of the industry and governments to address the problem. There are 33 organisations who are members of the GCAQE. This organisation is hoping to make people aware of the issue, including aircraft crews and public to pressure the industry into taking action to prevent long term health issues for crew and passengers and to potentially avert a fatal aircraft incident (GCAQE 2019).

FreshAircraft (FACTS) is a research study funded by the Directorate-General for Mobility and Transport (DG-MOVE). The main remit of this project is to determine if engine oil can enter the bleed air system and affect aircraft cabin air (FACTS 2017).

The FACTS project is organised by the following tasks.

- Task 1. Review of the State of the Art and Establishment of the Baseline for the Work – this part of the project continued the monitoring in-flight air quality including simulations within real aircraft but on the ground (FACTS 2017).
- Task 2. Exposure Monitoring: Identification of the causes of bleed air contamination and assessment of the impact on the quality of cockpit/cabin air – determination of the toxicity and the effect of the body. Limited tests have been conducted so far, so further analysis of body fluids and tissues will be undertaken (FACTS 2017).
- Task 3a and 3b Toxicological risk assessment and Health risk assessment – there is limited data on the effects of specific chemicals such as organophosphates (FACTS 2017).
- Task 4. Engineering controls- Risk mitigation strategy - will provide an overview of technical measures that potentially can be taken to reduce or eliminate the intrusion of engine oil into the aircraft (FACTS 2017).
- Task 5. Conclusions and recommendations.

3.16 Case studies of organophosphate contaminations

The first well-documented case was of a C-130 Hercules navigator becoming incapacitated after breathing contaminated cabin air in 1977 (Hanel et al. 2005). An Australian study of three defence aircraft (Hawk, Hercules C-130 and the F-111) was undertaken in 2005. The tests were carried out while the aircraft was on the ground when the auxiliary power units were in operation. The experiments found that in the Hawk the highest concentration of TCP was 21.7 and 49µg/m^3, in the Hercules and the F-111 results showed that <3.5µg/m^3 and 0.35µg/m^3 OP were present. These values are low when compared with the maximum allowable time-weighted 8-hour average (TWA) exposure of 1005µg/m^3 for TCP. In most of the tests the most toxic components of TCP (mono-*o*-cresyl phosphate isomers) calculated to be present were less than 1/200 of the TCP TWA after allowing for the fact that these isomers are 10 times more toxic.

During the 1990‘s a number of incidents occurred on BAe 146 passenger aircraft, operating in the UK and Australia. It was suggested that these incidents could be related to contamination of the cabin air. The contamination was suspected to be fumes from the engine oil, which contained TCP (PACTS 2010). The BAe 146 is a jet used mainly for short haul trips. The aircraft first flew in 1981. There are three sizes of fuselage, but all have common types of engines and systems. The dimensions of the different BAe 146 aircraft available are provided in Table 12.

Table 12: Dimensions of the three BAe 146 aircraft (BAE Systems)

	BAe 146-100	BAe 146-200	BAe 146-300
Wingspan (m)	26.34	26.34	26.34
Gross wing area (m^2)	77.3	77.3	77.3
Overall length (m)	26.16	28.55	30.99
Overall height (m)	8.61	8.61	8.59
Wheelbase (m)	10.09	11.2	12.52
Passenger cabin			
Length (m)	15.42	17.81	20.20
Headroom (m)	2.03	2.03	2.03
Internal diameter (m)	3.42	3.42	3.42
Floor width (m)	3.24	3.24	3.24

The BAe 146 is powered by four Honeywell ALF502R-5 high by-pass engines shown in Figure 24 below. They are also fitted with auxiliary power units which supply the bleed air for the air conditioning at high altitude and electrical power for ground services and emergency services. A report by the Senate Rural and Regional Affairs and Transport References Committee (Senate Rural and Regional Affairs and Transport 2000) in Australia conducted an enquiry into the air quality on the BAe 146. The report looked into the BAe 146 air supply and the circulation routes throughout the aircraft and identified the key engine components as a fan module, compressor, combustion chamber and a turbine section as shown in Figure 24.

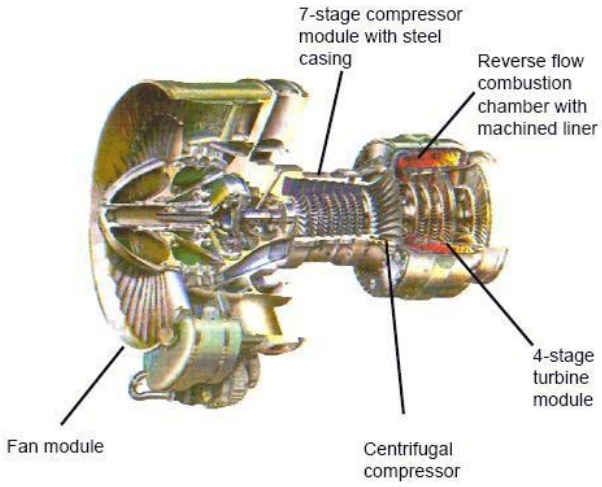

Figure 24: Schematic showing the Honeywell ALF502R-5 (Bae Systems 2009)

Mobile Jet II Oil is the main type of engine oil used in the BAe 146 engines. High pressure bleed air is taken from the rear of the compressor stage. It is then diverted to various systems including the environmental control system, to the cabin and flight deck. The design of the BAe 146 allows the aircraft to operate with the air conditioning system re-circulating a proportion of cabin air. It is generally considered that re-circulated air improves humidity levels in the aircraft cabin and cockpit and is a feature designed to reduce symptoms of watering eyes as well as nasal and throat dryness caused by dry air (Senate Rural and Regional Affairs and Transport 2000). The air in the BAe 146 is changed 16 times an hour. This air is approximately 60 per cent fresh and 40 per cent recycled. The United States Aviation Transport Safety Board noted that there had been 93 fumes events between 1991 and 1999 (Senate Rural and Regional Affairs and Transport 2000), but no substantial investigations were undertaken. The most serious fume event in Australia occurred in 1997 on a freight flight in the final stages of decent. The crew smelt strong oily odours and fumes were observed in the cockpit. The captain began to feel confused and had difficulty in concentrating. The co-pilot noticed the captains' deteriorating state, took control of the aircraft and landed safely. All crew members showed varying symptoms from nausea to headaches. Within two months of the incident the crews' health began to improve. Medical examinations failed to find a

cause for the symptoms. Before the flight had commenced one of the crew had examined the maintenance logs and noted that oil residue had been noticed at the two air conditioning packs as a result of oil transfer from one of the engines. The problem was linked to a failing oil seal. However, the aircraft was still cleared for flight (Senate Rural and Regional Affairs and Transport 2000).

The Committee's (Senate Rural and Regional Affairs and Transport 2000) inquiry into the possible impact on air safety of cabin air quality in the BAe 146 aircraft indicates, that safe and comfortable operation requires adequate quality air, if the air contains contaminants, it has the potential to detrimentally effect the levels of crew operation. Excessive levels of chemical contamination can affect two aspects of aircraft operations: the operational environment and the working and travelling environment; a fact apparent to airline operators, to aircrew and to every airline passenger (Senate Rural and Regional Affairs and Transport 2000). Oil fumes entering passenger cabins and cockpits are not limited to the BAe 146, although it has been the focus of the majority of complaints of fume contamination made to Australian airlines and has been the source of a number of serious incidents of pilot incapacitation resulting from oil fume contamination of cabin air.

It has been argued that fume events cannot be eradicated as long as air is brought into cabins by bleeding air from the engines. It is also unlikely that an alternative engineering arrangement can being implemented on current aircraft. It appears to the Committee that contamination of cabin aircraft air on the BAe 146 aircraft has led to short-term and medium-term health problems for a number of BAe 146 flight crew. Some scientists link these health problems to contaminants, although the link has not yet been definitively established. Similarly, while definitive links have not been made between the toxic chemical components of Mobil Jet Oil II and illness in flight crew, this remains a question to be further investigated and assessed (Senate Rural and Regional Affairs and Transport 2000). The central issue of this research is the composition of the fumes entering the aircraft cabin and their potential to distribute toxic substances throughout

the aircraft cabin and cockpit, potentially affecting passengers and crew. The research will attempt to establish if there are adequate safety systems in operation.

3.17 Other possible contaminant of aircraft cabin air

Is it possible that the air can become contaminated from other sources than through the jet oil contaminating the recycled air?

Whilst the aircraft is on the runway following landing, or whilst waiting to take off, the aircraft cabin air could become contaminated by fumes generated by other surrounding aircraft and airport vehicles. There are a number of toxic species within these exhausts that can cause adverse health effects. These include but are not limited to carbon monoxide, nitrogen oxides and hydrocarbons. Aircraft and vehicles are under air pollution restrictions when on the ground, so the amount of these compounds emitted is controlled and reduced. Whilst these compounds can cause respiratory irritation and other health effects, there is little available information from monitoring that indicates the exposure of cabin occupants to these substances.

Carbon dioxide is also a potential source of ill health. As part of the normal respiratory process, we expel CO_2 into the atmosphere. In an aircraft, the Environmental Protection Agency (EPA) have stated that the following standards for CO_2 exposure should be adhered too: 10 mg/m^3 (9ppm) for an 8-hour exposure and 40 mg/m^3 (35ppm) for a 1-hour exposure. Studies have shown that the levels of CO_2 are typically below 1 ppm.

The materials used to construct the aircraft and the furnishings within as well as the cleaning products used regularly within the cabin, could also be a potential source for air contaminants. Volatile organic chemicals (VOCs) can be emitted from the materials and leach into the air. There is little data on the potential of this chemical leaching within aircraft, but there are studies in which chemical leaching is being considered within homes and working environments. Whilst this may be a potential source of contamination, the amount of chemicals would be considered to be extremely small and prolonged exposure

would have to occur. Studies have shown that cleaning materials may emit some VOCs but that this period of emission peeks 2 hours after use, decaying exponentially thereafter. De-icing fluids are also another source for contamination, although this is not used on all flights all year round. Glycols (ethylene glycol and propylene glycol) are the main constituents of de-icing fluids used for aircraft. Ethylene glycol is extremely toxic when ingested in high doses whereas propylene glycol is not. Table 13 below shows the level of toxicity of ethylene and propylene glycols. Propylene glycol is the preferred choice for aircraft de-icing (70%), reducing the potential for de-icing fluids to be the cause of adverse health effects in cabin crew and passenger.

Table 13: Toxicity of Ethylene and Propylene Glycol

Routes of exposure	**Ethylene Glycol**	**Propylene Glycol**
Oral	1.4 mL/kg	No intrinsic oral toxicity
Dermal	Unlikely	-
Inhalation	3–67 mg/m^3 for 20–22 h/d for about 4 weeks	-

3.18 Air travel and COVID 19

March 2020 saw the rise of infections due to the Coronavirus (COVID-19). This initially saw many countries introducing travel restrictions, reducing the amount of travel across their borders. This led to an increase in research into many aspects of transmission of the virus, including the risk of contracting COVID-19 during air travel, particle distribution and air flows within the aircraft cabin (Davis et al. 2021, Desai et al. 2021, Gupta 2020, Linder 2020, Wang et al. 2021, Yan 2021).

Aircraft cabins have a high occupant density, and the occupants could be exposed to virus particles for a long period of time.

Due to the potential increased risk of COVID-19 transmission a number of studies have been conducted to investigate the airflow within aircraft cabins. One such study (Aviation Public Health Initiative, 2020) identified the flow velocities and patterns in a number of

different aircraft. Illustrated below is velocities and directions of particles identified within and Airbus A320 aircraft.

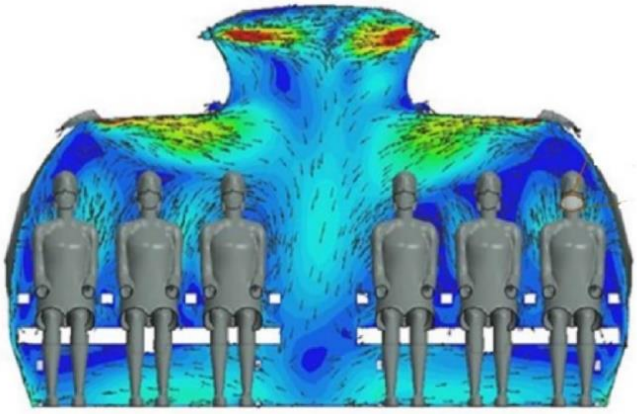

Figure 25: Airflow within an aircraft cabin (Runway Girl 2020)

Figure 25 illustrates the air entering the cabin from inlets at the top of the cabin, flowing down between the seats in the central isle and then leaving the cabin via the outlets at floor level. The figure shows there is some circulation around the occupants, but this is minimal. COVID-19 is emitted when a person talks, coughs, sneezes or sings mainly in droplets that can be propelled a short distance, and sometimes in smaller aerosol particles that can remain suspended and travel further (World Heart Federation 2021). Another person can be infected if these particles reach their mouth or nose, directly or via hands. Transmission via surface contact is also important in some cases. The ease of transmission has raised concerns that the risk of contracting COVID-19 in an enclosed space, such as an aircraft cabin.

One study by Zee et al. (2021) analysed the transport of particles from a coughing individual in a Boeing 737 aircraft cabin. Computational fluid dynamic simulations using Ansys Fluent, were used to illustrate the particle pathways. The aircraft cabin environment was compared with an indoor commercial space. It was shown that particles were removed from the cabin environment by the air outlets as well as by particles depositing onto surfaces. The study showed that most of the particles were deposited within 30 seconds of release within the aircraft cabin. The study showed that the flow rate within

the aircraft cabin affect the rate of deposition. Supply flow rates were between 9.15 m^3/min and 16.65 m^3/min. At higher flow rates particles were rapidly removed as can be seen in Figure 26.

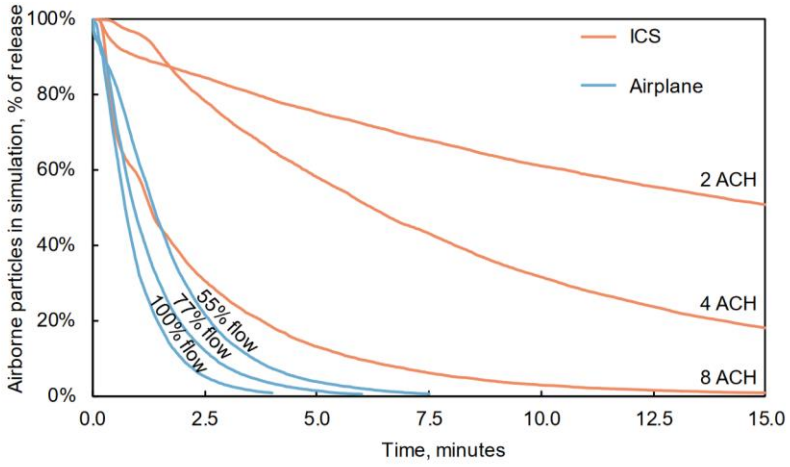

Figure 26: Decay of total expiratory particles vs time after initial release at 2, 4 and 8 air exchanges per hour (ACH) in the indoor commercial space (ICS) compared to 100%. 77% and 55% supply air flow in the aircraft cabin (Davis 2021)

The study showed that supply airflow rate had a large effect on the rate of particle removal. Indicating that with a 100% flow rate of 95% of the particles were removed from circulation within 2.5 minutes. With a 55% flow rate it took 4.6 minutes to reach 95% removal of particles. Figure 27 shows the velocity vectors at maximum flow rates. The air is introduced through nozzles located near the overhead storage cabins. The highest flow rates are shown in red. It can be seen that as the air enters the cabin it is at its highest velocities.

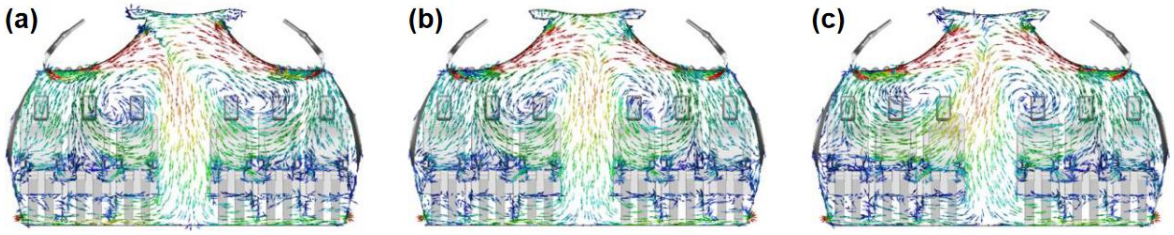

Figure 27: Maximum flow rate at a) 0 seconds, b) 90 seconds c) 120 seconds, high velocities are indicated with the red arrows.

It has been shown that droplet size plays a vital role in the transportation of particles within an aircraft cabin environment. Yan et al. (2021) studied a range of particle sizes (4 – 200μm) determining the horizontal and vertical velocities. Figure 28 illustrates the horizontal and vertical transportation of the particles. The positive horizontal velocity represented particles traveling to the right-hand side, whereas negative velocity means traveling in the opposite direction. Also, a positive vertical velocity indicated the particle was ascending, and the converse meant descending. The figure illustrates the larger particles (100 μm) fell to the floor quickly whereas smaller particles travelled horizontally but did not fluctuate vertically and remained suspended for some time. These particles could then be inhaled much more readily.

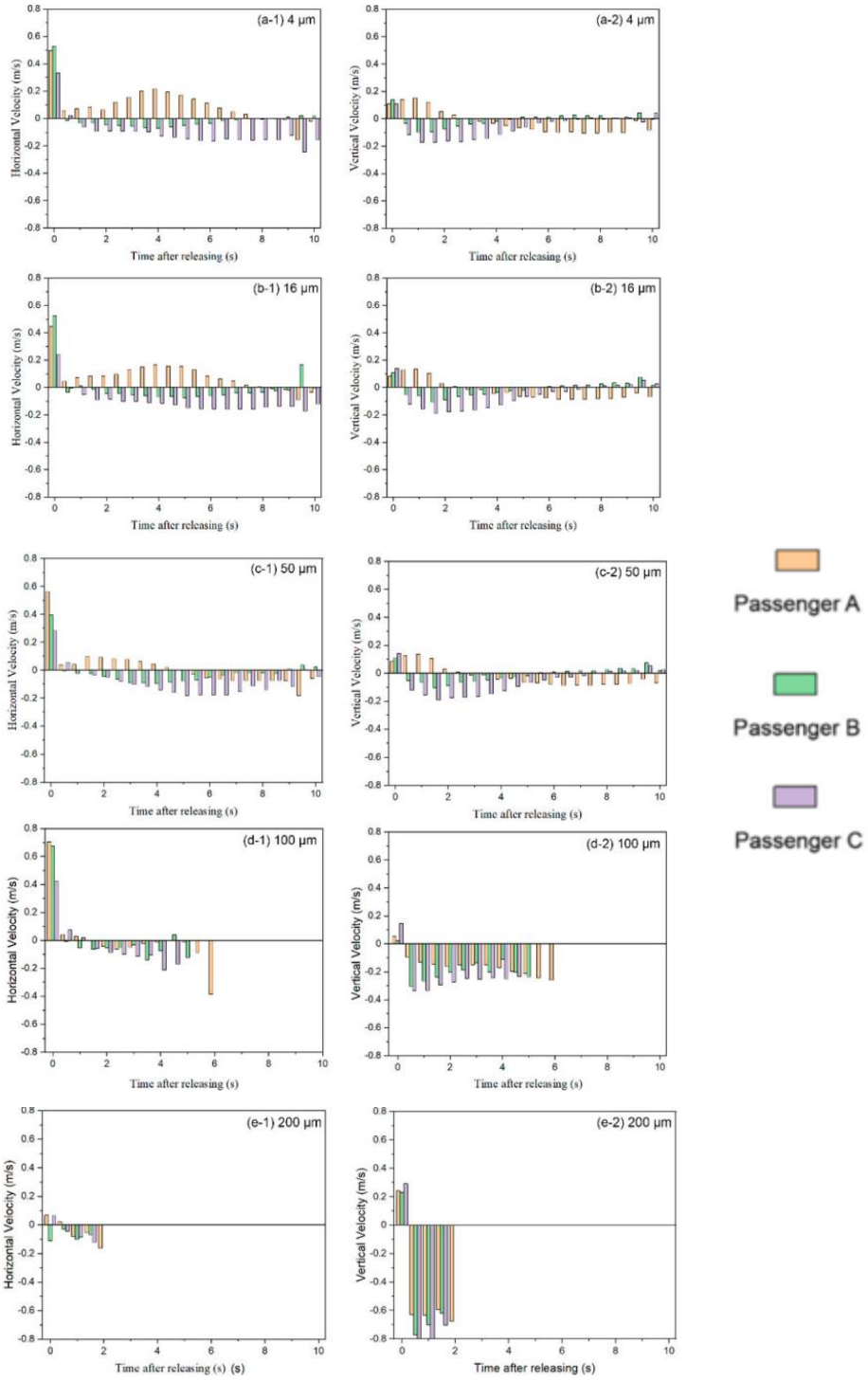

Figure 28: Horizontal velocities (left figures) and vertical velocities (right figures) for time-dependent particles for five sizes (4 μm, 16 μm, 50 μm, 100 and 200 μm)(Yan, 2021)

3.19 Particle Deposition

It is important to understand how particles move and deposit on surfaces within an aircraft cabin to determine the exposure to the occupants. Several studies have looked at release of noxious material or biological pathogens as well as ventilation within an aircraft cabin using simulation software to determine the deposition rates or flow patterns (Aboosaidi et al., Gao et al., Pan et al., Sing et al., Talaat et al. and Zhang et al.). Wang et al. (2011) simulated the deposition of particles within a mock-up of an aircraft cabin using ANYSYS FLUENT software. The mock-up was a four-row twin aisle seating arrangement, with 28 seats. The air flow rate was 0.23 m^3/s. Three particle diameters of 0.7, 10 and 100 µm were studied. Particle release was either slow (representing occupants breathing) or faster (representing occupants coughing). This study found that the distribution of particle deposition onto surfaces depended on particle size and particle velocity. At the higher release velocity, particle velocity increased by 14% for the 0.7 and 10 µm. The larger particles size all particles were deposited at both release velocities (Wang et al. 2011). Zhang et al. (2013) used ANSYS/CFX to model contaminant (SARS) distribution within an Airbus 320 aircraft cabin. Inlet air velocity was 2.6 m/s. Figure 29 shows the flow field of the contaminant within this simulation.

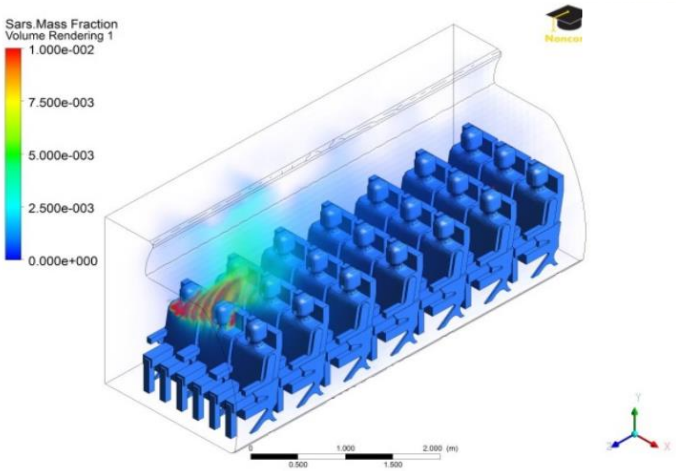

Figure 29: Contamination flow field from front row occupant (Zhang et al., 2013)

Particles may differ is size, shape and composition. Size is the most important factor which influences the particle transport (Tsuda 2013). Shape will affect the particles

aerodynamic and diffusive nature. Density is an intensive property of the particle, therefore the density of the particle will remain the same, density will affect the deposition of particles (Tsuda 2013).

3.20 Regulations and Authorising Bodies

Aircraft design is generally considered to be one of the safest forms of transport in the world. Aircraft design, maintenance, repair and operation are all governed by strict standards and regulations. There are a number of governing bodies which enforced these standards and regulations across the world. Within the United Kingdom this is performed by the Civil Aviation Authority (CAA), in Europe this is the European Aviation Safety Authority (EASA), in the United States it is the Federal Aviation Administration (FAA). The International Civil Aviation Organization (ICAO) was established in 1944 to manage the administration and governance of the Convention on International Civil Aviation (known as the Chicago Convention), which was established to promote cooperation, this agreement was set up by 54 nations, setting the minimum level of safety performance of civil aviation in a State, expressed in terms of safety targets; and safety performance indicators. The level of safety within the aviation sector for each state is defined by the Acceptance Level of Safety Performance (ALoSP). The UK was one of the 54 states, it has its own version of the AloSP. This outlines:

“No accidents involving commercial air transport that result in serious injuries or fatalities. No serious injuries or fatalities to third parties as a result of aviation activities”.

The UK aims to achieve this AloSP through State safety objectives that:

- Protect people from aviation safety risks.
- Reinforce the UK position as a global leader in aviation safety.
- Positively influence aviation safety through collaboration working with our international partners.

Chapter 4 Experimental investigation

This research endeavours to understand if it is possible for organophosphates from engine oil to contaminate the air within aircraft cabins and if there are organophosphates present are, they insufficient quantities to pose a risk to health of the aircraft occupants. However, it is not possible to “cause” a fume event within an actual aircraft as this could have severe consequences therefore understanding of the thermal decomposition and the deposition patterns and rates is required in order to successfully predict the potential hazards within the aircraft cabin. An understanding of the thermal decomposition and flow patterns within the aircraft is needed.

The main tools for such analysis used in this work are gas chromatography (GC) coupled with mass spectrophotometry (MS) to determine the thermal decomposition products of pure tri-cresyl phosphate and Mobile Jet II oil, computer modelling to analyse the air flows within the aircraft and then to determine the possible deposition rates of potentially hazardous particles, to mathematically determine the potential hazards of chemicals over a period of time.

4.1 Introduction to Gas Chromatography / Mass Spectrophotometry (GC-MS)

GC is an analytical technique which separates compounds within a mixture, indicating the presence or absence of specific chemical components and how much is present. MS is an analytical technique that ionises chemical species and sorts them based on their mass to charge ratio, therefore determining the molecular weight and elemental composition (Turner 2022). These two methods can be combined to provide a more detailed analysis of a chemical sample. The sample is initially separated by the GC before being transferred to the MS for detection. The instrument consists of three main components as shown in Figure 30.

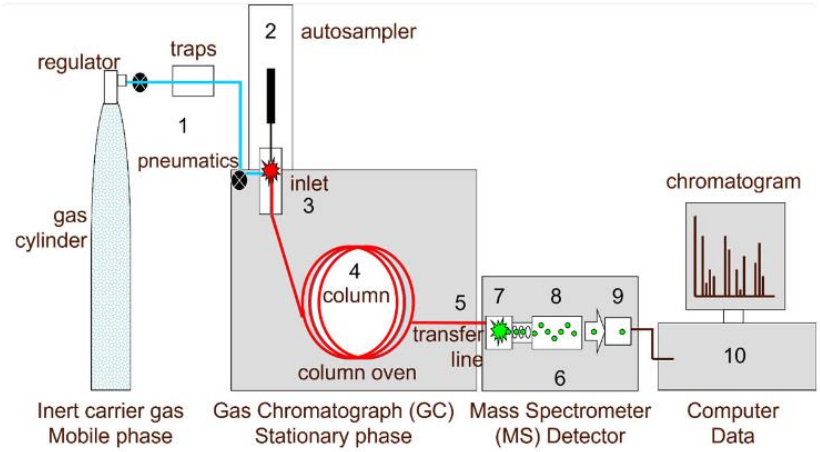

Figure 30: A simplified diagram of a gas chromatograph–mass spectrometer showing (1) carrier gas, (2) autosampler, (3) inlet, (4) analytical column, (5) interface, (6) vacuum, (7) ion source, (8) mass analyser, (9) ion detector and (10) PC (Turner 2022)

A liquid sample is initially introduced into the GC component of the instrument either manually or by the use of an autosampler. The sample is heat to about 300°C and vapourised in the heat at the GC inlet and the sample vapour is transferred to the analytical column. The sample is not thermally decomposed. As with all chromatography techniques a mobile and stationary phase are required. The mobile phase is usually an inert gas (helium). The stationary phase consists of a silica packed capillary column. The inert mobile phase is flowing through the machine, this picks up the vaporised sample and carries it to the capillary column. The sample passes through the column and injected into a detector at the other end. The detector records the amount of sample hitting it. The information from the detector allows a graph to be produced which shows the amount of sample reaching the detector and at what time – this is called a chromatograph – Figure 31. A gas chromatograph consists of a base line and a number of peaks.

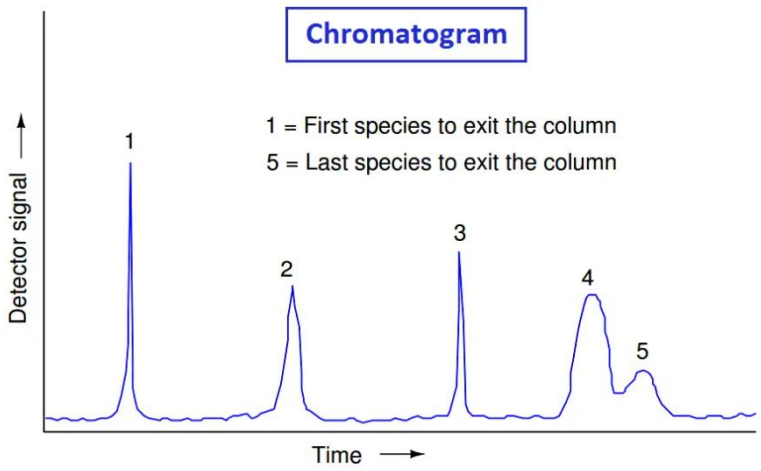

Figure 31: Chromatograph chart – showing peak start and end markers

If the molecules are bunched together, the chart will present narrow peaks, as all the molecules are exiting the column at nearly the same time. Wide peaks represent more diffuse groupings of similar (or identical) molecules. Once the sample is separated its components leave the GC part of the machine one at a time and are sent to the mass spectrophotometer. Here they are ionised and accelerated through the mass analyser. The components are separated into the different mass-to-charge ratios (m/z) (Tuner 2022). The result from the MS is a graph of mass per charge against relative abundance – Figure 32 (Fox 1994).

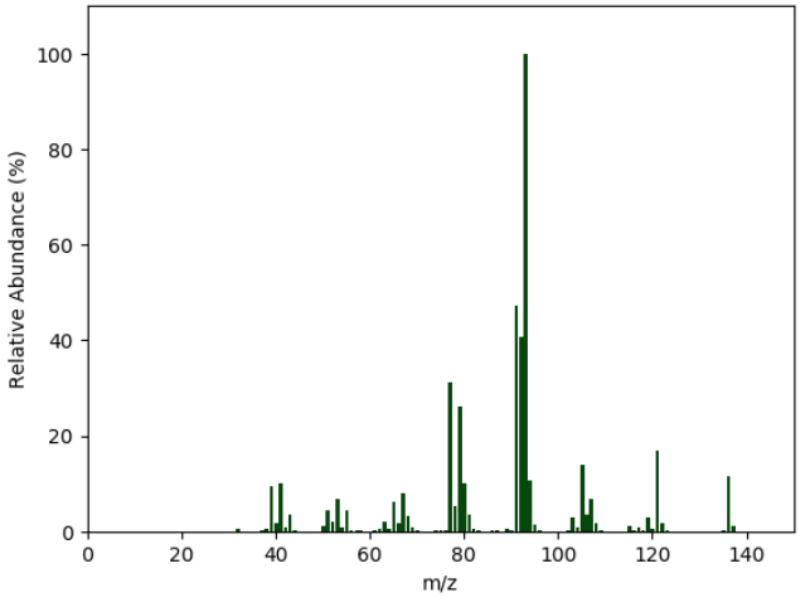

Figure 32: Example of a mass spectrum (Fox 1994)

The smaller more positively charged fragment ions will be detected first. Each fragment corresponds to a peak with a particular m/z value in the mass spectrum (Figure 32). The heights of the peaks in the mass spectrum show the proportion of each isotope present (Fox 1994). The most intense ion is assigned an abundance of 100, and it is referred to as the base peak. Most of the ions formed in a mass spectrometer have a single charge, so the m/z value is equivalent to mass itself.

4.2 Analytical studies of hydraulic fluids

Oil analysis by GC has been significantly important in the last 50 years. Powerful separation techniques can determine the purity and therefore any contaminants within oil samples (Blomberg et al. 2002). GC analysis has been used extensively to analyse complex organic mixtures and has been found to be particularly useful when determining low levels of contaminants in complex organic materials is required (Hiltz and Haggett 1991). Jet engine oils contain several different compounds including synthetic esters, (pentaerythritol and dipentaerythritol), TCP, phenyl-alpha-naphthylamine, Benzamine as

well as some unknown substances and impurities (Sholz 2017). Material safety data sheets provided by manufacturers do not include elemental analysis of their products or provide a complete breakdown of the additives (van Netten 1999). Jet engine oils have been analysed using different methods in trying to identify their components. van Netten (1999) analysed hydraulic fluids and jet engine lubricating oils using inductively coupled plasma mass spectrometry (ICPMS). The samples were analysed for several elements which were found to be present in concentrations below the various limits of detection (van Netten 1999). The data is presented in Table 14 illustrates the mixture of compounds which can be found in hydraulic fluids and lubricating oils.

Table 14: Elemental concentrations found in hydraulic fluids and lubricating oils

Element	**Hydraulic Fluids**		**Jet engine lubricating oils**		
	Skydrol	**HyJet**	**Exxon**	**Castrol**	**Mobil**
Boron	<5000	5000	<5000	<5000	<5000
Sodium	3000	4000	<3000	<3000	3000
Magnesium	900	1900	1500	500	1100
Aluminium	1100	1200	1400	1000	1000
Silicon	56 000	58 000	54 000	63 000	64 000
Phosphorous %	11.1	11.3	0.23	0.28	0.29
Potassium	22 000	38 000	<5000	<5000	<5000
Calcium	<10 000	110 000	<10 000	<10 000	<10 000
Titanium	20	60	100	110	<10
Vanadium	600	700	700	800	9000
Chromium	2190	900	3360	2230	115 000
Manganese	300	<100	200	<100	2200
Cobalt	50	30	50	20	520
Zinc	13 900	12 300	14 300	10 900	5400
Rubidium	<3	4	<3	<3	<3
Strontium	12	58	14	10	13
Yttrium	3	4	<3	<3	<3
Cadmium	<2	<2	<2	<2	7
Antimony	<5	5	<5	<5	15
Barium	7	390	5	9	10
Tungsten	<5	<5	<5	<5	57
***All concentrations are in ppb except where otherwise stated**					

van Netten (1999) found that none of the elements identified in Table 14 related to the symptoms that passengers and flight crew were reporting. van Netten (1999) concluded that the hydraulic fluids contained higher levels of phosphorous than the lubricating oils. hydraulic fluids can contain high levels of tributyl phosphates (79%) and mixtures of phenyl dibutyl phosphates, diphenyl butyl phosphates and tricresyl phosphates. Lubricant engine oils are allowed to contain 3% cresyl phosphates of which only 0.1% can be the neurotoxic ortho isomer. In hydraulic fluids this isomer can be as high as 1% (van Netten 1999).

When fluids are exposed to high temperatures within the engines, a mixture of thermally degraded components will be produced. EASA (2015) conducted a study to determine the toxicity of the aviation turbine engine oils after pyrolysis. The study analysed three oils under a variety of conditions and were characterized using two-dimensional gas chromatography coupled with time-of-flight mass spectrometry (GCxGC-ToF-MS). During a flight the turbine oil undergoes a series of temperature changes caused by changes in engine power. A basic temperature pattern is shown in Figure 33. During the study, the oil samples were heated following the temperature outlined in Figure 33.

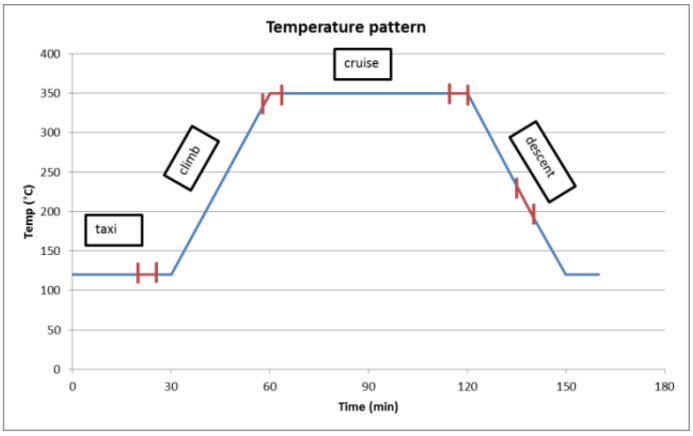

Figure 33: Schematic overview of a typical engine temperature profile for a flight duration of approximately 90 minutes (EASA 2015)

The study (EASA 2015) found 21 compounds were identified in the new oil that were not present in the chromatograms of used oil, whilst 30 compounds were found in the used

oil that were not in the new oil. The 10 compounds with the highest similarities are shown in Table 15 below. The oils analysed contain TCP, however no tri-ortho cresyl phosphate isomers could be detected.

Table 15: Compound found in new and old oil samples

Name	Present in new oil	Present in old oil	Compounds present in all oils
Cyclopropane, ethyl	X	-	
trans-3-Decene	X	-	
Decane	X	-	
3-Undecene, (Z)-	X	-	
Heptane, 3-ethyl-	X	-	
Isopropyl Myristate	X	-	
Decane, 3,6-dimethyl-	X	-	
Ethanone, 1,2-diphenyl-	X	-	
Cyclopropane, 1,1,2,2-tetramethyl-	X	-	
Homomenthyl salicylate	X	-	
2-Ethylacrolein	-	X	
2-Hexanone	-	X	
2-Heptanone	-	X	
Cycloprop[a]indene,1,1a,6,6a-tetrahydro- tetrahydro-	-	X	
Pentadecane	-	X	
3-Tetradecene, (Z)-	-	X	
2-Butanone	-	X	
Benzonitrile	-	X	
Tetradecane	-	X	
Pentadecane, 2,6,10-trimethyl-	-	X	
Acetic acid	X	X	X
Benzene	X	X	X
Benzonitrile	X	X	X
Decane	X	X	X
Heptane	X	X	X
Isobutane	X	X	X
Pentane	X	X	X
Pentanoic acid, methyl ester	X	X	X
Phenol	X	X	X
TCP isomer	X	X	X

Solbu et al. (2007), studied personal occupational exposure assessment of airborne trialkyl and triaryl organophosphates originating from hydraulic fluids by active combined aerosol and vapor sampling. Determination of the organophosphates was performed by gas chromatography–mass spectrometry. Solbu et al. (2007) experimental set up included an oil aerosol generator coupled to an exposure chamber. Sampled air from oil aerosol atmospheres, showed after subtracting the background from the alkyl phosphates, recovery of TiBP, TnBP and TmCP for all concentration levels in mineral oil aerosol was 99 ± 7%, 93 ± 9% and 106 ± 5% (n = 4), respectively, and in synthetic oil aerosol 105 ± 23%, 96 ± 18% and 96 ± 6% (n = 4), respectively. The organophosphate sampler was then used for determination of exposure of aviation workers within a workshop area to airborne organophosphates (Solbu et al. 2007). Figure 34 shows the GC-MS chromatogram of one of the samples taken from the workshop area.

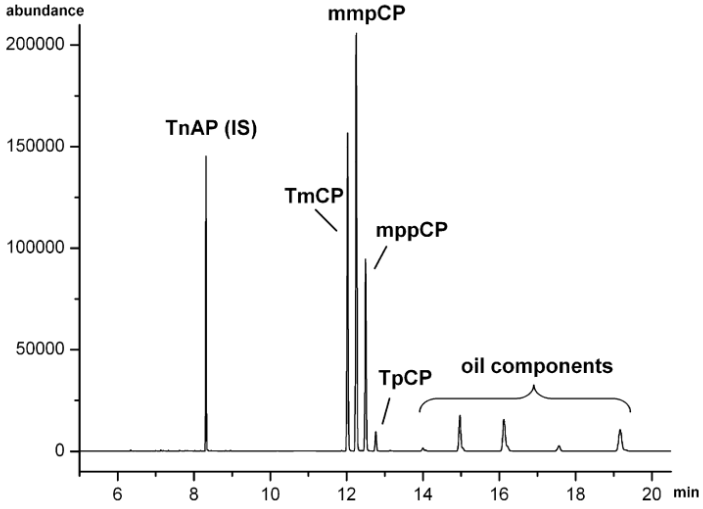

Figure 34: GC-MS chromatogram of air sample exposed to aerosols from engine oil (Solbu 2007)

Figure 34 shows the presence TCP isomer tri-m-cresyl phosphate (TmCP) tri-*p*-cresyl phosphate (TpCP).

Spila et al. (1999) used two methods to analyse jet oils to determine the presence of organophosphate compounds, both methods were based on GC techniques, one included MS detector and the second included a flame photometric detector. Standard

solutions were used. The study determined that both methods were suitable for determining organophosphate compounds in complex mixtures such as hydraulic fluids and engine fuels.

Solbu et al. (2011) applied different sampling methods to obtain samples from different aircraft, these included collection of the high-efficiency particulate air filters and surface wipes. These were then analysed using GC to determine the presence of organophosphates.

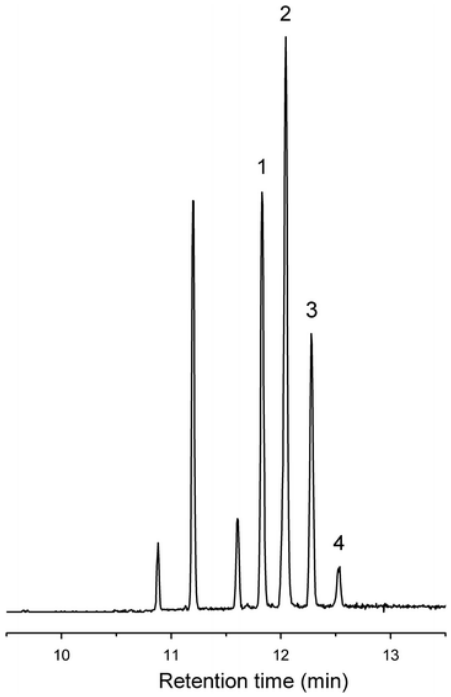

Figure 35: Chromatographic profile (extracted ion chromatogram, m/z 368) from analysis (Solbu et al. 2011)

Figure 35 shows the chromatographic profile obtained by Solbu et al. (2011). TCP was identified. The TCP peaks shown in the chromatogram are: (1) *m*-TCP, (2) *mmp*-TCP, (3) *mpp*-TCP and (4) *p*-TCP. The three peaks to the left were also due to compounds with *m*/*z* 368 in the mass fragment pattern, but from the mass spectra and analysis in SIM mode were confirmed not to origin from TCP isomers.

Table 16 shows a number of studies investigating the analysis of organophosphate compounds using GC-MS.

Table 16: Studies investigating analysis of organophosphate compounds using GC-MS

Reference	Title	Short description	Predictions
Crump et al. (2011)	Aircraft Cabin Air Sampling Study	Analyse cabin air for volatile organic compounds semi-volatile organic compounds, particles and carbon monoxide in normal operations during all phases of flight and to detect and characterise any anomalous elevations of target compounds and particle concentrations during any fume events or events in which unusual smells or similar occurrences were reported.	Samples specifically taken during recorded air quality events did not have notably elevated concentrations of any of the individually measured pollutants.
Denola et al. (2011)	Determination of tricresyl phosphate air contamination in aircraft	Analysis of air samples from 46 different aircraft (commercial and military) to determine the concentration of TCP.	Highest total TCP concentration was 51.3 µg m(-3), while most were generally found to be <5 µg m(-3) compared with the 8-h time-weighted average exposure limit of 100 µg m(-3) for tri-o-cresyl phosphate.
Solbu (2011)	Organophosphates in aircraft cabin and cockpit air—method development and measurements of contaminants	Analysis of different methods for determining organophosphate contamination, analysed by GC.	TCP was detected in sufficient quantities.
Spila et al. (1999)	Determination of organophosphate contaminants in jet fuel	Two methods based on GC analysis were used to determine organophosphate compounds in jet fuels. One included MS detector and the second included a flame photometric detector. The study determined that both methods were suitable for determining organophosphate compounds in complex mixtures such as hydraulic fluids and engine fuels.	Both methods detected organophosphate compounds effectively
Tiffany et al. (2015)	Analysis of organophosphate flame retardants and plasticisers in water by isotope dilution gas chromatography–electron ionisation tandem mass spectrometry	A rapid and reliable analytical method was developed for the analysis of five organophosphate flame retardant in water using gas chromatography tandem mass spectrometry (GC–MS/MS) with electron ionisation (EI) and a run time of 13 min.	Validation of this method confirmed satisfactory method stability with less than 1% coefficients of variation, verifying that this approach produced good reproducibility.
van Netten C (1999)	Multi-elemental analysis of jet engine lubricating oils and hydraulic fluids and their implication in aircraft air quality incidents	Analysing different hydraulic fluids and lubricating oils for a number of different elements	Levels of phosphorous were detected but not in excessive levels.

These studies have shown that the instrumental combination of GC with MS detection offers sensitive single-ion-monitoring of the organophosphates of interest, providing supporting evidence that this is a suitable technique to be used in this research.

4.3 GC-MS analysis

To determine if engine jet oil and pyrolysed samples of engine jet oil contained isomers of TCP, GC-MS analysis was conducted. GC–MS measurements were conducted by use of a PerkinElmer Clarus 600 Mass Spectrometer (MS) is a detector that is interfaced to the Clarus 600 Gas Chromatograph (GC) with a mass range of 1.0-1200 g/mol. The mass stability is ±0.1 m/z mass accuracy over 48 hours. The scan rate was up to 12, 500 amu/sec. The detector was a sealed long-life photomultiplier, with a quadrupole with prefilter analyser. The system can accommodate flow rates up to 5 mL/min. The entire system is controlled through the PerkinElmer TurboMass GC-MS software. Samples of technical grade tricresyl phosphate (TCP) and Mobile Jet II oil were analysed. Identification of compounds and chemical structures of the products is supported using the Xcalibur analysis software (Xcalibur 2007) and the NIST library (Stein et al. 2005). 1ml of TCP or its burnt sample was dissolved into 10 ml ethanol 5 µl of solution was then injected into PerkinElmer TurboMass GC-MS system, with injector temperature at 280 °C. The GC Column was PerkinElmer PE-5 30 meter by 0.25 mm x 0.25 µm film thickness. This column was a general-purpose column low polarity phase, commonly used for the analysis of drugs, pesticides, hydrocarbons, PCBs, essential oils, semi-volatiles and solvent impurities (Perkin Elmer 2023). 99.9999% helium was used as carrier gas at a flow rate of 1.5 mL/min. The GC oven temperature was initially held at 90 °C for 1 min, then heated at 20°C/min to 150°C and held for 1 min; finally heated at 10 °C/min to 300°C and held for 10 min. The GC incorporated a flame ionization detector with a sensitivity of >0.015 coulombs/g C. The GC calibration sequence was followed, the oven was calibrated. The GC oven was calibrated using a platinum resistance thermometer with 0.01 °C readout and a probe inserted into the GC oven. Background compensation was applied by running a calibrated blank sample which did not contain any analytes of interest within a detectable level, using the temperature program. Calibration run time was greater than 2 minutes. Mass Spectra were recorded under EI

positive mode with an ionization energy of 70 eV. The mass detector was scanned from m/z 35 to 550. The spectrum was analysed to match the NIST library (Stein et al. 2005). Technical grade TCP, vapour from pyrolyzed TCP, jet oil and a vapour from pyrolyzed jet oil samples were analysed. These were analysed in duplicate (eight tests in total). Table 17 shows the information on the test.

Table 17: Summary of parameters for the GC-MS tests

Parameters			
Case	**Material**	**Injection volume**	**Flow rate**
GC-MStest 1 & 2	Technical grade TCP	5µl	1.5 mL/min
GC-MStest 3 & 4	Vapour from pyrolyzed TCP	5µl	1.5 mL/min
GC-MStest 5 & 6	Jet oil	5µl	1.5 mL/min
GC-MStest 7 & 8	Vapour from Pyrolyzed Jet Oil	5µl	1.5 mL/min

Duplicate samples gave the same results so only 1 of each test is illustrated in the results in the following sections.

4.3.1 Test case 1

Test case 1 analysed technical grade TCP, from Sigma Aldrich, this contains a mixture of isomers. The sample was tested as per the parameters outlined in Section 4.3. The chromatogram obtained is shown in Figure 36. The retention time for TCP was a total of 25 minutes. As can be seen on Figure 36, there are three large peaks detected during the chromatographical analysis. The retention time of the three large peaks was 18.07 min, 18.74 min and 19.41 min. There are two smaller peaks at 5.38 min and 20.14 min. Each of these peaks was then analysed and identified.

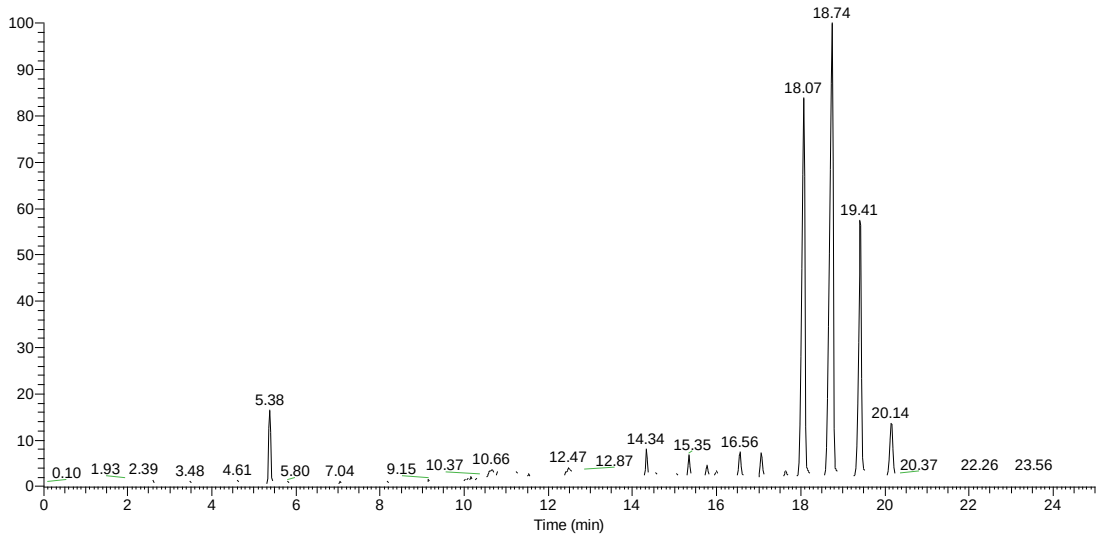

Figure 36: Chromatogram of TCP indicating main peaks at 18.07, 18.74, 19.41 and 20.14 minutes

The spectral analysis of the peak retained at 18.07 min is shown in Figure 37. The most abundant ion has a m/z of 367.96. Using Xcalibur Qual Browser library this spectrum was identified as Phosphonic acid, tris (3-methylphenyl) ester (phosphonic acid, tri-m-tolyl ester).

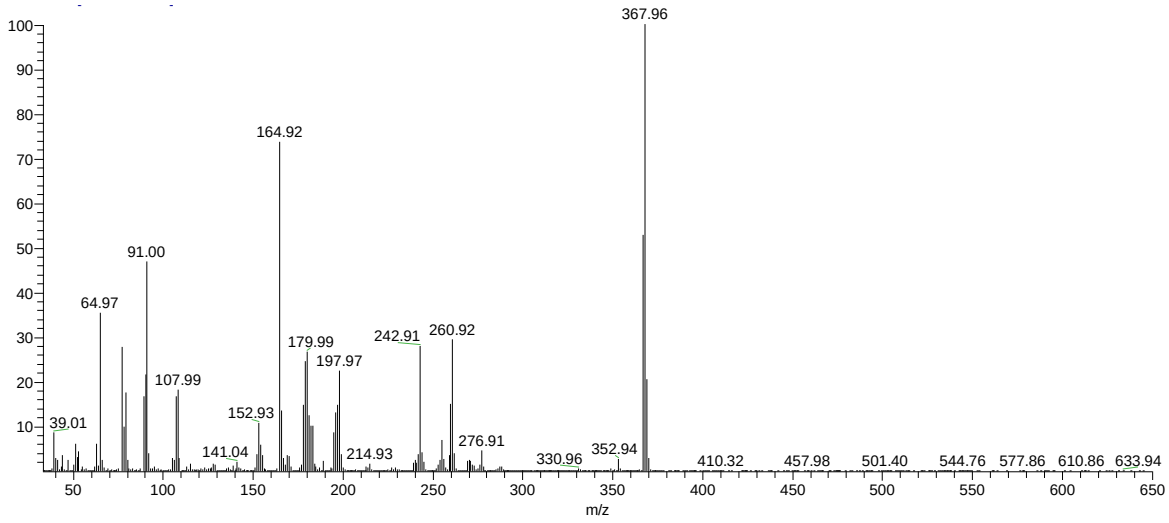

Figure 37: Spectral analysis of peak at 18.07 min on TCP Chromatograph

The spectral analysis of the peak retained at 18.74 min is shown in Figure 38. The most abundant ion has a m/z of 367.95, this spectrum was identified as using Xcalibur Qual Browser library this as Phosphonic acid, tris (3-methylphenyl) ester (phosphonic acid, tri-m-tolyl ester).

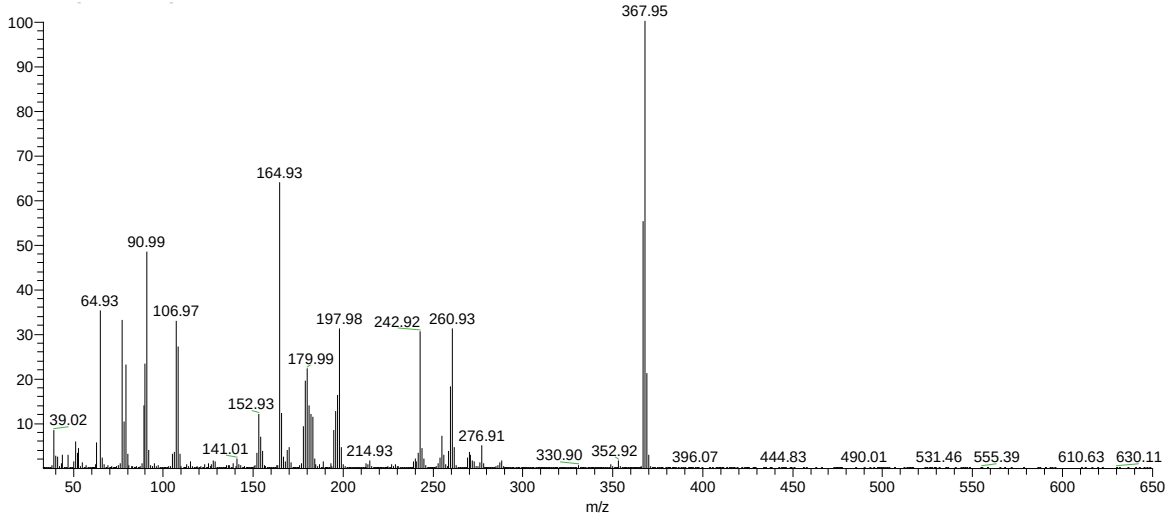

Figure 38: Spectral analysis of peak at 18.74 min on TCP Chromatograph

The spectral analysis of the peak retained at 19.41 min is shown in Figure 39. The most abundant ion has a m/z of 367.97., Using the Xcalibur Qual Browser library software this spectrum was identified as Phosphonic acid, tris (4-methylphenyl) ester (phosphonic acid, tri-p-tolyl ester).

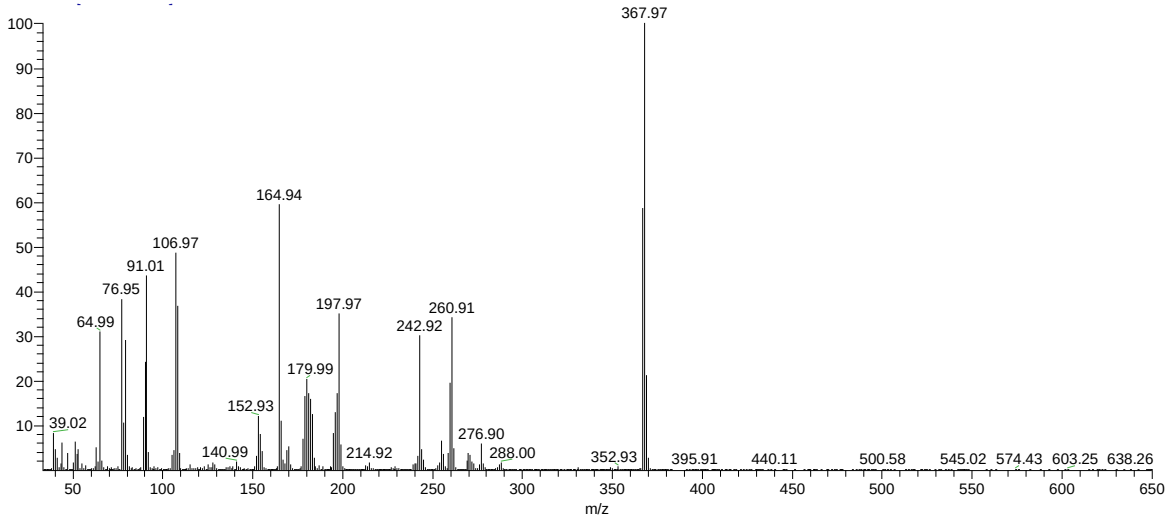

Figure 39: Spectral analysis of peak at 19.41 min on TCP Chromatograph

The spectral analysis of the peak retained at 5.38 min is shown in Figure 40. The most abundant ion has a m/z of 106.97, this was identified using Xcalibur Qual Browser library this as Phenol, 4methyl p-Cresol.

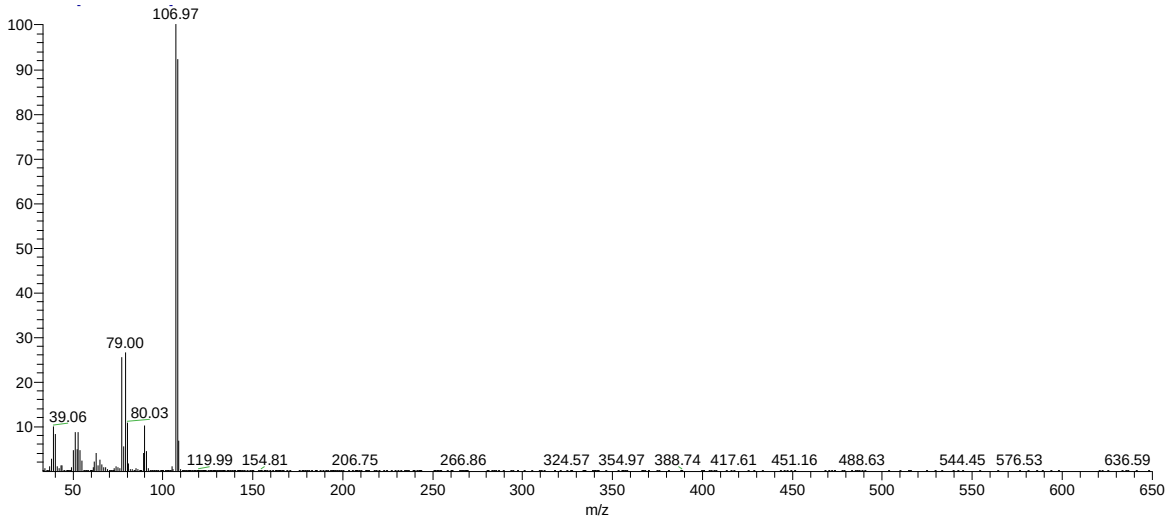

Figure 40: Spectral analysis of peak at 5.38 min on TCP Chromatograph

The spectral analysis of the peak retained at 20.14 min is shown in Figure 41. The most abundant ion has a m/z of 367.97, this was identified as using Xcalibur Qual Browser library as Phosphonic acid, tris (4-methylphenyl) ester (phosphonic acid, tri-p-tolyl ester).

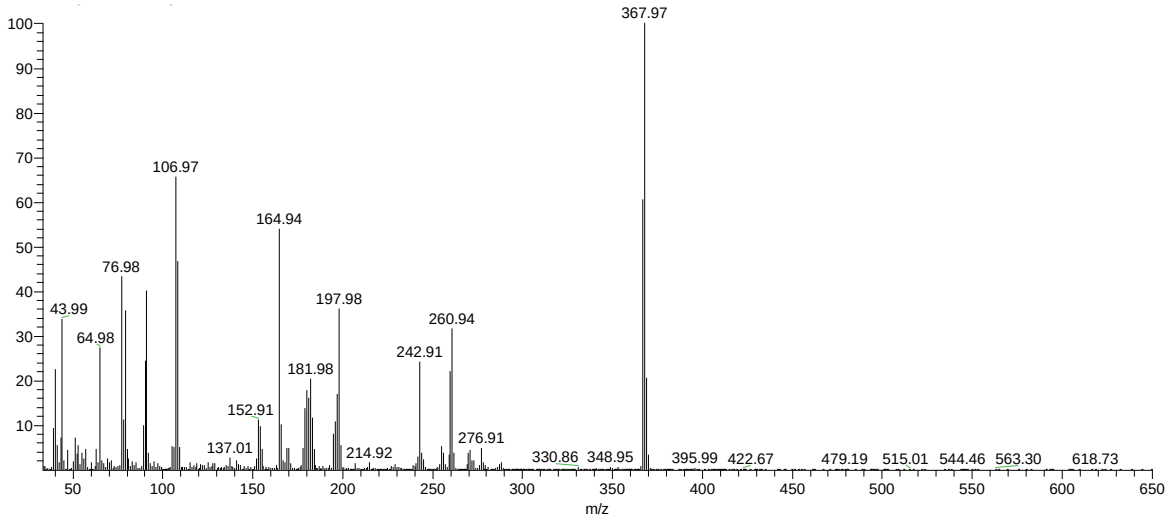

Figure 41: Spectral analysis of peak at 20.14 min on TCP Chromatograph

A further analysis of the peak at 18.74 min, the highest abundant ion observed, with the NIST library. The NIST library confirmed the identification of the sample as Phosphonic

acid, tris (3-methylphenyl) ester (TCP). The comparison of the spectra of peak form sample tested with the library spectra can be seen in Figure 42. The red peaks in Figure 42 represent the tested sample and the blue peaks represent the standard sample of TCP, there is good correlation between the m/z of the red peaks and those of the standard blue peaks, confirming that the sample tested was TCP.

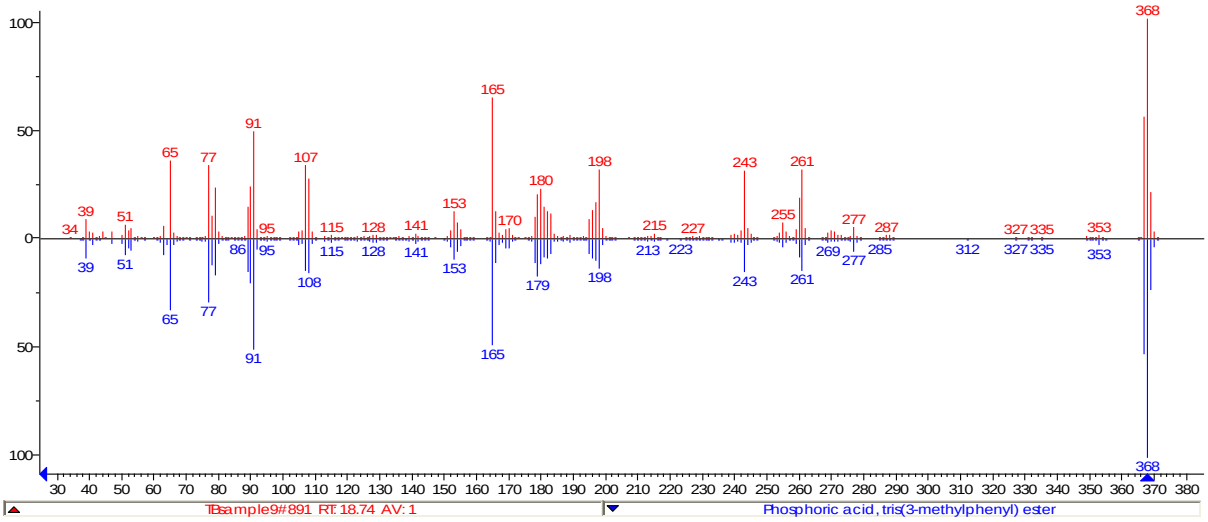

Figure 42: Comparison of m/z profiles of standard TCP data (blue data lines)and test sample (peak 18.74 min) (red data lines)

4.3.2 Test case 2

Test case 2 analysis of the vapours from heated technical grade TCP, from Sigma Aldrich, this contains a mixture of isomers, this sample was heated to 500 ˚C prior to being tested as per the parameters outlined in Section 4.3. The chromatogram obtained is shown in Figure 43. The retention time for TCP was a total of 21 minutes. As can be seen on Figure 43, there are three large peaks detected during the chromatographical analysis. The retention time of the three large peaks was 16.02 min, 16.58 min and 17.05 min. With smaller peaks at 4.86 min, 13.05 min, 13.81 min, 14.72 min, 17.48 min. Each of these peaks was then analysed and identified.

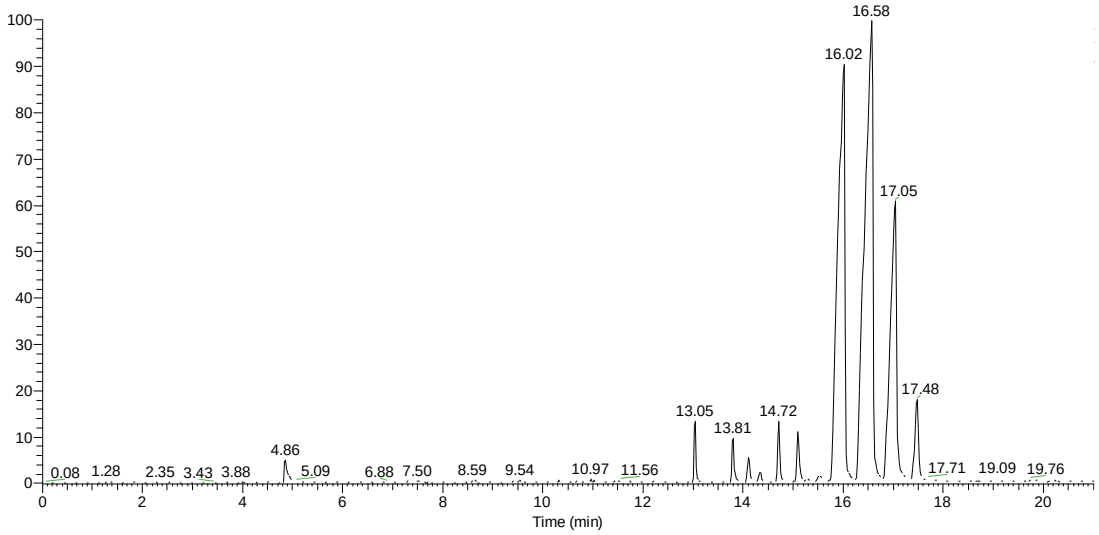

Figure 43: Chromatogram of the vapour of heat TCP indicating main peaks at 16.02, 16.58, 17.05 and 17.48 minutes

The spectral analysis of the peak retained at 16.02 min is shown in Figure 44. The most abundant ion has a m/z of 368.12. Using Xcalibur Qual Browser library this spectrum was identified as Phosphonic acid, tris (3 methylphenyl) ester (phosphonic acid, tri-m-tolyl ester).

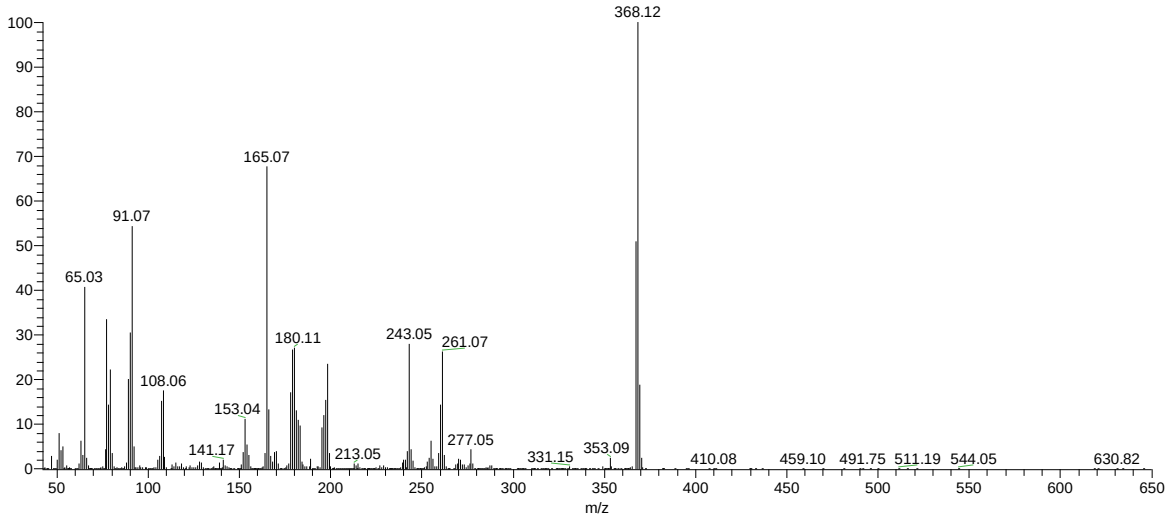

Figure 44: Spectral analysis of peak at 16.02 min on TCP vapour Chromatograph

The spectral analysis of the peak retained at 16.58 min is shown in Figure 45. The most abundant ion has a m/z of 368.11. Using Xcalibur Qual Browser library this spectrum was identified as Phosphonic acid, tris (3 methylphenyl) ester (phosphonic acid, tri-m-tolyl ester).

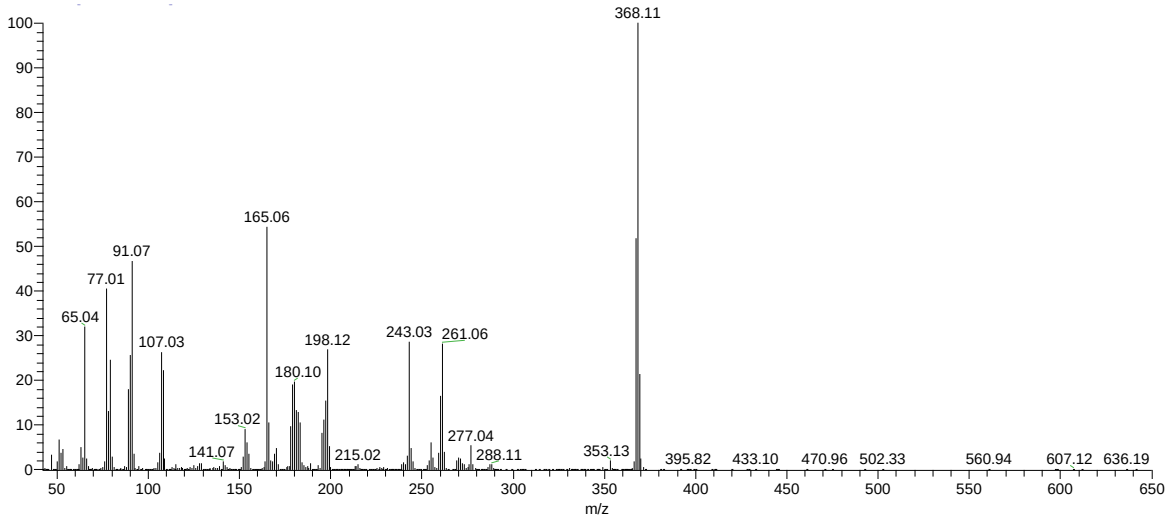

Figure 45: Spectral analysis of peak at 16.58 min on TCP vapour Chromatograph

The spectral analysis of the peak retained at 17.05 min is shown in Figure 46. The most abundant ion has a m/z of 368.14. Using Xcalibur Qual Browser library this spectrum, was identified as Phosphonic acid, tris (4 methylphenyl) ester (phosphonic acid, tri-p-tolyl ester).

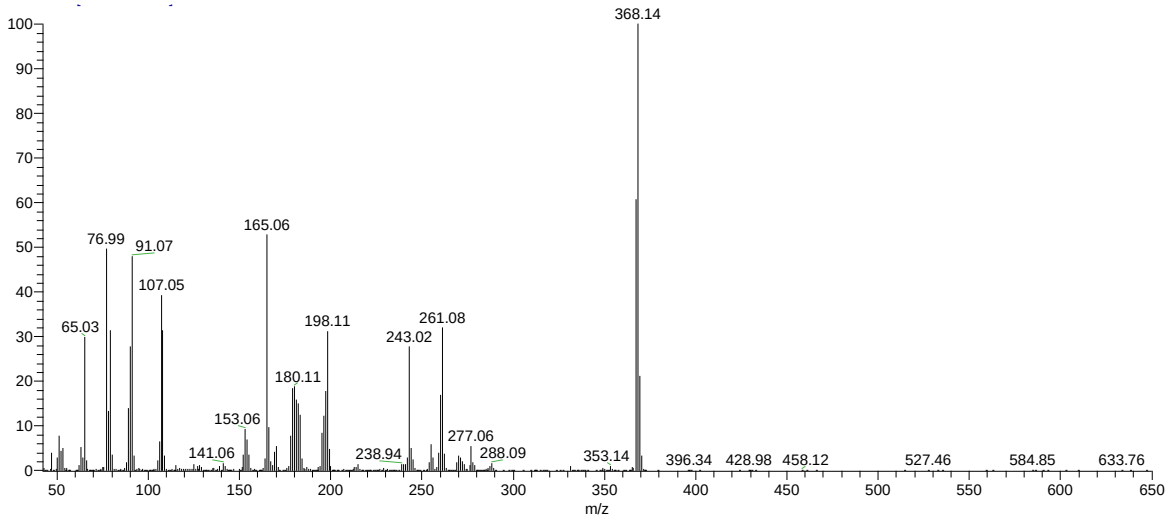

Figure 46: Spectral analysis of peak at 17.05 min on TCP vapour Chromatograph

The spectral analysis of the peak retained at 4.86 min is shown in Figure 47. The most abundant ion has a m/z of 107.04. Using Xcalibur Qual Browser library this spectrum was identified using the Qualbrowser phenol, 3-methyl m-Cresol.

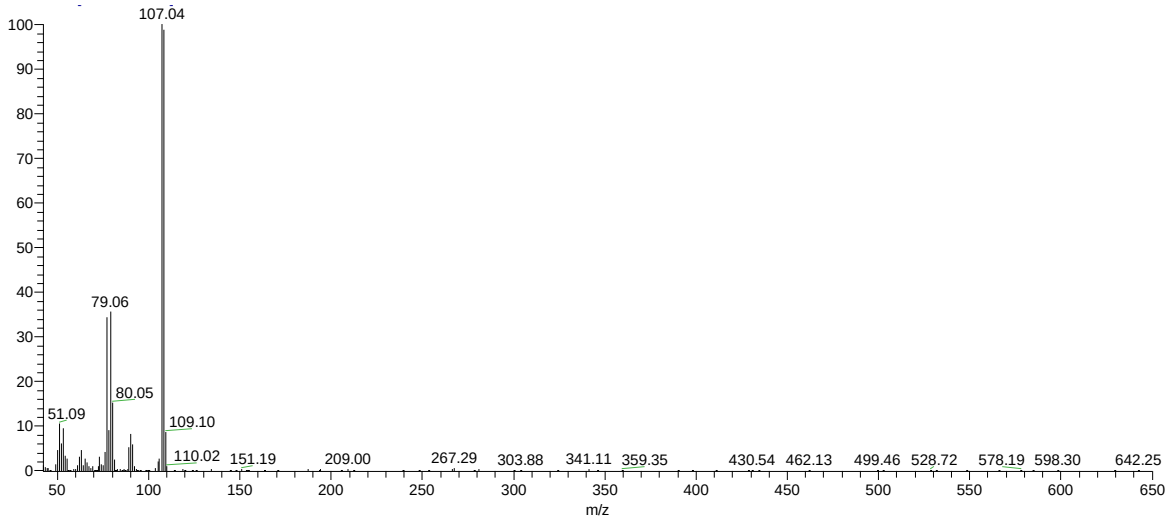

Figure 47: Spectral analysis of peak at 4.86 min on TCP vapour Chromatograph

The spectral analysis of the peak retained at 13.05 min is shown in Figure 48. The most abundant ion has a m/z of 326.06. Using Xcalibur Qual Browser library this spectrum was identified as triphenyl phosphate TPP.

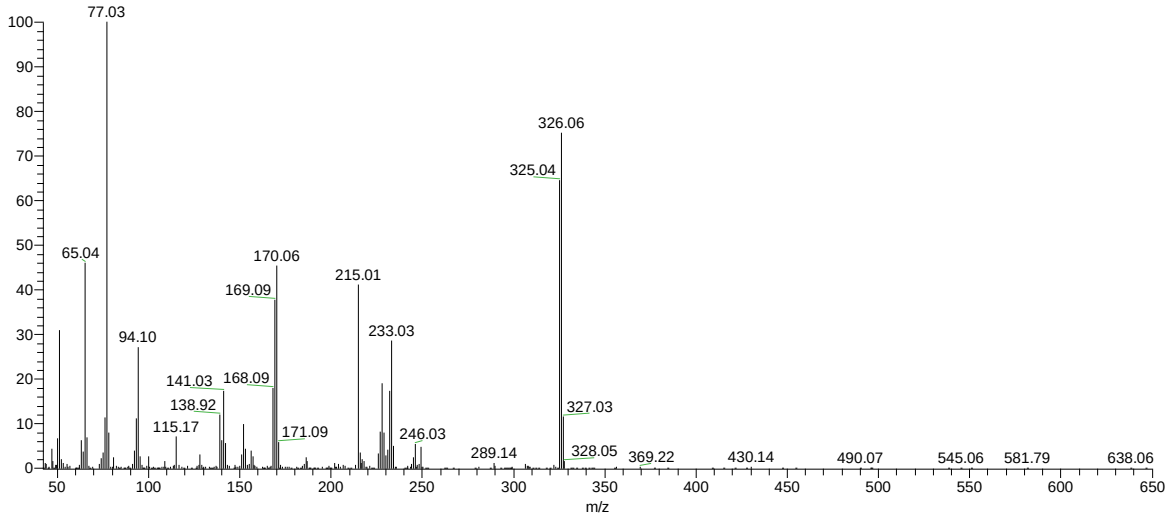

Figure 48: Spectral analysis of peak at 13.05 min on TCP vapour Chromatograph

The spectral analysis of the peak retained at 13.81 min is shown in Figure 49. The most abundant ion has a m/z of 340.08. Using Xcalibur Qual Browser library this spectrum was identified as cresyl diphenylphosphate diphenylcresyl phosphate.

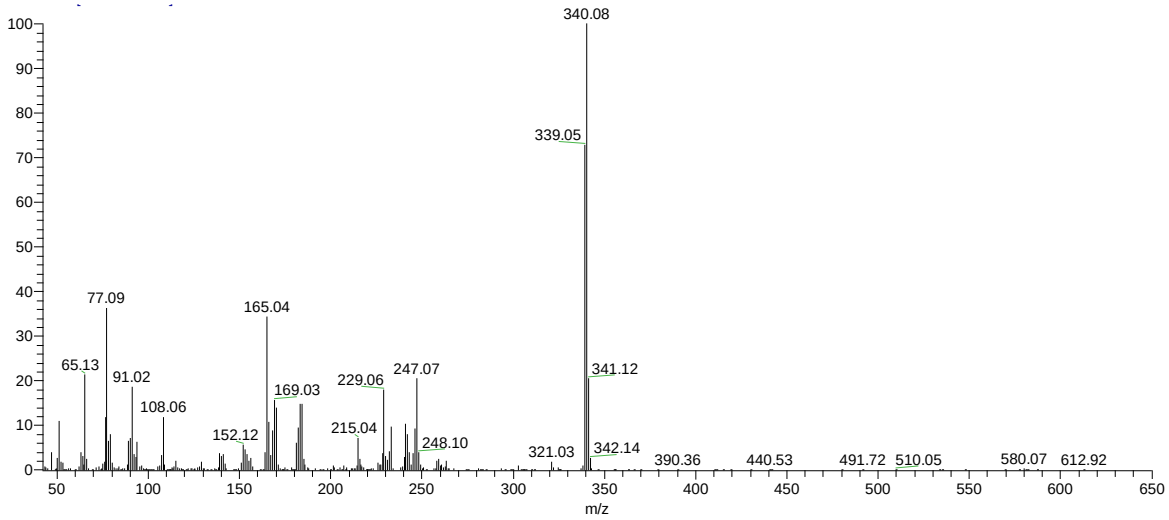

Figure 49: Spectral analysis of peak at 13.81 min on TCP vapour Chromatograph

The spectral analysis of the peak retained at 14.72 min is shown in Figure 50. The most abundant ion has a m/z of 354.09. Using Xcalibur Qual Browser library this spectrum was identified as phosphoric acid, bis(4-methylphenyl) phenyl ester (monophenyl ditolyl phosphate).

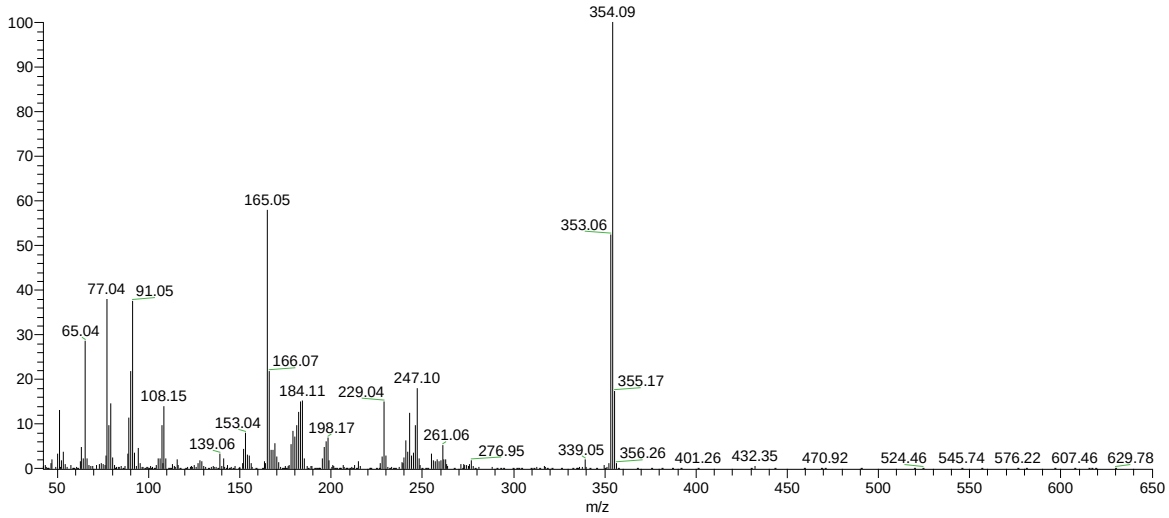

Figure 50: Spectral analysis of peak at 14.72 min on TCP vapour Chromatograph

The spectral analysis of the peak retained at 17.48 min is shown in Figure 51. The most abundant ion has a m/z of 368.14. Using Xcalibur Qual Browser library this spectrum was identified phosphoric acid bis(4-methylphenyl) phenyl ester (phosphoric acid tri-p-tolyl ester).

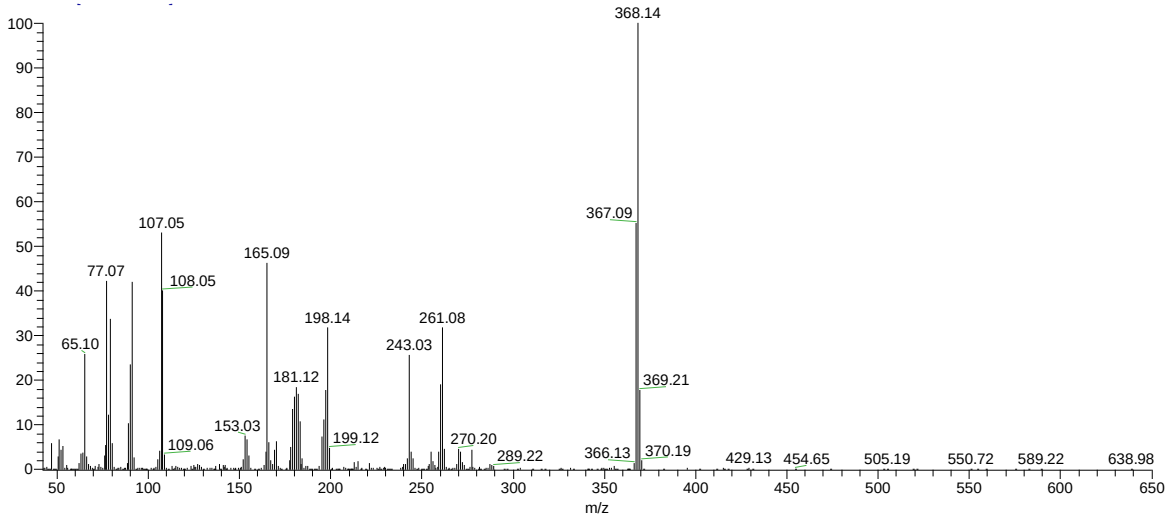

Figure 51: Spectral analysis of peak at 17.48 min on TCP vapour Chromatograph

A comparison of the m/z profile of the peak observed at 17.05 min from the tested sample is made with the NIST library. NIST library identified the sample to be Phosphonic acid. Comparison with the test substance with the library profile of phosphonic acid, as can be seen in Figure 52. The red peaks in Figure 52 represent the tested sample and the blue peaks represent the standard sample of phosphonic, there is good correlation between the m/z of the red peaks and those of the standard blue peaks, confirming that the sample tested was phosphonic acid.

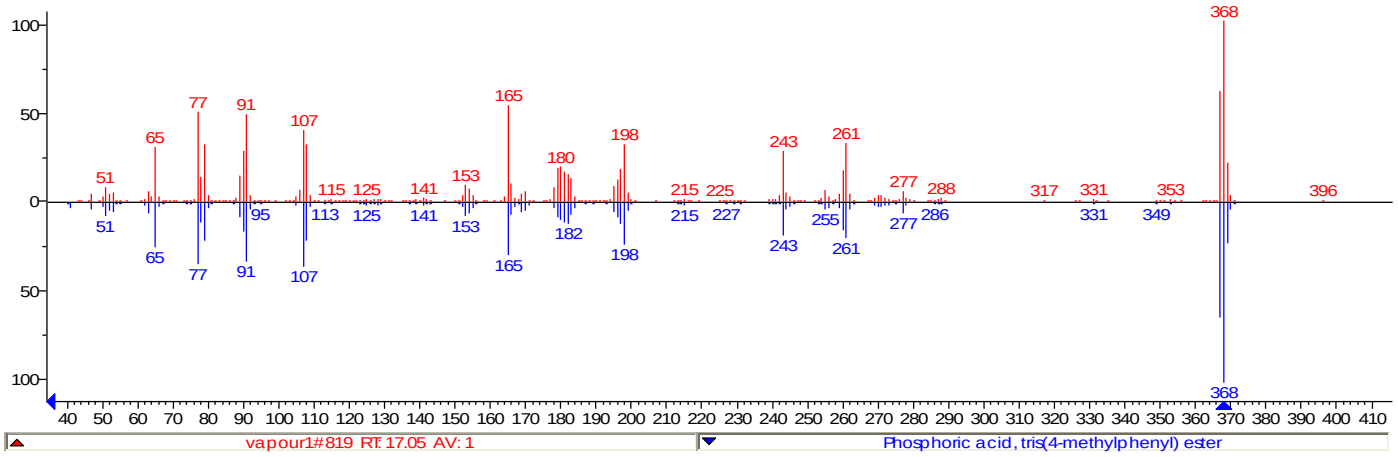

Figure 52: Comparison of m/z profiles of standard TCP data (blue data lines) and test sample (peak 17.05 min) (red data lines)

4.3.3 Test case 3

Test case 3 was analysis of Mobile Jet II Oil (Lubricant Supplies). The sample was tested as per the parameters outlined in Section 4.3. The chromatogram obtained is shown in Figure 53. The retention time for the Mobile Jet II oil was a total of 25 minutes. As can be seen on Figure 53, there are three large peaks detected early in the spectrum with retention times of 5.06 min, 6.89 min and 8.02 min during the chromatographical analysis. Three further smaller peaks were observed with retention times of 17.59 min, 18.22 min, and 18.89 min. Each of these peaks was then analysed and identified.

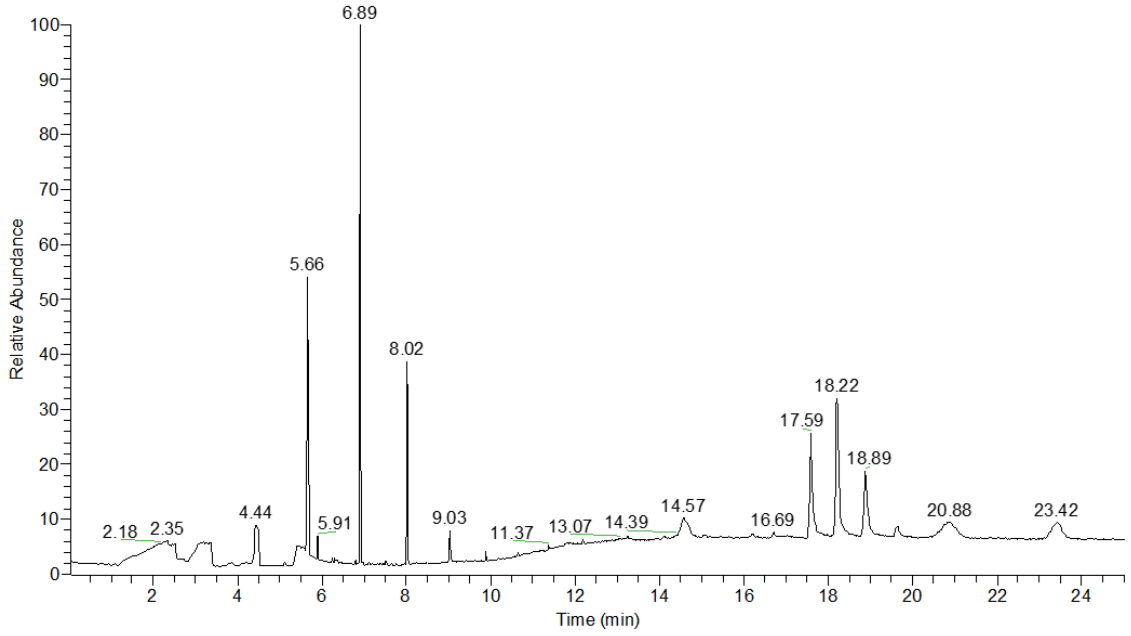

Figure 53: Chromatogram of Mobile Jet II Oil indicating main peaks at 17.59, 18.22, 18.89 minutes

The spectral analysis of the peak retained at 5.66 min is shown in Figure 53. The most abundant ion has a m/z of 72.92. Using Xcalibur Qual Browser library this spectrum was identified as identified as decamethyl cyclpentasiloxane.

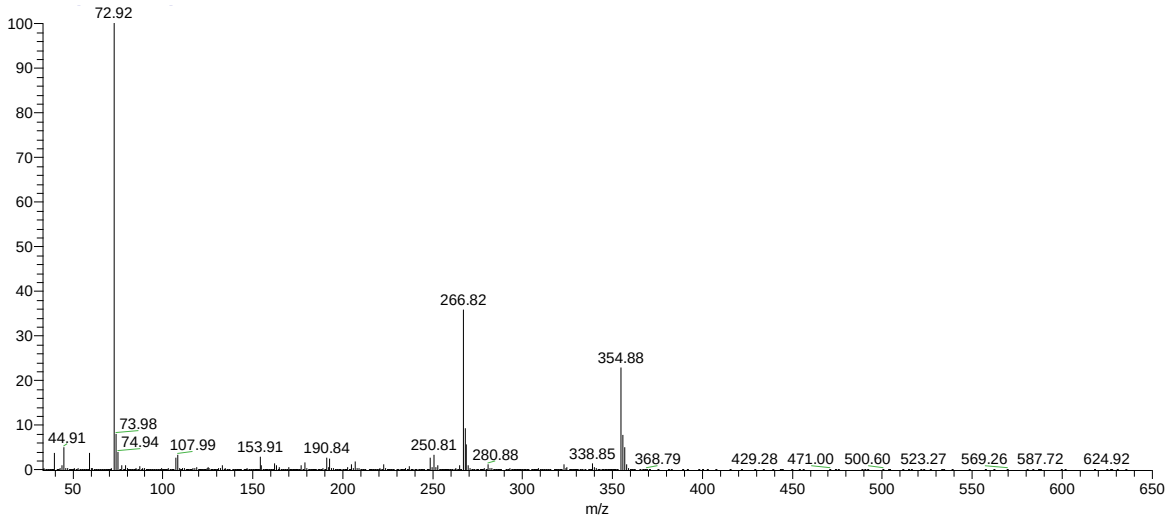

Figure 54: Spectral analysis of peak at 5.66 min on Mobile Jet II Oil Chromatograph

The spectral analysis of the peak retained at 6.89 min is shown in Figure 55. The most abundant ion has a m/z of 340.82. Using Xcalibur Qual Browser library this spectrum was identified as identified as Cyclohexasiloxane, dodecamethyl (Dodecamethylcyclohexasiloxane).

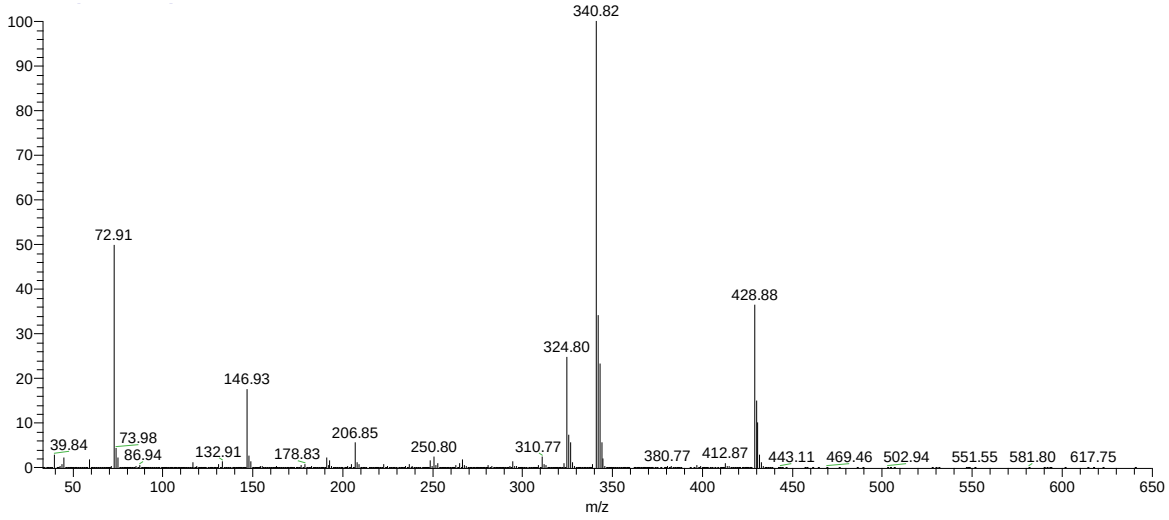

Figure 55: Spectral analysis of peak at 6.89 min on Mobile Jet II Oil Chromatograph

The spectral analysis of the peak retained at 8.02 min is shown in Figure 56. The most abundant ion has a m/z of 72.90. Using Xcalibur Qual Browser library this spectrum was identified as identified as identified as tetradecamethylcyclopentasiloxane.

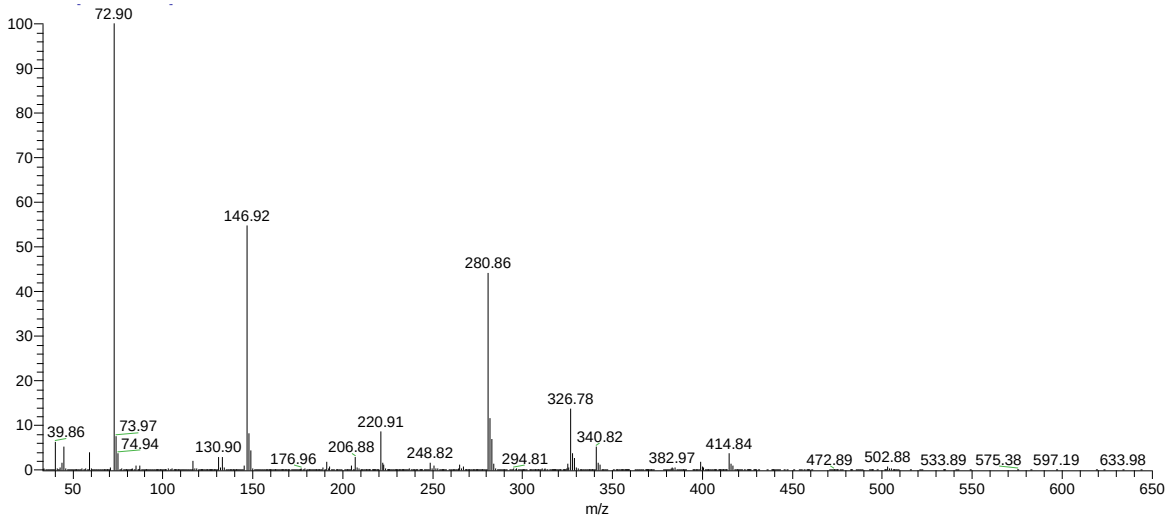

Figure 56: Spectral analysis of peak at 8.02 min on Mobile Jet II Oil Chromatograph

The next set of major peaks was detected at 17.59 min, 18.22 min and 18.89 min. The spectral analysis of the peak retained at 17.59 min is shown in Figure 57. The most abundant ion has a m/z of 164.92. Using Xcalibur Qual Browser library this spectrum was, as identified as Phosphonic acid, tris (3 methylphenyl) ester (phosphoric acid, tri-m-tolyl ester.

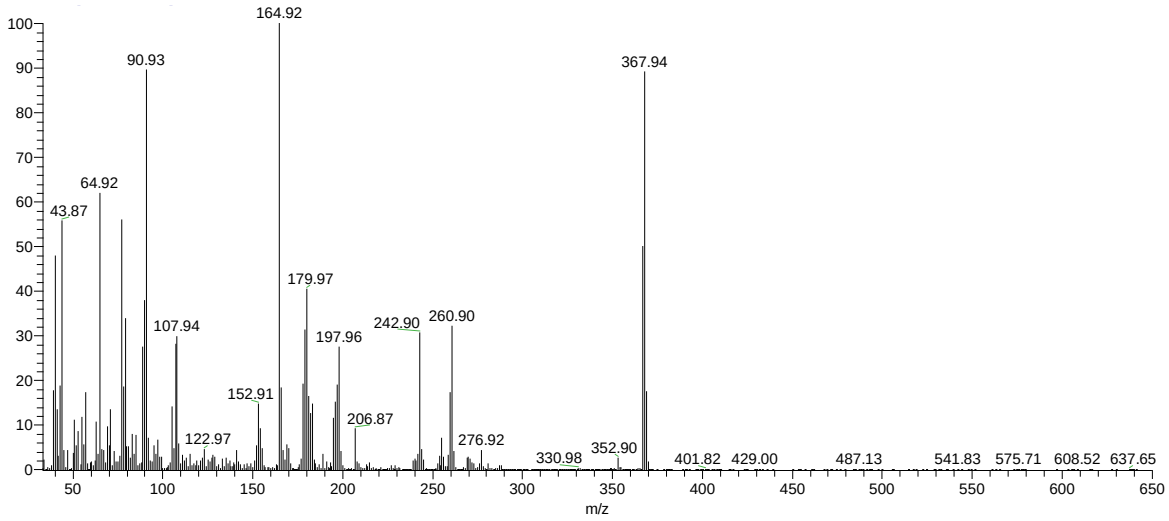

Figure 57: Spectral analysis of peak at 17.59 min on Mobile Jet II Oil Chromatograph

The spectral analysis of the peak retained at 18.22 min is shown in Figure 58. The most abundant ion has a m/z of 90.93. Using Xcalibur Qual Browser library this spectrum was identified as Phosphonic acid, tris (3 methylphenyl) ester. (phosphoric acid, tri-m-tolyl ester.

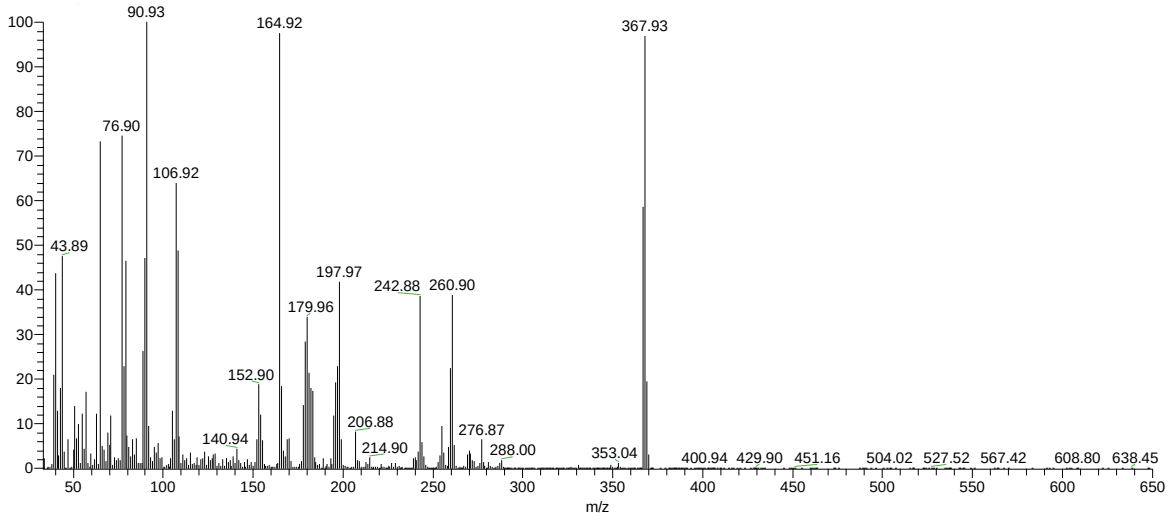

Figure 58: Spectral analysis of peak at 18.22 min on Mobile Jet II Oil Chromatograph

The spectral analysis of the peak retained at 18.89 min is shown in Figure 59. The most abundant ion has a m/z of 43.89. Using Xcalibur Qual Browser library this spectrum was

identified as Phosphonic acid, tris (3 methylphenyl) ester (phosphoric acid, tri-m-tolyl ester.

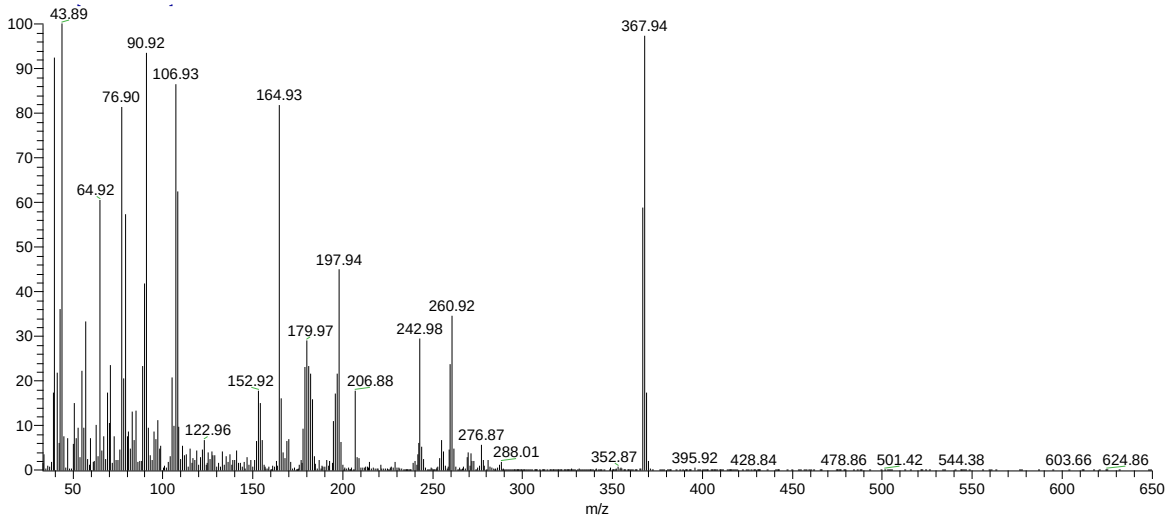

Figure 59: Spectral analysis of peak at 18.89 min on Mobile Jet II Oil Chromatograph

A further analysis of the peak at 18.89 min, the highest abundant ion observed, at the far side of the chromatograms, with the NIST library. The NIST library confirmed the identification of the sample as Phosphonic acid, tris (2-methylphenyl) ester (TCP). The comparison of the spectra of peak form sample tested with the library spectra can be seen in Figure 60. The red peaks in Figure 60 represent the tested sample and the blue peaks represent the standard sample. There is good correlation between the m/z of the red peaks and those of the standard blue peaks, confirming that the sample tested was Phosphonic acid.

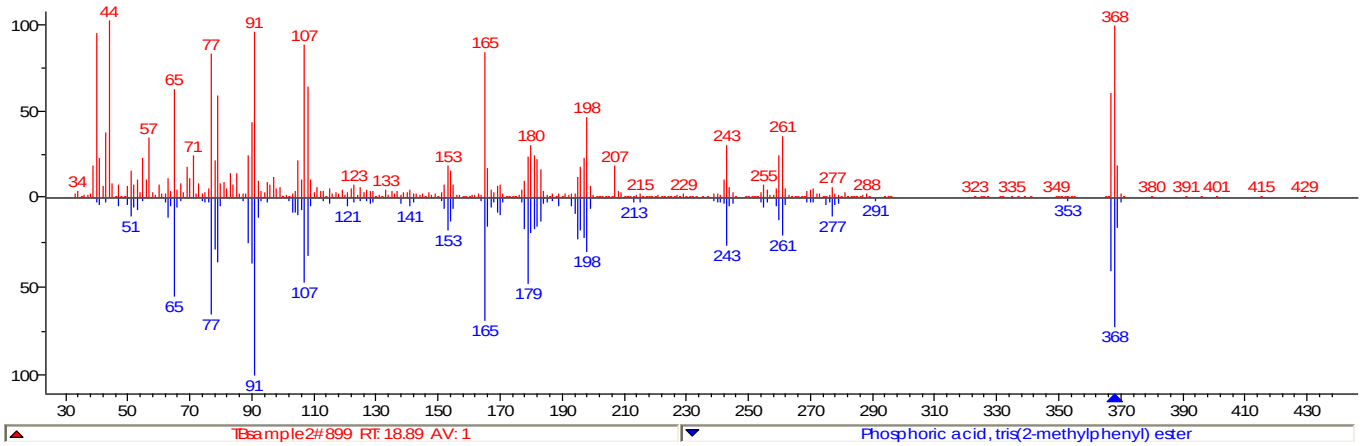

Figure 60: Comparison of m/z profiles of standard TCP data (blue data lines) and test sample (peak 18.89 min) (red data lines)

4.3.4 Test case 4

Test case 4 was analysis of the vapour from heated Mobile Jet II Oil (Lubricant Supplies). When oils are exposed to high temperatures in the engines or APU, a complex mixture of thermally degraded (thermolysis) components is produced (Burdon et al. 2023). The sample was heated to 500°C in a calibrated oven and then the sample was tested as per the parameters outlined in Section 4.3. The chromatogram obtained is shown in Figure 61. The retention time for the Mobile Jet II oil was a total of 41 minutes. As can be seen on Figure 61, there is one very large peak at 4.85 min, followed by four large peaks detected during the chromatographical analysis. The retention time of the peaks was 13.54 min, 16.40 min, 16.91 min and 17.37 min. Each of these peaks was then analysed and identified.

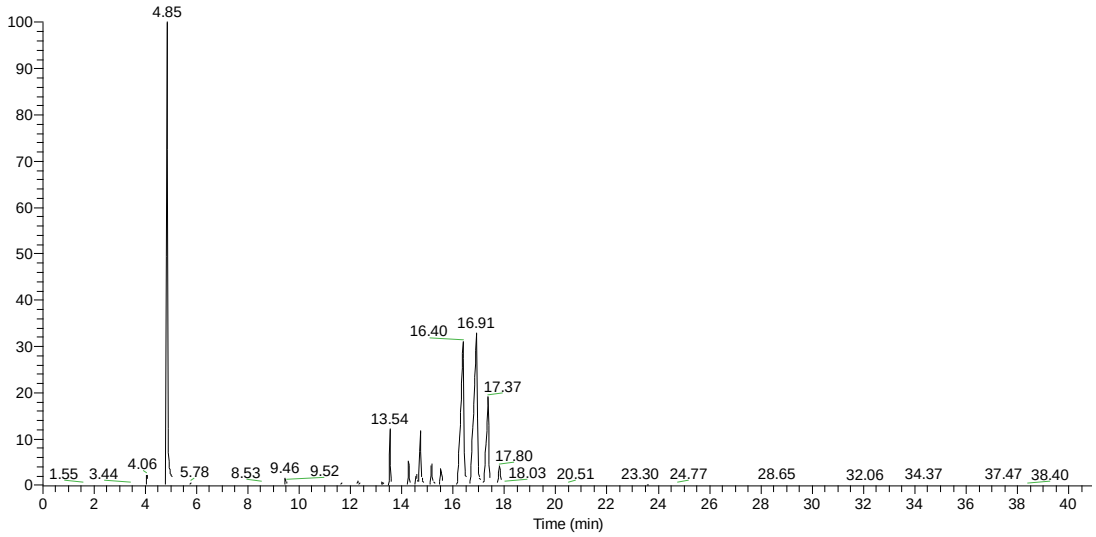

Figure 61: Chromatogram of vapour from Mobile Jet II Oil indicating main peaks at 16.40, 16.91, 17.37 minutes

The spectral analysis of the peak retained at 4.85 mins is shown in Figure 62. The most abundant ion has a m/z of 108.08. Using Xcalibur Qual Browser library this spectrum was identified as identified as phenol 3 methyl m-cresol.

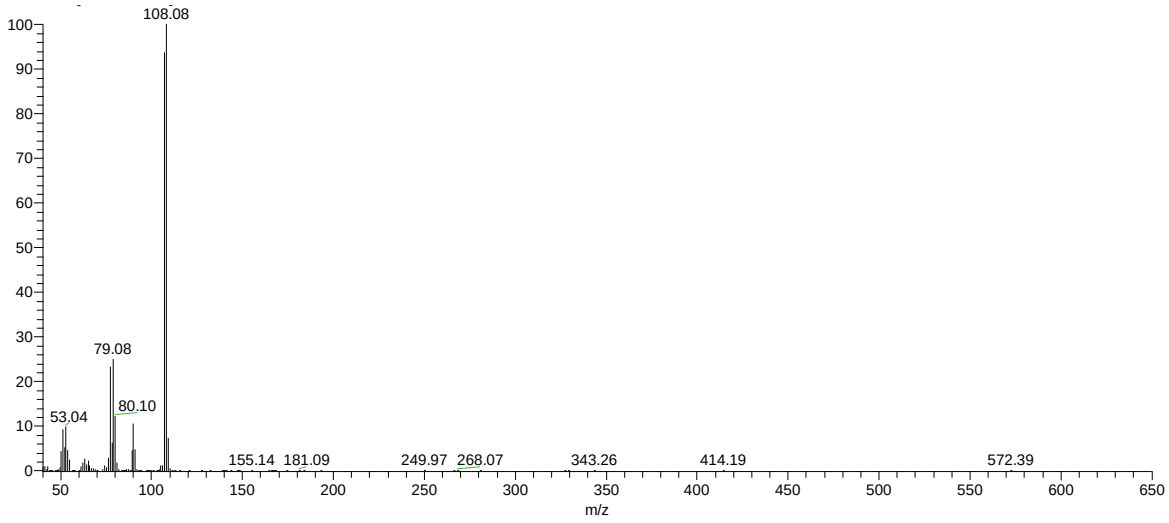

Figure 62: Spectral analysis of peak at 4.85 min on vapour from the Mobile Jet II Oil Chromatograph

The spectral analysis of the peak retained at 13.54 min is shown in Figure 63. The most abundant ion has a m/z of 326.05. Using Xcalibur Qual Browser library this spectrum was identified as identified as triphenol phosphate TPP.

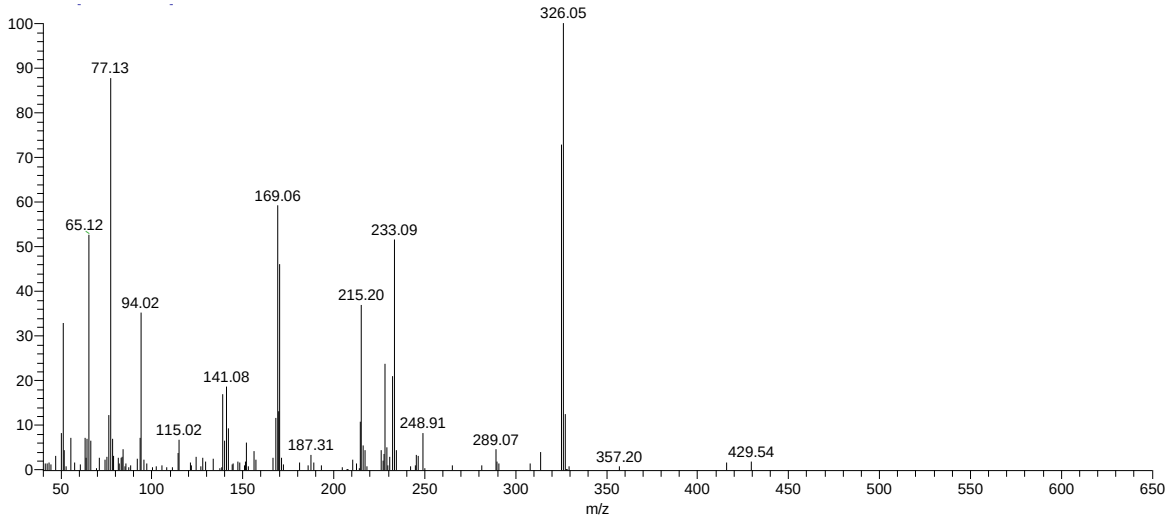

Figure 63: Spectral analysis of peak at 13.54 min on vapour from the Mobile Jet II Oil Chromatograph

The spectral analysis of the peak retained at 16.40 min is shown in Figure 64. The most abundant ion has a m/z of 368.15. Using Xcalibur Qual Browser library this spectrum was identified as identified as phosphoric acid tri (3-methylphenyl) ester.

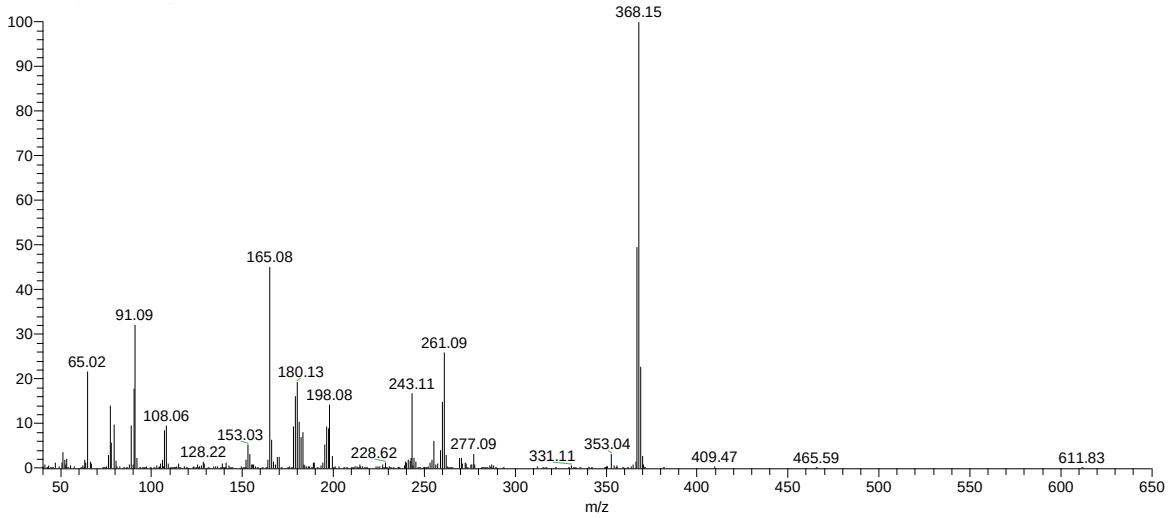

Figure 64: Spectral analysis of peak at 16.40 min on vapour from the Mobile Jet II Oil Chromatograph

The spectral analysis of the peak retained at 16.91 mins is shown in Figure 65. The most abundant ion has a m/z of 368.12. Using Xcalibur Qual Browser library this spectrum was identified as phosphoric acid, tri(3-methyphenyl) ester Phosphoric acid, tri-m-tolyl ester.

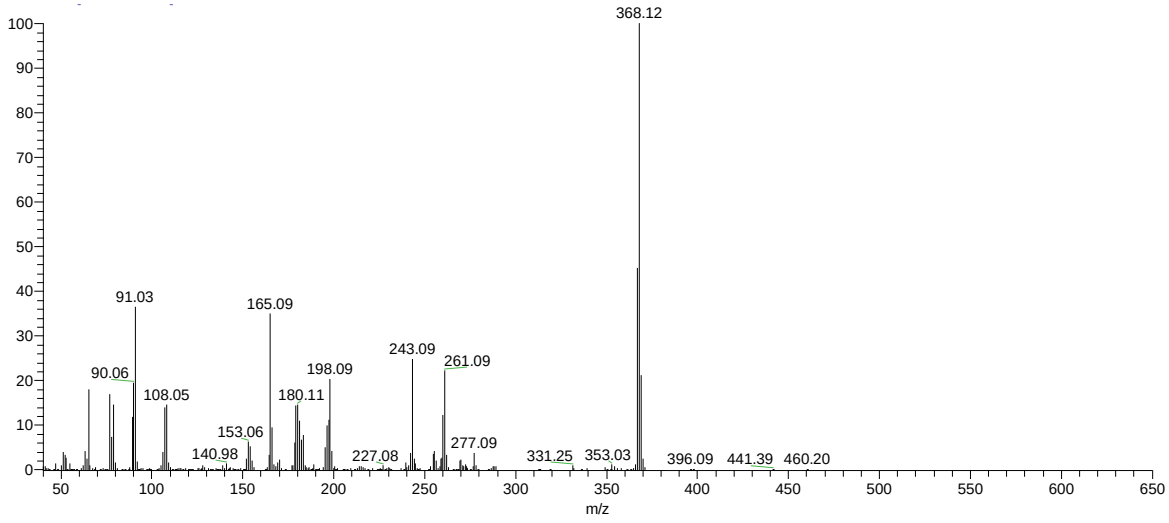

Figure 65: Spectral analysis of peak at 16.91 min on vapour from the Mobile Jet II Oil Chromatograph

The spectral analysis of the peak retained at 17.37 mins is shown in Figure 66. The most abundant ion has a m/z of 368.12. Using Xcalibur Qual Browser library this spectrum was identified as identified as phosphoric acid, tris (4-methylphenyl) ester Phosphoric acid tri-p-tolyl ester.

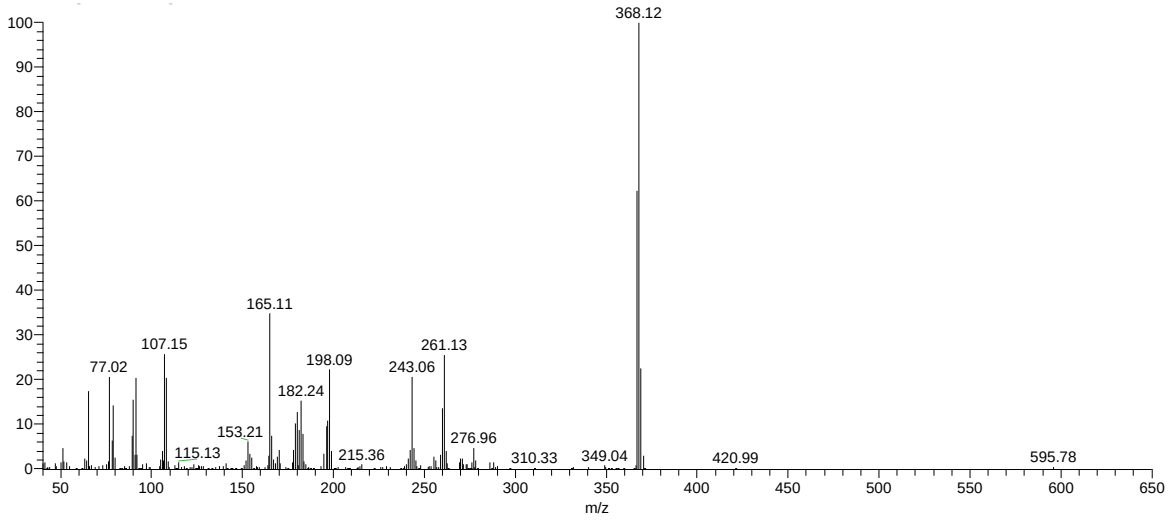

Figure 66: Spectral analysis of peak at 17.37 min on vapour from the Mobile Jet II Oil Chromatograph

The spectral analysis of the peak retained at 17.80 mins is shown in Figure 67. The most abundant ion has a m/z of 368.23. Using Xcalibur Qual Browser library this spectrum was identified as identified as phosphoric acid, tris (4-methylphenyl) ester Phosphoric acid tri-p-tolyl ester.

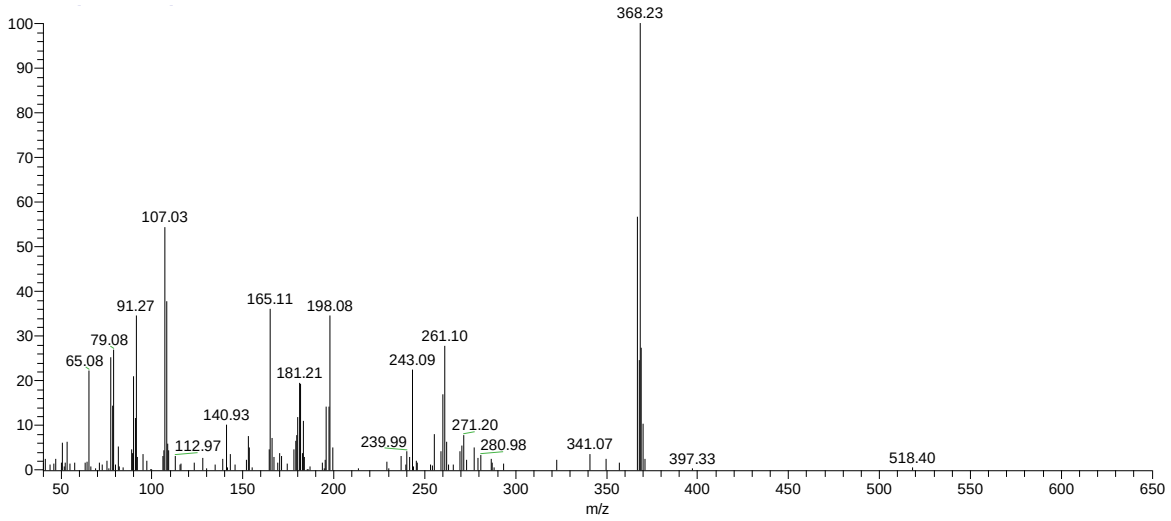

Figure 67: Spectral analysis of peak at 17.80 min on vapour from the Mobile Jet II Oil Chromatograph

A comparison of the m/z profile of the peak observed at 16.91 min from the tested sample is made with the NIST library. NIST library identified the sample to be Phosphonic acid. Comparison with the test substance with the library profile of phosphonic acid, as can be seen in Figure 68. The red peaks in Figure 68 represent the tested sample and the blue peaks represent the standard sample of phosphonic, there is good correlation between the m/z of the red peaks and those of the standard blue peaks, confirming that the sample tested was phosphonic acid.

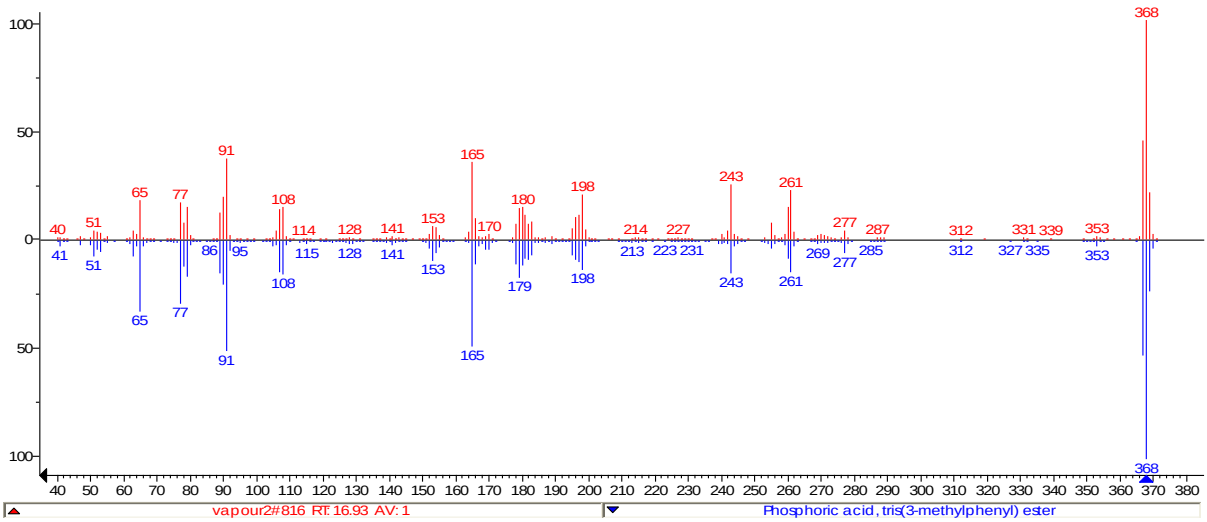

Figure 68: Comparison of m/z profiles of standard TCP data (blue data lines) and test sample (peak 16.91 min) (red data lines)

4.4 Summary of GC/MS analysis

All samples tested showed the presence of TCP isomers in varying concentrations, this has shown that whether the sample is the standard jet oil or a pyrolyzed sample, there is TCP present. The technical grade TCP indicated that peaks of the TCP isomers should show a retention time between 18 and 20 minutes, as the different samples were analysed the retention times decreased slightly, this is due to the compounds being in different compositions. The MS spectra was used to identify the compound with retention times in the same region – between 16 and 19 minutes. The main peak observed on the GC chromatographs were identified as can be seen in Table 18.

Table 18: Retention times and MS identification of the main peaks observed in the chromatographs on the 4 tested samples

Test case	Material tested	Peak retention time (min)	Identification	Other names
Test 1 & 2	TCP	18.07	Phosphoric acid	Tri-m-cresyl phosphate
		18.74	Phosphoric acid	Tri-m-cresyl phosphate
		19.41	Phosphoric acid	Tri-p-cresyl phosphate
		20.14	Phosphoric acid	Tri-p-cresyl phosphate
Test 3 & 4	Vapour of pyrolyzed TCP	16.02	Phosphoric acid	Tri-m-cresyl phosphate
		16.58	Phosphoric acid	Tri-m-cresyl phosphate
		17.05	Phosphoric acid	Tri-p-cresyl phosphate
		17.48	Phosphoric acid	Tri-p-cresyl phosphate
Test 5 & 6	Engine jet oil	17.59	Phosphoric acid	Tri-m-cresyl phosphate
		18.22	Phosphoric acid	Tri-m-cresyl phosphate
		18.89	Phosphoric acid	Tri-m-cresyl phosphate
Test 7 & 8	Vapour of pyrolyzed engine jet oil	16.40	Phosphoric acid	Tri-m-cresyl phosphate
		16.91	Phosphoric acid	Tri-m-cresyl phosphate
		17.37	Phosphoric acid	Tri-p-cresyl phosphate
		17.80	Phosphoric acid	Tri-p-cresyl phosphate

Isomers of TCP are found in engine jet oil and the vapour from the pyrolyzed sample of engine jet oil. This will be present in the aircraft engine and the potentially contaminate the air returning the cabin via the bleed air. Whilst it has been shown that isomers of TCP are present the major isomer of concern TOCP was not identified within the samples test.

TOCP is a highly poisonous compound. Its toxicity is greater than that of the meta- or para-isomer. Studies have shown that tri-o-cresyl phosphate, tri-p-cresyl phosphate and tri-m-cresyl phosphate are toxic (WHO 1990). The toxicity of the different isomers is summarised in Table 19.

Table 19: LD_{50} values for TCP and its isomers (WHO 1990)

Compounds	Route of administration	Species	LD_{50} (mg/kg)
TCP mixed isomers	Oral	Rat	5190
	Oral	Rat	>4640
	Oral	Rat	>15 800
	Oral	Mouse	3900
	Oral	Chicken	>10 000
	Dermal	Rabbit	>7900
	Dermal	Cat	1500
Tri-*o*-cresyl phosphate	Oral	Rat	8400
	Oral	Rat	1160
	Oral	Rabbit	3700
	Oral	Chicken	500
	Oral	Chicken	100-200
Tri-*p*-cresyl phosphate	Oral	Rabbit	>3000
	Oral	Chicken	>1000
Tri-*m*-cresyl phosphate	Oral	Rabbit	>3000
	Oral	Chicken	>2000

The acute toxicity of TCP depends on the relative proportions of the different isomers.
The GC-MS data for the analysis of the jet engine oil (Figures 53- 60) show that the peaks with a retention time of 17.59, 18.22 and 18.89 minutes are isomers of TCP as the molecular weight was determined as 367.94, 367.93 and 367.94 g/mol respectively. The GC-MS data for the analysis of the pyrolyzed jet engine oil (Figures 61-68) show that the peaks with a retention time of 16.40, 16.91, and 17.37 minutes are isomers of TCP as the molecular weight was determined as 368.15, 368.12, and 368.12 g/mol respectively.

The molecular weight of TCP is 368.4 g/mol. There is a slight difference in the molecular weights observed in this study to the published molecular weight of TCP, due to the presence of the isomers and different isotopes of carbon.

As can be seen in Figures 53 and 61, the GC chromatography the different isomers have a different relative abundance. This data is reproduced in Table 20.

Table 20: Molecular weight and relative abundance of TCP isomers determined from analysis of engine jet oil and pyrolysed engine jet oil

Material tested	Retention time (minute)	Molecular weight (g/mol)	Relative abundance (%)
Engine jet oil	17.59	367.94	26
	18.22	367.93	30
	18.89	367.94	18
Pyrolysed engine jet oil	16.40	368.15	32
	16.91	368.12	34
	17.37	368.12	20

This analysis has shown that there is potential for TCP to be present in engine oils, this potentially could contaminate aircraft cabin air and therefore supports the need for further analysis to show the possible concentrations which could enter the aircraft cabin. A mathematical model will be used to determine how much contaminant could enter the air supply and therefore enter the cabin. This is developed in Chapter 5. The findings from Chapter 5 will then allow the development of the numerical analysis to determine the particle flow paths and distribution within the cabin and identify the hazardous seat locations (Chapter 6).

Chapter 5 – Development of a mathematical model

In this section of the thesis the contaminant-cabin problem is examined using the well-known tank mixing problem. The chapter is structured to develop the mathematical theory from a crude one-dimensional ODE to the inhomogeneous eigenvalue approach. Then conclusions are made in light of the holistic problem.

Ramsden (2013) conducted a study on the consumption of jet engine oil as a surrogate for measuring chemical contamination within an aircraft cabin. This study found that comparing the known rate of loss of engine oil during jet engine operation with measurements of ultrafine particle concentration could determine the levels of oil leaking into the cabin to be inhaled by cabin crew and passengers (Ramsden 2013).

Scholz (2017) undertook a study of aircraft cabin air and engine oil. The study tries to determine how much oil could get into the aircraft cabin using mathematical modelling. This was based on the oil consumption per flight hour, and estimation of how much oil could leak out of the engine seals (a conservative value of 2% was used). A value of 17.2 mg/m^3 was determined. This was then compared to in-flight measurements which can be seen in Figure 69.

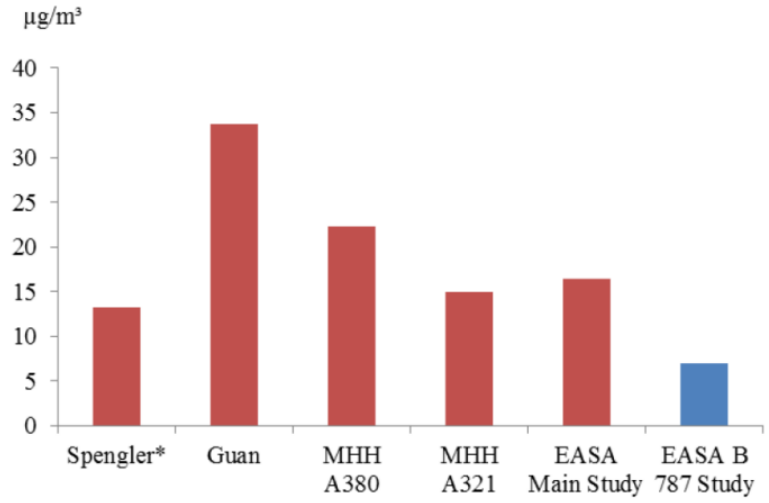

Figure 69: In-flight measurements from 6 studies (Scholz 2017)

As can be seen the results of the mathematical solution presented by Scholz are comparable to those observed from the in-flight measurements.

Lakies (2019) went on to develop the theory from Scholz (2017) to derive an equation to calculate the dynamic effect of primary and secondary aircraft cabin air contamination. Primary contamination is from an outside source in form of normal low-level contamination or high-level contamination in a failure case. Secondary contamination originates from deposited material released into the cabin by a trigger event. This study was not limited to the contamination of aircraft cabin air by organophosphate compounds. This study found that the results calculated ranged from 17 $\mu g/m^3$ to 4600 $\mu g/m^3$ dependant on the size of the proportion of recycled air, the total air exchange rate. aircraft and the type of filters present (Lakies 2019).

Within the aircraft cabin, air flows into the cabin at head height at a flow rate of 1.2 m/s and leaves the cabin a floor level at the a flow rate of 1.4 m/s. Prior to the air entering the cabin, recycled air and new air mix within the engine. At this stage, if the seals are leaking, the air has the potential to become contaminated with organophosphates. This chapter will set up the mathematical problem using:

- One tank mixing
- Two tanks – vertical orientation
- Two tanks – horizontal orientation
- The aircraft-toxin system, two tanks in the homogenous problem

5.1 The Mixing Problem – One tank

Initially the problem can be illustrated using the air flow into and out of the cabin environment. This can be considered as a one tank mixing problem.

In this situation there is a holding tank which contains a solution of a fluid containing a dispersed substance. There is normally fluid entering the holding tank as well as leaving it. The fluid entering the tank may or may not contain more of the suspended substance,

but fluid leaving the holding tank will contain the dispersed substance. It is assumed that the concentration of the suspension in the holding tank is uniform thorough out, and that the volume of the fluid also remains constant (Boelkins et al. 20016).

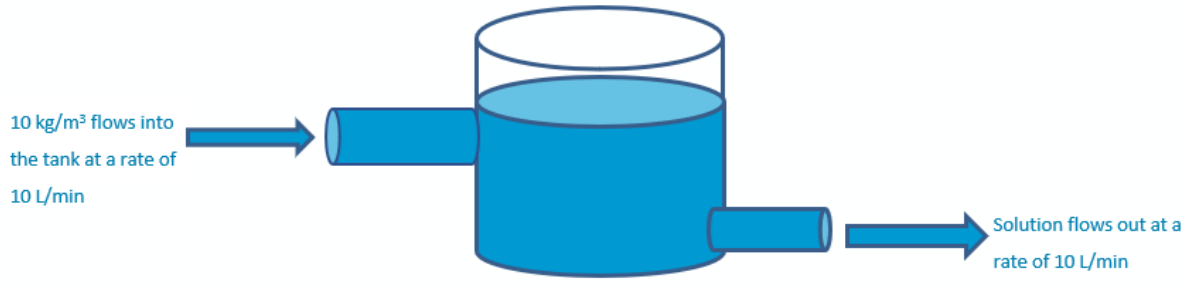

Figure 70: Illustration of one tank with flow in and flow out

Let m(t) describe the mass (kg) of suspended substance at time (t). The rate of change of this mass is given by the difference of inflow and outflow, equation 5-1.

$$\frac{dm}{dt} = \frac{dm_{in}}{dt} - \frac{dm_{out}}{dt} \qquad (5\text{-}1)$$

Consider the following situation: There is a holding tank, as in Figure 70, which contains 100 L of water and 10 kg of salt. There is an outlet flow from the tank, removing the solution at a rate of 0.01 m^3/min. Salt water with a concentration of 10 kg/m^3 flows into the tank at a rate of 0.01 m^3/min l/min. The aim is to find how much salt is in the tank after a period of time, for example, after 11 minutes. As the flow into the tank is the same as the flow out, the volume of the solution in the tank will remain the same. As there is a different concentration flowing into the tank, the co9ncentration in the tank will change over time, as will the solution flowing out.

The initial conditions of the tank are: m(0) = 10 kg (t = 0 minutes)

The solution flowing into the tank is a different concentration to that already in the tank, this will change the concentration over time. The rate of suspension flowing in would be equal to the concentration and the flow rate.

$$Rate\ of\ suspension\ in = 10\frac{kg}{m^3} * 0.01\frac{m^3}{min} = 0.1\ kg/min \quad (5\text{-}2)$$

The flow rate out needs to be calculated based on the flow rate out of the tank. The problem statement does not give the concentration of the solution flowing out of the tank. As the concentration of the tank is changing with time, the concentration flowing out will change with time. This is assuming the contents of the tank itself are well mixed. The full mathematical solution can be seen in Appendix 1.

In the tank problem illustrated above, the initial conditions are 10 kg of salt in 100 l of water. The concentration of salt at time 0 is 10 kg. this can be included to give:

$$m(0) = 10 = De^{-0.1(0)} + 1 \quad (5\text{-}3)$$

$$D = 9$$

Equation (5-3) can be written

$$m = 9e^{-0.1t} + 1 \quad (5\text{-}4)$$

This is the solution. It is an exponential decay with relaxation period 1/0.1 = 10 minutes. Using the example time of 11 minutes mentioned above.

$$m(11) = 9e^{-0.1\ (11)} + 1 = 4kg \quad (5\text{-}5)$$

This is expressed graphically in Figure 71, it can be seen that if the initial condition is 10 kg, the concentration will decrease over time.

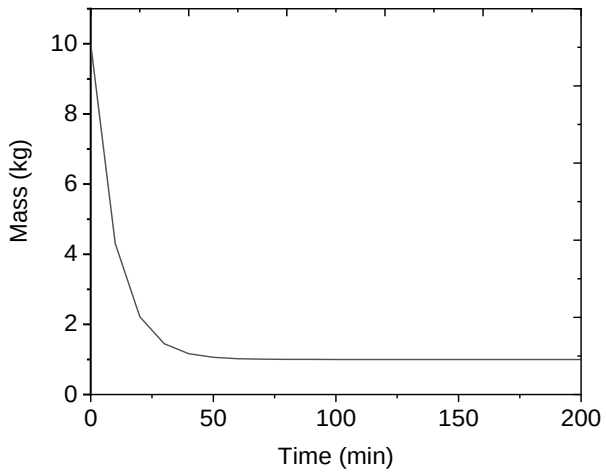

Figure 71: Graphical representation of the solution illustrating the initial concentration of 10 kg being diluted over time

This is a classic example of a relaxation process. Where the mass exponentially decreases over time to a steady state value. From equation 5-5 the steady value is (t=∞), m (∞)=1 and the relaxation period is 1/0.1 = 10 minutes.

5.2 Two tank mixing problem – vertical tanks

Moving on from a one tank mixing problem, a two-tank mixing problem needs to be considered. In the following formulation it is shown how two tanks lead to a second order problem. In this scenario there is an outlet from one tank feeding into a second tank below it, but there is no pipe connecting the two tanks. As illustrated in Figure 72. There is a flow into tank one (f_{in1}) and a flow out (f_{12}) showing the flow is from tank one to tank 2. The depth of the solution in tank one is at a given height (h_1) and thank two is (h_2). There is also flow out of tank two (f_{out}).

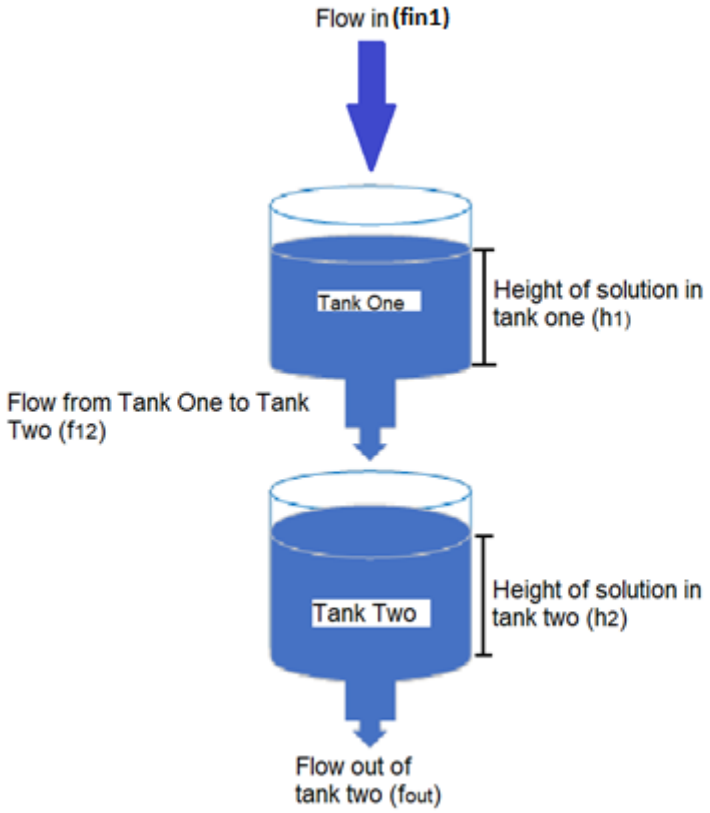

Figure 72: Two vertical tanks

To model this scenario the flow through a restriction from tank one to tank two can be represented by the formula in Equation 5-6 where f_{12} in the flow from tank one to two, h_1

is the height of the solution in tank one and R_{12} is a constant, this is because the pressure at the bottom of the thank is proportional to the depth:

$$R_{12}h_1 = f_{12} \tag{5-6}$$

Therefore, we can write an equation for the depth of fluid in tank one, Equation 5-7 (where A_1 is the cross-sectional area of tank one):

$$A_1 \frac{dh_1}{dt} = f_{in1} - f_{12} \tag{5-7}$$

For tank two a similar equation can be determined, Equation 5-8 ((where A_2 is the cross-sectional area of tank two):

$$A_2 \frac{dh_2}{dt} = f_{12} - f_{out} \tag{5-8}$$

We also need to consider the flow out of tank two:

$$[R_2]h_2 = f_{out} \tag{5-9}$$

These four equations (5- 6 to 5 -9) represent the tanks in series and the flow into and out of each. The depth in tank one is represented by Equation 5-7. Equations 5-8 and 5-9 need to be combined giving equation 5-10 to give the depth of tank two.

$$A_2 \frac{dh_2}{dt} = R_{12}h_1 - R_2h_2 \tag{5-10}$$

To determine the depth of fluid in tank two we need to initially rearrange the formula for the depth in tank 2 to isolate h_1:

$$\frac{A_2}{R_{12}} \frac{dh_2}{dt} + \frac{R_2}{R_{12}} h_2 = h_1 \tag{5-11}$$

This formula can now be used for h_1 and used to illuminate h_1 from the equation:

$$A_1 \frac{d}{dt}\left(\frac{A_2}{R_{12}}\frac{dh_2}{dt} + \frac{R_2}{R_{12}}h_2\right) = f_{in1} - R_{12}\left(\frac{A_2}{R_{12}}\frac{dh_2}{dt} + \frac{R_2}{R_{12}}h_2\right) \quad (5\text{-}12)$$

This is h_2 and f_{in1}

We can rearrange this for a 2nd order ODE

$$\frac{A_1 A_2}{R_{12}}\frac{d^2h_2}{dt^2} + \left(\frac{A_1 R_2}{R_{12}} + A_2\right)\frac{dh_2}{dt} + R_2 h_2 = f_{in1} \quad (5\text{-}13)$$

Having demonstrated this is a second order problem, the solution of such a mathematical problem can include wavelike behaviour, resonance and could be formulated as one ODE or two coupled first order equations.

5.3 Two tank mixing problem – horizontal tanks

Two tanks in parallel - There are two interconnect tanks as shown in Figure 73. The two tanks are of equal volume (24 L). Both tanks contain an homogenous salt solution. Fresh water flows into Tank one at a rate of 6 L per minute. Fluid is drained from Tank two at a rate of 6 L per minutes. There is a rate of flow of 2 L per minute from Tank two to Tank one and a flow of 8L per minute from Tank one to Tank two. Initially Tank one contains 1 kg of salt and Tank two contains 6 kg of salt. Concentration of salt in each tank will vary with time, but the volume of solution in the tanks will not change over time.

The mass of salt in tank one is m_1 and the mass of salt in tank two is m_2 at time (t). From the one tank mixing problem, it was determined that the rate of change of salt was determined by the amount if salt going in mins the rate of salt flowing out.

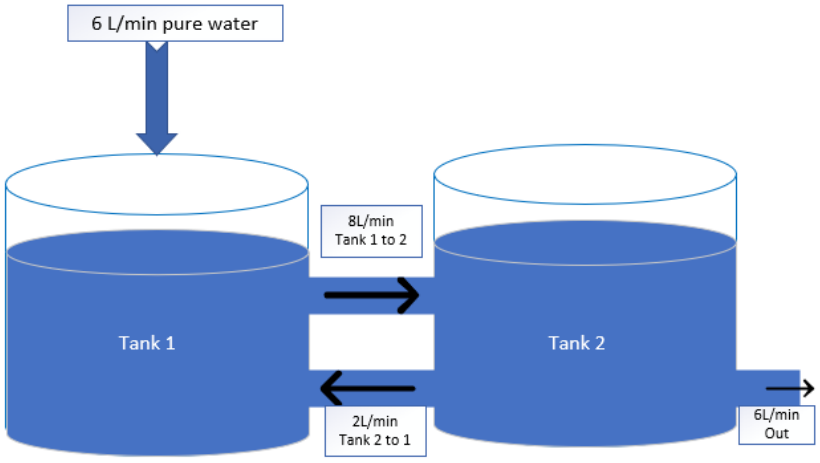

Figure 73: Two interconnected tanks

Both tanks will initially contain 24 L of water (this will not change over time). Therefore, if we consider the rates of flow in and out of each tank, we can show the volume is a constant 24 L, tank one has a volume of 24 L, there is 6 L flowing into this tank, but 8 L flowing out to tank two. There is 2 L flowing to tank one from tank two – this maintains the

constant 24 l volume. Tank two is the same. The rate of change in concertation of salt is depending on the flows in and out of each tank.

Rate of change in concentration for Tank one is shown in Equation 5-14, where m_1' is the rate of change of salt concentration in tank one.

$$m_1'(t) = (0)(6) + \left(\frac{m_2}{24}\right)(2) - \left(\frac{m_1}{24}\right) \tag{5-14}$$

Rate of change in concentration for Tank two is shown in Equation 5-15, where m_2' is the rate of change of salt concentration in tank two.

$$m_2'(t) = \left(\frac{m_1}{24}\right)(8) - \left(\frac{m_2}{24}\right)(2) - \left(\frac{m_2}{24}\right) \tag{5-15}$$

This can be simplified

$$m_1'(t) = -\frac{1}{3}m_1 + \frac{1}{12}m_2 \tag{5-16}$$

$$m_2'(t) = \frac{1}{3}m_1 - \frac{1}{3}m_2 \tag{5-17}$$

Initial states of amount of salt in each tank: tank one had 1 kg of salt, tank two had 6 kg of salt.

To solve this the matrix form is used:

$$\overline{m}' = \begin{bmatrix} -\frac{1}{3} & \frac{1}{12} \\ \frac{1}{3} & -\frac{1}{3} \end{bmatrix} \overline{m} \tag{5-18}$$

$$\overline{m}(0) = \begin{bmatrix} 1 \\ 6 \end{bmatrix}$$

This is a classical Eigenvalue problem equivalent to

Eigenvalue of the matrix:

$$0 = |\lambda I - A| 0 = \begin{vmatrix} \lambda + \frac{1}{3} & -\frac{1}{12} \\ -\frac{1}{3} & \lambda + \frac{1}{3} \end{vmatrix} \tag{5-19}$$

$$0 = \left(\lambda + \frac{1}{3}\right)\left(\lambda + \frac{1}{3}\right) - \frac{1}{36} \tag{5-20}$$

$$0 = \frac{1}{12}(2\lambda + 1)(6\lambda + 1) \tag{5-21}$$

So Eigen values are:

$$\lambda = -\frac{1}{2}, -\frac{1}{6} \tag{5-22}$$

The corresponding Eigenvectors are therefore:

First consider $\lambda = -\frac{1}{2}$ we need to solve $\left(-\frac{1}{2}I - A\right)m = 0$ we get:

$$-\frac{1}{2}I - A = \left[\begin{array}{cc|c} -\frac{1}{6} & -\frac{1}{12} & 0 \\ -\frac{1}{3} & -\frac{1}{6} & 0 \end{array}\right] \rightarrow \left[\begin{array}{cc|c} 1 & \frac{1}{2} & 0 \\ 0 & 0 & 0 \end{array}\right] \tag{5-23}$$

For m_2 = t, then the Eigenvectors would be:

$$m = \begin{bmatrix} m_1 \\ m_2 \end{bmatrix} = t \begin{bmatrix} -\frac{1}{2} \\ 1 \end{bmatrix} = t \begin{bmatrix} -1 \\ 2 \end{bmatrix} \tag{5-24}$$

The second Eigenvalue would be:

$\lambda = -\frac{1}{6}$ we would need to solve the equation $\left(-\frac{1}{6}I - A\right) m = 0$ we get:

$$-\frac{1}{6}I - A = \left[\begin{array}{cc|c} \frac{1}{6} & -\frac{1}{12} & 0 \\ -\frac{1}{3} & \frac{1}{6} & 0 \end{array}\right] \rightarrow \left[\begin{array}{cc|c} 1 & -\frac{1}{2} & 0 \\ 0 & 0 & 0 \end{array}\right] \tag{5-25}$$

If m_2=t the Eigenvectors are:

$$m = \begin{bmatrix} m_1 \\ m_2 \end{bmatrix} = t \begin{bmatrix} \frac{1}{2} \\ 1 \end{bmatrix} = t \begin{bmatrix} 1 \\ 2 \end{bmatrix} \tag{5-26}$$

The Eigenpairs for the two-tank problem are

$$\lambda_1 = -\frac{1}{2} \bar{v}_1 = \begin{bmatrix} -1 \\ 2 \end{bmatrix} \tag{5-27}$$

$$\lambda_2 = -\frac{1}{6} \bar{v}_2 = \begin{bmatrix} 1 \\ 2 \end{bmatrix} \tag{5-28}$$

The general solution

$$\bar{m}(t) = C_1 e^{-t/2} \begin{bmatrix} -1 \\ 2 \end{bmatrix} + C_2 e^{-t/6} \begin{bmatrix} 1 \\ 2 \end{bmatrix} \tag{5-29}$$

To solve this for the constants C1 and C2, remembering our initial conditions: $\bar{m}(0) = \begin{bmatrix}1\\6\end{bmatrix}$ this gives

$$\begin{bmatrix}1\\6\end{bmatrix} = \bar{m}(0) = C_1\begin{bmatrix}-1\\2\end{bmatrix} + C_2\begin{bmatrix}1\\2\end{bmatrix} \quad (5\text{-}30)$$

or

$$\left.\begin{aligned}1 &= -C_1 + C_2\\ 6 &= 2C_1 + 2C_2\end{aligned}\right\} \begin{aligned}C_1 &= 1\\ C_2 &= 2\end{aligned}$$

Plug in to the general equation:

$$m(t) = 1e^{-t/2}\begin{bmatrix}-1\\2\end{bmatrix} + 2e^{-t/6}\begin{bmatrix}1\\2\end{bmatrix} \quad (5\text{-}31)$$

So the solution to the systems is:

$$\text{Row 1} = \bar{m}(t) = -e^{-t/2} + 2e^{-t/6} \quad (5\text{-}32)$$

$$\text{Row 2} = \bar{m}(t) = 2e^{-t/2} + 4e^{-t/6} \quad (5\text{-}33)$$

Remembering that $m_1(t)$ is the amount of salt ion Tank 1 at any time (t) and that $m_2(t)$ is the amount of salt ion Tank 2 at any time (t) if we wish to determine the amount of salt in Tank 1 after 2 hours, we can substitute this in the equation:

$$\bar{m}(2) = 2e^{-2/2} + 4e^{-2/6}\ 1.07\text{kg of salt} \quad (5\text{-}34)$$

The settling of the two tanks can be plotted graphically. Figure 74 shows that the concentration of both tanks decreases over time.

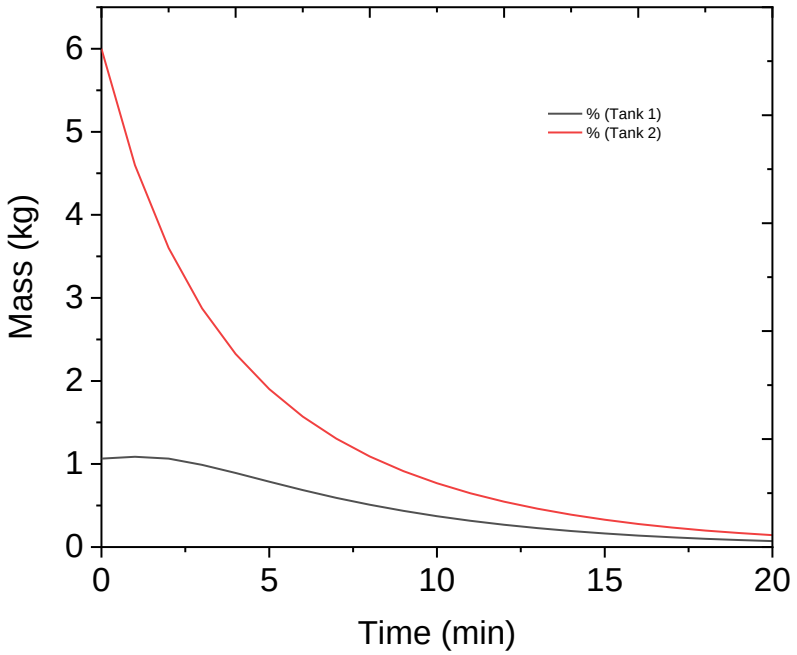

Figure 74: Concentration in tank one within initial concentration of 1 kg of salt and two with initially concentration of 6 kg of salt showing dilution over time

The two tanks relax or settle to zero mass eventually with decay time of 6 minutes.

5.4 Application - aircraft cabin contamination

The configuration of the aircraft contamination problem is shown in Figure 75. The volume of the oil tank within the engine is 20-30 litres (Aircraft Nerd 2009). The concentration of organophosphates within the oil is 3 % (0.372 kg/m^3). We assume flow in, and flow out are equal and that the initial conditions (before air becomes recycled) the air is clean and contains no organophosphates. Air flow through the engine is 0.00025 m^3/min (250 mL/min) as there are two engines this would be 500 mL/min.

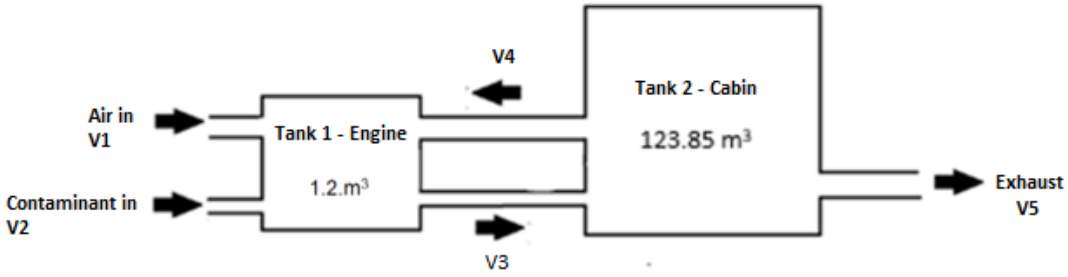

Figure 75: Tank set-up for mathematical model

The rate of change of the mass (mg/m^3) is given by the sum of the flow rate and the density of the of the contaminant. This is given in Equation 5-35. Where Q = flow rate l/min and ρ = density kg/m^3.

$$\frac{d_m}{dt} = \sum Q\rho \qquad (5\text{-}35)$$

If we consider the mass flow through the engines and into the cabin, the mass flow from the cabin back to the engine as well as the mass flow out of the cabin to the exhaust, Equations (5-36) and (5-37) show this process, m_1 is the mass (kg) of the contaminant entering from the engine, m_2 is the mass (kg) of contaminant in the cabin, m_0 is the initial state (no contaminant). $\dot{m}_0$is the rate of supply of the contaminant, treated here as the mean a value over the total time of release. The volume for this solution is in litres.

If we consider that the air is exchanged completely twice in one hour, the rate of gas/ contaminant mixture is 123.85 * 2 per 60 minutes which gives 4.128 m^3/min.

$$\frac{d}{dt}m_1 = -4.128 * \frac{m_1}{1.2} + \frac{4.128}{2} * \frac{m_2}{123.85} + \dot{m}_0 \quad (5\text{-}36)$$

$$\frac{d}{dt}m_2 = 4.128 * \frac{m_1}{1.2} - 4.128 * \frac{m_2}{123.85} \quad (5\text{-}37)$$

This is an inhomogeneous Eigenvalue problem. To solve this, the homogeneous problem must be solved first.

$$\dot{m} = Am + m_0 \quad (5\text{-}39)$$

In matrix form this is equation 5-40.

$$m = \begin{pmatrix} m_1 \\ m_2 \end{pmatrix} = \begin{pmatrix} m_{engine} \\ m_{cabin} \end{pmatrix} \quad A = \begin{bmatrix} -3.44 & 0.0167 \\ 3.44 & -0.0333 \end{bmatrix} \quad m_0 = \begin{pmatrix} \dot{m}_0 \\ 0 \end{pmatrix} \quad (5\text{-}40)$$

The solution to the problem is the sum of the homogeneous and the inhomogeneous parts

$$m = m_h + m_p \quad (5\text{-}41)$$

Using on-line solvers such as Symbolab, the homogeneous problem can be solved easily. The Eigenpairs are:

$$\lambda_1 = -3.46 \quad e_1 = \begin{pmatrix} -0.995 \\ 1 \end{pmatrix} \quad (5\text{-}42)$$

$$\lambda_2 = -0.0165 \qquad e_2 = \begin{pmatrix} 0.00488 \\ 1 \end{pmatrix} \quad (5\text{-}43)$$

The homogenous solution is then Equation 5-44

$$m_h = c_1 e^{\lambda_1 t} e_1 + c_2 e^{\lambda_2 t} e_2 \quad (5\text{-}44)$$

Which becomes Equation 5-45

$$m_h = c_1 e^{-3.46t} \begin{pmatrix} -0.995 \\ 1 \end{pmatrix} + c_2 e^{-0.0165t} \begin{pmatrix} 0.00488 \\ 1 \end{pmatrix} \quad (5\text{-}45)$$

For the particular solution we can use ansatz (an educated guess).

The guess used is $m_p = \begin{pmatrix} x \\ y \end{pmatrix} e^{-t}$ where the constants x, y are unknown. Furthermore, we will formulate the supply of toxin to the engine manifold volume in the same manner – Equation 5-46

(5-46)

$$m = \begin{pmatrix} m_0 e^{-t/10} \\ 0 \end{pmatrix}$$

Where $m_0 \approx 92 \times 10^{-6}$ kg/min and this decreases over a ten-minute interval. This is the initial amount of contaminant in the engine.

Hence

$$\dot{m} = Am + m_0 \quad (5\text{-}39)$$

Therefore giving:

$$-\begin{pmatrix} x \\ y \end{pmatrix} e^{-t} = \begin{pmatrix} -3.44 & 0.0167 \\ 3.44 & -0.0333 \end{pmatrix} \begin{pmatrix} x \\ y \end{pmatrix} e^{-t} + \begin{pmatrix} m_0 e^{-t/10} \\ 0 \end{pmatrix} \quad (5\text{-}47)$$

This is two simultaneous equations (or can be solved as a matrix inversion problem).

$$-xe^{-t} = -3.44xe^{-t} + 0.0167ye^{-t} + m_0 e^{-t/10}$$
$$-y = 3.44x - 0.0333y \qquad \text{(i)} \quad (5\text{-}48)$$

Solving the second equation:

$$y = \frac{3.44}{1 - 0.0333} x = 3.56x \quad (5\text{-}48)$$

$$y = \frac{-3.44}{1 - 0.0333}x = -3.56x$$

$$m_p = x\begin{pmatrix}1\\-3.56\end{pmatrix}e^{-t}$$

And the first simultaneous equation, Equation 5-48(i) gives

$$x = \frac{92 \times 10^{-6}}{-1 + 3.44 + 0.0167(3.56)}e^{0.9t} = 3.68 \times 10^{-5}e^{0.9t} \quad (5\text{-}49)$$

It follows

$$m_p = 3.68 \times 10^{-5}\begin{pmatrix}1\\-3.56\end{pmatrix}e^{-0.1t} \quad (5\text{-}50)$$

The final solution is therefore Equation 5-41 is:

$$m = c_1 e^{-3.46t}\begin{pmatrix}-0.995\\1\end{pmatrix} + c_2 e^{-0.0165t}\begin{pmatrix}0.00488\\1\end{pmatrix} + 3.68 \times 10^{-5}\begin{pmatrix}1\\-3.56\end{pmatrix}e^{-0.1t} \quad (5\text{-}51)$$

Again there are two unknown constants here and the initial values are used to resolve these.

$$-0.995c_1 + 0.00488c_2 = 0.0000552$$
$$c_1 + c_2 = 0.000131 \quad (5\text{-}51)$$

Hence

$$c_1 = -0.00055, \qquad c_2 = 0.000682$$

We have:

$$m = -0.00055e^{-3.46t}\begin{pmatrix}-0.995\\1\end{pmatrix} + 0.000682e^{-0.0165t}\begin{pmatrix}0.00488\\1\end{pmatrix} + 3.68 \times 10^{-5}\begin{pmatrix}1\\-3.56\end{pmatrix}e^{-0.1t} \quad (5\text{-}52)$$

We only want the cabin = row 2.

$$m = -0.00055e^{-3.46t} + 0.000682e^{-0.0165t} - 0.000131e^{-0.1t} \quad (5\text{-}53)$$

The solution in Equation 5-53 can be plotted graphically as seen in Figure

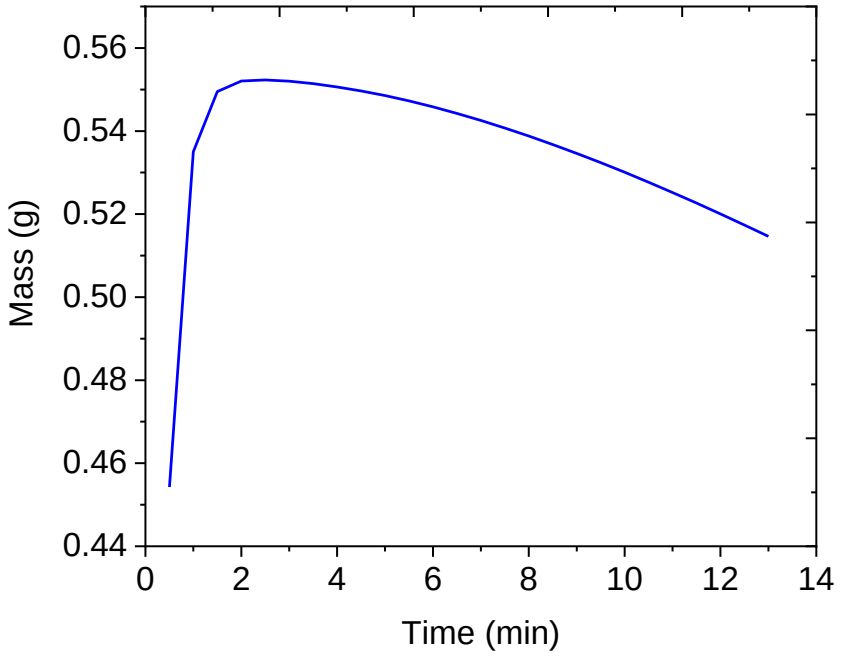

Figure 76: Temporal evolution of contaminant mass within the BAe 146 aircraft cabin using the two-tank approximation

This is a dynamical model with three transient processes on the right-hand side. The first two terms arise from the homogeneous part of the eigenvalue problem. These represent the recirculation between two volumes.

$$\tau_1 = \frac{1}{3.46} \approx 17 seconds$$
$$\tau_2 = \frac{1}{0.0165} \approx 61\ minutes \quad (5\text{-}54)$$
$$\tau_3 = \frac{1}{0.1} \approx 10\ minutes$$

The first-time factor of 17 seconds is when the contaminant is rapidly dispersed into the cabin, this gives the smell associated with fume events, as the peak level of contamination is achieved. The second time factor is for a slow distribution and removal over an hour. Notably the levels have dropped significantly after 10 minutes. The third time factor is the time during the flight that the contaminant is released into the cabin, this is an input

parameter. No more contaminant is being supplied, but the original supply has dispersed around both the cabin and the engine.

Figure 76 shows that initially there is a higher level of contaminant supplied to the aircraft cabin 0.55 grams. After 2 minutes the level of contamination being injected into the cabin decreases. After 5 minutes contamination levels are lower and would not cause significant. The timescales of 1 and 2 depend on the rate of air changes within the cabin. Timescale 3 was a chosen value.

5.5 Summary of mathematical model

The mathematical model has shown how it can be used to represent a real process such as combining solutions in chemistry (Bhopale 2019), fertilizer irrigation tanks or water storage plants (Mott 2020). Initially the mathematical solution for a one tank problem was shown, illustrating the contaminant flowing into a tank with an outlet flow equalling the flow entering. The mathematical model has been widely established and agreed on (Bronson et al. 2022).

As the problem in this research is more complicated than a one tank flow, the mathematical problem was developed to understand two tank flow problems (horizontal and vertical flow). The mathematical problem showed as the level of contaminant in tank 1 increased initially by a small amount, tank 2 starts with a high concentration but both tanks after a period of time level off and reduce the concentration (Figure 74).

If we consider the application the aircraft cabin environment it can be seen in Figure 76 how the levels of contaminant would change over time.

The mathematical model showed that significant amounts of contaminant such as TCP would get into the aircraft cabin. There would be a significant peak at the start of the flight which would tail off as the flight proceeded. This is what was expected. Studies have shown it is the initial stages of flight that are greatly affected by fume events. The occupational exposure limits for TCP are 0.1 mg/m^3 (New Jersey Department of Health 2015) as can be seen the mathematical model is showing 0.55 g entering the cabin within

the first two minutes. This is throughout the whole of the cabin area so 0.004 mg/m^3 this is below the threshold limits. Whilst this is below limits, continued exposure at this level over several flights would impact health.

As the air is entering the cabin via ceiling high vents the distribution of the particles needs to be analysed to determine the concentrations within the cabin in different areas as this 0.55 g will not initially be distributed uniformly throughout the cabin. To determine the flow path of the particles numerical simulations were conducted, this analysis is found in Chapter 6.

The mathematical model can be developed in a number of ways such as solving by integrating factors method (which uses matrix exponentials) but the principal sensitivity is the numbers used within the input.

For future work this could include analysis of different aircraft which would have different air supply rates, different air exchange rates and linked with numerical modelling could then determine exposure of one occupant at a particular location.

Chapter 6 Computational Fluid Dynamics

This chapter introduces the subject of computational fluid dynamics (CFD) and opens with an introduction to fluids and the complexity of fluid dynamics. It continues with an introduction to CFD simulations. A description of the Fire Dynamics Simulator (FDS) software which is the chosen software for this study. This chapter also includes a parametric study which was made to determine the FDS parameters for the validation study.

The aim of the presented numerical methodology is to determine the of the currently available CFD tools to accurately predict the airflow and particle distribution within aircraft cabins. This research has developed a dedicated numerical model where specific toxic species have been injected into the aircraft cabin. The model has been implemented in the CFD code and has been validated against available experimental measurements. A detailed review of grid resolution has enabled a grid sensitivity study to consolidate model and computer accuracy. Appropriate choice of model geometry, grid resolution and boundary conditions are essential and may define the analysis outcome. In order to test these uncertainties, the grid sensitivity analysis conducted, and the simulation details are discussed in this chapter.

6.1 Introduction to Computational Fluid Dynamics

Computer modelling has been used extensively for a number of years to model environmental conditions within buildings (Nielsen 1975, Guan Heng Yeoh 2009). These studies have analysed factors such as air flow and velocity profiles as well as thermal analysis both for building insulation properties and occupant comfort. CFD software uses numerical algorithms to solve equations which describe the motion of fluids (Guan Heng Yeoh 2009). CFD is a tool for generating solutions for fluid flows with or without solid interaction.

CFD is a computer based mathematical modelling tool which analyses fluid flow under varying conditions. It is extensively used throughout the engineering industry and is

recognised a valid, cost effective and beneficial tool. CFD tools can provide a vast array of information regarding the characteristics of fluid flow developing within a specified system.

CFD calculations are based on solving fundamental mathematical fluid flow equations, namely the conservation of mass, momentum and energy. These equations form the Navier-Stokes (N-S) equations which are a set of partial differential equations which are extremely difficult to solve analytically. CFD gives values of the flow quantities at a large number of locations within the system. This allows a greater understanding of the way the fluid will interact with the obstacles within its flow path and can be applied to both laminar and turbulent flow. The area of interest is divided into many small volumes, where the equations are discretised into algebraic equations.

CFD are utilised when engineers are interested in predicting the dynamic behaviour of systems to understand the relationship between the system variables. Within the field of fluid dynamics, this was originally performed by using a large number of complex partial differential equations. These equations can now be numerical modelled using computer simulation.

The purpose of flow simulations is to determine how the flow of the fluid of interest interacts with surroundings, given different inlet and outlet flows, or boundary conditions.

6.1.1 Introduction to Fire Dynamics Simulator Software

There are a number of commercially available modelling software but due to the extensive use of FDS software, this has allowed it to be validated for use within a number of different scenarios. FDS is predominantly used to model the development of fire scenarios. FDS has been used extensively for other applications such as particle distribution and deposition (McGrattan et al. 2022). Aerosol deposition is determined by applying an empirical deposition velocity to aerosols near surfaces. The model takes into account the effects of a temperature gradient, gravitational settling and turbulent deposition

(McGrattan et al. 2022). Each mechanism is determined separately and then combined to determine the total deposition.

FDS code is a CFD tool, developed by NIST in 2000, to enable the study and analysis of fire dynamics. It is aimed at solving practical fire problems within fire engineering (McGrattan et al. 2022). FDS code numerically solves a form of the Navier-Stokes equations appropriate for low-speed thermally driven flows, with emphasis on smoke and heat transport from fires. Development of FDS has also enabled aerosol particle deposition, velocity and flow patterns.

FDS is an open-source code (Version 6.7.9) has been used to determine the particle flow within the aircraft cabin and quantify particle concentrations. A graphical user interface (Pathfinder Version 2022.2.0803) has been used to aid visualisation within FDS.

The core algorithm of FDS is an explicit predictor-corrector scheme, second order accurate in space and time. Turbulence is treated by using Large Eddy Simulation (LES approach). Particles are Lagrangian particles which can be assigned a set of surface properties. Partial derivatives of the conservation equations of mass, momentum and energy are approximated as finite difference and the solution is updated in time on a three-dimensional, Cartesian grid (McGrattan et al. 2022).

Development of FDS has been undertaken since its first iteration in 2000. Rehm and Baum (1978) originally determined the form of the Navier-Stokes equations now utilised within FDS and describe the low-speed (often referred to as low-Mach) motion of a gas driven by chemical heat release and buoyancy forces. The governing equations for CFD modelling are Reynolds-averaged form of the Navier-Stokes equations (RANS), in particular the k-ε turbulence model pioneered by Patankar and Spalding.

FDS has been utilised to simulate the airflow within an aircraft cabin and therefore the particle distribution. FDS is predominantly used to model the development of fire scenarios but can include aerosol flow paths and deposition. Aerosol deposition is determined by applying an empirical deposition velocity to aerosols near surfaces. The model takes into account the effects of a temperature gradient, gravitational settling and

turbulent deposition. Each mechanism is determined separately and then combined to determine the total deposition.

The equations governing the evolution of a low-Mach, variable density fluid are continuity, species concentration, momentum, energy and the ideal gas equation of state - Equation 6-1 to 6-5 (McGrattan et al. 2022)

$$\frac{\partial \rho}{\partial t} + \nabla \cdot (\rho u) = 0 \quad (6\text{-}1)$$

$$\frac{\partial \rho Y_a}{\partial t} + \nabla \cdot (\rho Y_a u) = \nabla \cdot (\rho D_a \nabla Y_a) + \dot{m}_a^{'''} \quad (6\text{-}2)$$

$$\frac{\partial \rho u}{\partial t} + \nabla \cdot (\rho u u) = \nabla \tilde{p} - \nabla \cdot \tau + (\rho - \rho_{amb}) g \quad (6\text{-}3)$$

$$\frac{\partial \rho h_s}{\partial t} + \nabla \cdot (\rho h_s u) = \frac{D\bar{p}}{Dt} + \dot{q}^{'''} - \nabla \cdot \boldsymbol{q}^{'''} \quad (6\text{-}4)$$

$$\rho = \frac{\bar{p}\bar{W}}{RT} \quad (6\text{-}5)$$

In the above equations ρ is mass density, u is the velocity, Y_a is the mass fraction of species a, $\rho D_a \nabla Y_a$ is the diffusive mass flux of a and $\dot{m}_a^{'''}$ is the reaction source term. In momentum equations τ is the deviatoric stress sensor, h_s is the sensible enthalpy per unit mass, $\dot{q}^{'''}$ is the heat release rate per unit volume and $\boldsymbol{q}^{'''}$ is the heat flux vector. The ideal equation of state (equation 6-5) is based on the thermodynamics background pressure $\bar{p}$, the perturbation of pressure that drives the fluid motion, $\bar{p}$, the mixture molecular weight, $\bar{W}$, the temperature, T and the ideal gas constant, R.

NIST continuously evaluate FDS and add new capabilities. Most of these efforts are focused on increasing the model's ability to predict the transport of heat and exhaust products from a fire through and enclosure (McGratten et al. 2022). Recently other aspects for fire dynamics such as fire growth, flame spread, suppression, sprinkler and detection activation have also included and improved.

FDS has been formally and extensively validated by its developers (McGrattan et al. 2022).

6.1.2 Computational Grid

The size of the numerical grid is an important factor when running simulations. This is normally best determined in relation to the size of the fire. Typically, the smaller the fire size the smaller the cell size should be in order to adequately resolve the fluid flow and fire dynamics.

This is normally determined using the following equation:

$$Q^* = \frac{\dot{Q}}{\rho_\infty C_p T_\infty \sqrt{g} D^{5/2}} \qquad (6\text{-}6)$$

Where $\dot{Q}$ is the heat release rate, ρ_∞ is the ambient density, C_p is the specific heat , T_∞ is the ambient temperature and *g* is the acceleration due to gravity.

Since there is no fire source, a grid sensitivity analysis has been performed as part of this work.

6.2 Numerical Simulation of Air Flow and Particle Distribution

Lagrangian particles are used in FDS to model small objects such as water, liquid fuel droplets, tracers or other particles of interest, with individual parameters, including droplet size distribution and material properties. The functionality of Lagrangian particles also included heat transfer and pyrolysis models. Some particles can be given a defined mass, diameter and shape.

The movement of Lagrangian particles over the course of a time step is calculated using an analytical solution and remains stable regardless of the time step used by the flow solver. However, if the particle moves over the width of several grid cells in a single time step, the momentum transferred between the particle and the gas cannot be allocated properly to all of the affected cells. To overcome this problem, FDS subdivides the gas phase time step based on each particle's velocity (McGratten et al. 2022).

Lagrangian particles can be used to represent a wide variety of objects that are too small to resolve on the numerical grid. FDS considers three major classes of Lagrangian particles: massless tracers, liquid droplets, and everything else. Particles are introduced into the calculation in several different ways: they may be introduced via a sprinkler or nozzle (liquid droplets are usually introduced this way), they may be introduced at a blowing vent or burning surface (mass tracer particles or particles representing embers are usually introduced this way), and they may be introduced randomly or at fixed points within a designated volume -solid particles that represent subgrid-scale objects are usually introduced this way(McGratten et al. 2022).

In studies where particles are not considered massless, particles can be considered as either solid or liquid.

If a liquid particle is to be studied properties of the liquid and the resulting gas have to be included, including thermal properties of the substance. By default, liquid droplet evaporation uses the Ranz-Marshall correlation. Ranz and Marshall performed a set of droplet evaporation experiments which ultimately led to the development of the Nusselt and Schmidt number correlations for droplet. These experiments have been modelled effectively in FDS.

The size distribution of liquid particles is specified using a cumulative volume fraction, the default setting is “Rosin-Rammler-Lognormal” as is shown in equation 6-7.

$$F(D) = \begin{cases} \frac{1}{\sqrt{2\pi}} \int_0^D \frac{1}{\sigma D'} \, exp\left(- \frac{\left[In\left(\frac{D'}{D_{v,0.5}} \right) \right]^2}{2\sigma^2} \right) dD' & (D \le D_{v,0.5}) \\ 1 - exp\left(-0.693 \left(\frac{D}{D_{v,0.5}} \right)^{\gamma} \right) & (D > D_{v,0.5}) \end{cases} \quad (6\text{-}7)$$

Solid can be used to represent a wide variety of material, from office clutter to vegetation. The thermophysical and geometric properties of the particle must be defined. Particle shape must also be defined, by default this is monodisperse spherical. Diameter distribution can be specified.

6.2 Numerical Studies of Particle Deposition and Flow

CFD models provide effective solutions to physical phenomenon involving fluid flow an particle movements in several different environments, including aircraft cabins. A number of experimental studies have been conducted to determine particle flow and distribution within aircraft cabins, these then can be recreated within FDS to validate the simulation used.

A number of numerical studies dedicated to the contamination transport of pathogens within hospitals have been conducted (Dunn et al. 2005). Analysis of air flow around the external surface of an aircraft have also been studied for decades. Recently the capacity to study airflow, velocity and particle distribution has been utilised in analysing the environmental conditions within aircraft cabins, analysing ventilation, thermal comfort and possible airborne contamination.

A number of studies have been conducted, some of which have been summarised in Table 18. Benji et al. (2017) used FDS to predict water spray patterns ejected from nozzles at a pressure of 750 kPa with a flow rate of 0.084 lpm, determining that grid size is influenced by particle diameters. Bellas et al. (2020) used FDS to model water mist extinguishing systems within a ship environment. The simulation results are compared to data from full-scale tests conducted at recognized fire testing laboratories. A good agreement was found between the compartment temperature evolution and fire extinguishing time for the modelled fire scenarios. Wadhwani et al. (2017) used FDS to model the transport of short-range fire brands. Uniform, non-combusting cubiform and cylindrical firebrands are projected using the firebrand generator. The experimentally observed distribution of particles on the ground is compared with a simulated distribution using the fire dynamic simulator. The results show that the existing Lagrangian model gives a good agreement with the experimental data.

These three cases illustrate the varied use of FDS and the inclusion of particles distribution in the form of water mist or fire brands. This shows that FDS is suitable to be used for simulating the distribution of oil particles as part of this study.

Table 21: FDS numerical studies on airflow and particle distribution

Reference	Title	Short description	Particles	Predictions
Beji T et al. (2017)	Influence of particle injection rate, droplet size distribution and volume flux angular distribution on the results of computational time of water spray CFD simulations	Water spray patterns using CFD.	Water	Grid size is influenced by particle diameter.
Bellas R et al. (2020)	Assessment of Fire Dynamic Simulator for modelling fire suppression in engine rooms of ships with low pressure water mist	Water based fire extinguishing systems – use of simulation tools (FDS)	Water mist, diesel and heptane	Simulation showed good agreement with experimental studies.
Wadhwani R et al. (2017)	Verification of a Lagrangian particle model for short range fire brand transport	Modelling of short-range fire brands travel patterns in wildfires	Fire brands	Successful representation of the firebrands was shown, transport dynamics was determined illustrating that the Lagrangian particle model of FDS was capable of simulating transport of non-burning solid firebrands accurately.

CFD can be used in simulating and predicting changes in these environmental factors. CFD uses numerical methods and algorithms to solve partial differential equations to analyse problems that involve detailed fluid flow developing within a compartment. CFD can be utilised to determine air flow and therefore potential airborne contaminations within the aircraft cabin environment. This has prompted the development of a numerical methodology specifically aimed at providing an in-depth tool and analysis of toxic particle flow and distribution within an aircraft cabin.

It is important to understand how particles move and deposit on surfaces within an aircraft cabin to determine the exposure to the occupants. Several studies have looked at release of noxious material or biological pathogens as well as ventilation within an aircraft cabin using simulation software to determine the deposition rates or flow patterns (Aboosaidi et al., Gao et al., Pan et al., Sing et al., Talaat et al. and Zhang et al.).

Wang et al. (2011) simulated the deposition of particles within a mock-up of an aircraft cabin using ANYSYS FLUENT software. The mock-up was a four-row twin aisle seating arrangement, with 28 seats. The air flow rate was 0.23 m^3/s. Three particle diameters of 0.7, 10 and 100 µm were studied. Particle release was either slow (representing occupants breathing) or faster (representing occupants coughing). This study found that the distribution of particle deposition onto surfaces depended on particle size and particle velocity. At the higher release velocity, particle velocity increased by 14% for the 0.7 and 10 µm. The larger particles size all particles were deposited at both release velocities (Wang et al. 2011).

Zhang et al. (2013) used ANSYS/CFX to model contaminant (SARS) distribution within an Airbus 320 aircraft cabin. Inlet air velocity was 2.6 m/s. As can be seen in Figure 77 air enters the aircraft cabin at the top of the luggage cabin and flows downward. A large fraction of air flows out through outlets at the bottom of the right-side wall. A small fraction of air remains in the cabin and creates some circulated loops above the passengers on left side as shown in Figure 77.

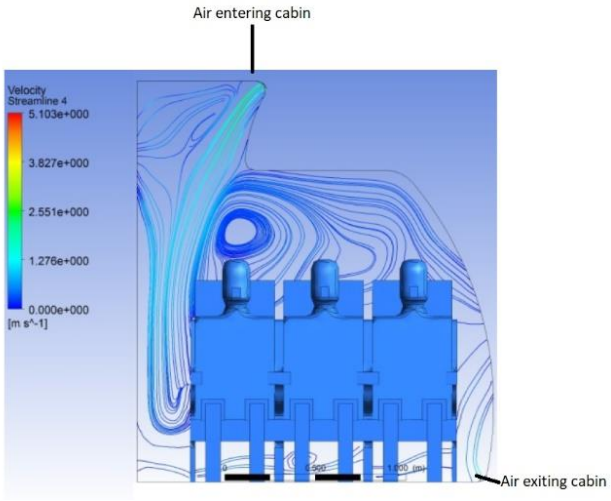

Figure 77: Cross-plane velocity streamlines (Zhang et al. 2013)

Figure 77 shows the flow field of the contaminant (in this case SARS) within the aircraft cabin. One passenger sitting in the middle of the first-row breaths out contaminated air. As can be seen in Figure 78 the highest concentration is around that passenger and spreads out to other passengers (Zhang et al. 2013).

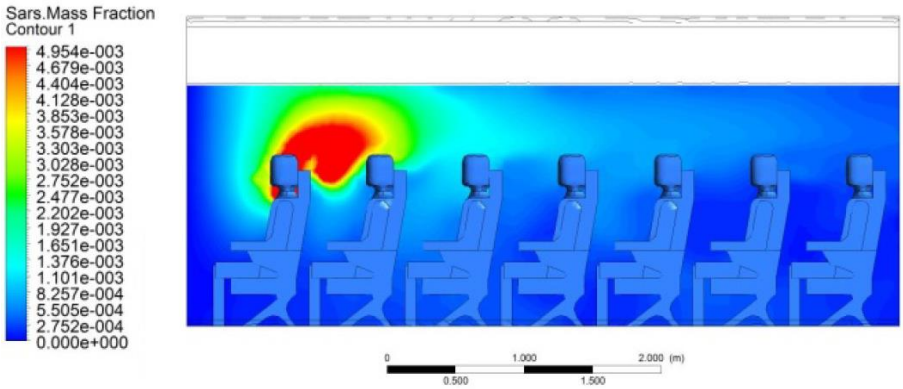

Figure 78: Flow field of contaminant (SARS) (Zhang et al. 2013)

This study shows the ease with which contaminated particles can move around an aircraft cabin due to the circulation paths of the incoming and outgoing air stream.

Beneke et al. (2010) created a test chamber representing 11 rows of a Boeing 767 aircraft cabin. The dimensions were 9.6 m long from front wall to the rear wall, 4.7 m wide at widest point (above armrests). Ventilation in this chamber is via blowers, heater, chiller and filter (similar to those in building) 660 l/s of air at 16 °C. 100% outside air, 18 cfm for each of the 77 seats, humidity was not controlled. Air enters through diffusers the lengths of the cabin at ceiling height (165 mm) on either side of the centreline. The exhaust was via 127 mm opening at the base of exterior walls. Talcum powder was used to illustrate the fine particles. The particles were 0.87-1.70 μm and injected using compressed air across the width of the cabin via 7 injection points (one in each of the seats in the second row), as illustrated in Figure 79. Particle's measurements were made at 27 locations the centreline of the cabin across rows 4 and 7 and then various seats in rows 1, 3 and 5. Figure 79 shows the overhead view of the test cabin. Seats marked with stars represent the injection locations and those marked with an X represent the location where measurements were taken.

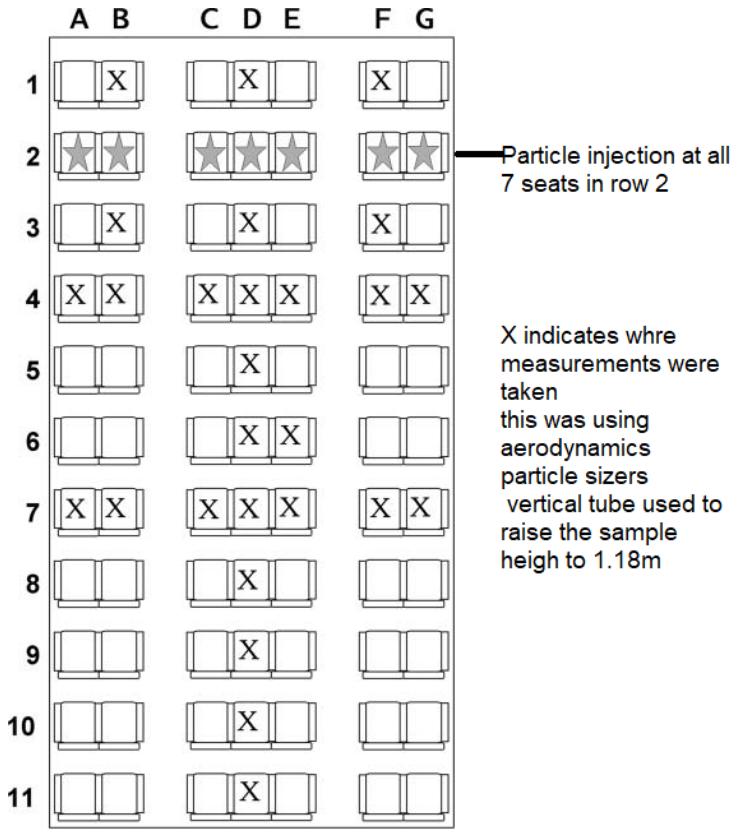

Figure 79: Injection points (Benzeke 2010)

The data collected provided two different views of particle dispersion within the cabin. Firstly, the total exposure analysis looked at the average total number of particles at the 27 locations, secondly looked at particle counts at each location relative to a reference location during the same test. Table 22 illustrates the particles at different seat locations. As the table indicates those seats nearest the injection point have the highest contamination. As can be seen those farthest away in the centre of, the aircraft received the lowest contamination.

Table 22: Numerical investigation of airflow inside a BOEING 737 (Benzeke et al. 2010)

Average Particle Counts							
	A	**B**	**C**	**D**	**E**	**F**	**G**
1	-	15,687	-	13,538	-	17,400	-
2	-	-	-	-	-		-
3	-	-	-	-	-	10,471	-
4	3187	-	6168	-	8192	7587	6951
5	-	-	-	-	4576	-	-
6	-	-	-	2094	-	-	-
7	1442	1087	1067	2068	-	1317	1437
8	-	-	-	956	-	-	-
9	-	-	-	837	-	-	-
10	-	-	-	736	-	-	-
11	-	-	-	397	-	-	-

6.3 Airflow and Particle Distribution Investigation inside a Boeing 737

In this section the relevant data from a numerical analysis of the air flow and particle distribution inside a Boeing 737 are presented. The aim is to validate the use of FDS for use in the current study by performing a grid independence study and using different turbulent models. Experimental data from You et al. are used to validate the numerical model developed.

6.3.1 Reference Case: You et al. (2016)

An experimental study by You et al. (2016) was chosen as the reference scenario. This study was chosen as the experimental mock up examined velocity profiles within an aircraft cabin as well as particle distribution, which is relevant to this research. You et al. (2016) created a full-scale mock-up, see Figure 80, of half a row of a single aisle recreation of a Boeing 737. This was 3.5 m wide x 0.9 m deep x 2.2 m high. Airflow entered the cabin at ceiling level and exhausts were located on the right side of floor

velocity. Airflow was 1.44 m/s. Gaspers used to supply air, 1.2 l/s inlet area of 33.4 m^2. Total airflow was 27.1 l/s. To simulate the presence of a person a human simulator was created in the centre of the mock-up emitting 75 W. Particles with a diameter of 1- 2 µm entered the cabin aircraft and were measured using particle image velocimetry (PIV) and hot-sphere anemometers.

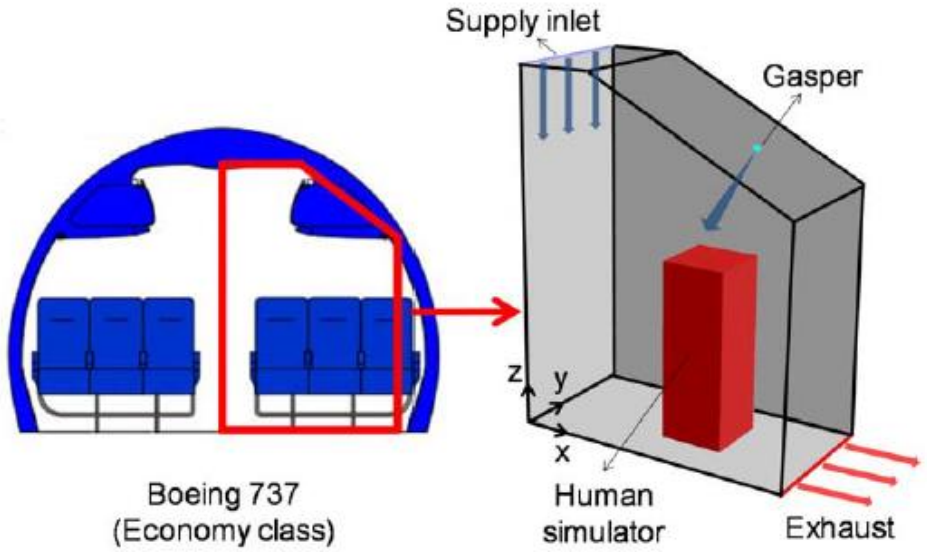

Figure 80: Experimental mock-up of air supply and exhaust location (You et al. 2016)

This investigation measured the airflow within the aircraft cabin mock-up, using a gasper to inject particles into the cabin. PIV techniques was used to obtain high resolution distribution of the airflow.

The airflow field in this section of the cabin mock up is shown in Figure 81. This figure shows the air flow from the amin supply vent (blue line in Figure 81) flows directly downwards past the first seat and then rotates towards the centre and window seats. Figure 81 shows there is little impact form the gasper induced airflow.

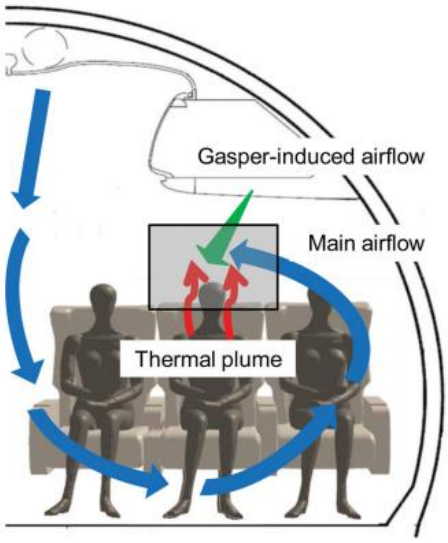

Figure 81: Experimental set up and air flow paths

6.4 Validation

Validation of computer simulation models has been conducted during the development of the simulation model to ensure that the results presented are accurate and credible. Using velocity and temperature data presented by You et al. (2016) from the cabin mock-up experiment, the computer simulation used in this research has been validated. You et al. (2016) collected data using 15 hot sphere anemometers (HAS). These we located in three lines at varying heights as shown in Figure 82.

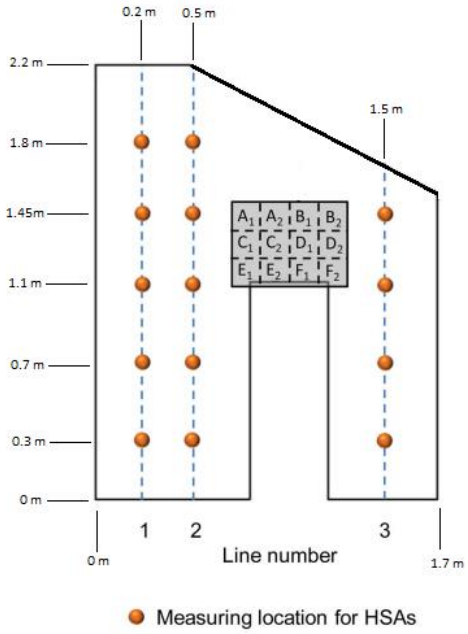

Figure 82: Location of HSA devices

You et al. (2016) experimental data showed that the gasper flow had little impact on the velocity profiles and data measured by the HSAs therefore this data was suitable to use in verification of the intended numerical model for this research. You et al. (2016) determined the average velocity profile for each of the three lines indicated on Figure 82. The location of the devices was replicated in the numerical simulation for this research.

The geometry of the simulation matched that from the experiments conducted by You et al. This consisted of a simplified full-scale mock-up of half of a one-row, single-aisle aircraft cabin with dimensions of 1.75 m in width (x), 0.9 m in depth (y), and 2.2 m in height (z), as shown in Figure 83. Air flow into the cabin was via an inlet vent at the top of the cabin, air flow was 1.44 m/s. The gaspers situated on the sloping roof injected the particles with an average diameter of 100 µm.

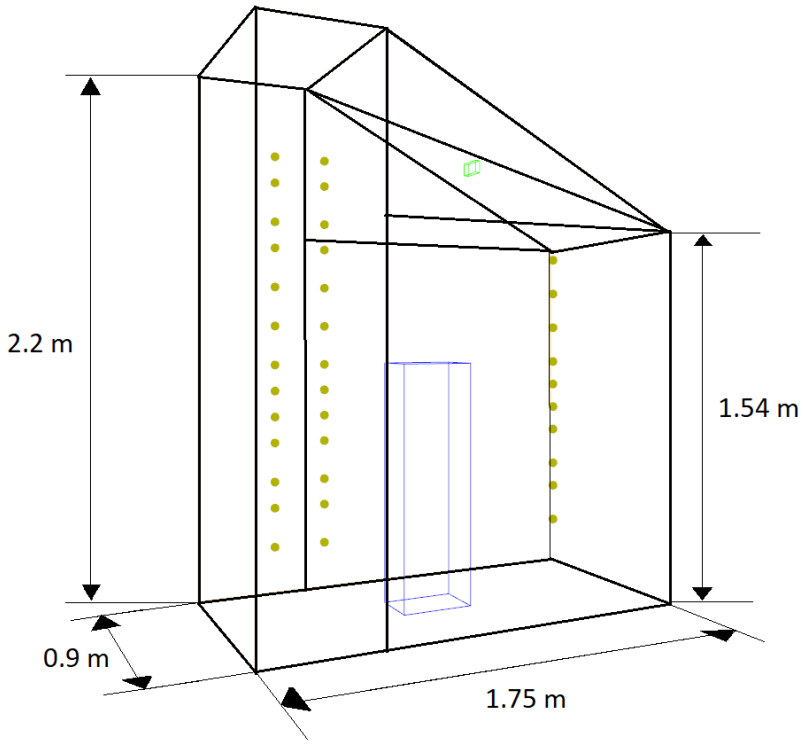

Figure 83: Geometry of numerical model

The numerical model was run with devices in the same vertical lines as in the experimental set up, but additional devices were included at different heights from 0.3 m to 1.8 m, as shown in Figure 84. The additional data captured allowed for a reliable trend line to be produced.

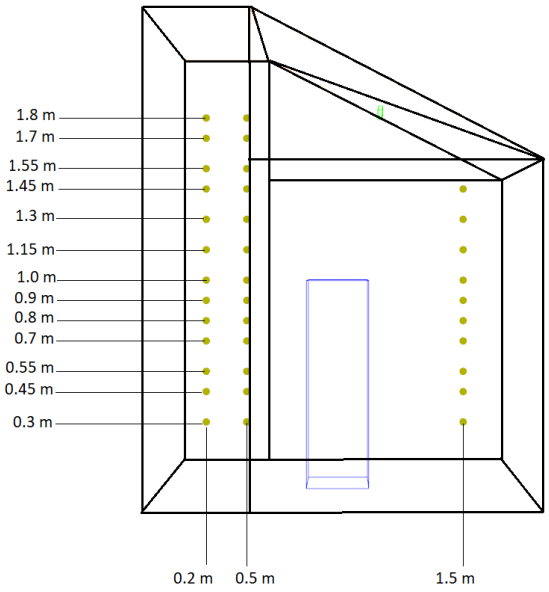

Figure 84: Location of velocity and temperature devices

Numerical simulations were completed with the parameters as indicated in Table 20.

Table 23: Parameters of numerical validation

Simulation name	Gird Size	VLES /LES	Duration	Number of computational cells
Simulation 1	0.03*0.03*0.03	VLES	1000s	129,600
Simulation 2	0.03*0.03*0.03	LES	1000s	129, 600
Simulation 3	0.02*0.02*0.02	VLES	1000s	437,400
Simulation 4	0.015*0.015*0.015	VLES	1000s	1, 080, 000

Four different numerical models have been conducted. In simulations 1, 3 and 4 the effect of the grid size has been investigated. The results showed particle velocity was independent of grid size. In simulations 1 and 2 the effect of the different turbulent models has been investigated. VLES stands for Very Large Eddy Simulation and LES stands for Large Eddy Simulation from the FDS user guide. These modes govern a number of physical and numerical parameters that determine the level of physics and the accuracy of the numerical model. Simulations 1 and 2 showed the different turbulent models had no effect on particle velocity.

The velocity data from the numerical simulation has been plotted alongside the data from the experiment conducted by You et al. (2016) and can be seen in Figure 85 below.

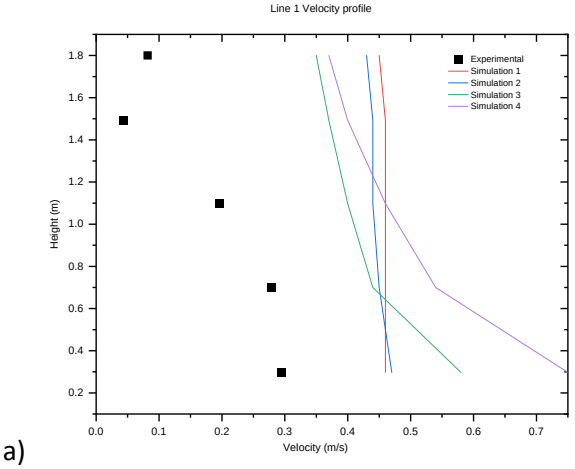

a)

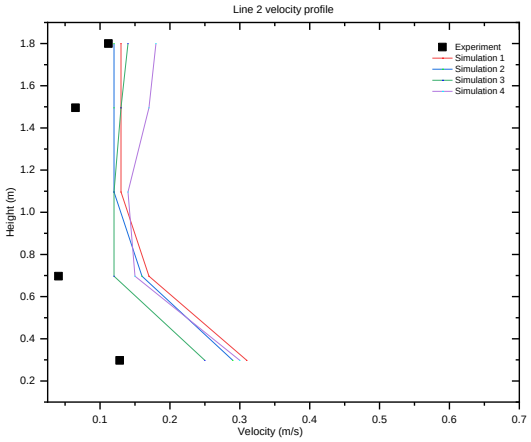

b)

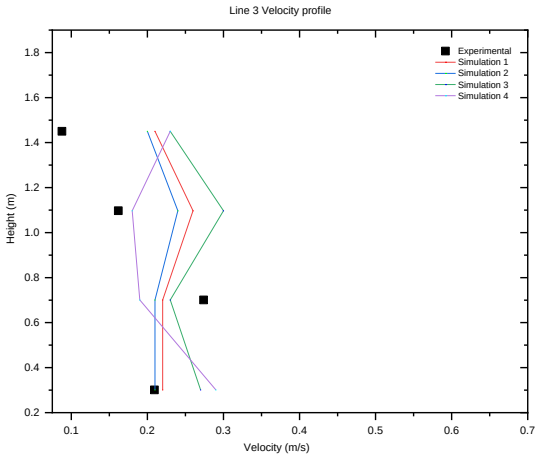

c)

Figure 85: Experimental correlation with simulated data a)line 1 at 0.2m b)line 2 at 0.5 m c)line 3 at 1.5 m

Figure 85a, b and c show good correlations between the simulations and the experimental data. Figure 85a represents velocity profile data for Line 1 located below the air inlet at 0.2 m (see Figure 82) this represents the centre of the cabin. Simulations 1 and 2 show good correlation indicating that the turbulence model used – either VLES or LES – does not affect the velocity of the particles. Increasing the number of computational cells (decreasing the grid size) as in simulations 3 (number of cells 437, 400) and simulation 4 (number of cells 1, 080, 00) showed that this had little effect on the velocity of the particles. These 2 simulations showed good correlation between each other. There was a slight deviance between these 2 simulations and simulations 1 and 2 below 0.7 m. At 0.7 m simulations 1 and 2 showed a velocity of 0.46 and 0.57 m/s respectively whilst simulations 3 and 4 showed an increase in velocity to 0.58 and 0.75 m/s respectively. As indicated by You et al. (2016) this lower region in Line 1 was greatly affected by the main air supply (see Figure 81), the reduced grid size gave a more accurate prediction of the velocities in this area. The trend of the simulations corresponds with the trend observed in the experimental data.

Line 2 which is located further to the right of the mock up cabin (see Figure 82) also shows good correlation between experimental and simulated data as shown in Figure 85b. Similar trends were observed between the experimental data and simulation data. Higher velocities were observed at 0.3 m for the experimental and simulation data. Experimental observed values of 0.13 m/s, simulations 1 to 4 observed values of 0.31, 0.29, 0.25 and 0.3 respectively.

Line 3 which is near the “window” side of the aircraft at 1.5 m (see Figure 82), showed good correlation between simulations 1, 2 and 3 as seen in Figure 85c. Figure 85c shows that the general trend of the experimental data matches that of simulations 1, 2 and 3. Simulation 3 as can be seen in Figure 85 gave the best correlation with the experimental data in all 3 positions and the parameters within in this model will be used for the initial simulations for this research.

Line 2, the middle of the experimental space and look at the velocities measured at 1.8 m high for simulation 3 this was 0.1 m/s for the experimental study this was 0.11 m/s giving a 10% error.

Figure 86 compares the simulated and measured velocities for line 1 and 2. Error bars indicate the percentage error for the values this ranges from 10% to 50%.

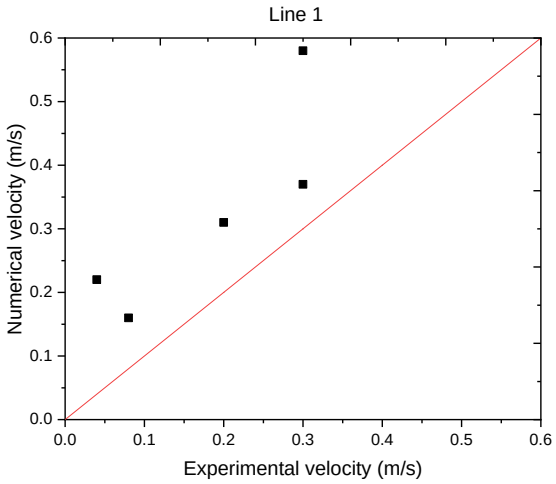

a)

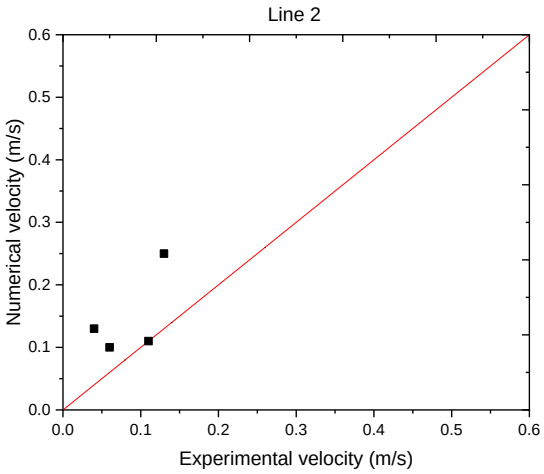

b)

Figure 86: Comparison of simulated and experimental velocity data for a)Line 1 b)Line 2

The correlation between the experimental data and the simulation data is due to the similarities in the flow paths within the geometries. Figure 87a shows the flow paths determined during the simulations, this closely resembles the flows paths determined by You et al. (2016) in the experimental data. Both experimental and simulated images show air flowing in from the inlet and flowing vertically downwards with some circulation loops created to the side of the simulated occupant. You et al. (2016) found that the gasper jet had little impact on the airflow pattern, this is shown in Figure 87b. Figure 87a provides a visualisation of simulation 4 at 300 seconds, this figure shows the flow path from the gasper jet has little impact on the flow path from the main supply in the simulations.

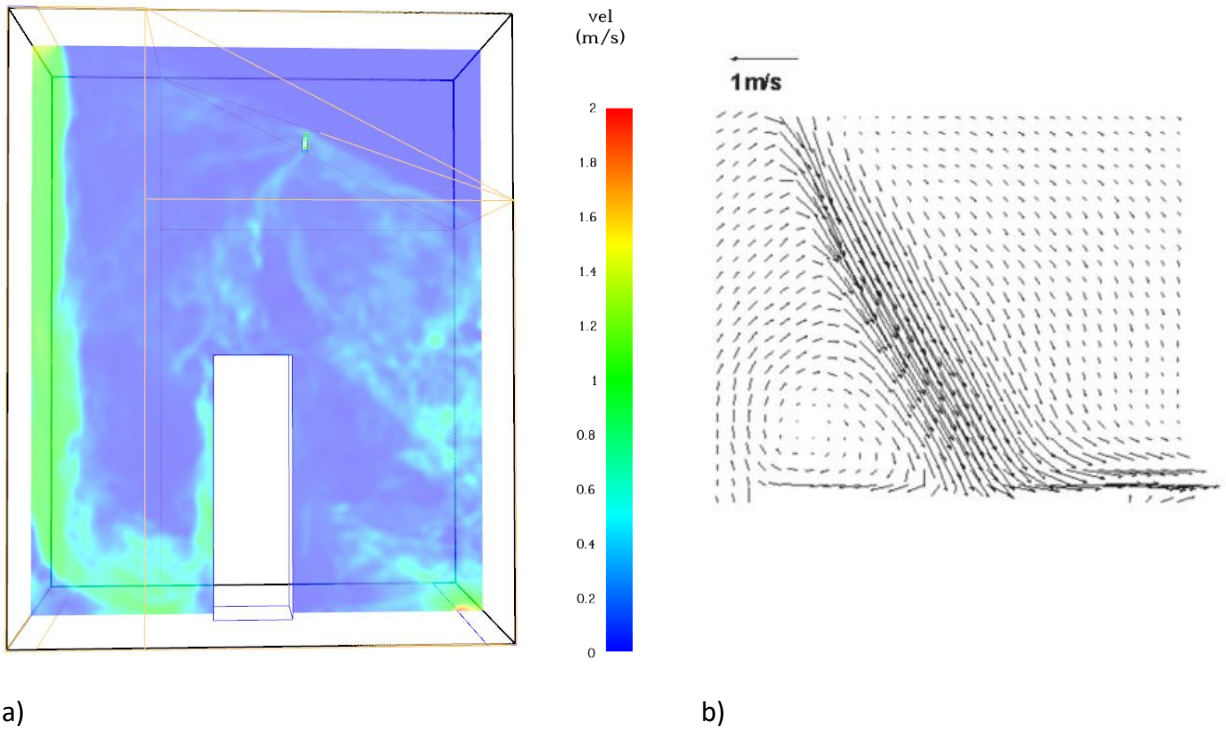

Figure 87: Flow path from a) numerical simulation at 300 seconds and b) experimental

Airflow into from the ceiling supply vent is 1.44 m/s as can be seen on the Figure 87 (green on the scale). Figure 88 shows the velocity profiles of simulation 4 at 50, 100, 250, 500, 750 and 1000 seconds

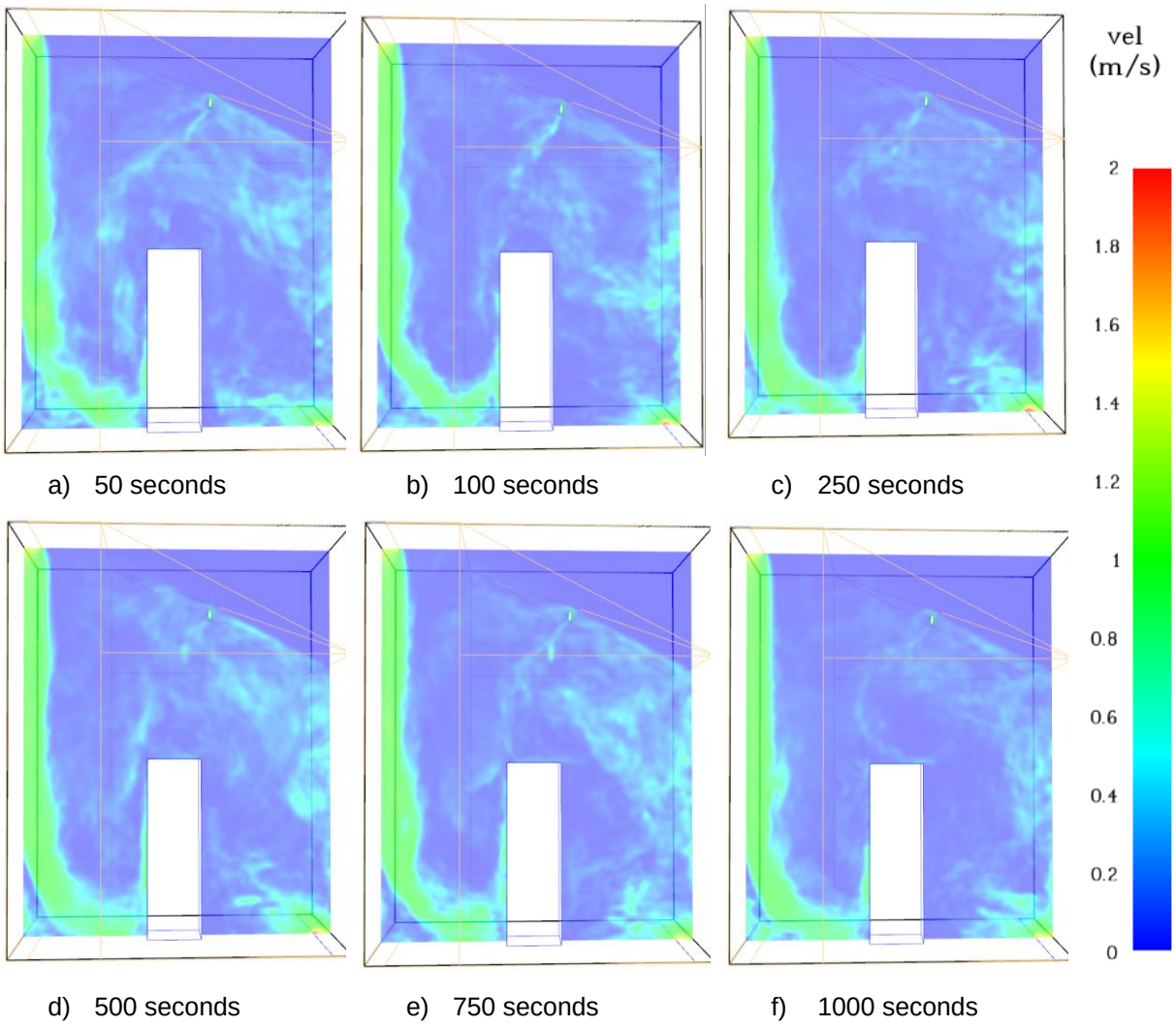

a) 50 seconds b) 100 seconds c) 250 seconds

d) 500 seconds e) 750 seconds f) 1000 seconds

Figure 88: Velocity profile for simulation 4 at a)50 seconds, b) 100seconds, c) 250 seconds, d) 500 seconds, e) 750 seconds and f) 1000seconds

The green particles are injected at the gasper location and can be seen to follow the flow path of the air, falling vertically and then recirculating in the airflow as indicated in Figure 88. Figure 89 shows the particle flow paths at 50, 100, 250, 500, 750 and 1000 seconds. As can been seen some particles exit with the outflowing air.

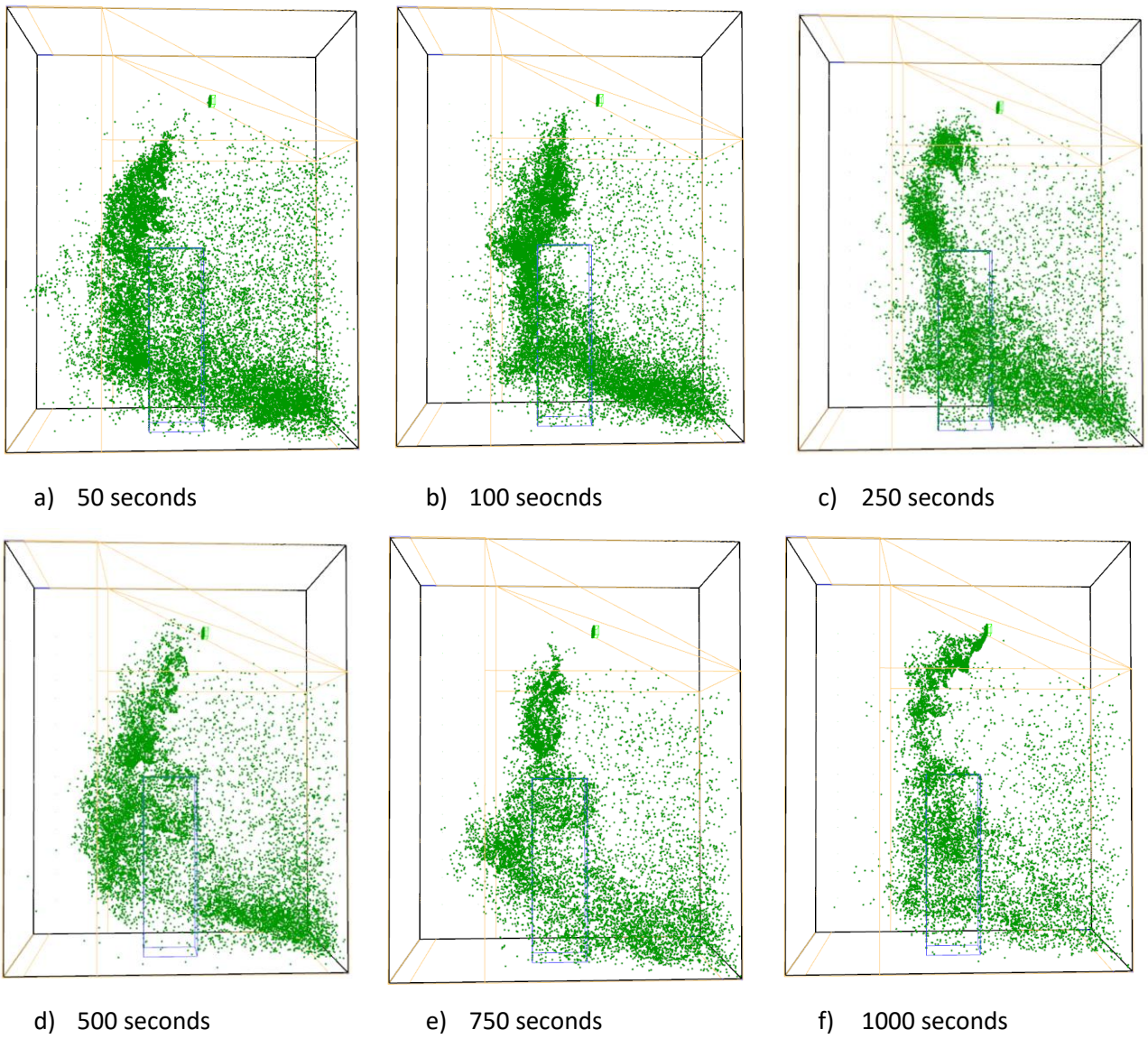

Figure 89: Particle flow profile for simulation 4 at a)50 seconds, b) 100seconds, c) 250 seconds, d) 500 seconds, e) 750 seconds and f) 1000seconds

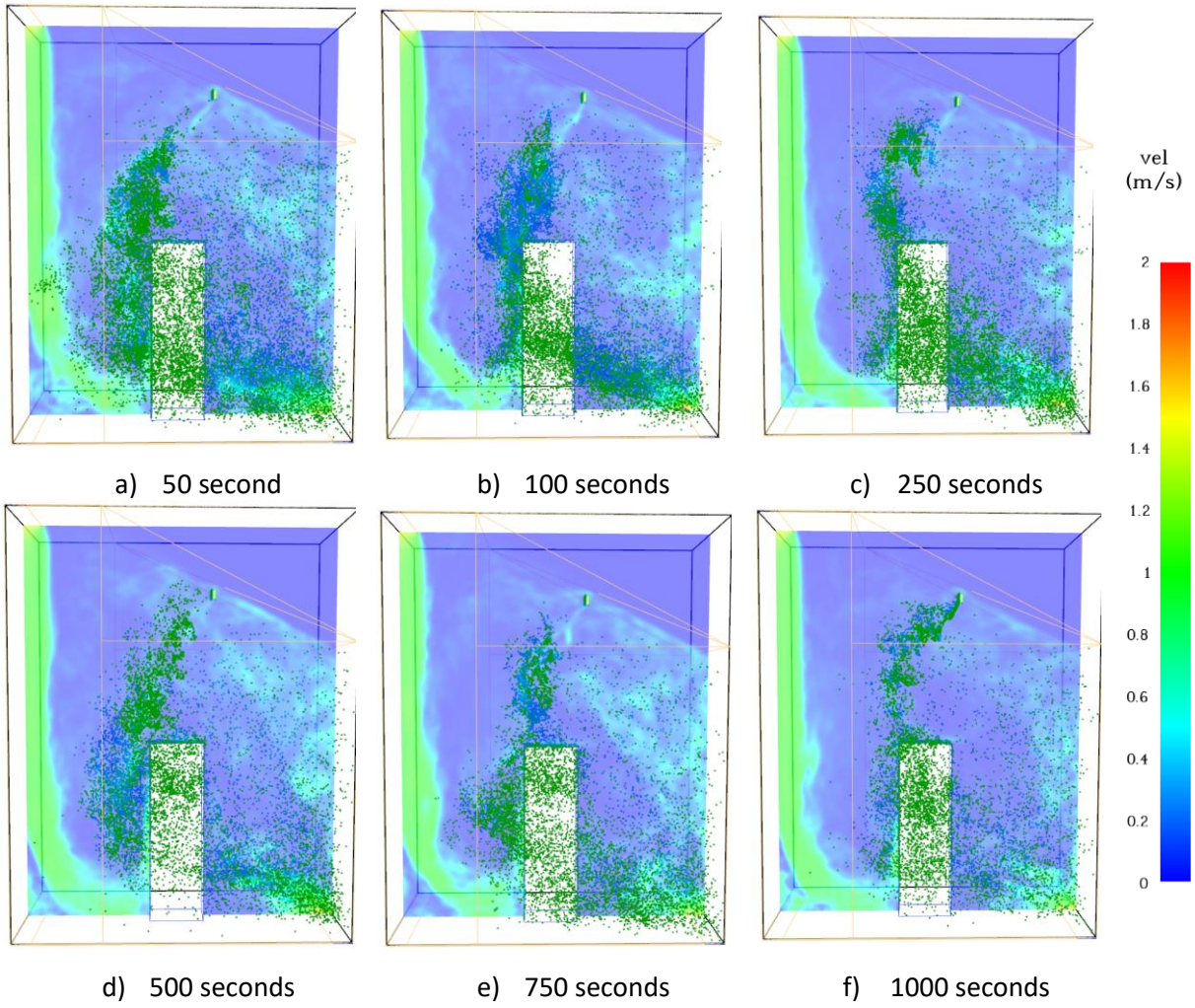

Figure 90: Air flow in cabin a)300 seconds b)700 seconds

The velocity profile and the particle flow can be seen in Figure 90 for 50, 100, 250, 500, 750 and 1000 seconds. Average velocity values were determined for each vertical line tested – line 1 at 0.2 m, line 2 at 0.5 m and line 3 at 1.5 m. Although the experimental mock-up was different to that of a real cabin, the main flow features were present, including the circulated main airflow and gasper induced airflow. The aim was to replicate the experimental data in a numerical model, this has been achieved, meaning the numerical model is meaningful and suitable to be used in this research.

6.5 Airflow and Particle Distribution investigation inside a Bae 146 aircraft

This numerical simulation can be used to calculate airflow and particle distribution and reliably relate this to actual aircraft. Simulations based on BAe 146 aircraft will be conducted on the basis of these results with confidence in the reliability of the data. Simulations will be conducted to determine the velocities of particles and the distribution of these particles within a BAe 146 cabin. Parameters such as particle size and concentration will be adjusted to enable this study to provide a full understanding of these effects on particle distribution and therefore the likelihood of contaminated air becoming a health issue for passengers.

The mesh independence analysis is made in order to secure a solution which is not depending on the quality or size of the mesh. The analysis is performed by starting with a coarse mesh and then gradually refining the mesh until the results do not show any appreciable difference.

The BAe 146 aircraft was chosen for the simulation as several reports have highlighted issues with this particular aircraft such as the report published by the Parliament of the Commonwealth of Australia (Senate Rural and Regional Affairs and Transport References Committee 2000). The UK Civil Aviation Authority issued an airworthiness directive requiring operators to inspect engine oil seals due to several incidents reported (Flight Global 2001).

Whilst studies by Winder et al. (among others) have explored the chemical makeup of engine oils, little work has been done to characterise the resulting aerosol (Mann 2014). Characterisation of the oil aerosol size distribution entering the aircraft cabin during a contamination event is important as this will affect the particle distribution throughout the cabin as illustrated in the study by Yan et al. (2021). Mann et al. (2014) determined that the mean diameter of aerosols from oil was in the range of 0.106-0.045 μm. Droplets larger than 5 μm will usually get trapped in the upper airways and swallowed later or expectorated. Smaller droplets will be carried down and retained in the lungs. Shang et al. (2021) demonstrated particles up to 50 μm show deposition in the upper airway. The aerosol particle size of TCP was determined to be 0.1 μm (Environment Agency 2009).

The particle sizes of 16, 50, 100 and 200 µm were chosen for study due to determine the effect of particle size on the distribution within the cabin. Pyrolysed products will have a different diameter than non-pyrolysed material as there is no direct evidence of aerosol particle size of a range needed to be studied.

6.6 Cabin Specification of Bae 146

Cabin geometry for the simulation is based on the dimensions of the BAe 146 airplane (Quality Wings 2013). There are three models of the BAe-146 namely BAe-146-100, BAe-146-200, BAe-146-300 (BAe Systems 2009). The dimensions of the BAe 146 are similar for all models. The Bae 146 cabin geometries were used as this type of aircraft has been implicated in having a number of contamination events.

Table 24 indicates the internal dimensions of Bae-146-100 used for in the simulations. The cabin width is 3.42 m and 2.03 m high. The cabin is 16.0 m in length. There are six seats abreast, three either side of a centre aisle of 0.53 m. There are 15 rows of seats. The seats have a pitch of 0.79 m (this is the space between a point on one seat and the same point on the seat in front of it).

Table 24: Dimensions of Bae-146 (Quality Wings 2013)

Cabin data	BAe-146-100
Number of passengers	70
Economy seat pitch (m)	0.79
Cabin length (m)	15.45
Cabin width (m)	3.42
Cabin height (m)	2.03
Aisle width (m)	0.53
Seat width (m) max	0.54

There are two air inlet vents are located in the roof space either side of the aisle as indicated on Figure 91. Extract vents are located at floor level, under the seats. The inlet vents run the length of the aircraft cabin (16.0 m) with an area of 3.2 m^2. Air flow into the cabin is 1.2 m/s.

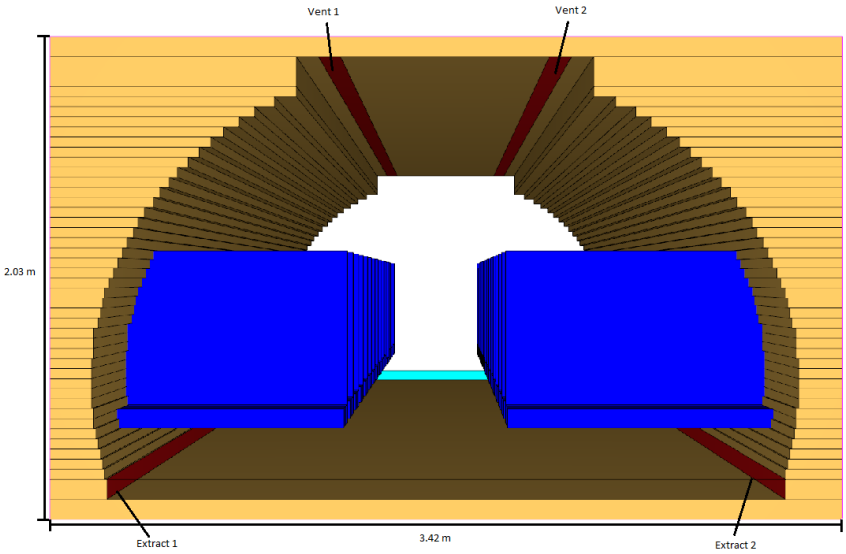

Figure 91: Internal cabin dimensions and location of vents

The extract vents run the full length of the cabin (16.0 m), each with an extract area of 1.6 m^2. One on either side of the cabin. The extract vents are removing air at 1.40 m/s (National Research Council, 2002) as can be seen in Figure 91.

There are 108 devices located within the cabin geometry 54 measuring the number of particles and 54 measuring mass per unit volume (kg/m^3). These were located at the front of the cabin, the middle and the rear. The front location was on the first row of seats, 1.2 m from the cabin boundary. The middle was 7.7 m into the cabin and the rear was located 13.35 m. The locations are indicated on Figure 92. The additional devices in the centre aisle were measuring velocity.

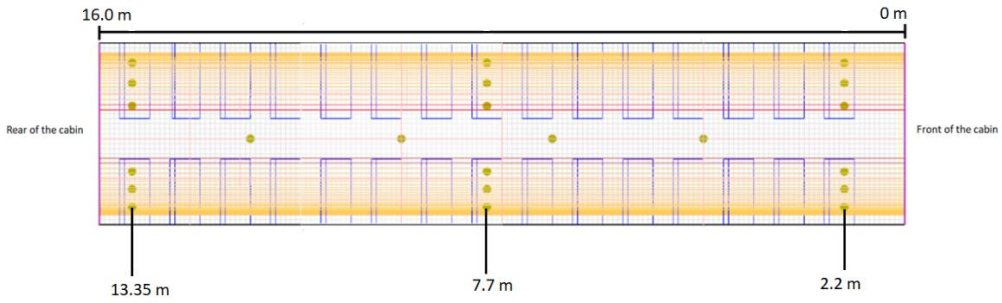

a)

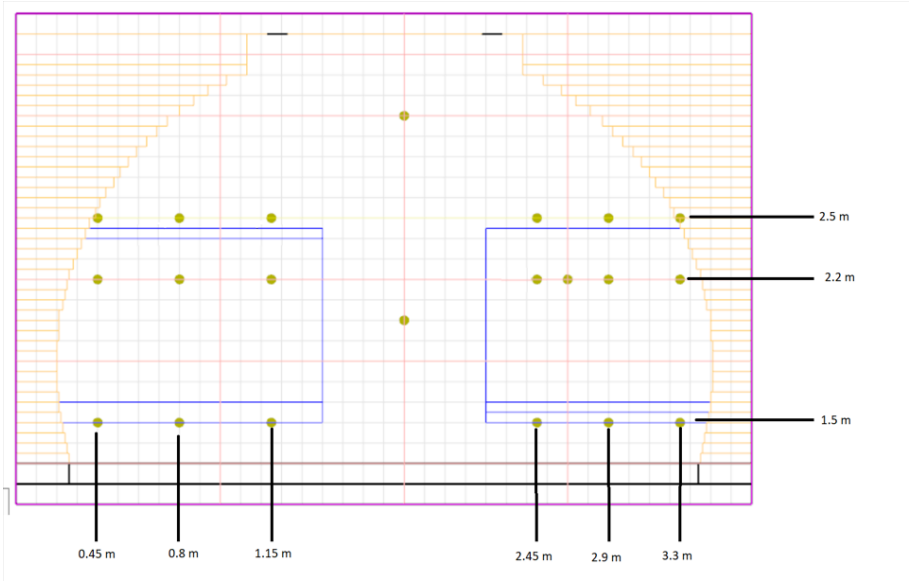

b)

Figure 92: Location of measuring devices a) location along the length of the cabin, b) location in height and width of the cabin

The devices at the front, middle and rear of the cabin were positioned at seat height (1.5 m) head height (2.2 m) and top of the seat height (2.5 m). In locations representing the aisle seat (either 1.15 m left side or 2.45 m right side) the centre seat (either 0.8 m left side or 2.9 m right side) and the window seat (either 0.45 m left side or 3.3 m right side) as shown in Figure 92b.

6.7 Parametric study

This section contains the parametric study in order to obtain the setup of the FDS simulation for the validation study. The objective of this research is to determine the influence of particle size, particle injection rate and number of particles on the accumulation of particles available for potential inhalation by occupants.

Table 25 shows the different parameters studies. Table 25 also defines the names of the configurations.

Table 25: Summary of main operational parameters for the examined test cases

Parameters		
Case	**Particle size (μm)**	**Number of particles**
PS16_NP4	16	400000
PS50 _NP4	50	
PS100 _NP4	100	
PS200 _NP4	200	
PS16_ NP5	16	500000
PS50_NP5	50	
PS100_NP5	100	
PS200_NP5	200	

To perform the simulations the computer system specifications were:

- Processor – Intel(R) Core (TM) I7-6950X COU @ 3.00 GHz
- Installed memory – 32.0 GB
- System type – 64-bit Operating System, x64 based processor
- Core 10

The simulation model used was Very Large Eddy Simulation.

Simulations took approximately 13 hours to run. Eight simulations were performed. Four simulations were completed where there were 400000 particles available for injection into the aircraft cabin. Each of these four runs had a different particle size- 16 μm, 50 μm, 100 μm and 200 μm. The remaining four simulations were completed where there were

500000 particles available for injection into the aircraft cabin. Each of these four runs had a different particle size- 16 µm, 50 µm, 100 µm and 200 µm. All runs were for 600 s.

The simulations represent the flow of particles within the aircraft cabin. The graphs represent the left and right side of the aircraft cabin, indicating the amount of materials at different heights at the front, the middle and the rear of the cabin.

Figure 93 shows a general representation of the result which are going to be presented in this section. The figure has two distinct sections – left and right. These represent the left and the right side of the cabin. The data points represent a specific location within the aircraft cabin as indicated on Figure 93, representing either aisle, centre or window seats at the heights 1.5 m, 2.2m and 2.5 m as indicated.

To visualise the particle flow, the particles were given a “particle trail time” of 0.6 seconds. This enabled a good visualisation of the paths the particles take without obscuring the image.

For the analysis of eight cases, time slices were provided for each case at 50, 100, 150, 300, 450 and 600 seconds. These times were chosen to show how the particles move in the first stages of the simulation (50, 100 and 150 seconds), as time progressed, and more particles were added the density of the particles was of interest. 300 seconds was chosen as this was the midpoint of the simulation. 450 and 600 seconds were the final stages of the simulation.

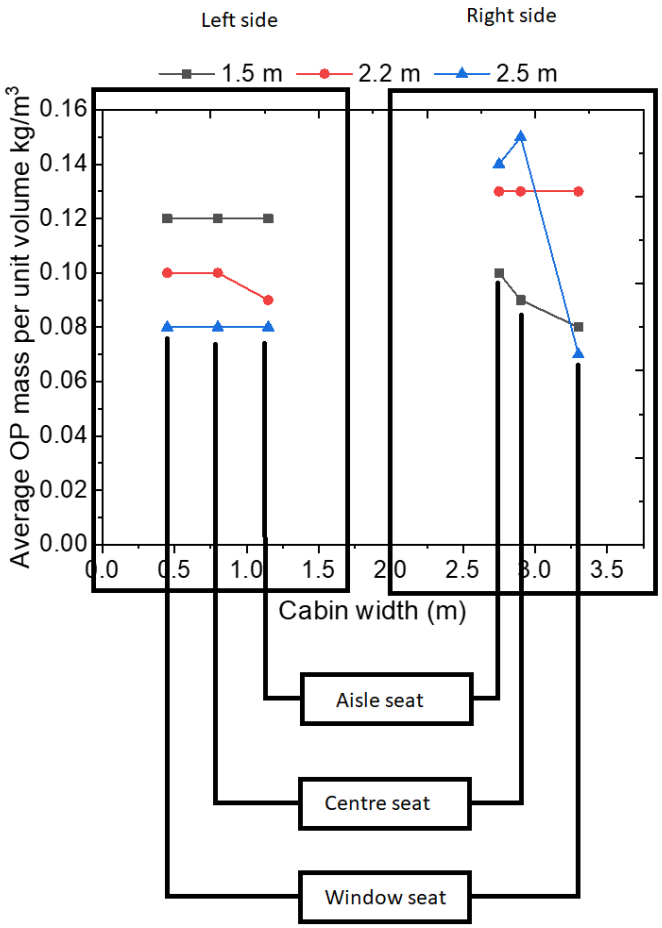

Figure 93: Illustration of the aircraft cabin layout represented in the graphs

6.7.1 Case PS16_NP4

Case PS16_NP4 injected 40000 particles of 16 µm diameter into the aircraft cabin via both inlet vents at the top of the cabin. Figure 94 shows the average density measured at the front (a), middle (b) and rear (c) of the cabin (see Figure 93 to identify location). Figure 94 clearly indicate the density on the left and right side of the cabin at heights of 1.5 m, 2.2 m and 2.5 m. As can be seen in Figure 94, the left of the cabin shows there is a higher average density of particles at a height of 1.5 m in the front (0.12 kg/m^3) and rear (0.11 kg/m^3). In the middle of the cabin on the left the highest average value (0.12kg/m^3) observed was at 2.2 m high at the window seat. On the right average high levels of 0.15kg/m^3 was observed at 2.2 m and 2.5 m at the front, middle and rear. In all cases on the right side of the cabin the highest levels observed (0.15 kg/m^3) were observed in the aisle or centre seat. Figure 94 indicates that there is a higher density on the right side compared to the left side of the cabin at 22 m and 2.5 m. At the front, Figure 94a, the highest average level of 0.15 kg/m^3 was observed on the right side at 2.5 m in the centre seat. In the middle Figure 93b, the highest average level of 0.15 kg/m^3 was observed on the right side at 2.5 m in the aisle seat as well as at 2.2 m in the window seat. At the rear, Figure 94c, the highest average level of 0.15 kg/m^3 was observed on the right side at 2.5 m in the aisle seat as well as at 2.2 m in the aisle and window seat.

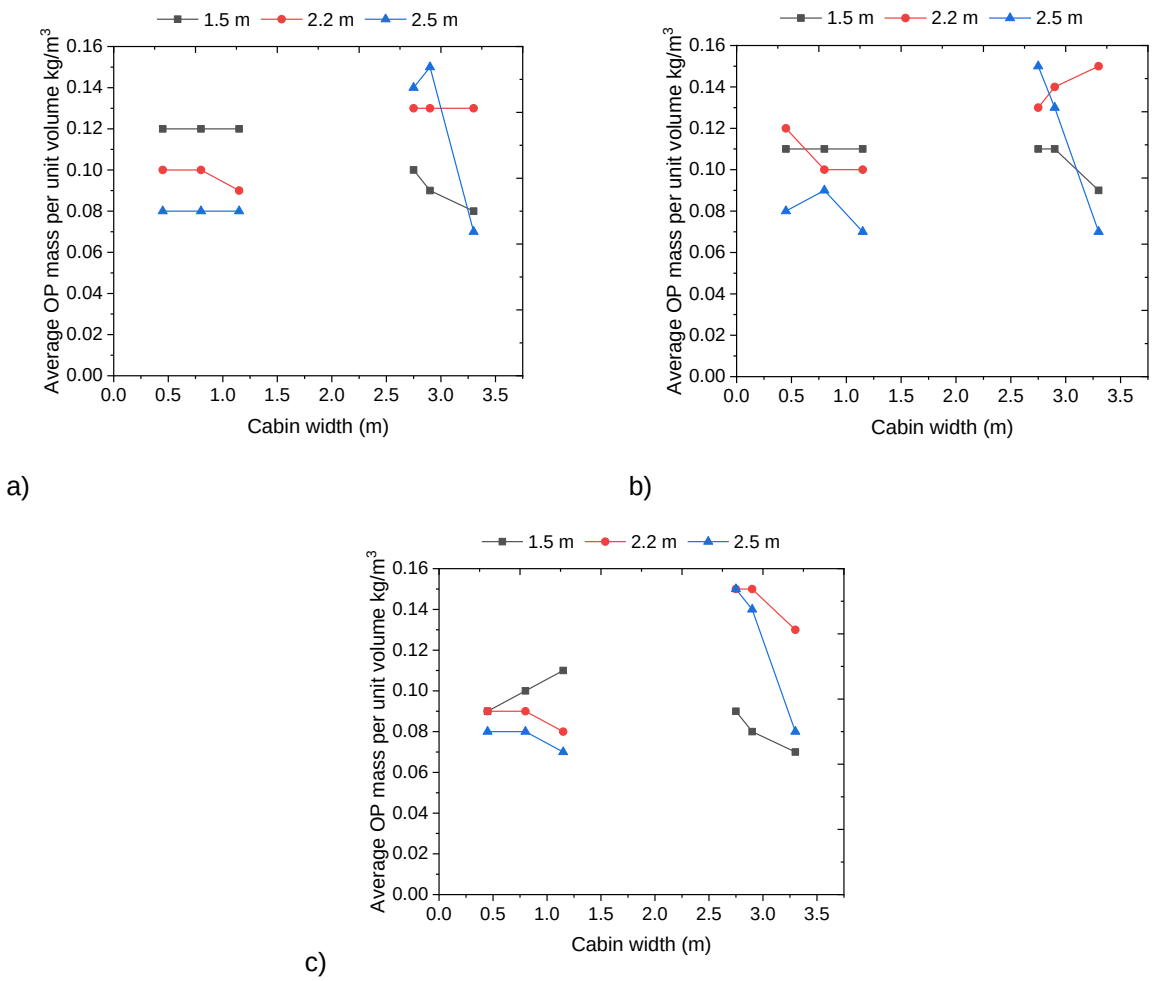

Figure 94: Average density of contamination for case PS16_NP4 at the (a) front, (b) middle and (c) rear of the cabin

Figure 95 shows the total amount of oil material injected over the duration of the simulation. As can be seen in Figure 95 the right side of the cabin receives a greater level of exposure. With a maximum of 180.55 kg/m^3 of material being observed at 2.5 m at the rear of the cabin. The highest levels of oil material on the left-hand side are found at 1.5 m high, with a value of 143.84 kg/m^3. On the right side consistent high levels are observed at 2.2 m. At the front, Figure 95a of the cabin there is little variation on seat location (at

the same height). In the middle, Figure 95b on the left side the window seat receives a higher concentration than the aisle seat 137.96 kg/m^3 compared to 130.92 kg/m^3. A greater concentration of 180.55 kg/m^3 was observed at the rear, Figure 95c, of the cabin in the aisle seat.

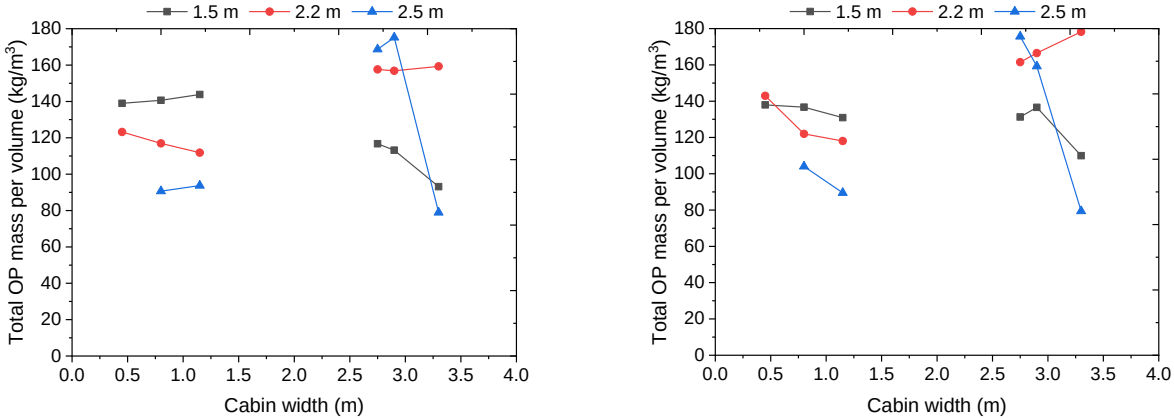

a) b)

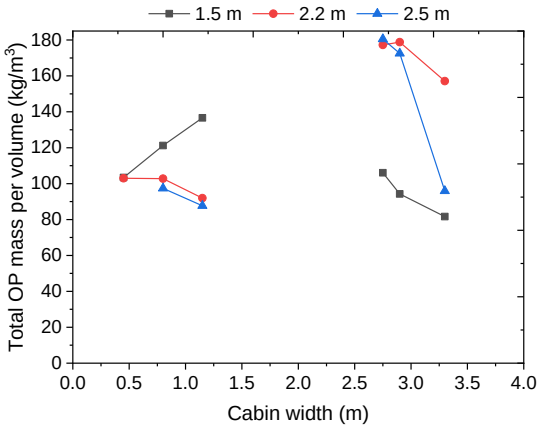

c)

Figure 95: Total: density of contamination for PS16_NP4 at the front (a), middle (b) and rear (c) of the cabin

Figure 96 illustrates the motion of the particles during the 600 s simulation 1.8 m from the rear of the cabin. All particles are given a 0.6 second trail so the direction and flow path can be clearly seen. Within the first 50 seconds, Figure 96a, of the simulation, particles

are observed to be evenly distributed around the cabin, as the simulation progresses a slight increase in the number of particles can be seen on the right at 100 seconds, Figure 96b. After 300 seconds the particles become evenly distributed, Figure 96d. Figure 96 clearly illustrates the recirculation of the particles. If we compare the motion of the particles in Figure 96 with the graphs of average densities, Figure 94 and total densities, Figure 95, it can be why slightly higher levels of particles are observed on the right side of the cabin. After 150 seconds, the particles on the left are flowing onto the right side of the cabin, this is increasing the values observed on the right side, in particular at heights of 2.2 m and 2.5 m. At the lower level of 1.5 m the particle flow is consistent on both sides of the cabin and not influenced by the velocity from the input vents.

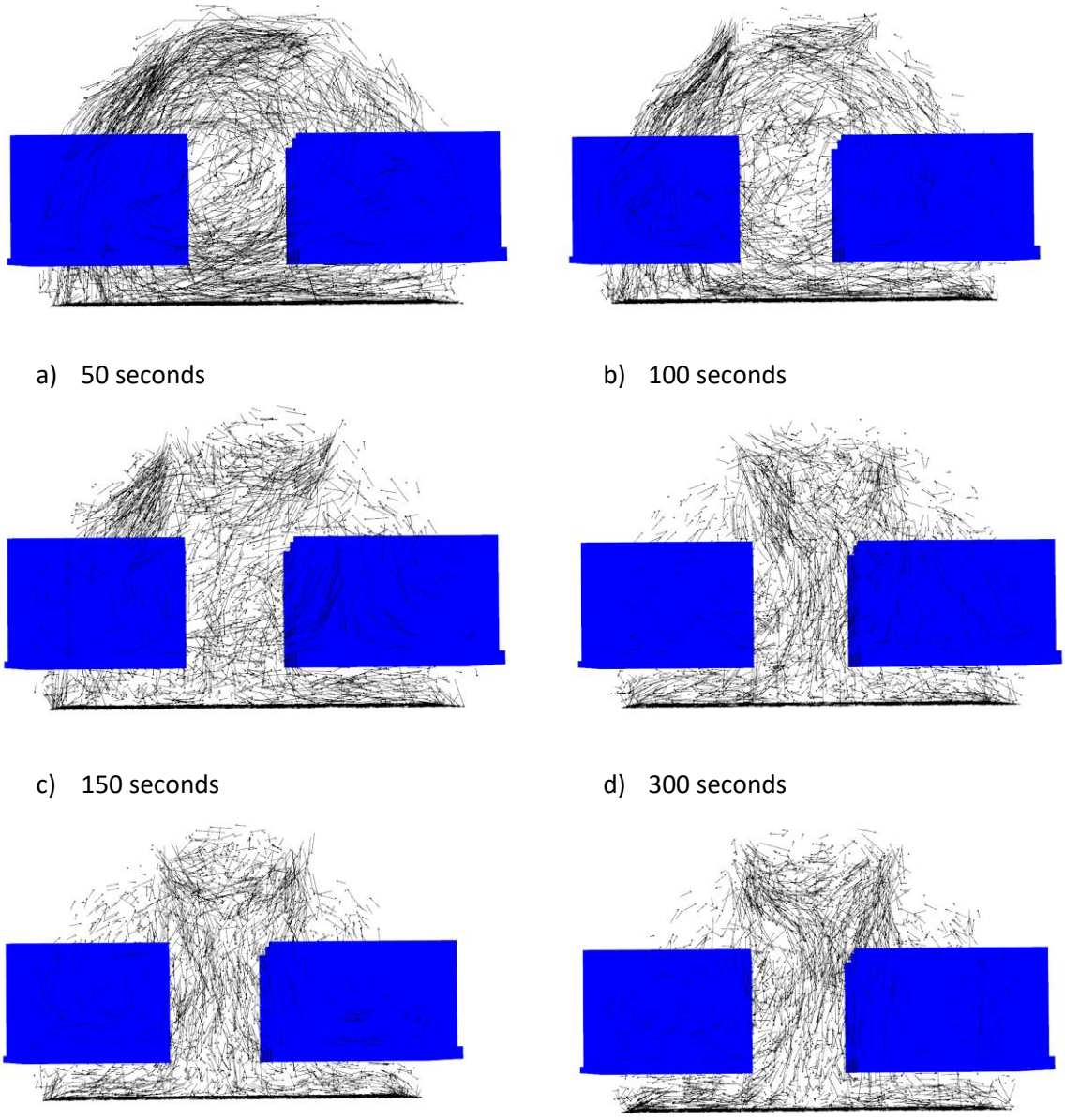

a) 50 seconds

b) 100 seconds

c) 150 seconds

d) 300 seconds

e) 450 seconds

f) 600 seconds

Figure 96: Motion of particles for case PS16_NP4 a-f: 50- 600 seconds

Comparison of the distribution of the particles as observed in Figure 96, with the velocity profile within the cabin as can be seen in Figure 97 shows particles are following the air contours.

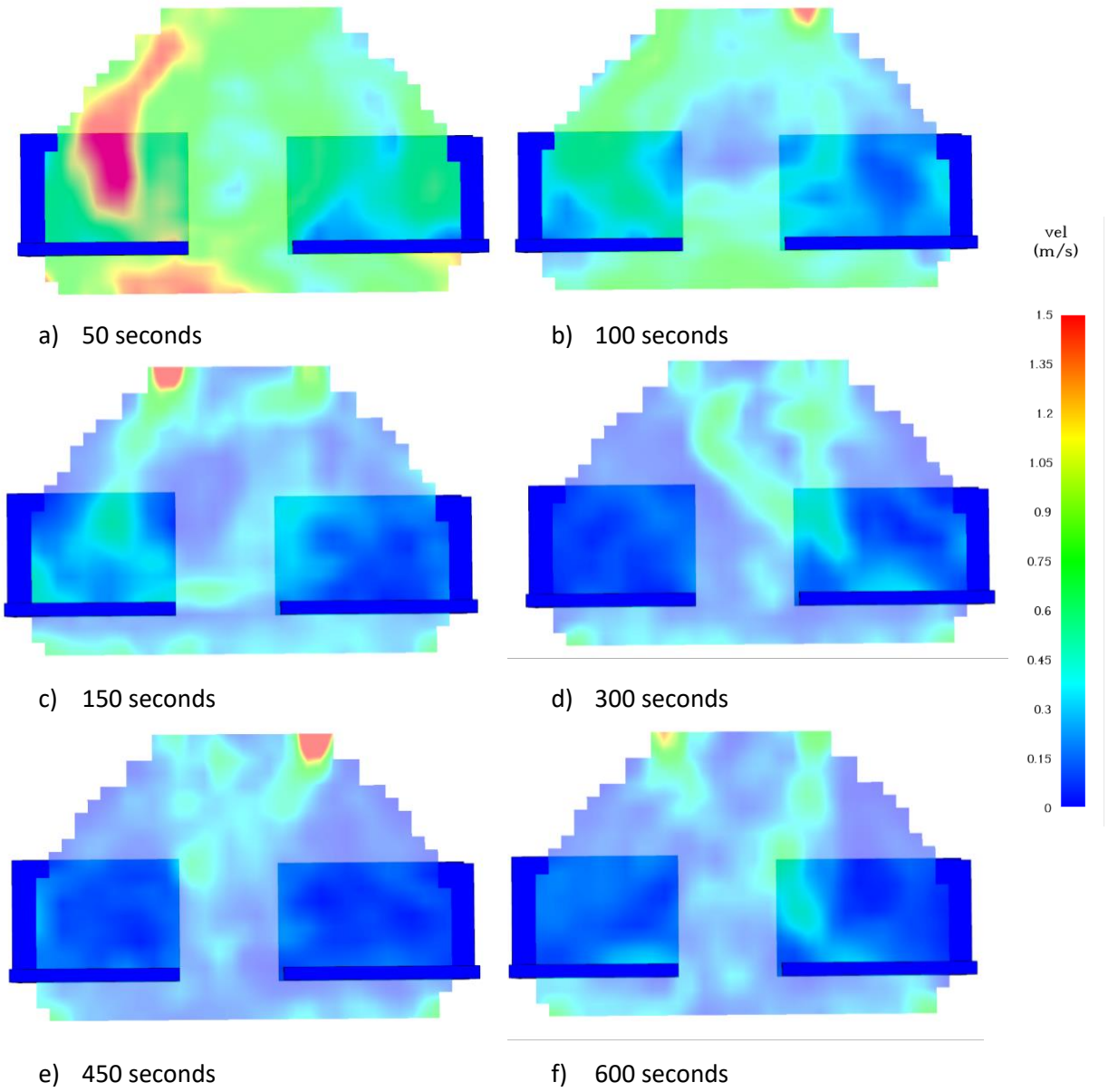

Figure 97: Velocity profile for case PS16_NP4 a-f: 50 -600 seconds

Figure 97 illustrates the contours of air and gas velocity 1.8 m from the rear of the cabin. Flow can be seen entering from the top of the cabin via the two supply vents and flowing downwards towards the seating area and to the extract vents on the floor. Initially at 50 seconds there is a high velocity on the left side, represented by the red colouring on Figure 97a. Figure 97a is mirrored in Figure 96a which illustrates a high concentration of

particles at this time on the left. As the simulation progresses the velocity becomes even on the left and right-side Figure 97d after 300 seconds. After 450 seconds in Figure 97e a higher velocity is seen at the supply vent on the right side of the cabin. The initial higher levels of velocity observed on the left of the cabin at 50 seconds and then on the right at 450 seconds could be due to the geometry of the cabin. As the geometry created in FDS is not a smooth curve for the ceiling of the aircraft cabin, the “squared” corners could affect the velocity and the motion of the particles. Velocities observed at 600 second, Figure 97f, mirrors the pattern of the particles as shown in Figure 96, reinforcing the observed values for he average and total densities as shown in Figures 94 and 95.

6.7.2 Case PS50_NP4

Case PS50_NP4 injected 40000 particles of 50 µm diameter into the aircraft cabin via both inlet vents at the top of the cabin. Figure 98 shows the average density measured at the front (a), middle (b) and rear (c) of this cabin, (see Figure 93 to identify location). Figure 98 clearly indicates the average density on the left and right side of the cabin at heights of 1.5 m, 2.2 m and 2.5 m. Higher average levels were observed on the left of the cabin at front, middle and rear. At the front, Figure 98a, of the cabin the highest level of 0.11 kg/m^3 was observed at 2.2 m and 2.5 m on the left, these were both in the aisle seat. On the left at the front the densities observed were in the range of 0.06 – 0.011 kg/m^3. On the right at the front, the highest value observed, 0.09 kg/m^3 was at 2.2 m at the window seat. Values observed on the right at the front ranged from 0.03 – 0.09 kg/m^3. In the middle, Figure 98b, of the cabin, the highest values of 0.10 kg/m^3 were observed on the left side, at 2.2 m and 2.5 m in all three seats. On the left the values ranged from 0.05 – 0.1 kg/m^3. On the right in the middle the highest values 0.08 kg/m^3 at 2.2 m and 2.5 m this were observed in the aisle seats (2.2 m and 2.5 m) and the window seat (2.2 m). On the right the values observed ranged from 0.02 – 0.08 kg/m^3. At the rear, Figure 98c, of the cabin, highest values were again observed on the left of the cabin. At 2.2 m the seat in the centre and at 2.5 m seats in the aisle and centre observed levels of 0.1 kg/m^3. On the left the values observed ranged from 0.04 – 0.1 kg/m^3. On the right at the rear, the aisle seat observed the highest levels of 0.08 kg/m^3 at all heights (1.5 m, 2.2 m and 2.5 m). On the right the observed values ranged from 0.02 – 0.08 kg/m^3.

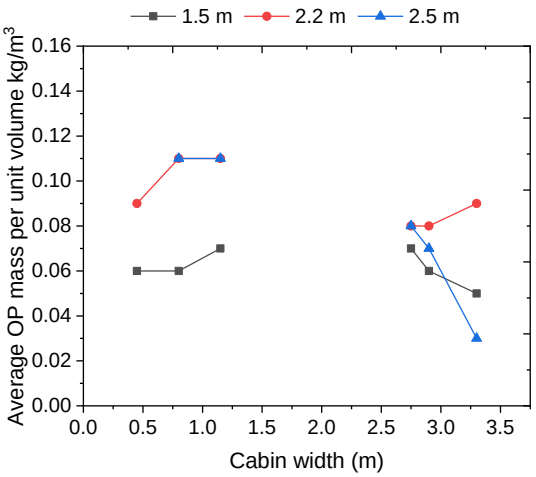

a)

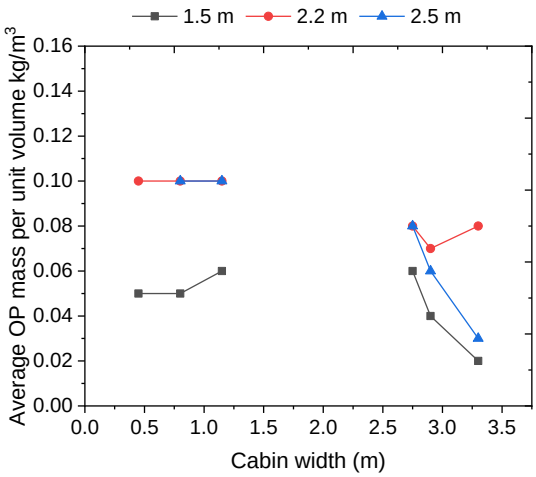

b)

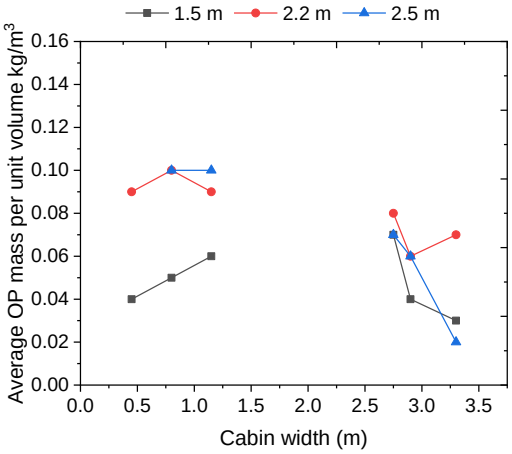

c)

Figure 98: Average density of contamination for PS50_NP4 at the front (a) middle (b) and rear (c) of the cabin

Figure 99 shows that the high total concentrations observed at the front, middle and rear of the cabin. Highest levels were found to be on the left side at 2.2 m and 2.5 m at the front, middle and rear, Figure 99a, b and c. The highest value recorded was 130.26 kg/m^3, this was at the front of the cabin, the middle seat at 2.2 m high, Figure 99a. In all locations on the left, the lowest observed values were at 1.5 m high. On the right, in the middle, Figure 99b, the aisle seat observed the highest levels 100.59 kg/m^3 at 2.5 m high. With the lowest levels of 27.98 kg/m^3 observed in the window seat at 1.5 m high. In the rear,

Figure 99c, the right side observed highest levels in the aisle seat for both 2.2 m and 2.5 m with the highest level of 91.16 kg/m^3 at 2.2 m. The lowest levels of 23.56 kg/m^3 were observed at 1.5 m in the window seat. In general, on the right-hand side 2.2 m recorded the highest concentrations.

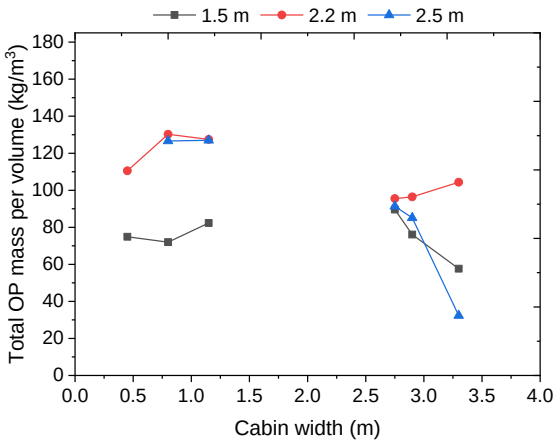

a)

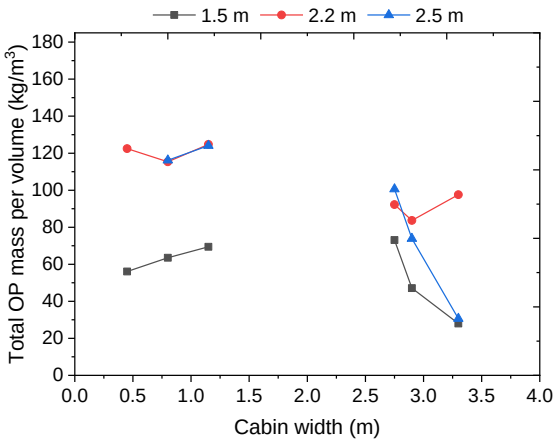

b)

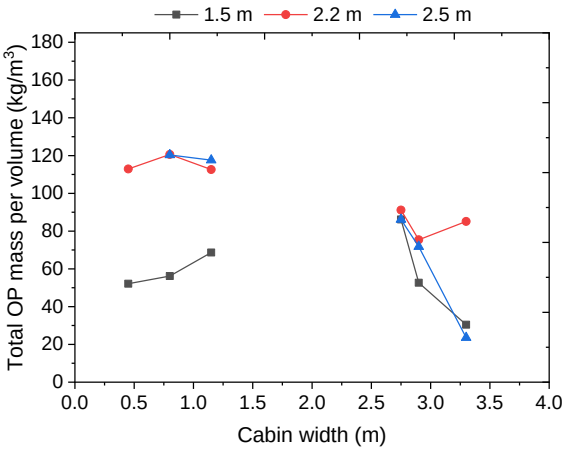

c)

Figure 99: Total density of contamination for PS50_NP4 at the front (a) middle (b) and rear (c) of the cabin

Figure 100 illustrates the motion of the particles during the 600 s simulation 1.8 m from the rear of the cabin. All particles are given a 0.6 second trail so the direction and flow path can be clearly seen. Within the first 50 seconds, Figure 100a, of the simulation, particles are observed in a larger density on the right side. As the simulation progresses, from 300 seconds, Figure 100d, particles are observed as having an even distribution across both sides of the cabin. Figure 100 clearly illustrates the recirculation of the particles.

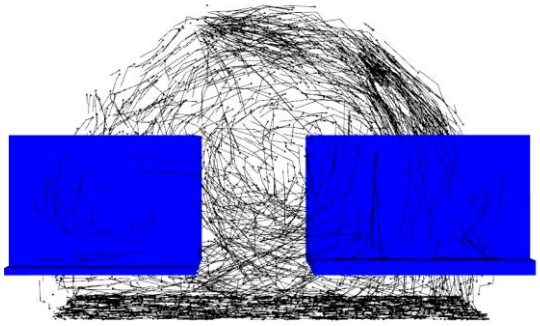

a) 50 seconds

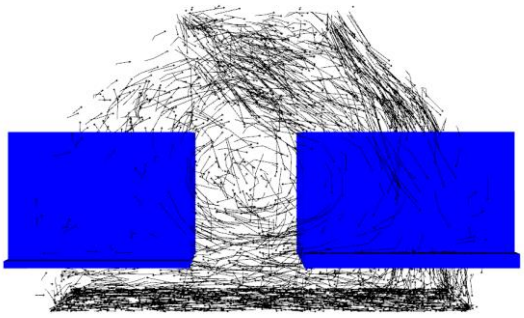

b) 100 seconds

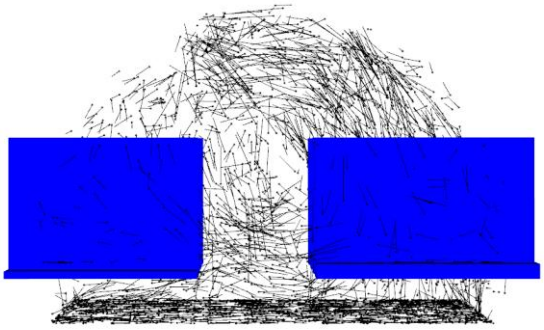

c) 150 seconds

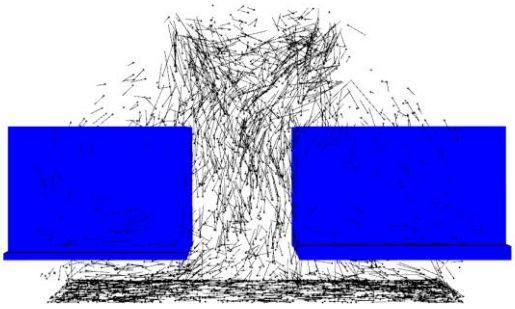

d) 300 seconds

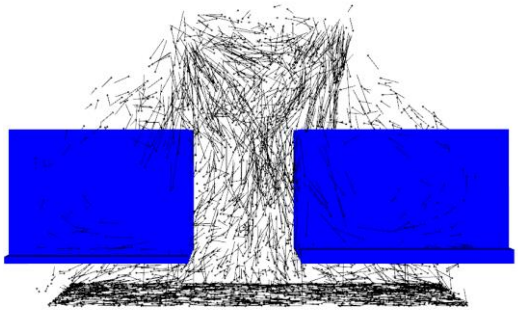

e) 450 seconds

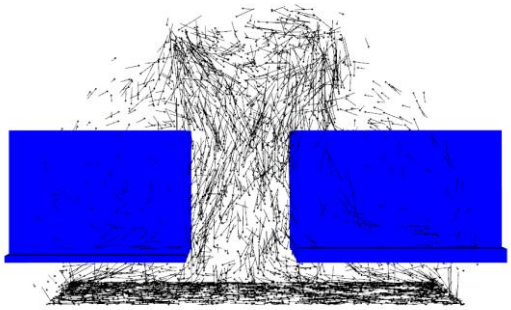

f) 600 seconds

Figure 100: Motion of particles for case P50_NP4 a-f:50-600 seconds

Comparison of the distribution of the particles as observed in Figure 100 with the velocity profile within the cabin as can be seen in Figure 101 shows the particle are following the air contours.

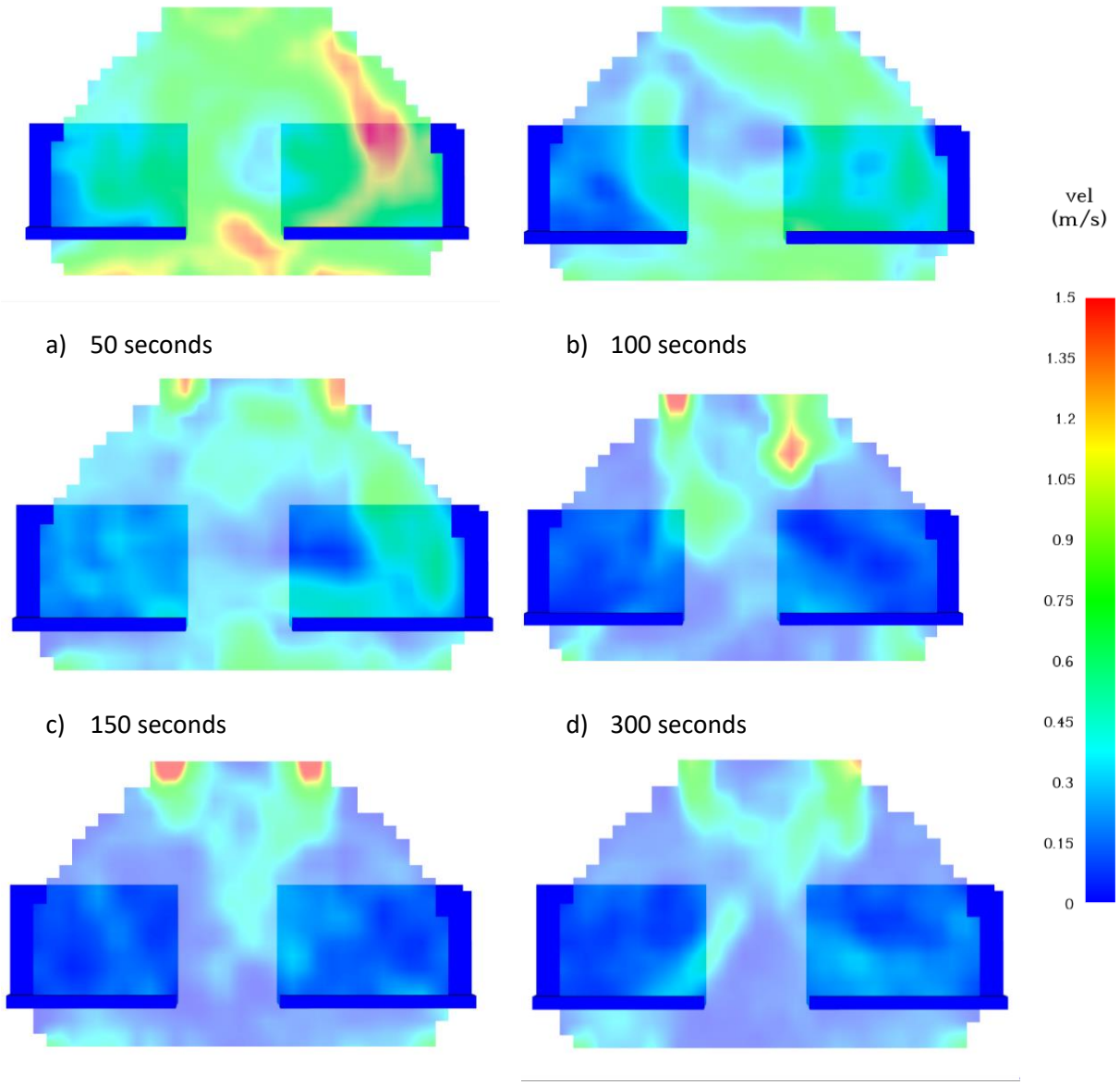

Figure 101: Velocity profile for case PS50_NP4 a-f:50-600 seconds

Figure 101 illustrates the contours of air and gas velocity 1.8 m from the rear of the cabin. Flow can be seen entering from the top of the cabin via the two supply vents, initially there is a high velocity on the right side. Figure 101a, this mirrors the path the particles are taking in Figure 100a. As the simulation progresses the velocity settles but clearly identifies the highest velocities at the supply vents.

6.7.3 Case PS100_NP4

Case PS100_NP4 injected 40000 particles of 100 µm diameter into the aircraft cabin via both inlet vents at the top of the cabin. Figure 102 shows the average density measured at the front (a), middle (b) and rear (c) of this cabin (see Figure 93 to identify location). Figure 102 indicates the average density on the left and right side of the cabin at heights of 1.5 m, 2.2 m and 2.5 m. As the particle size increases, the left and right side start to see similar patterns in the concentrations. Higher average levels were observed on the right of the cabin at front, middle and rear. At the front, Figure 102a, the highest average observation of 0.05 kg/m^3 at 2.5 m in the aisle seat, compared to a highest average value of 0.04 kg/m^3 on the left at 2.2 m and 2.5 m in the aisle and centre seat. In the middle, Figure 102b, highest average levels were observed on the right at 2.2 m with a value of 0.08 kg/m^3, this was observed int eh aisle seat, the highest observation of 0.04 kg/m^3 on the left was at 2.2 m and 2.5 m in the aisle and centre seat. At the rear, Figure 102c, the highest average level of 0.08 kg/m^3 was observed on the right side at 2.2 m in the aisle seat, compared the highest observed value of 0.03 kg/m^3 on the left.

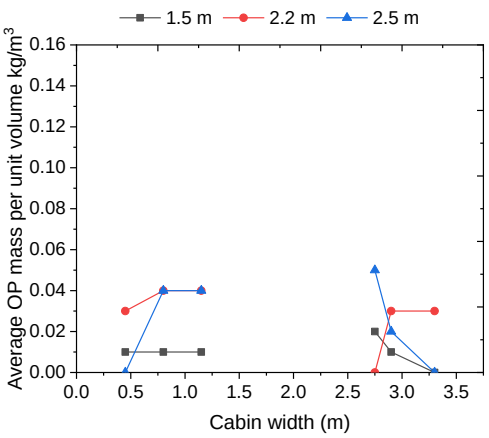

a)

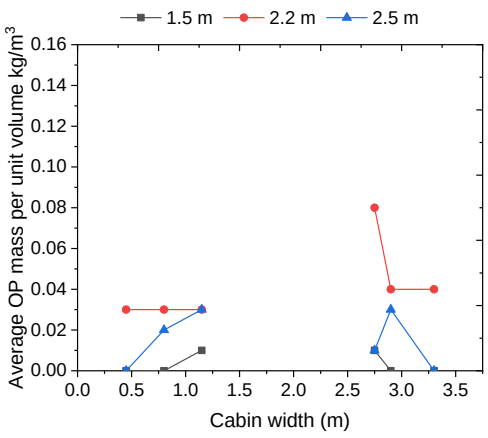

b)

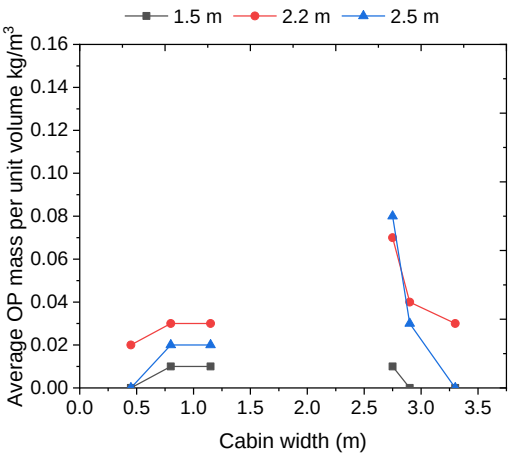

c)

Figure 102: Average density of contamination for PS100_NP4 at the front (a) middle (b) and rear (c) of the cabin

Figure 103 shows the total density measurements for particles of 100 µm. Highest levels were observed on the right side at the front, middle and rear. At the front, Figure 103a, highest observations of 64.41 kg/m^3 were on the right at 2.5 m in the aisle, compared to levels of 52.56 kg/m^3 on the left at 2.2 m in the centre seat. In the middle, Figure 103b, highest observations of 116.17 kg/m^3 were on the right, centre seat at 2.5 m, compared to 39.73 kg/m^3 on the left, at 2.2 m in the aisle seat. At the rear, Figure 103c, highest observations of 96.16 kg/m^3 were on the right at 2.5 m in the aisle, compared to levels of 31.8 kg/m^3 on the left at 2.2 m in the centre seat.

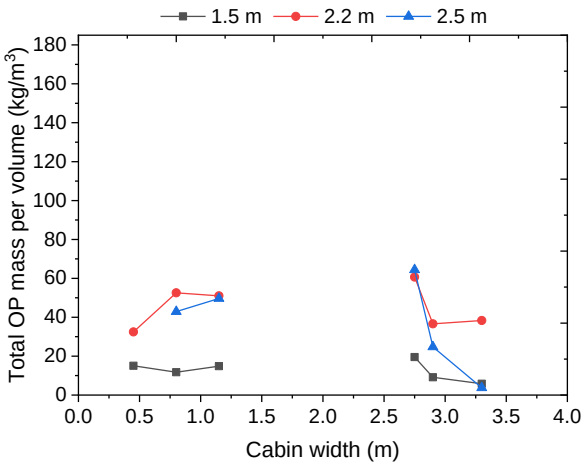

a)

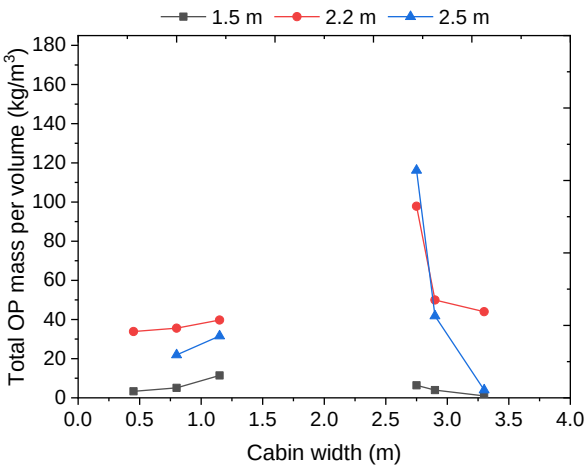

b)

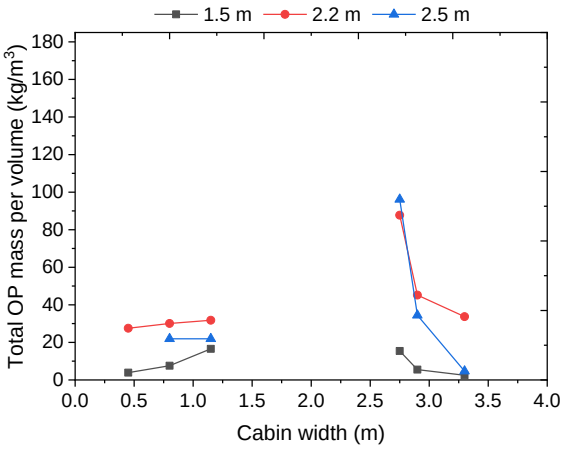

c)

Figure 103: Total density of contamination for PS100_NP4 at the front (a) middle (b) and rear (c) of the cabin

Figure 104 illustrates the motion of the particles during the 600 s simulation 1.8 m from the rear of the cabin. All particles are given a 0.6 second trail so the direction and flow path can be clearly seen. Within the first 100 seconds of the simulation, Figure 104b, particles are observed in a larger density on the right side. As the simulation progresses, from 300 seconds, Figure 104d, particles are observed as having an even

distribution across both sides of the cabin. Figure 104 clearly illustrates the recirculation of the particles.

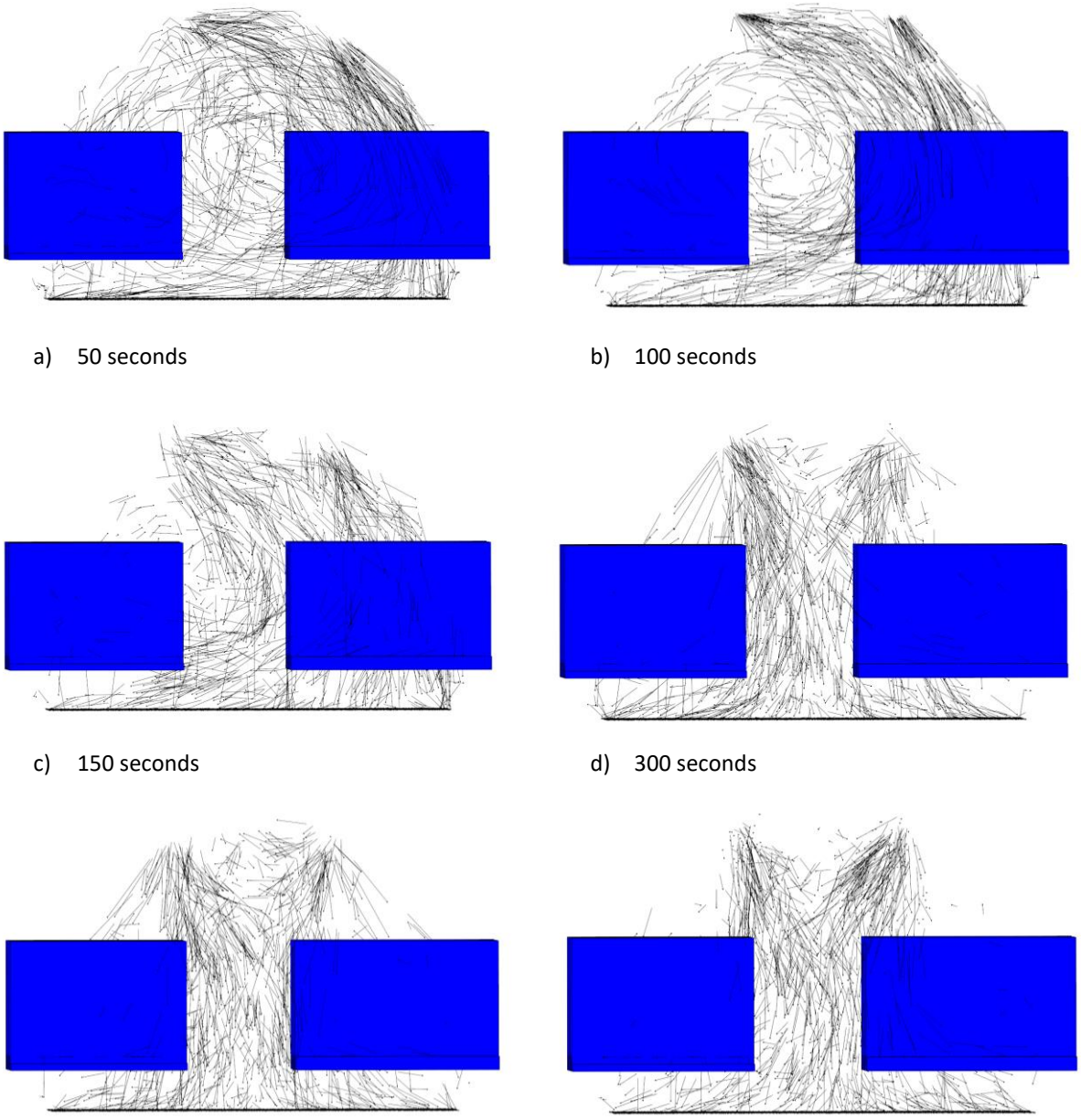

a) 50 seconds

b) 100 seconds

c) 150 seconds

d) 300 seconds

e) 450 seconds

f) 600 seconds

Figure 104: Motion of the particles for case PS100_NP4 a -f 50-600 seconds

Comparison of the distribution of the particles as observed in Figure 104, with the velocity profile within the cabin as can be seen in Figure 105 shows particles are following the air contours.

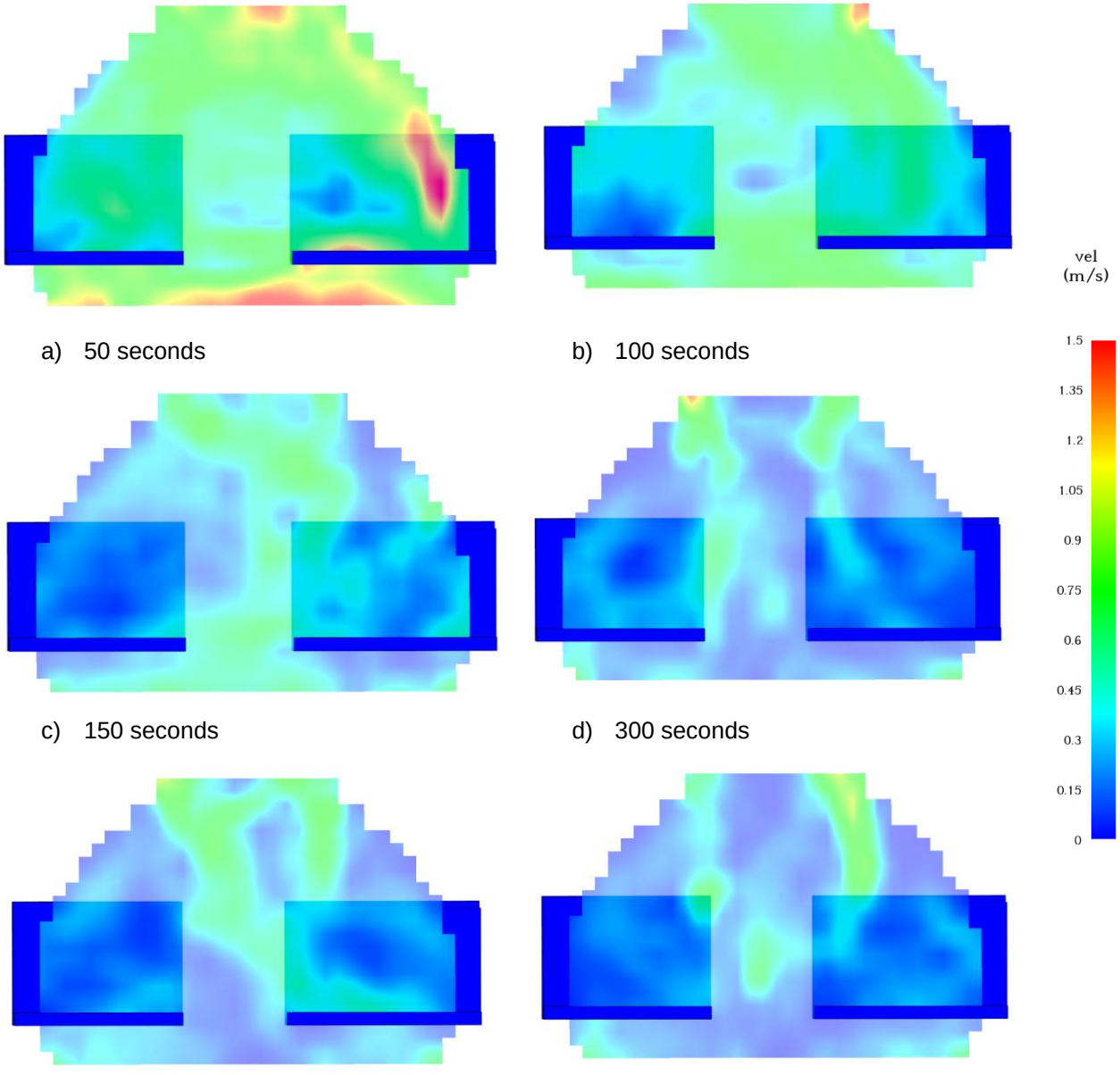

a) 50 seconds

b) 100 seconds

c) 150 seconds

d) 300 seconds

e) 450 seconds

f) 600 seconds

Figure 105: Velocity profile for case PS100_NP4 a-f 50-600 seconds

Figure 105 illustrates the contours of air and gas velocity 1.8 m from the rear of the cabin. Flow can be seen entering from the top of the cabin via the two supply vents and flowing downwards towards the seating area and to the extract vents on the floor. Initially after 50 seconds, there is a high velocity on the right side, Figure 1059a, this mirrors the path the particles are taking Figure 105a. As the simulation progresses the velocity settles but clearly identifies the highest velocities at the supply vents.

6.7.4 Case PS200_NP4

Case PS200_NP4 injected 40000 particles of 200 µm diameter into the aircraft cabin via both inlet vents at the top of the cabin. Figure 106 shows the average density measured at the front (a), middle (b) and rear (c) of this cabin (see Figure 93 to identify location). Figure 106 indicates the density on the left and right side of the cabin at heights of 1.5 m, 2.2 m and 2.5 m. As the particle size increases, the levels on the left are similar at the front, middle and rear, as are those for the right at the front, middle and rear. There is a difference between the levels on the left and right. Higher average levels were observed on the right of the cabin at front, middle and rear. At the front, Figure 106a, the highest average observation of 0.06 kg/m^3 at 2.2 m and 2.5 m in the aisle seat, compared to a highest average value of 0.01 kg/m^3 on the left at 2.5 m in the aisle seat. In the middle, Figure 106b, highest average levels were observed on the right at 2.5 m with a value of 0.09 kg/m^3, this was observed in the aisle seat, the highest observation of 0.02 kg/m^3 on the left was at 2.2 m in the aisle seat. At the rear, Figure 106c, the highest average level of 0.09 kg/m^3 was observed on the right side at 2.5 m in the aisle seat, compared the highest observed value of 0.01 kg/m^3 on the left at 2.2 m and 2.5 m in the aisle seat. In the front, middle and rear of the cabin this illustrates that the aisle seat was exposed to a higher concentration.

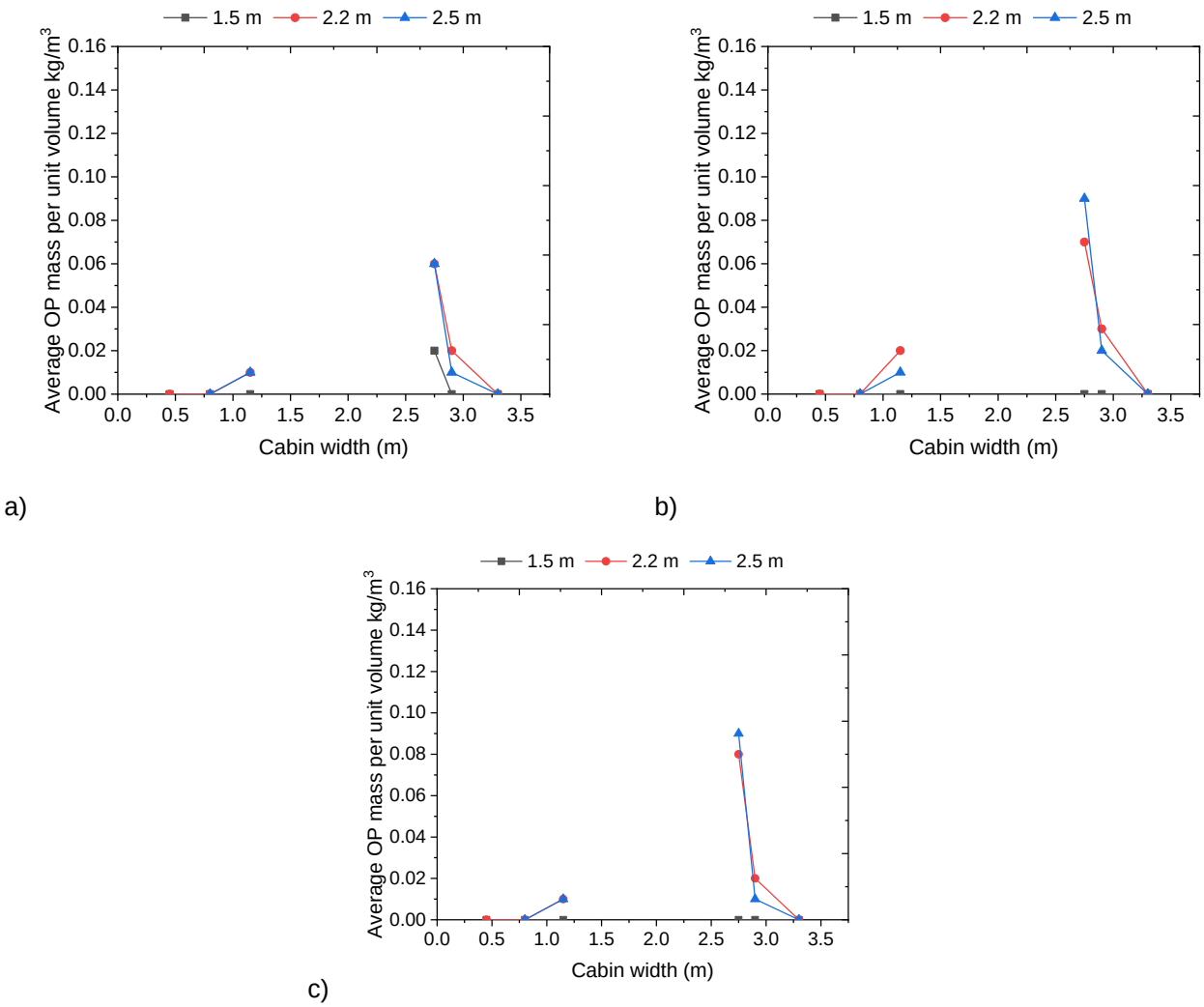

Figure 106: Average density of contamination for PS200_NP4 at the front (a) middle (b) and rear (c) of the cabin

Figure 107 shows that high levels are measured in the middle of the cabin and at the rear. Again, the aisle seats show the greatest exposure. At the front, Figure 107a the highest total density observed was 76.97 kg/m^3, at 2.5 m high in the aisle seat, compared to 7.84 kg/m^3 on the left, this was at 2.2 m high and on the aisle seat. In the middle, Figure 71b, the highest total density observed was 104.87 kg/m^3, at 2.5 m high in the aisle seat, compared to 19.82 kg/m^3 on the left, this was at 2.2 m high and on the aisle seat. At the

rear, Figure 107c, the highest total density observed was 106.99 kg/m^3, at 2.5 m high in the aisle seat, compared to 11.75 kg/m^3 on the left, this was at 2.2 m high and on the aisle seat.

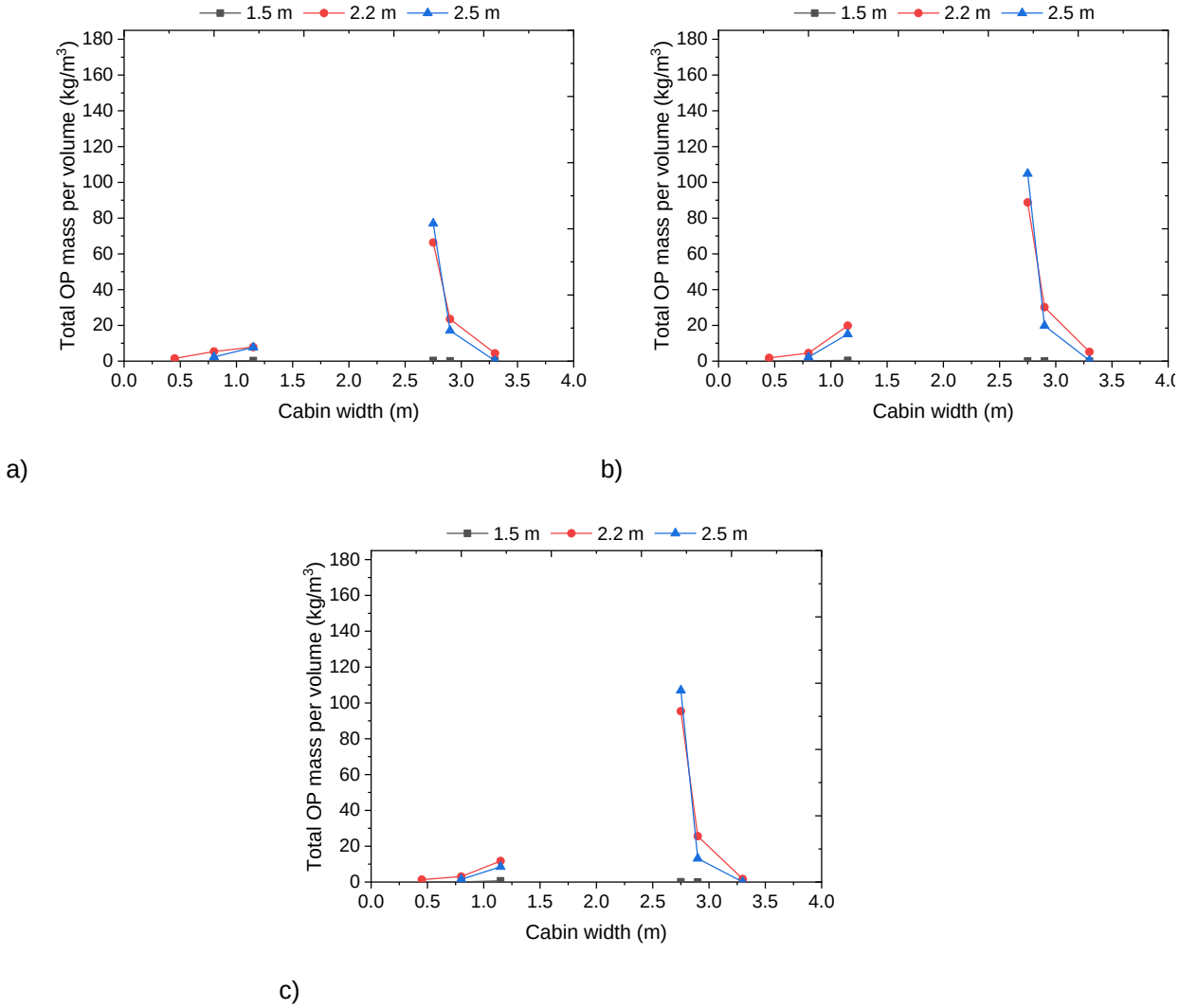

Figure 107: Total density of contamination for PS200_NP4 at the front (a) middle (b) and rear (c) of the cabin

Figure 108 illustrates the motion of the particles during the 600 s simulation 1.8 m from the rear of the cabin. All particles are given a 0.6 second trail so the direction and flow path can be clearly seen. Within the first 100 seconds of the simulation, Figure 108b

particles are observed in a larger density on the right side. As the simulation progresses, from 300 seconds, Figure 108d, particles are observed as having an even distribution across both sides of the cabin.

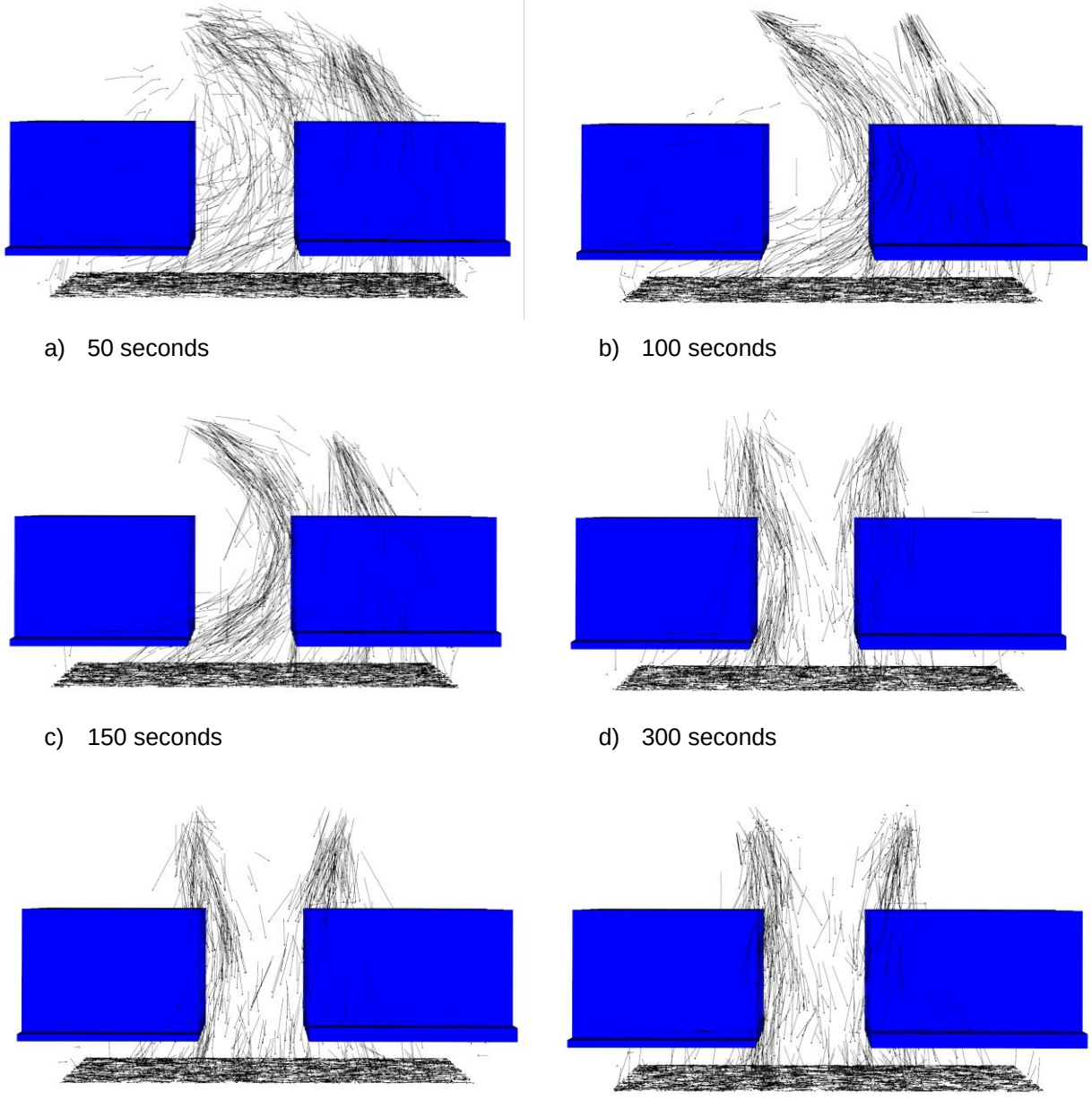

a) 50 seconds

b) 100 seconds

c) 150 seconds

d) 300 seconds

e) 450 seconds

f) 600 seconds

Figure 108: Motion of particles for case PS200_NP4 a-f 50-600 seconds

Comparison of the distribution of the particles as observed in Figure 108 with the velocity profile within the cabin as can be seen in Figure 109 shows particles are following the air contours.

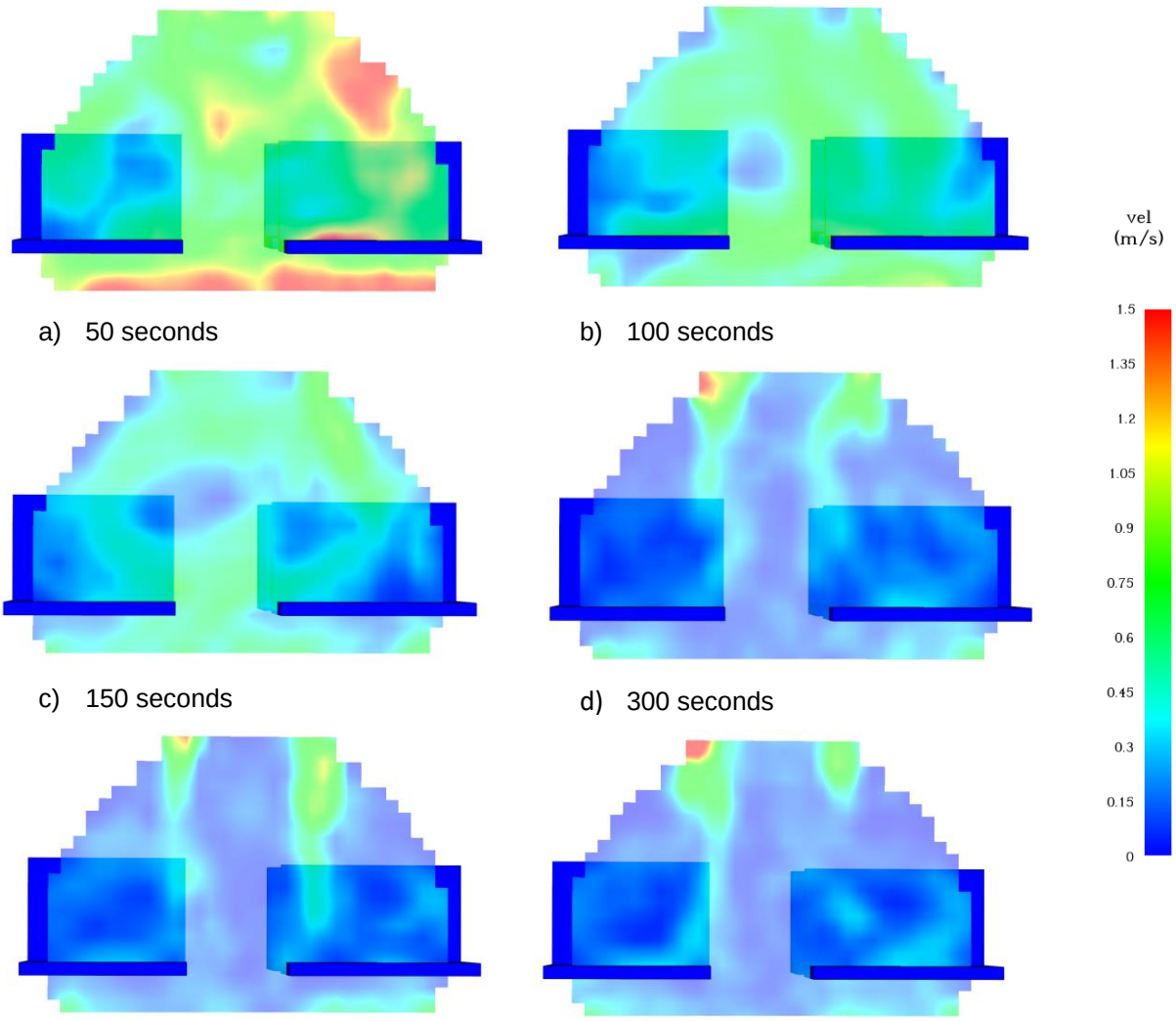

a) 50 seconds b) 100 seconds

c) 150 seconds d) 300 seconds

e) 450 seconds f) 600 seconds

Figure 109: Velocity profile for case PS200_NP4 a-f 50-600 seconds

Figure 109 illustrates the contours of air and gas velocity 1.8 m from the rear of the cabin. Flow can be seen entering from the top of the cabin via the two supply vents and flowing

downwards towards the seating area and to the extract vents on the floor. Figure 109a after 50 seconds shows a higher velocity on the right side of the cabin. This becomes balanced and uniform after 100 seconds Figure 109b. The velocity profiles illustrated in Figure 109 mirror the paths of the particles as shown in Figure 108.

6.7.5 Case PS16_NP5

Case PS16_NP5 injected 50000 particles of 16 µm diameter into the aircraft cabin via both inlet vents at the top of the cabin. Figure 110 shows the average density measured at the front (a), middle (b) and rear (c) of this cabin (seeFigure 93 to identify location). Figure 110 indicates the density on the left and right side of the cabin at heights of 1.5 m, 2.2 m and 2.5 m. Higher average levels were observed on the right of the cabin at front, middle and rear. At the front, Figure 110a, the highest average observation of 0.15 kg/m^3 at 2.5 m in the centre seat, compared to a highest average value of 0.12 kg/m^3 on the left at 1.5 m in all three seats (aisle, centre and window). In the middle, Figure 110b, highest average levels were observed on the right at 2.5 m with a value of 0.15 kg/m^3, this was observed in the aisle seat, the highest observation of 0.11 kg/m^3 on the left was at 2.2 m in the window seat. At the rear, Figure 110c, the highest average level of 0.15 kg/m^3 was observed on the right side at 2.2 m and 2.5 m in the aisle seat, compared the highest observed value of 0.11 kg/m^3 on the left at 1.5 m in the aisle seat.

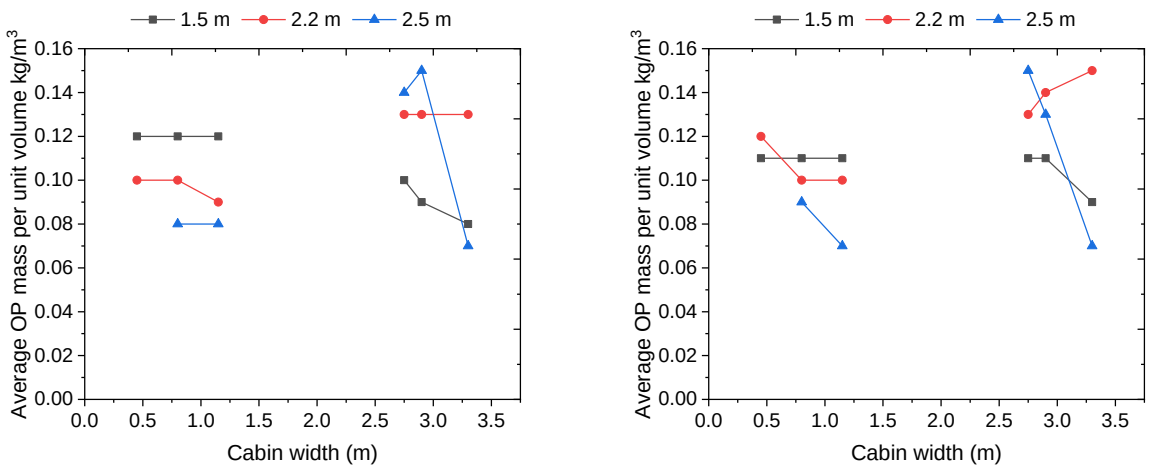

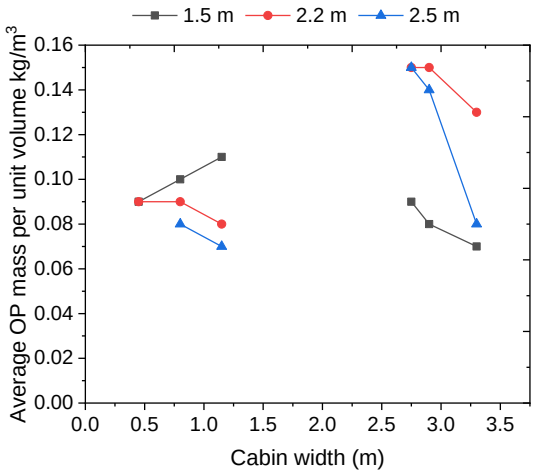

Figure 110: Average density of contamination for PS16_NP5 at the front (a) middle (b) and rear (c) of the cabin

Figure 111 shows the total density measurements for particles of 16 µm. Highest levels were observed on the right side at the front, middle and rear. At the front, Figure 111a, highest observations of 168.68 kg/m^3 were on the right at 2.5 m in the centre seat, compared to levels of 143.84 kg/m^3 on the left at 1.5 m in the aisle seat. In the middle, Figure 111b, highest observations of 178.22 kg/m^3 were on the right, window seat at 2.2 m, compared to 142.97 kg/m^3 on the left, at 2.2 m in the aisle seat. At the rear, Figure

111c, highest observations of 180.55 kg/m^3 were on the right at 2.5 m in the aisle, compared to levels of 136.66 kg/m^3 on the left at 1.5 m in the aisle seat.

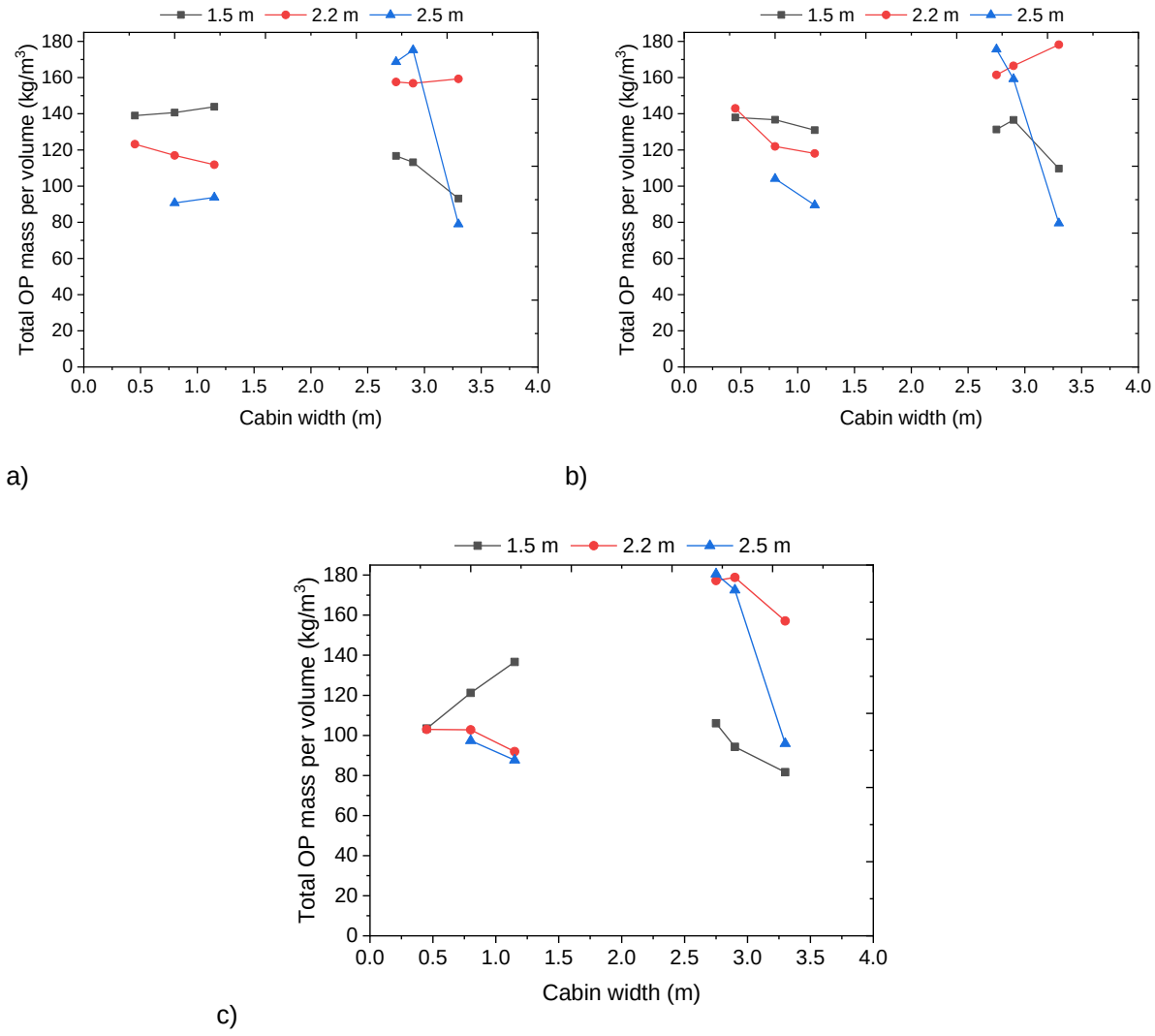

Figure 111: Total density of contamination for PS16_NP5 at the front (a) middle (b) and rear (c) of the cabin

Figure 112 illustrates the motion of the particles during the 600 s simulation 1.8 m from the rear of the cabin. All particles are given a 0.6 second trail so the direction and flow path can be clearly seen. As can be seen from the start the particles are evenly distributed

on both sides of the cabin. As the simulation progresses, from 300 seconds Figure 112d, particles are observed as having a slightly higher density on the right side. Figure 112 clearly illustrates the recirculation of the particles.

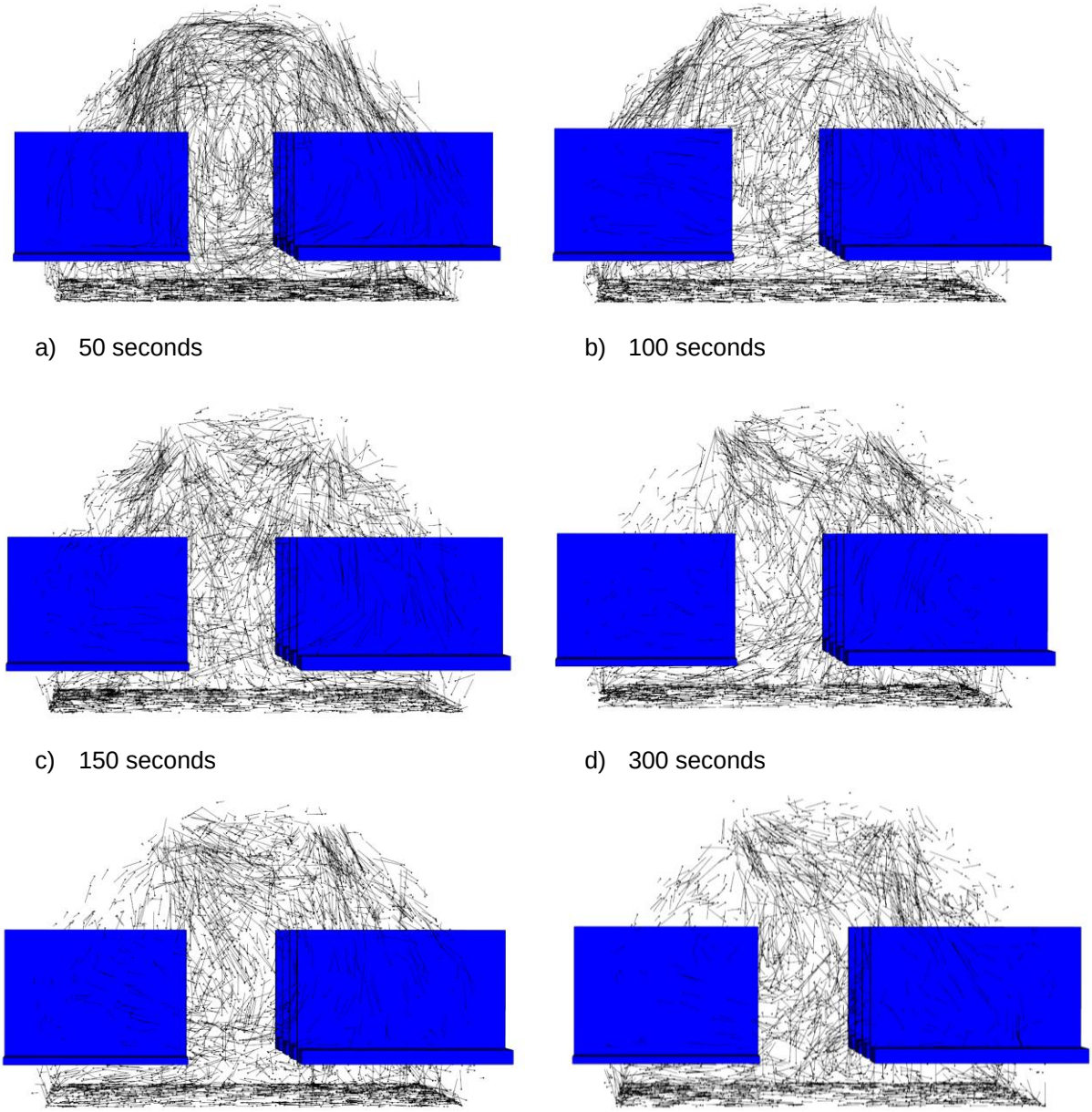

a) 50 seconds

b) 100 seconds

c) 150 seconds

d) 300 seconds

e) 450 seconds

f) 600 seconds

Figure 112: Motion of particles for case PS16NP5 a-f 50-600 seconds

Comparison of the distribution of the particles as observed in Figure 112 with the velocity profile within the cabin as can be seen in Figure 113 shows particles are following the air contours.

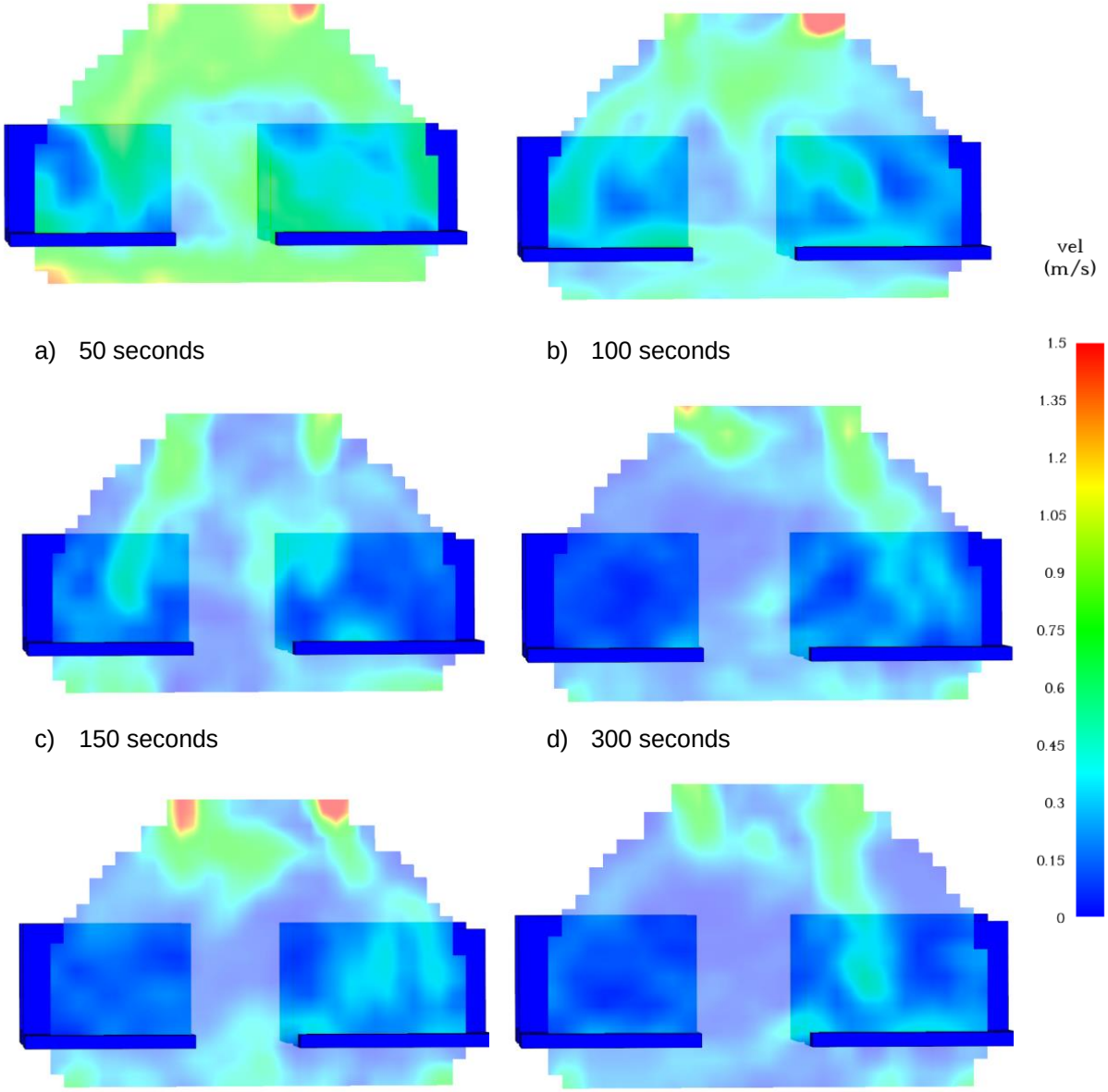

a) 50 seconds b) 100 seconds

c) 150 seconds d) 300 seconds

e) 450 seconds f) 600 seconds

Figure 113: Velocity profile for case PS16NP5 a-f 50-600 seconds

Figure 113 illustrates the contours of air and gas velocity 1.8 m from the rear of the cabin. Flow can be seen entering from the top of the cabin via the two supply vents and flowing downwards towards the seating area and to the extract vents on the floor. Initially there is a high velocity on the right side. Figure 113a, this mirrors the path the particles are taking Figure 112a. As the simulation progresses the velocity settles but clearly identifies the highest velocities at the supply vents.

6.7.6 Case PS50_NP5

Case PS50_NP5 injected 50000 particles of 50 µm diameter into the aircraft cabin via both inlet vents at the top of the cabin. Figure 114 shows the average density measured at the front (a), middle (b) and rear (c) of this cabin (see Figure 93 to identify location). The figures clearly indicate the density on the left and right side of the cabin at heights of 1.5 m, 2.2 m and 2.5 m. As the particle size increases, the left and right side start to see similar patterns in the concentrations. Similar average levels were observed on both sides of the cabin at front, middle and rear. At the front, Figure 114a, the highest average observation of 0.1 kg/m^3 at 2.5 m in all three seats (aisle, middle and window) as well as the aisle seat at 2.2 m. In the middle, Figure 114b, highest average levels were observed on the right at 2.2 m and 2.5 m with a value of 0.12 kg/m^3, this was observed in the aisle seat, the highest observation of 0.1 kg/m^3 on the left was at 2.2 m in the window seat. At the rear, Figure 114c, the highest average level of 0.1 kg/m^3 was observed on the right side at 2.5 m in the aisle seat, compared the highest observed value of 0.09 kg/m^3 on the left at 2.2 m in all three seats (aisle, centre and window) as well as the aisle seat at 2.5 m.

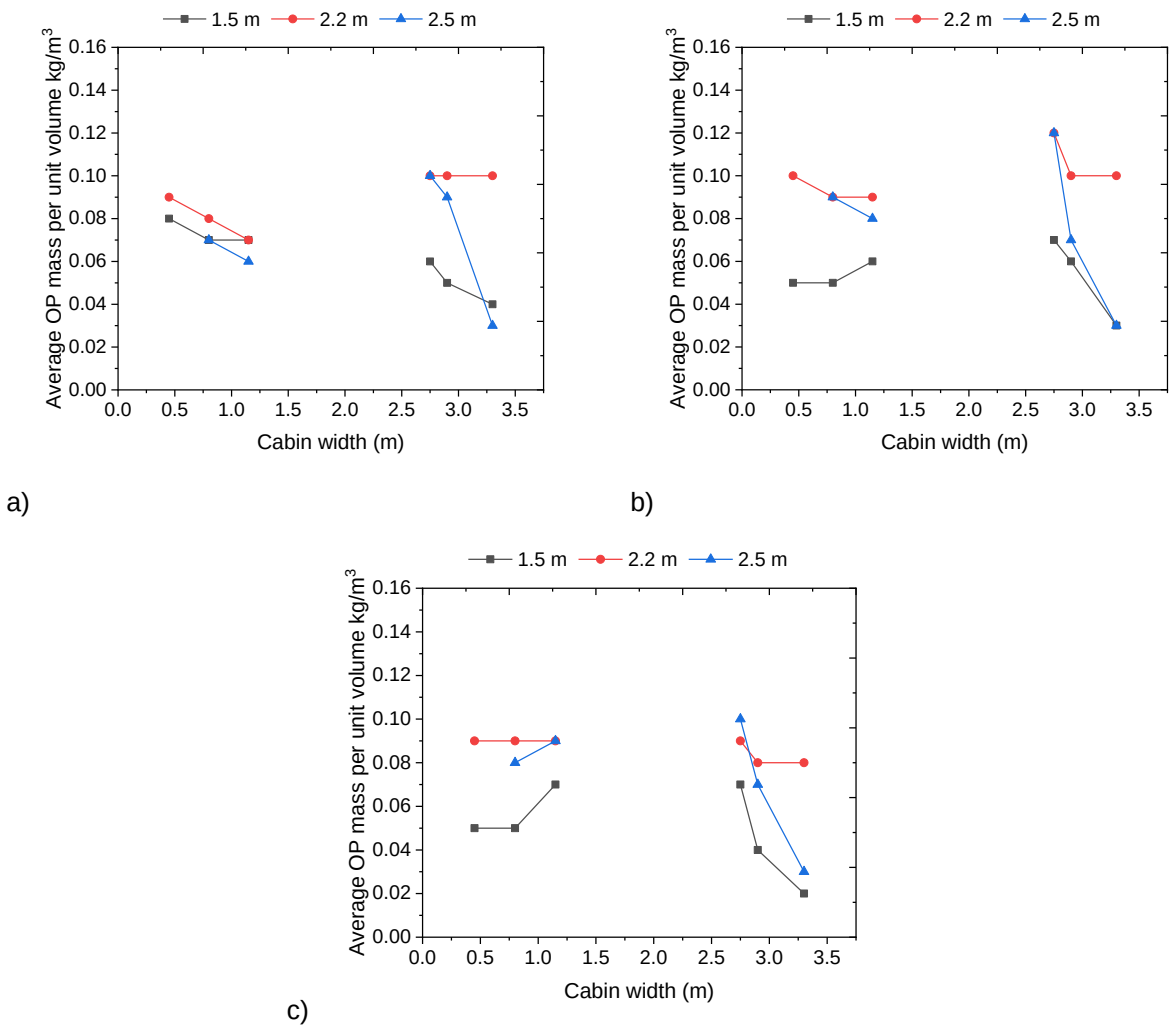

Figure 114:Average density of contamination for PS50_NP5 at the front (a) middle (b) and rear (c) of the cabin

Figure 115 shows the total density measurements for particles of 50 µm. Highest levels were observed on the right side at the front, middle and rear. At the front, Figure 115a, highest observations of 124.19 kg/m^3 were on the right at 2.5 m in the aisle, compared to levels of 105.15 kg/m^3 on the left at 2.2 m in the window seat. In the middle, Figure 115b, highest observations of 145.37 kg/m^3 were on the right, aisle seat at 2.5 m, compared to 104.94 kg/m^3 on the left, at 2.2 m in the aisle seat. At the rear, Figure 115c, highest

observations of 119.18 kg/m^3 were on the right at 2.5 m in the aisle, compared to levels of 109.55 kg/m^3 on the left at 2.2 m in the aisle seat.

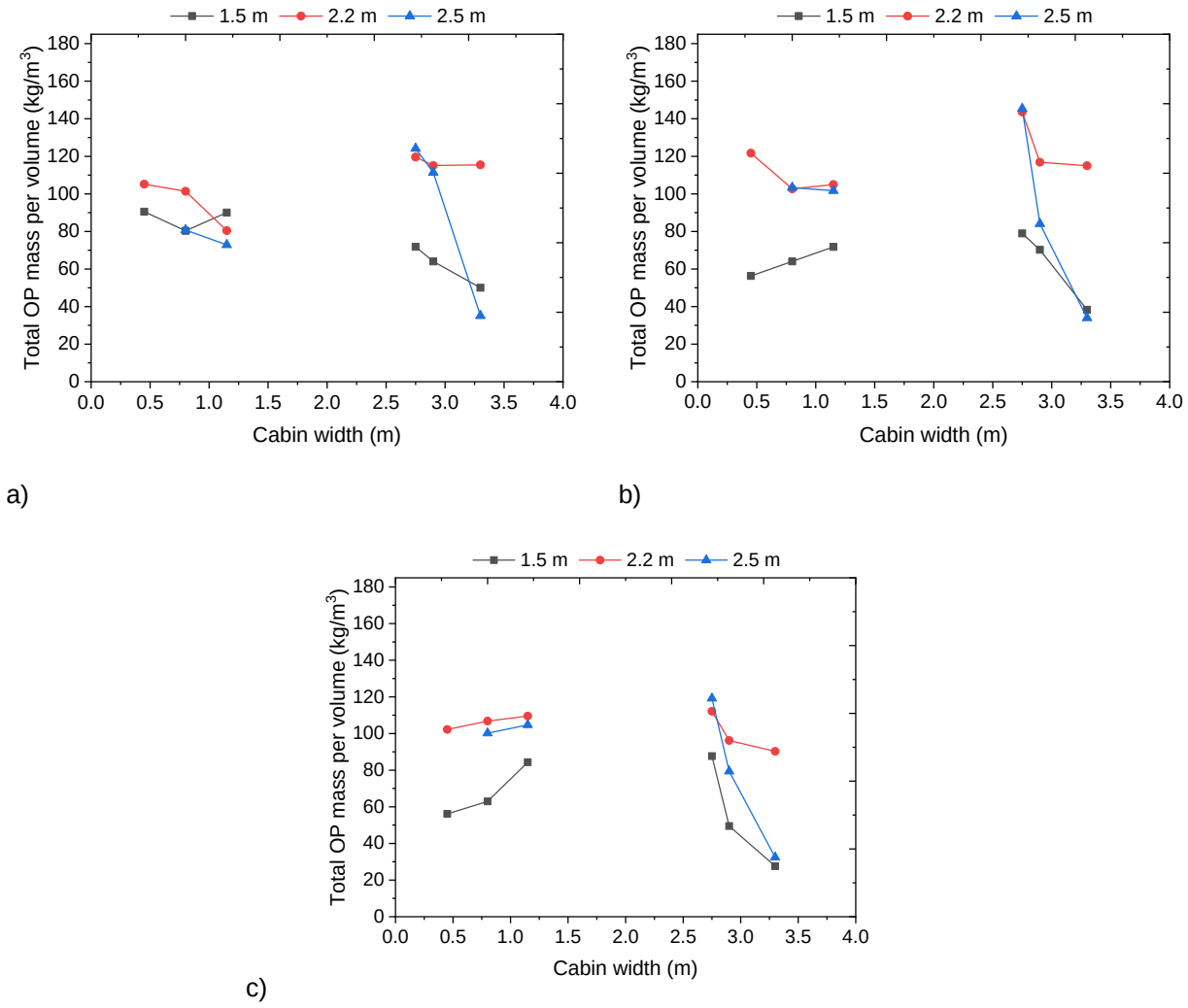

Figure 115:Total density of contamination for PS50_NP5 at the front (a) middle (b) and rear (c) of the cabin

Figure 116 illustrates the motion of the particles during the 600 s simulation 1.8 m from the rear of the cabin. All particles are given a 0.6 second trail so the direction and flow path can be clearly seen. Within the first 100 seconds Figure 116b, of the simulation,

particles are observed in a larger density on the left side. As the simulation progresses, from 300 seconds Figure 116d, the particles are observed as having an even distribution across both sides of the cabin. Figure 116 clearly illustrates the recirculation of the particles.

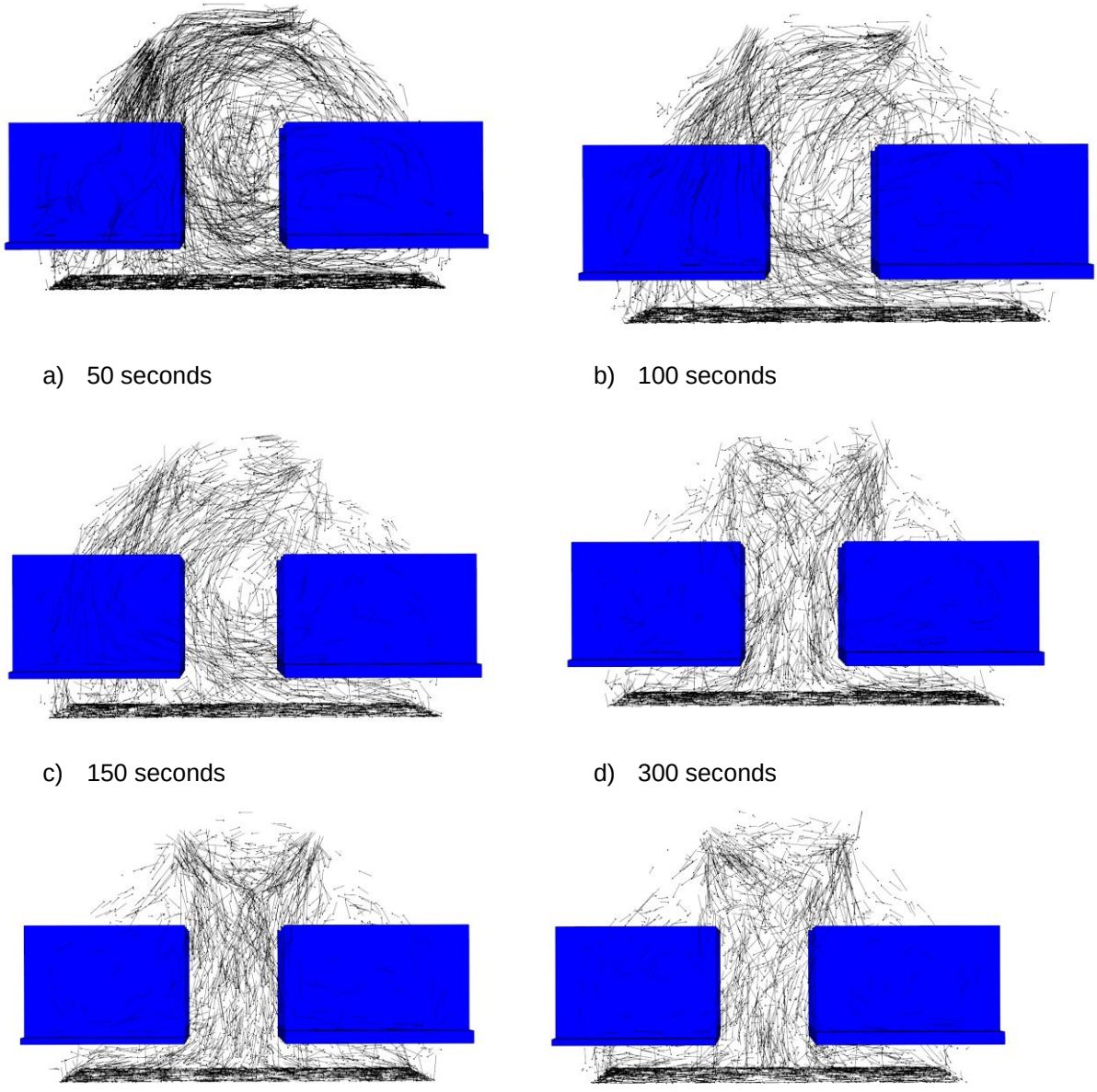

a) 50 seconds

b) 100 seconds

c) 150 seconds

d) 300 seconds

e) 450 seconds

f) 600 seconds

Figure 116: Motion of particles for case PS50NP5 a-f:50-600 seconds

Comparison of the distribution of the particles as observed in Figure 116, with the velocity profile within the cabin as can be seen in Figure 117 shows particles are following the air contours.

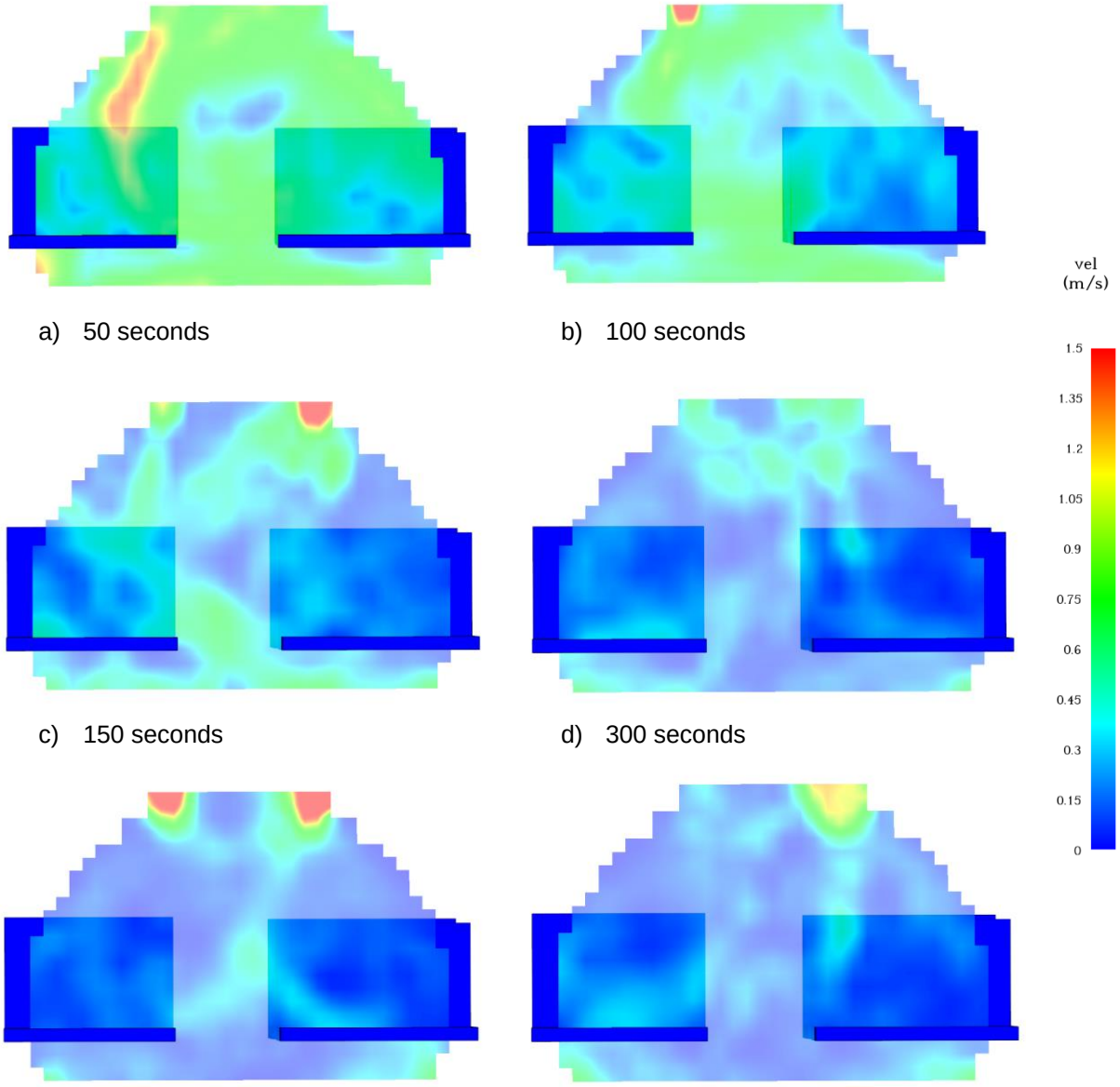

a) 50 seconds

b) 100 seconds

c) 150 seconds

d) 300 seconds

e) 450 seconds

f) 600 seconds

Figure 117: Velocity profile for case PS50_NP5 a-f: 50 -600 seconds

Figure 117 illustrates the contours of air and gas velocity 1.8 m from the rear of the cabin. Flow can be seen entering from the top of the cabin via the two supply vents and flowing downwards towards the seating area and to the extract vents on the floor. Initially there is a high velocity on the left side Figure 117a, this mirrors the path the particles are taking Figure 117a. As the simulation progresses the velocity settles but clearly identifies the highest velocities at the supply vents.

6.7.7 Case PS100_NP5

Case PS100_NP5 injected 50000 particles of 100 µm diameter into the aircraft cabin via both inlet vents at the top of the cabin. Figure 118 shows the average density measured at the front (a), middle (b) and rear (c) of this cabin (see Figure 93 to identify location). Figure 118 indicates the density on the left and right side of the cabin at heights of 1.5 m, 2.2 m and 2.5 m. As the particle size increases, the left and right side start to see similar patterns in the concentrations. Higher average levels were observed on the right of the cabin at front, middle and rear. At the front, Figure 118a, the highest average observation of 0.05 kg/m^3 at 2.2 m and 2.5 m in the aisle seat, compared to a highest average value of 0.04 kg/m^3 on the left at 2.2 m and 2.5 m in the aisle and centre seat. In the middle, Figure 118b, highest average levels were observed on the right at 2.5 m with a value of 0.10 kg/m^3, this was observed in the aisle seat, the highest observation of 0.03 kg/m^3 on the left was at 2.2 m in all three seats (aisle, centre and window) as well as 2.5 m in the aisle seat. At the rear, Figure 118c, the highest average level of 0.08 kg/m^3 was observed on the right side at 2.5 m in the aisle seat, compared the highest observed value of 0.03 kg/m^3 on the left at 2.2 m in the aisle and centre seat.

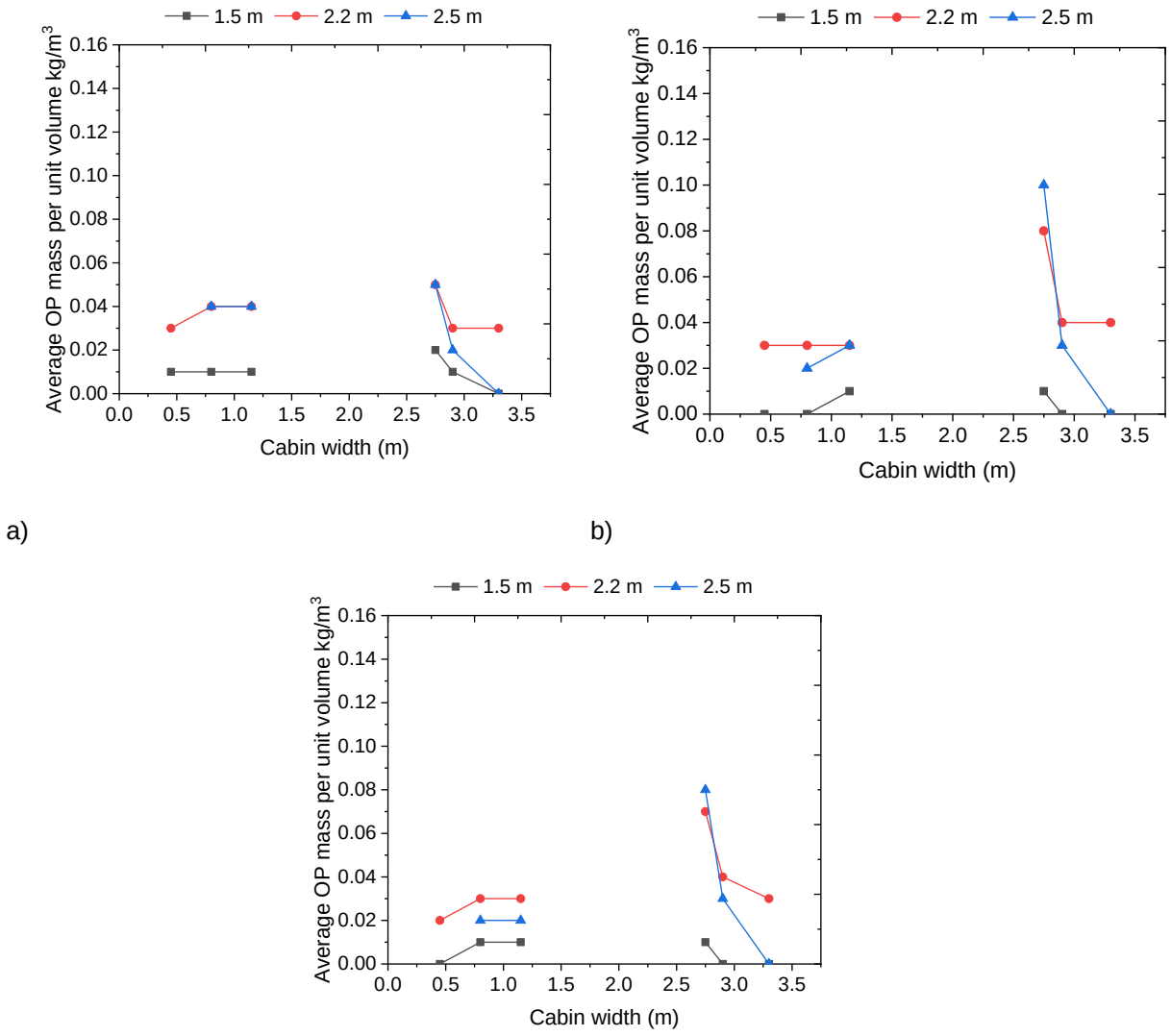

Figure 118: Average density of contamination for PS100_NP5 at the front (a) middle (b) and rear (c) of the cabin

Figure 119 shows the total density measurements for particles of 100 µm. Highest levels were observed on the right side at the front, middle and rear. At the front, Figure 119a, highest observations of 64.41 kg/m^3 were on the right at 2.5 m in the aisle, compared to levels of 52.56 kg/m^3 on the left at 2.2 m in the centre seat. In the middle, Figure 119b highest observations of 116.17 kg/m^3 were on the right, centre seat at 2.5 m, compared

to 39.73 kg/m^3 on the left, at 2.2 m in the aisle seat. At the rear, Figure 119c, highest observations of 96.16 kg/m^3 were on the right at 2.5 m in the aisle, compared to levels of 31.8 kg/m^3 on the left at 2.2 m in the centre seat.

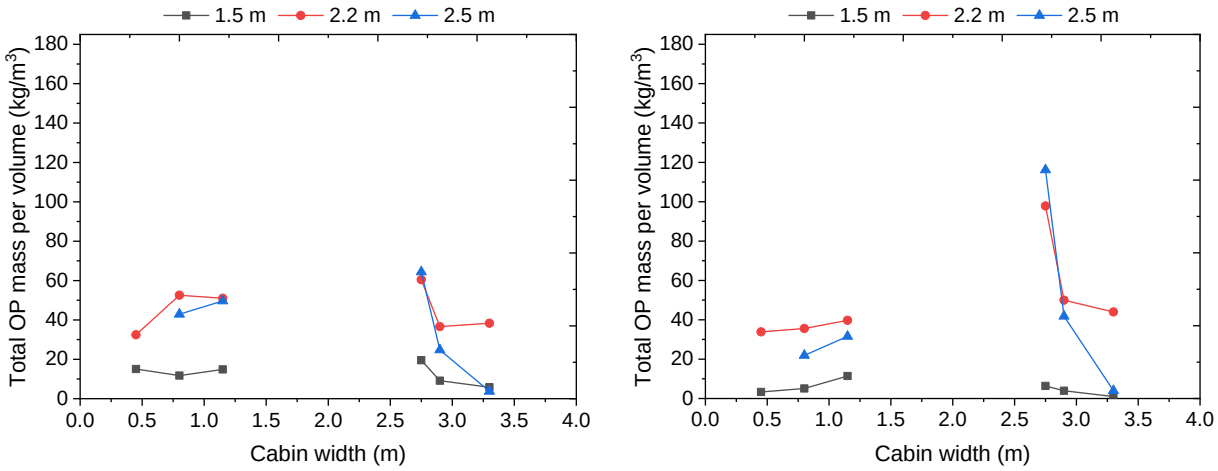

a) b)

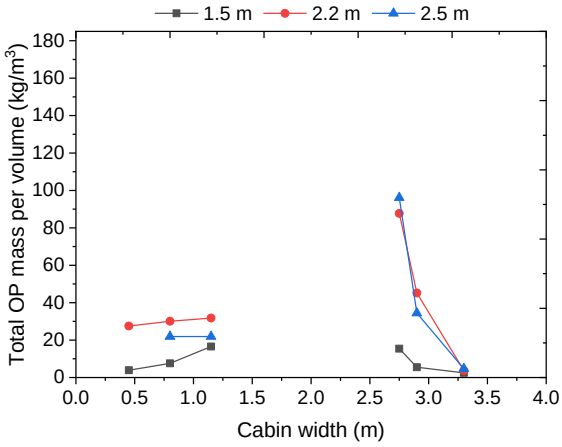

c)

Figure 119: Total density of contamination for PS100_NP5 at the front (a) middle (b) and rear (c) of the cabin

Figure 120 illustrates the motion of the particles during the 600 s simulation 1.8 m from the rear of the cabin. All particles are given a 0.6 second trail so the direction and flow

path can be clearly seen. Within the first 150 seconds of the simulation, Figure 120c, particles are observed in a larger density on the right side. As the simulation progresses, from 300 seconds Figure 120d, particles are observed as having an even distribution across both sides of the cabin. Figure 120 clearly illustrates the recirculation of the particles.

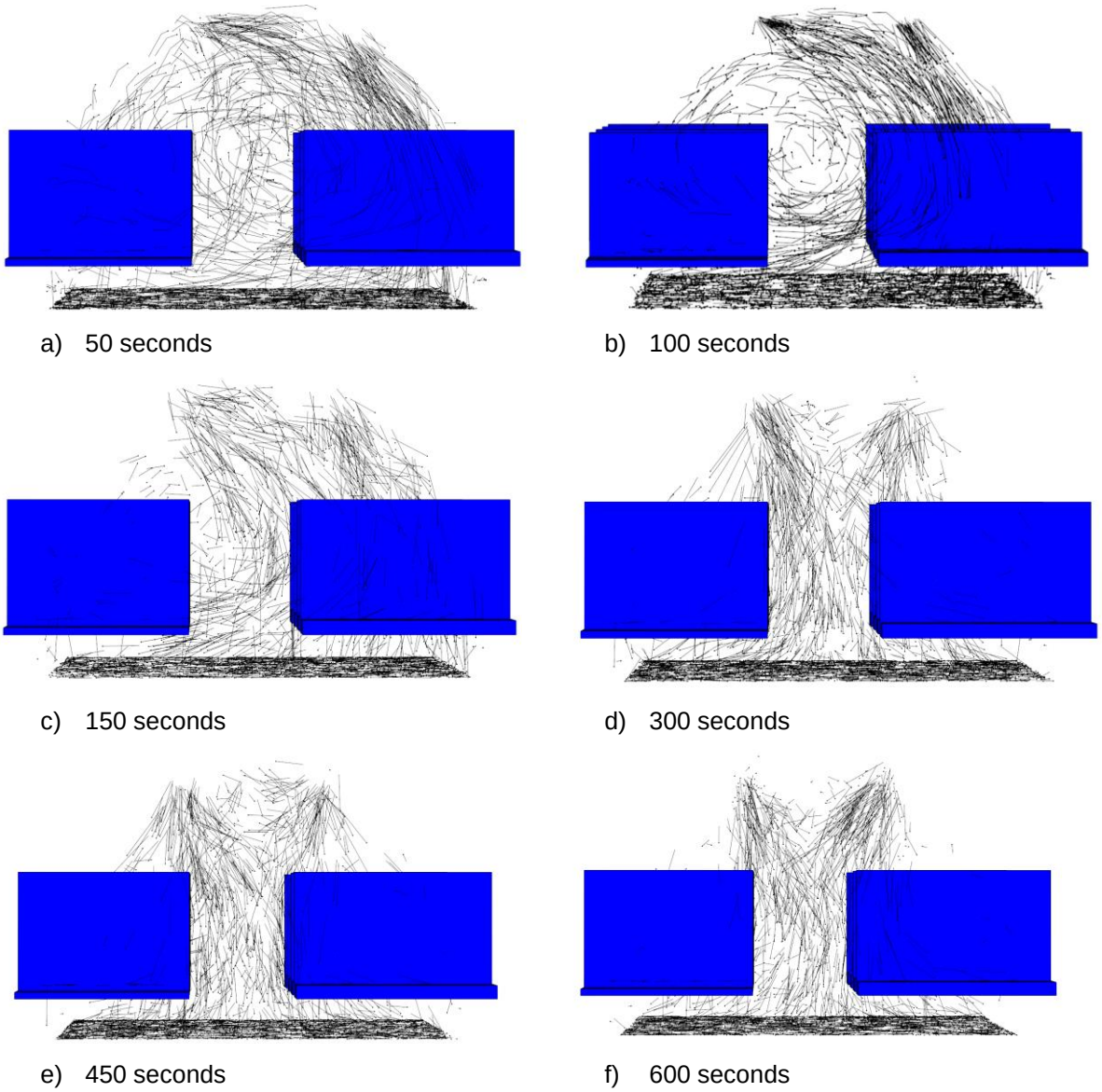

a) 50 seconds

b) 100 seconds

c) 150 seconds

d) 300 seconds

e) 450 seconds

f) 600 seconds

Figure 120: Motion of particles for case PS100_NP5 a-f:50-600 seconds

Comparison of the distribution of the particles as observed in Figure 120, with the velocity profile within the cabin as can be seen in Figure 121 shows particles are following the air contours.

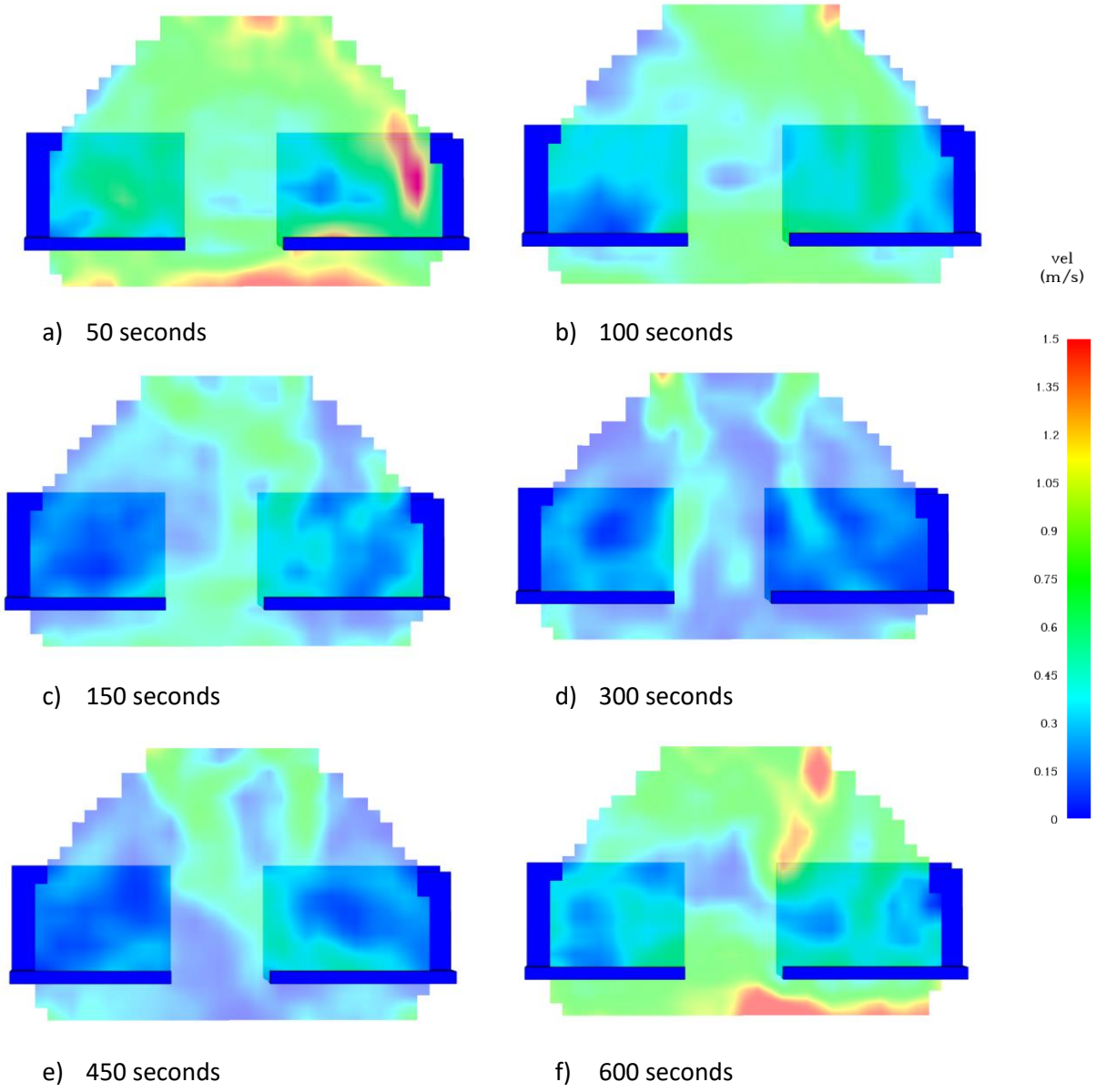

Figure 121: Velocity profile for case PS100_NP5 a-f: 50 -600 seconds

Figure 121 illustrates the contours of air and gas velocity 1.8 m from the rear of the cabin. Flow can be seen entering from the top of the cabin via the two supply vents and flowing

downwards towards the seating area and to the extract vents on the floor. Initially there is a high velocity on the right side, Figure 121a after 50 seconds this mirrors the path the particles are taking Figure 120a. As the simulation progresses the velocity settles but clearly identifies the highest velocities at the supply vents.

6.7.8 Case PS200_NP5

Case PS200_NP5 injected 50000 particles of 200 µm diameter into the aircraft cabin via both inlet vents at the top of the cabin. Figure 122 shows the average density measured at the front (a), middle (b) and rear (c) of this cabin (see Figure 93 to identify location). Figure 122 indicates the density on the left and right side of the cabin at heights of 1.5 m, 2.2 m and 2.5 m. As the particle size increases, the left and right side start to see similar patterns in the concentrations. Higher average levels were observed on the right of the cabin at front, middle and rear. At the front, Figure 122a, the highest average observation of 0.06 kg/m^3 at 2.2 m and 2.5 m was in the aisle seat, compared to the highest average value of 0.01 kg/m^3 on the left at 2.2 m and 2.5 m in the aisle seat. In the middle, Figure 122b, highest average levels were observed on the right at 2.5 m with a value of 0.09 kg/m^3, this was observed in the aisle seat, the highest observation of 0.02 kg/m^3 on the left was at 2.2 m in the aisle seat. At the rear, Figure 122c, the highest average level of 0.09 kg/m^3 was observed on the right side at 2.5 m in the aisle seat, compared the highest observed value of 0.013 kg/m^3 on the left at 2.2 m and 2.5 m in the aisle seat.

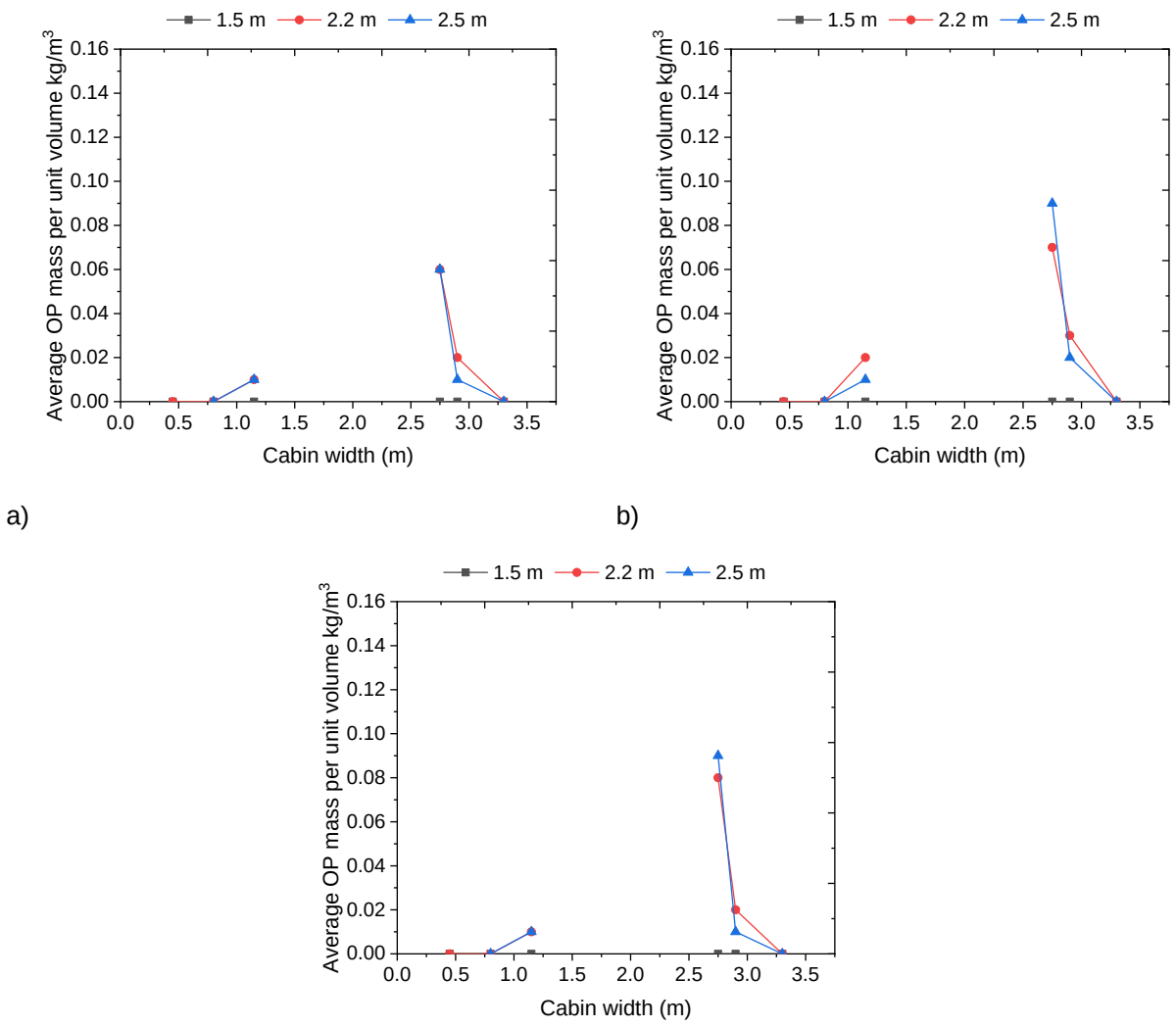

Figure 122: Average density of contamination for PS200_NP5 at the front (a) middle (b) and rear (c) of the cabin

Figure 123 shows the total density measurements for particles of 200 µm. Highest levels were observed on the right side at the front, middle and rear. At the front, Figure 123a, highest observations of 76.97 kg/m^3 were on the right at 2.5 m in the aisle, compared to levels of 7.84 kg/m^3 on the left at 2.2 m in the aisle seat. In the middle, Figure 123b, highest observations of 104.87 kg/m^3 were on the right, aisle seat at 2.5 m, compared to

19.82 kg/m^3 on the left, at 2.2 m in the aisle seat. At the rear, Figure 123c, highest observations of 169.0 kg/m^3 were on the right at 2.2 m in the window, compared to levels of 11.75 kg/m^3 on the left at 2.2 m in the aisle seat

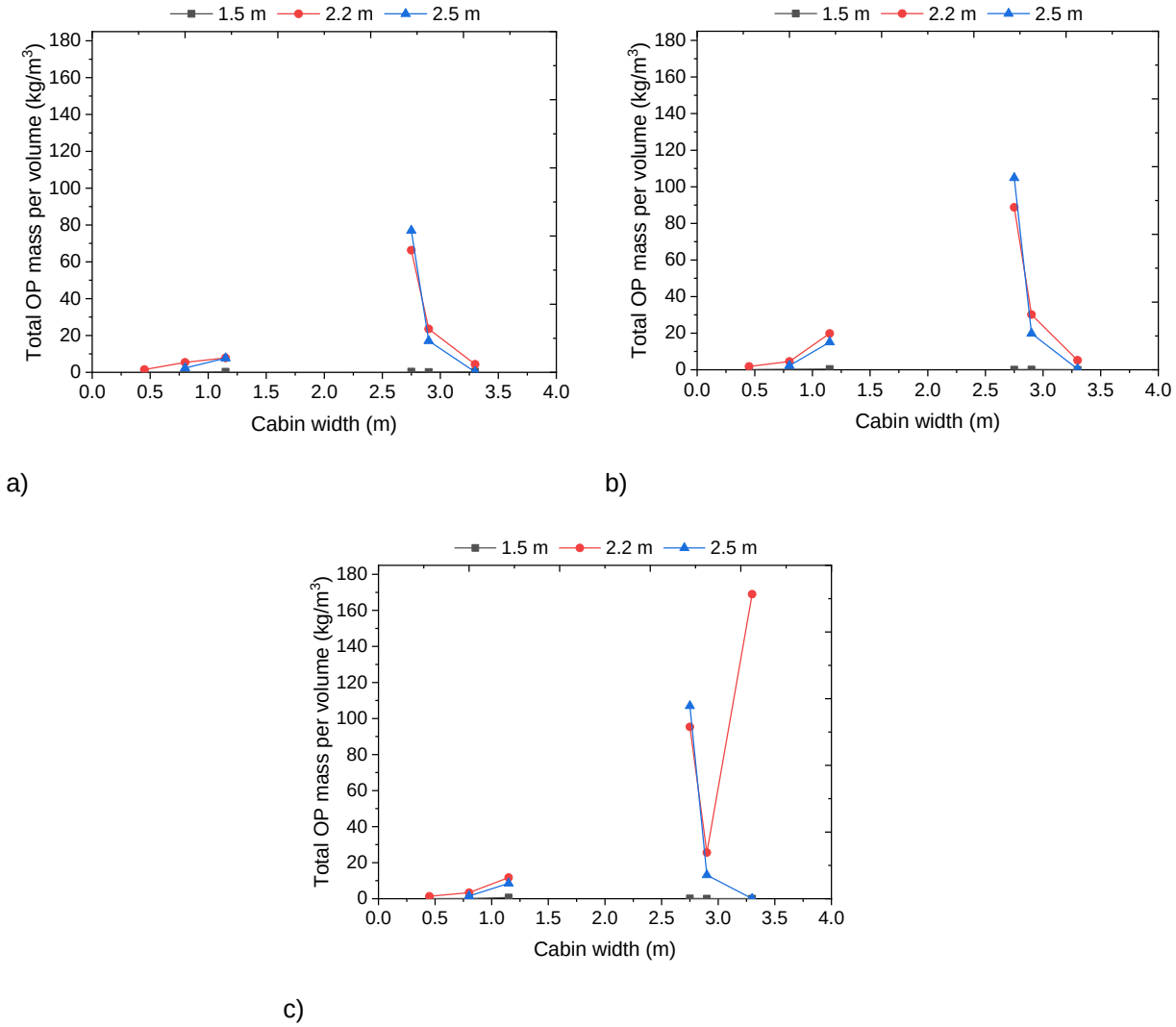

Figure 123: Total density of contamination for PS200_NP5 at the front (a) middle (b) and rear (c) of the cabin

Figure 124 illustrates the motion of the particles during the 600 s simulation 1.8 m from the rear of the cabin. All particles are given a 0.6 second trail so the direction and flow path can be clearly seen.

Within the first 100 seconds of the simulation, Figure 124b, particles are observed in a larger density on the right side. As the simulation progresses, from 300 seconds Figure 124d, particles are observed as having an even distribution across both sides of the cabin. Figure 124 clearly illustrates the recirculation of the particles.

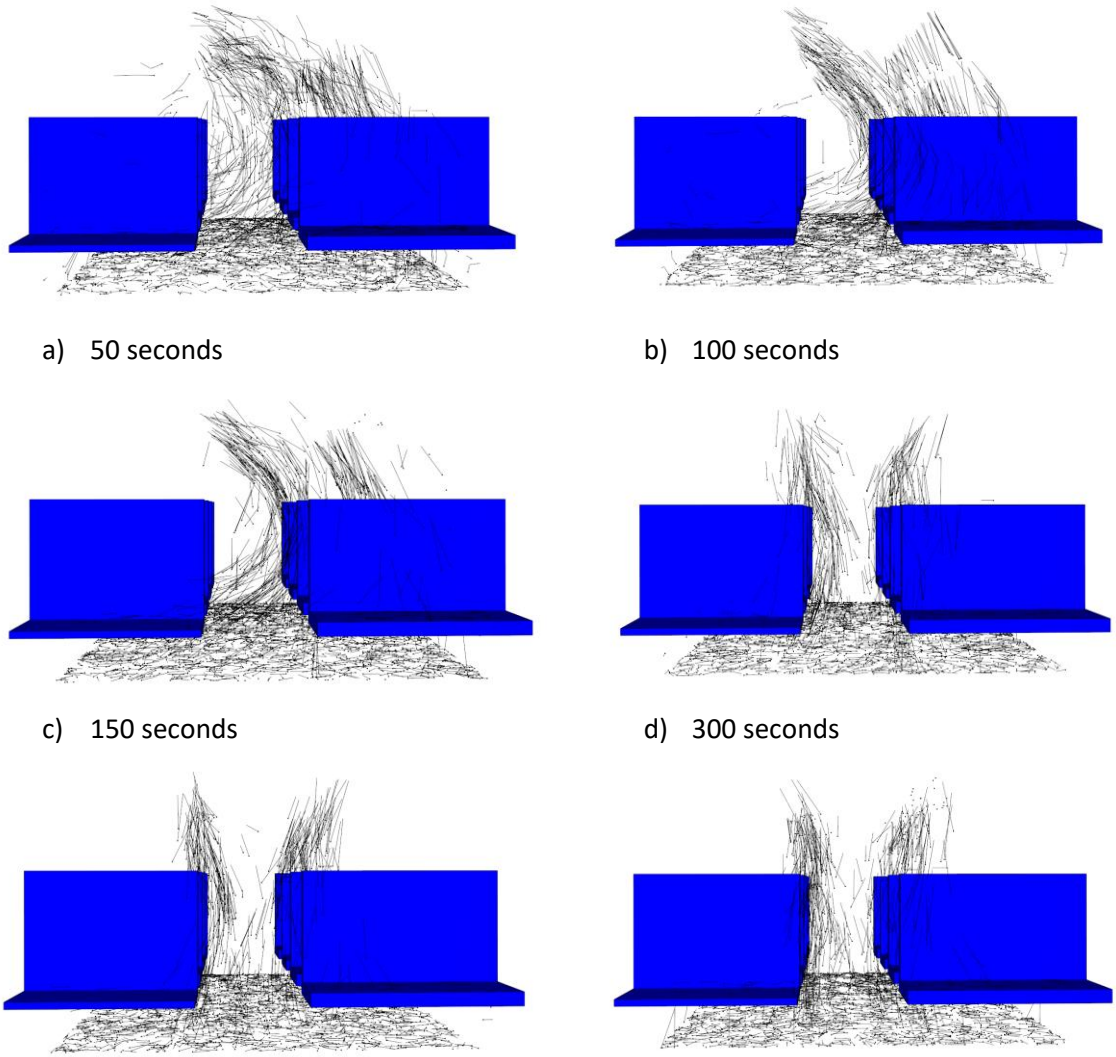

a) 50 seconds

b) 100 seconds

c) 150 seconds

d) 300 seconds

e) 450 seconds

f) 600 seconds

Figure 124: Motion of particles for case PS200_NP5 a-f: 50 - 600 seconds

Comparison of the distribution of the particles as observed in Figure 124, with the velocity profile within the cabin as can be seen in Figure 125 shows particles are following the air contours.

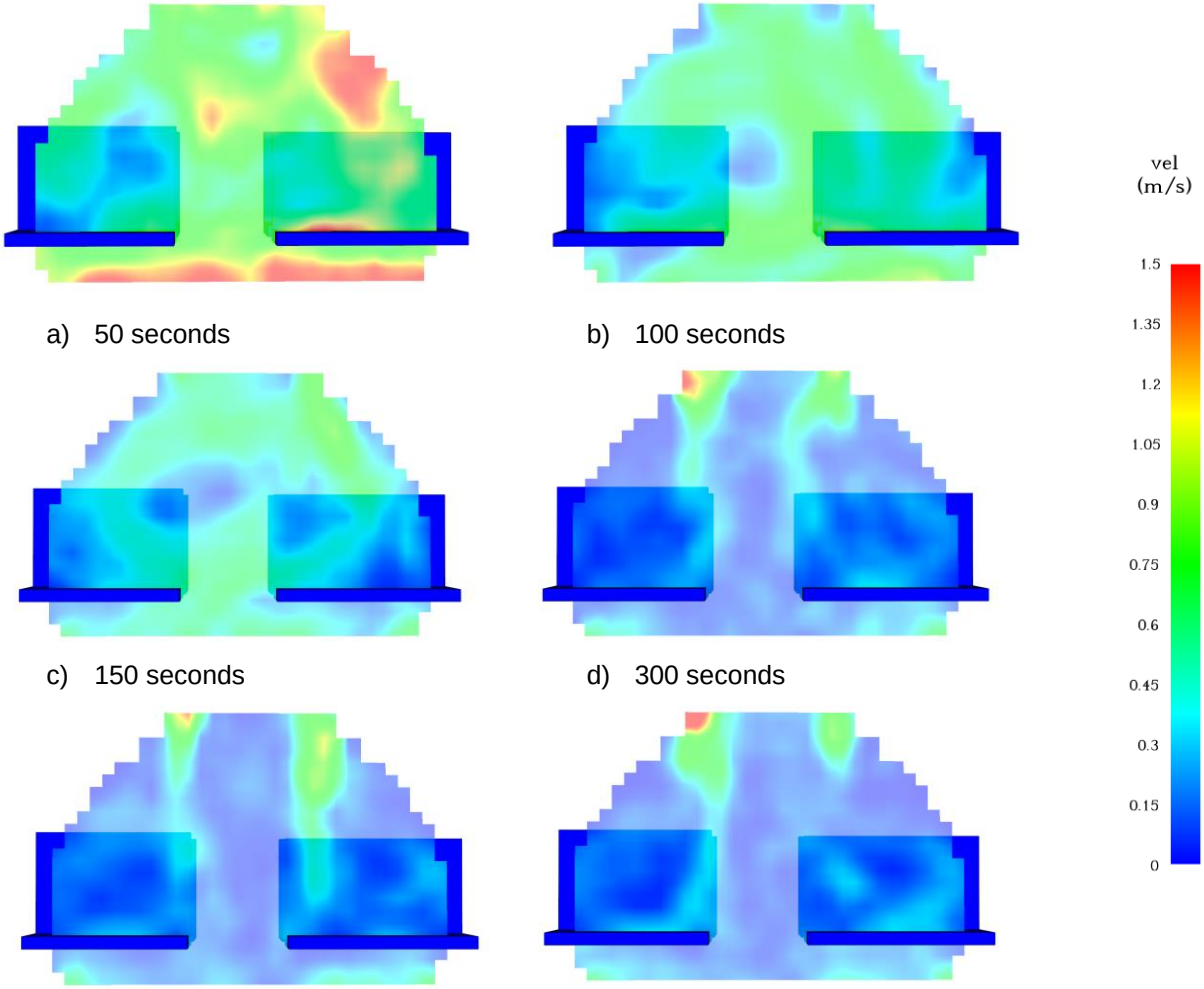

Figure 125: Velocity profile for case PS200_NP5 a-f: 50 - 600 seconds

Figure 125 illustrates the contours of air and gas velocity 1.8 m from the rear of the cabin. Flow can be seen entering from the top of the cabin via the two supply vents and flowing downwards towards the seating area and to the extract vents on the floor. Initially there is a high velocity on the right side, Figure 125a after 50 seconds, with a high velocity at

the extract vents on the floor level. As the simulation progresses the velocity settles but clearly identifies the highest velocities at the supply vents.

6.8 Discussion

As can be seen in the majority of cases it is the aisle seat which receives the highest concentration of material. The height does affect the exposure, with 2.5 m generally being the height at which the highest levels have been measured. Particle size does significantly impact on the distribution of the particles.

If we compare case PS16_NP4, PS50_NP4, PS100_NP4, PS200_NP4 where we are increasing the particle diameter from 16 µm to 200 µm, we can see that as the particle diameter increases, the number of particles observed in all locations decreases. With the range of average particles at 16 µm being from 0.07 kg/m^3 – 0.15 kg/m^3 compared to 0 – 0.09 kg/m^3. This is visibly seen if we compare Figures 94, 98, 103 and 106. A greater number of particles is seen when the particle diameter is low – 16 µm.

We can see if the number of particles inputted with the same diameter affects the distribution. By comparing case PS16_NP4 with PS16_NP5 we can see if increasing the number of particles injected from 40000 particles to 50000 affected the particle distribution within the cabin. By comparing Figure 94 with Figure 110, the levels observed in both cases mirror each other. Similar levels are observed, at the front of the cabin the highest average mass per unit volume was in the centre seat on the right at 2.5 m for both cases. In the middle, the highest value observed was on the right side, in the aisle seat at 2.5 m and the window seat at 2.2 m with levels of 0.15 kg/m^3. At the rear, the highest value observed was on the right side, in the aisle seat at 2.5 m and the centre seat at 2.2 m with levels of 0.15 kg/m^3.

By comparing case PS50_NP4 with PS50_NP5 we can see if increasing the number of particles injected from 40000 particles to 50000 affected the particle distribution within the cabin. By comparing Figure 98 with Figure 114, the levels observed in both cases similar to each other but did show some differences. At the front of the cabin, with the lower number of particles injected, the highest levels observed were on the left of the cabin – 0.11 kg/m^3 in the centre and aisle seat at both 2.2 m and 2.5 m. Whilst when we increased the number of particles inject to 50000 the highest levels observed at the front of the cabin

appeared on the right with highest levels observed in the aisle seat for 2.5 m and all three seats at 2.2 m. As we move through the cabin highest levels are observed on the right than the left when we have a higher level of particles injected, but similar patterns are observed.

By comparing case PS100_NP4 with PS100_NP5 we can see that if increasing the number of particles injected from 40000 particles to 50000 with larger diameter affected the particle distribution within the cabin. By comparing Figure 103 with Figure 118, the levels observed in both cases mirror each other. Similar levels are observed, at the front of the cabin the highest average mass per unit volume (0.05 kg/m^3) was in the aisle seat on the right at 2.5 m for both cases. In the middle, the highest value observed was on the right side for both cases. When the lower number of particles was injected, the aisle seat at 2.2 m observed levels of 0.08 kg/m^3 whereas when the larger number of particles was injected, the aisle seat observed values of 0.1 kg/m^3 but this was at 2.5 m high. At the rear, Similar patterns were observed, with the highest levels of 0.08 kg/m^3 observed in the aisle seat on the right at 2.5 m.

By comparing case PS200_NP4 with PS200_NP5 we can see if increasing the number of particles injected from 40000 particles to 50000 with larger diameter of 200µm affected the particle distribution within the cabin. By comparing Figure 106 with Figure 112, the levels observed in both cases mirror each other in all locations. Similar levels are observed, at the front of the cabin the highest average mass per unit volume (0.06 kg/m^3) was in the aisle seat on the right at 2.5 m for both cases. In the middle, the highest value observed was on the right side for both cases, this was in the aisle seat at 2.5 m and observed values of 0.09 kg/m^3. At the rear, Similar patterns were observed, with the highest levels of 0.09 kg/m^3 observed in the aisle seat on the right at 2.5 m.

To understand if the velocity throughout the cabin stable analysis of slice files at two locations was conducted. These are illustrated on Figure 126. A vertical slice through

the length of the cabin running through the centre of the aisle at 1.8 m. The second slice was just above head height at 3.0 m again running the length of the cabin.

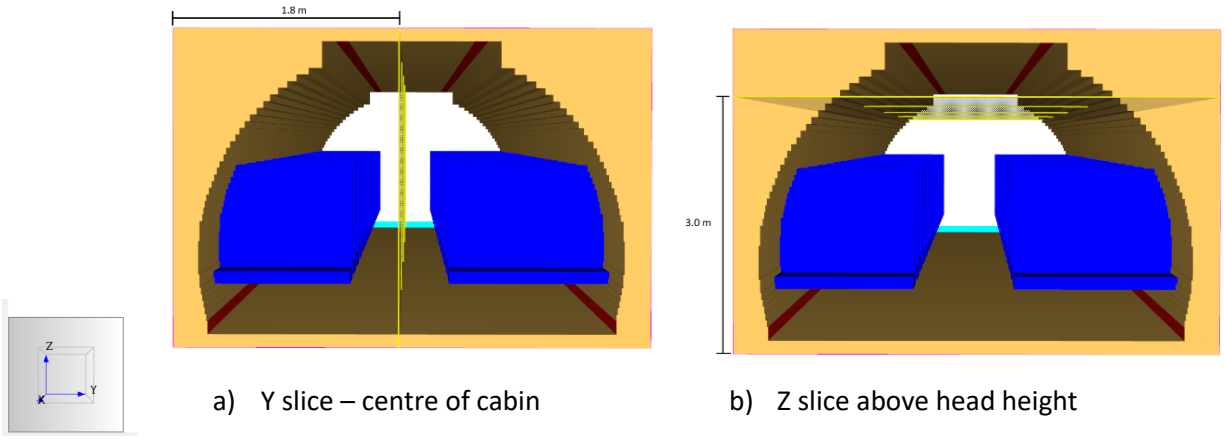

Figure 126: Location of slice files

Images were taken at 300 seconds for all eight cases to compare the velocity. As can be seen in Figure 127, turbulence can be observed at the top of the cabin, where the vents are supplying the air into the cabin. There is little variation in depth from top – 3.4 m to the bottom – floor level at 0 m. The length of the cabin again slows little variance. This is expected as the flow into the cabin is constant.

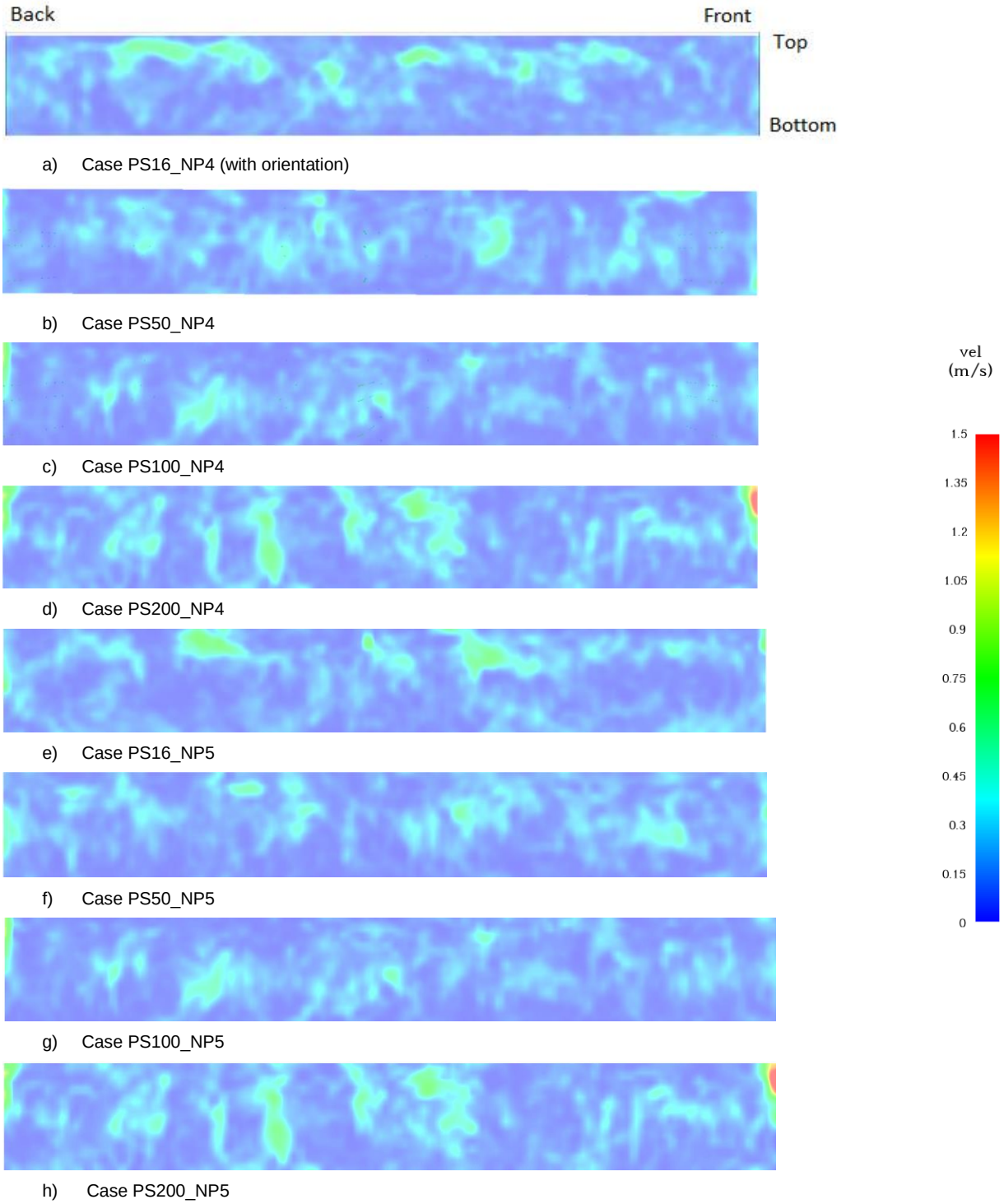

a) Case PS16_NP4 (with orientation)

b) Case PS50_NP4

c) Case PS100_NP4

d) Case PS200_NP4

e) Case PS16_NP5

f) Case PS50_NP5

g) Case PS100_NP5

h) Case PS200_NP5

Figure 127: Y-axis velocity profiles for all eight cases at 300 s

Figure 128 shows the velocity the width of the cabin at 3.0 m high. There is some variation on the left and right side as has been observed in the cases previously. This is minimal and is expected due to the nature of the model. As there is not a smooth curve the “corners” of the model will affect the turbulence. This is minimal and has not been seen as a impacting on the particle distribution greatly.

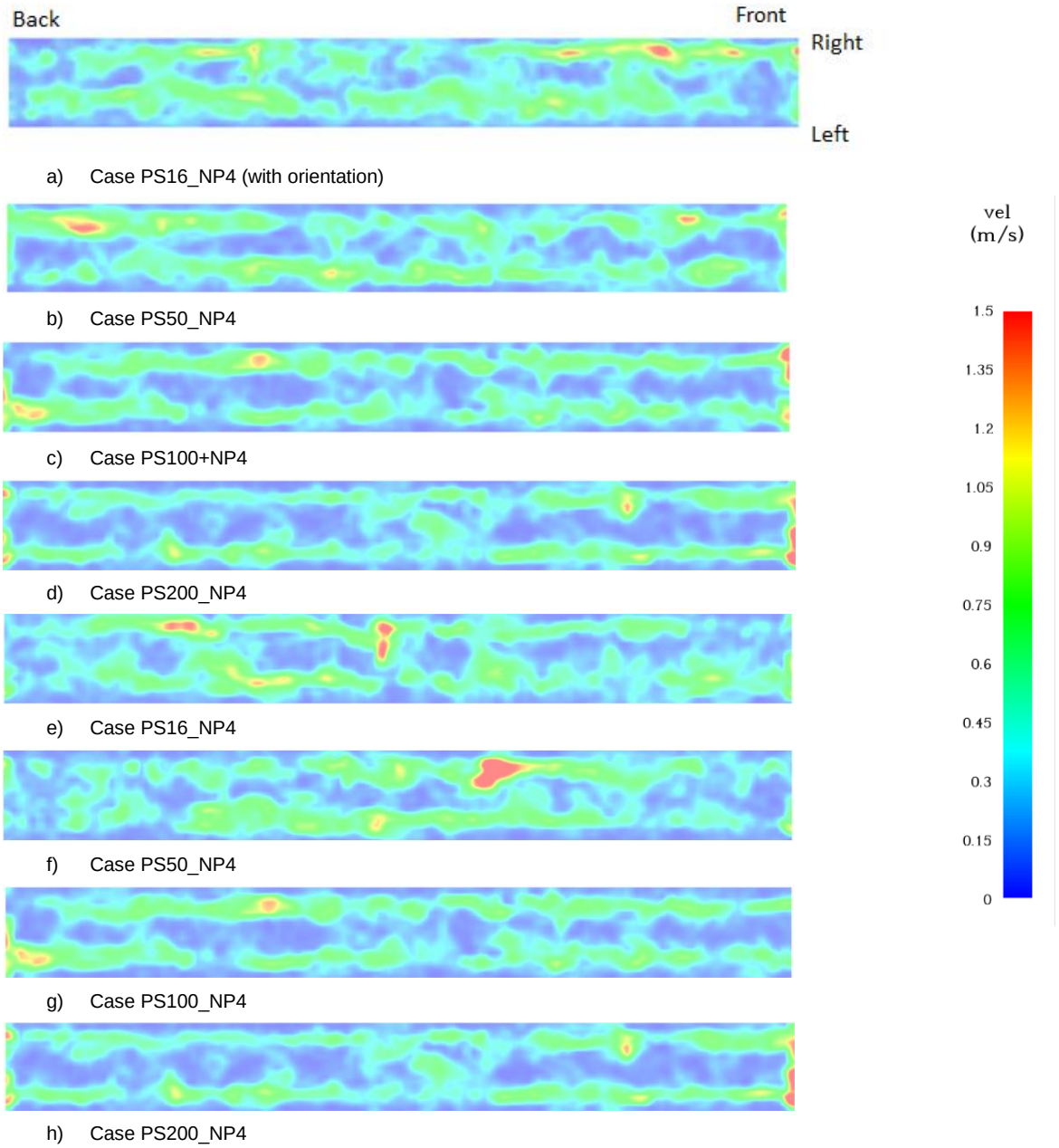

a) Case PS16_NP4 (with orientation)

b) Case PS50_NP4

c) Case PS100+NP4

d) Case PS200_NP4

e) Case PS16_NP4

f) Case PS50_NP4

g) Case PS100_NP4

h) Case PS200_NP4

Figure 128: Velocity profile in Z orientation

Figure 129 shows velocity profiles from the front, 12.0 m from the rear of the cabin, middle 6.0 m from the rear of the cabin and rear 1.8 m from the rear of the cabin as shown of Figure 92, for all four simulations: Cases: PS16_NP4, PS50_NP4, PS100_NP4 and

PS200_NP4. As can be seen there is a higher velocity at the top of the cabin where the air flow is being supplied (red is showing levels of 1.5 m/s). In all cases it can be seen that the flow decreases as it flows to the bottom of the cabin.

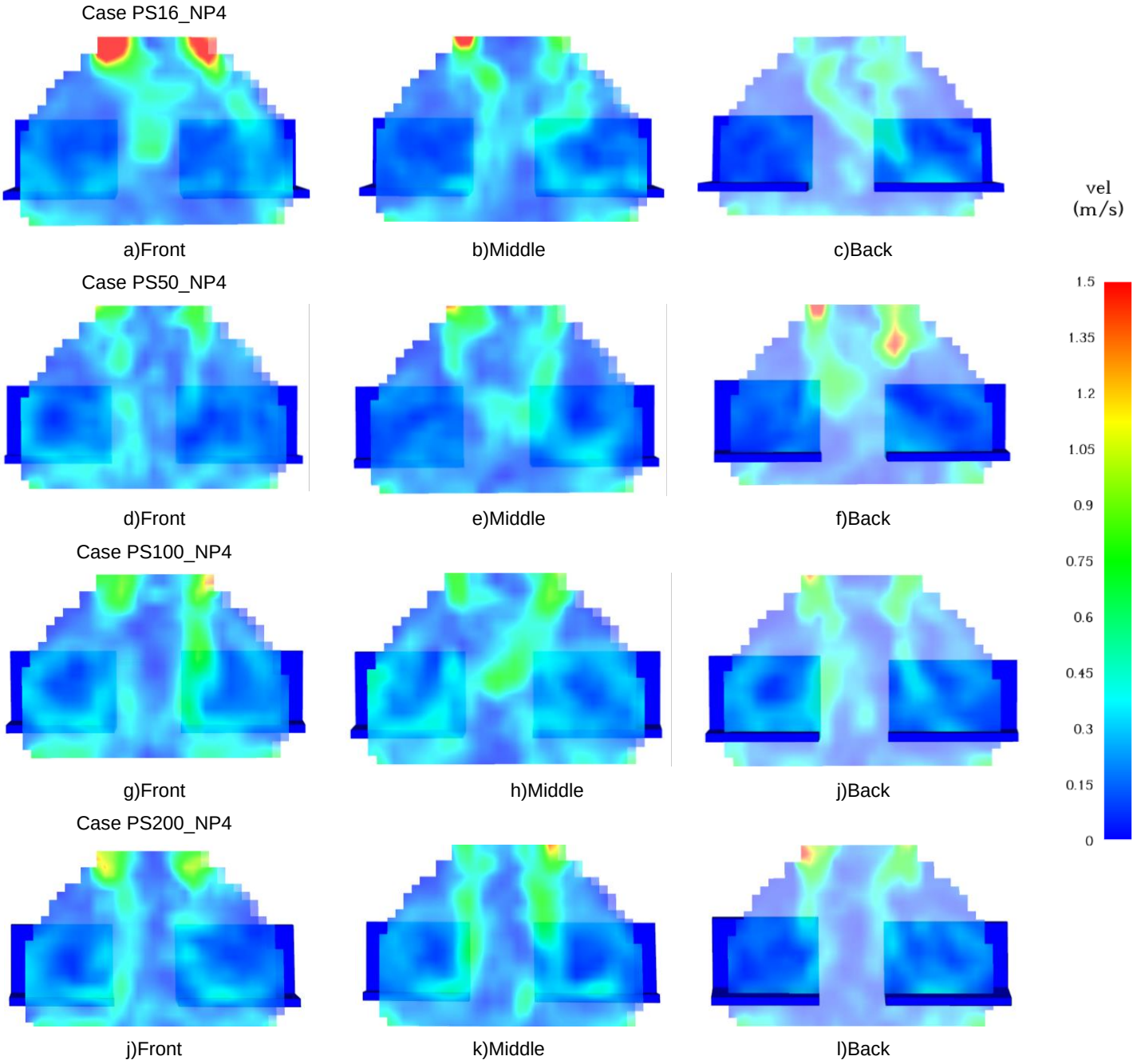

Figure 129: Velocity profile for four cases (1 to 4) simulations for the front, middle and rear of the cabin

Figure 130 shows velocity profiles from the front, 12.0 m from the rear of the cabin, middle 6.0 m from the rear of the cabin and rear 1.8 m from the rear of the cabin as can be seen on Figure 92, for four simulations: Cases: PS16_NP5, PS50_NP5, PS100_NP5 and PS200_NP5. As can be seen there is a higher velocity at the top of the cabin where the air flow is being supplied (red is showing levels of 1.5 m/s). In all cases it can be seen that the flow decreases as it flows to the bottom of the cabin.

As can be seen in Figures 129 and 130, there is little variation between the velocity contours of the gases when measured at the front, middle or rear. In Figure 129 and 130 in all cases a higher velocity is observed at the top of the cabin as this is where the air and gases are being supplied. As can be seen there is a turbulent flow down the centre of the cabin of the left and right and then this folds round under the seats and to the extract vents.

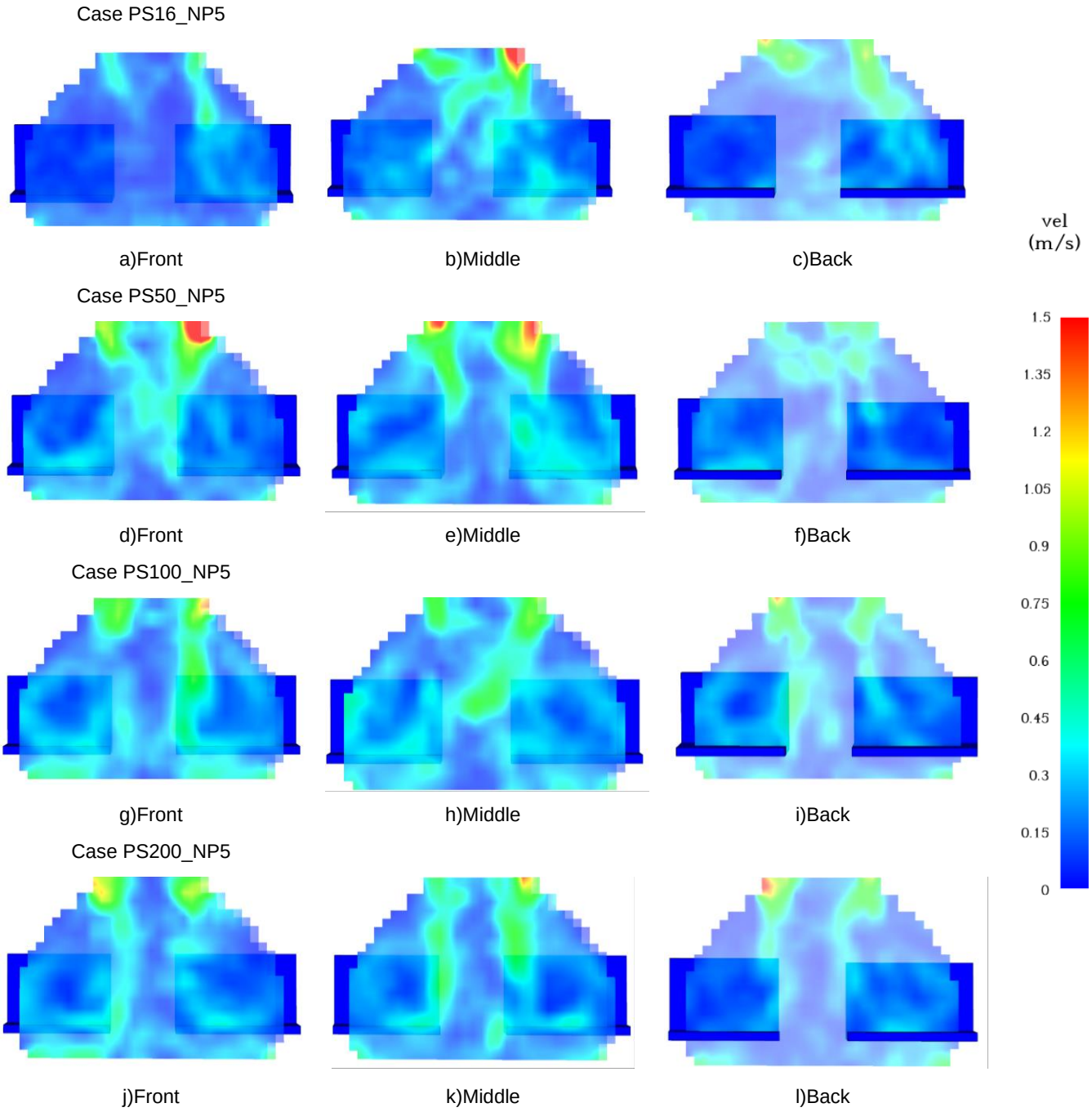

Figure 130: Velocity profile for four cases (5 to 8) simulations for the front, middle and rear of the cabin

Chapter 7 Conclusion

Although a variety of sources can contaminate the aircraft cabin air, jet engine oil was of primary concern. The use of TCP within engine oils has been the major concern as this could potentially contaminate the air supply. The determination of the presence of TCP in engine oil, the determination of the quantities entering the air supply and therefore the cabin and the potential flow paths of particles within the cabin was investigated in this research.

Based on the review of the previous studies on contamination of aircraft cabins, it was concluded that there was not a sufficient reporting methodology for air crew to report “fume” events. That there was a lack of trust in the official government and industry reports, which left a number of questions unanswered. There was a substantial gap in independently verifying that there was the possibility of contaminants entering the aircraft cabin at sufficient rates and quantities that can cause adverse health issues.

The experimental programme of this research used standard chemical analytical equipment (GC-MS), both technical grade TCP and Mobile Jet II engine oil were analysed, including pyrolysed samples. The results showed the presence of TCP isomers in both the pyrolysed and non-pyrolysed samples of TCP and the Mobile Jet II oil in significant quantities. This finding is in agreement with the findings of EASA (2015) study, in which samples of old and new oils were tested, TCP was identified in both types of oil. Two isomers of TCP, tri-p-cresyl phosphate and tri-m-cresyl, were found in all samples tested, the isomer tri—o-cresyl phosphate was not detected. This is supported by Solbu et al. (2007) who found both TmCP and TpCP in air samples tested exposed to oil aerosols. Exposure to TCP has been shown to have significant effects on health (Winder et al. 2001). Symptoms, such as irritation of the eyes, nose and throat or respiratory effects could occur immediately or soon after exposure. Other issues such as nervous system impairment and chemical sensitivity developed later, after exposure had stopped. These symptoms were sufficiently consistent to indicate the development of a discrete occupational health condition, and the term aerotoxic syndrome is introduced to describe it. It has been shown that TmCP and TpCP have LD_{50} between 1000 and 3000 mg/kg (WHO

1990), this may be less than that of TOCP but has been found to still have impact on health. This analysis proved that the presence of TCP isomer in engine jet oil could therefore potentially contaminate bleed air within aircraft and therefore present a hazard to the occupants – crew and passengers. Whilst the amounts may not have significant health impacts on a single exposure, as could be the case for passengers, multiple exposure, as in the case of cabin crew, could have detrimental health impacts. Average air consumo

As TCP was detected in the GC-MS analysis the mathematical model was developed to determine how much TCP could get into the cabin. Analysing the air flow into the cabin from the engine and taking into account the air exchange rate, the analysis show TCP would enter the aircraft cabin. The analysis showed 0.55 g would enter the cabin, this would be dispersed evenly throughout the cabin, exposing individuals to lower levels of contaminant 0.004 mg/m^3 after a short period of time. Within 2 minutes of the engine start up, the highest levels of TCP would enter the cabin, this would then reduce as the air exchange takes place, 50% recycled air and 50% fresh air, with a complete air exchange twice in one hour. The mathematical analysis supported the research showing that small levels of contamination could enter the cabin. This would affect some occupant's health. As shown by Winder et al. (2001) immediate effects of exposure to TCP include disorientation, headaches, dizziness as well as irritation to the eyes, nose and throat. The main issues are the continued exposure of cabin crew. Whilst this may only be low levels of exposure in each contamination event. Continued exposure can cause long term health issues such as conative impairment and chronic fatigue. A daily exposure from 6 hours of flight, with an average air consumption of 3 m^3 would give an exposure of 0.012 mg/m^3 per day. This is below the permissible exposure limit of 0.1 mg/m^3 averaged over and 8-hour period (New Jersey Health Department 2015).

The mathematical model developed in Chapter 5, does not take into account the injection point from the air vent supply that runs the length of the cabin, this would affect the distribution of the particles and therefore the exposure of occupants in different locations within the aircraft cabin.

The distribution of the particles needs to be analysed to determine the concentrations within the cabin in different areas. To determine the flow path of the particles numerical simulations were conducted, this can be found in Chapter 6.

From the numerical simulations, analysis to determine the effect of particle size and the number of particles being injected to the cabin was conducted. It was found that particle size did impact on the flow paths of the particles being supplied at a constant rate with a constant supply air velocity. As with the study with Yan et al. (2021) it was found that the particles of a larger diameter fell to the floor quicker.

Comparing particle size of 16, 50, 100 and 200 µm it was shown that as the particle diameter increases, the number of particles observed in all locations decreases. With the range of average particles at 16 µm being from 0.07 kg/m^3 – 0.15 kg/m^3 compared to 0 – 0.09 kg/m^3. This is visibly seen if we compare Figures 94, 98, 103 and 106. A greater number of particles is seen when the particle diameter is low – 16 µm.

It was shown that increasing the number of particles (40 000 to 50 000) with the same diameter had little impact on the distribution. Comparing Figure 94 showing the average density for the injection of 40 000 of 16 µm to with Figure 110 showing the average density for the injection of 50 000 of 16 µm, the levels observed in both cases mirror each other with an average density of 0.11 to 0.15 kgm^3 being recorded. Similar levels are observed, at the front of the cabin the highest average mass per unit volume was in the centre seat on the right at 2.5 m for both cases. In the middle, the highest value observed was on the right side, in the aisle seat at 2.5 m and the window seat at 2.2 m with levels of 0.15 kg/m^3. At the rear, the highest value observed was on the right side, in the aisle seat at 2.5 m and the centre seat at 2.2 m with levels of 0.15 kg/m^3.

The numerical simulation showed that seat location did impact on exposure (aisle, middle or window) but that sitting in the front, middle or rear of the cabin did not impact on levels of exposure. This is supported by the findings of Foxwell (2009), who also found that the aisle seat did increase the risk of exposure.

The analysis of the numerical simulations concluded that seat location did potentially affect the exposure of occupants to differing levels of contamination. In most cases the

aisle seat was exposed to higher levels of containment. The velocity profiles determined from the numerical study showed that the airflow was higher around the aisle seat carrying the particles to this location, as the velocity decreased, the particles were able to fall to the floor and not be transported to the middle or window seat in high concentrations. This follows the findings of You et al. 2016.

The GC-MS analysis showed that there is contamination available to enter the cabin, the mathematical analysis showed low levels of contamination would enter the cabin but diminish over the duration of the flight and the numerical simulations showed that the particles would affect occupants in the aisle, middle and window seat differently.

As seen in this thesis, there is sufficient evidence that there is a problem of aircraft air contamination. This research has shown that aircraft cabins have to potential to have contaminated air within the aircraft cabin.

The frequency of fume events occurring in aircraft is still uncertain, this research has shown that in the event of a fume event, there is area for concern. Occupants will be exposed to TCP. Frequent flyers and cabin crew will be regularly exposed leading to detrimental health effects. Whilst this research has shown low level exposure in a one-off event, if cabin crew are exposed these concentrations over the period of their working life, levels of exposure would be greater than the exposure limits.

Exposure to TCP has been shown to have significant effects on health (Winder et al. 2001). Symptoms, such as irritation of the eyes, nose and throat or respiratory effects could occur immediately or soon after exposure. Other issues such as nervous system impairment and chemical sensitivity developed later, after exposure had stopped. These symptoms were sufficiently consistent to indicate the development of a discrete occupational health condition, and the term aerotoxic syndrome is introduced to describe it.

7.1 Recommendations

This research has shown that contaminated air is possible and that the levels of contamination can cause adverse health effects. The industry needs to act to reduce the occurrence and the impact if such an event does occur. Detection and alarm systems need to be put in place to detect if contamination events take place. Real time sensors for detecting toxic compounds such as TCP are available and should be installed. Currently portable detectors are used but these only sample air in the local area after a potential event has been reported. Bleed air monitors should be retrofitted to existing aircraft to identify if air is becoming contaminated (Fox 2023), these would detect a leak and therefore the potential for the whole cabin to become contaminated. Installing such devices would not only confirm events had taken place to provide an accurate record, but also could be beneficial to aircraft companies as they could reduce aircraft down time.

The installation and operation of suitable filtration systems to remove fumes from the ventilation air supply, pending available technology. Filters should be placed in more strategic areas of the air supply system, after the bleed air and recirculated air are mixed. Whilst there are currently filters in place, high efficiency particulate filters (HEPA) for removing bacteria and viruses, these do not stop the passage of small particles such as TCP. Some HEPA filters have an activated charcoal filter attached; this would reduce the transmission of TCP, but these filters are only using in the recirculated air portion not the air coming from the bleed air (Pall Corporation 2020). If these were position so they did filter the bleed air, reduction in the concentration of particles and aerosols within the air could be achieved. HEPA filters remove at least 99.97% of dust, pollen, mould, bacteria, and any airborne particles with a size of 0.3 µm. The diameter specification of 0.3 µm corresponds to the worst case, the most penetrating particle size. Particles that are larger or smaller are trapped with even higher efficiency (US EPA 2019).

Some modern aircraft are removing the use of bleed air all together. In engines which do not use bleed air an electrically driven compressors provide the cabin pressurization function; fresh air is introduced to the cabin via dedicated cabin air inlets. This system would stop the contamination of bleed air with organophosphates and is more efficient as

it reduces energy extraction from the engines. Similar systems should be considered for all new aircraft design (Sinnett 2007).

Aircraft air exchange rates could be increased, increasing ventilation would introduce more dilutant air and extract contaminated air faster, so the residence time is reduced, but this could also increase the circulation of the contaminant more effectively.

Synthetic engine oils which do not contain TCP isomers are commercially available, these are more expensive and due to their relative “newness” have not been proven to be as effective as those oils containing TCP, research needs to be undertaken into the effectiveness of these oils so that they can become more widely used. (Scholz 2017).

Pilots and cabin crew need to be trained to respond to smoke or fume events on aircraft and to report any events. Cabin Air Quality Act 2022 was introduced to American Congress, this Act has not yet been passed, but similar forms of legislation should be introduced internationally. This Act requires the development of standardized form for reporting incidents as well as a system for filing the reports and recording incidents involving smoke or fumes. The Act also requires an investigation to be conducted following the submission of a report about incidents of smoke or fumes in the cabin or cockpit. It would also require air carriers to install and operate onboard detectors and other air quality monitoring equipment situated in the air supply system to enable pilots and maintenance technicians to locate the sources of air supply contamination, including carbon monoxide (Garamendi 2022).

Novelty of this work

- Experimental analysis of mobile jet II oil identifying the properties of TCP, jet engine oil aswell as the products from pyrolysed samples.
- Mathematical modelling of the level of contamination within the cabin environment over a period of time.
- Numerical simulation showing the flow paths of particles within the aircraft.
- Linking the simulations to the chemical analysis and the mathematical models.

7.2 Future work

More independent research is required to determine the how often these events occur. Surface swabs of a range of aircraft need to be taken independently and analysed to determine the actual levels of contaminant within the aircraft. Analysis of additive levels of tri-cresyl phosphate needs to be undertaken to determine if this would have an adverse effect on frequent flyers and cabin crew. Air samples need to be taken following the report of an event to determine if contaminants such as TCP are present, this would also help determine the rate of occurrence.

Analysis of enhanced filter systems needs to be conducted to determine if these would prevent the contamination of air from oil particles from the engine.

Studies should be undertaken to determine the particle size of pyrolysed oils as this will affect the flow paths and distribution throughout the cabin. Modelling should be conducted where the cabin is full of passengers and there is a temperature gradient to determine how much this would affect the deposition rate of the particles. Studies need to be conducted to determine the exposure of occupants in particular locations, such as the aisle seat. This study concentrated on BAe 146 aircraft, but tis is not the only aircraft in which incidents occur and have been reported, this mathematical model and numerical simulations needs to be extended to include different sized aircraft with different engines and different number of engines. This would give a greater representation of the issues and the impacts on occupant’s health.

References

Aircraft Nerds *How Aircraft engine oil system works?*, *(2023),* Available at: https://www.aircraftnerds.com/2018/09/the-oil-system-of-aircraft-engine.html (Accessed: Jun 19, 2023).

Airliner Cabin Environment and the Health of Passengers and Crew (2002) *Committee on Air Quality in Passenger Cabins of Commercial Aircraft Board on Environmental Studies and Toxicology* Staff National Research Council Staff National Academies Press 2002

Abou-Donia, M. (2003) *Organophosphorus Ester-Induced Chronic Neurotoxicity* Archives of Environmental Health

BAe Systems (2009) *BAe 146 General Data*

Bagshaw, M. (2013) *Health Effects of Contaminants in Aircraft Cabin Air Summary Report v2.5*

Bahri, N. and Abderrahmane, B. (2019) *Exponential Stability of a Transmission Problem with History and Delay*, *Statistics, optimization & information computing,* 7(4), pp. 731. doi: 10.19139/soic-2310-5070-728.

Balali-Mood, M. and Balali-Mood, K. (2008) *Neurotoxic Disorders of Organophosphorus Compounds and Their Management* Archives of Iranian Medicine; 11 (No 1): 65-89

Bardin, P., Eeden, S., Moolman, J., Foden, A., and Joubert, J. (1994) *Organophosphate and Carbamate Poisoning* International Medicine;154:1433-1441

Baviskar, J. (2015) *How do Gas turbines or Jet engines work ?* Available at: https://mechstuff.com/how-do-jet-engines-work/ (Accessed: Jun 1, 2023).

BBC Accessed on-line 19/11/2019 https://www.bbc.co.uk/news/world-australia-43530332

BBC Accessed on-line 19/11/2019 https://www.bbc.co.uk/news/world-australia-50114049

Beji, T., Zadeh, S.E., Maragkos, G. and Merci, B. (2017) *Influence of the particle injection rate, droplet size distribution and volume flux angular distribution on the results and computational time of water spray CFD simulations* Elsevier BV

Beneke, J.M., Jones, B.W. and Hosni, M. (2011) *Fine particle dispersion in a commercial aircraft cabin*, *HVAC&R research,* 17(1), pp. 107-117. doi: 10.1080/10789669.2011.543255.

Bhopale, M, B., (2019) *Application of differential equations to engineering* International Journal of Advanced Research and Innovative Ideas in Education 5 issue 3 ISSN(O)-2395-4396

Blomberg, J., Schoenmakers, P.J. and Brinkman, U.A.T. (2002) *Gas chromatographic methods for oil analysis*, *Journal of Chromatography A,* 972(2), pp. 137-173. doi: 10.1016/S0021-9673(02)00995-0.

Boedeker, W., Watts, M., Clausing, P. *,* (2020) *The global distribution of acute unintentional pesticide poisoning: estimations based on a systematic review*. *BMC Public Health **20**, 1*875 (2020). https://doi.org/10.1186/s12889-020-09939-0

Boelkins, M., Austin, D., Schlicker, S. *Active Calculus* (2016) Grand Valley State University Orthogonal Publishing

Bonora, S., Trinchero, A., Torreggiani, A. and Tamba, M. (2007) *A DSC and Raman Study of the Interaction between Tricresyl Phosphates (TCP) and Phospholipid Liposomes* Croatia Chemica Acta; 80 (1):81-89

Bronson, R., and Costa, G. B., 2022. *Applications of First-Order Differential Equations.* Chap. 7 in *Schaum's Outline of Differential Equations*. 5th ed. New York: McGraw Hill. https://www.accessengineeringlibrary.com/content/book/9781264258826/chapter/chapter7

Brooks, J., Erickson, T. B., Kayden, S., Ruiz, R., Wilkinson, S., & Burkle, F. M. (2018). *Responding To Chemical Weapons Violations In Syria: Legal, Health, And Humanitarian Recommendations.* Conflict and Health, 12 doi:10.1186/s13031-018-0143-3

Burdon, J., Budnik, L.T., Baur, X., Hageman, G., Howard, C.V., Roig, J., Coxon, L., Furlong, C.E., Gee, D., Loraine, T., Terry, A.V., Midavaine, J., Petersen, H., Bron, D., Soskolne, C.L. and Michaelis, S. (2023) *Health consequences of exposure to aircraft contaminated air and fume events: a narrative review and medical protocol for the investigation of exposed aircrew and passengers*, Environmental Health, 22, pp. 43. doi: 10.1186/s12940-023-00987-8.

CBS Interactive (online) Last accessed 12/02/2011 http://www.search.com/reference/Jet_engine

Centers for Disease Control and Prevention (2023) *Sarin (GB): Nerve Agent | NIOSH | CDC.* Available: https://www.cdc.gov/niosh/ershdb/emergencyresponsecard_29750001.html (Accessed: Jun 26, 2023).

Chambers, J. and Oppenheimer, S. (2004) *Toxicological Highlight – Organophosphates, Serine Esterase Inhibition and Modelling of Organophosphate Toxicity.* Society Of Toxicology

Chemical Terrorism *Organophosphates* (online) (2003) Last accessed October 2010 at http://bioterrorism.slu.edu/nerve/nerve.pdf

Committee on Toxicity COT, 1999. *Organophosphates. A Report of the Committee on Toxicology of Chemicals in Food*, Consumer Products and the Environment. UK Department of Health, London

Committee on Toxicology COT (2000) *Proceedings from Workshop on Research on Organophosphates* Society of Chemical Industry Headquarters London

Committee on Toxicology of Chemicals In Food Consumer Products And The Environment (2013) *Statement On The Review Of The Cabin Air Environment, Ill health In Aircraft Crews And The Possible Relationship To Smoke/Fume Events In Aircraft*

Costa, L. (2006) *Current Issues in Organophosphate Toxicology* Clinica Chimica Acta 2006;366:1-13

Crump, D., Harrison, P. and Walton, C. (2011) *Aircraft Cabin Air Sampling Study: Part 1 of the Final Report*, Institute of Environment and Health, Cranfield University, March 2011

Crump, D., Harrison, P. and Walton, C., (2011) *Aircraft Cabin Air Sampling Study; Part 2 of the Final Report*, Institute of Environment and Health, Cranfield University, April 2011

Department of Energy (DOE) (2016) *Handbook Temporary Emergency Exposure Limits for Chemicals:* Methods and Practice, Washington D.C

Department of Environmental & Occupational Health Sciences University of Washington opchild@u.washington.edu 2007

Denola, G., Hanhela, P.J. and Mazurek, W. (2011) *Determination of tricresyl phosphate air contamination in aircraft, The Annals of Occupational Hygiene,* 55(7), pp. 710-722. doi: 10.1093/annhyg/mer040.

Dunn, K.H. *et al.* (2005) *Numerical Simulation of Airflow and Airborne Pathogen Transport in Aircraft Cabins-Part I: Numerical Simulation of the Flow Field, ASHRAE transactions*, 111(1), pp. 755–763.

European Union Aviation Safety Agency *Preliminary cabin air quality (CAQ) measurement campaign*, (2015) *MENA Report,* Mar 17,

Excalibur Qual Browser Version 2.0.7, Thermofisher Scientific In 2007

FreshAirCraft (FACTS) *Task 1 Review of the state of the art and establishment of the baseline for the FACTS project* (2017)

Flight Delayed Accessed on-line 19/11/2019 https://www.flight-delayed.co.uk/news/2019/07/30/july-25-2019-aviations-busiest-day-in-history

Flight Global 2001, 2.A. *British European BAe 146 fume incident prompts UK CAA action*. Available at: https://www.flightglobal.com/british-european-bae-146-fume-incident-prompts-uk-caa-action-/37003.article (Accessed: Jun 20, 2023).

Fox, M.A., and Whitesell, J. K., (1994) *Organic Chemistry*, North Carolina State University Raleigh, North Carolina Jones and Bartlett

Fox, Richard. *Development and Application of a Real Time Bleed Air Contamination Monitor* SAE Transactions, vol. 111, 2002, pp. 432–39. JSTOR, http://www.jstor.org/stable/44718451. Accessed 22 June 2023.

Foxwell, A., Roberts, L., Lokuge, K., and Kelly, P. M. (2011). *Transmission of Influenza on International Flights*, May 2009. *Emerging Infectious Diseases*, *17*(7), 1188-1194. https://doi.org/10.3201/eid1707.101135.

Freudenthal, R.I., Rausch, L., Gerhart, J.M., Barth, M.L., Mackerer, C.R. and Bisinger, E.C. (1993) *Subchronic Neurotoxicity of Oil Formulations Containing Either Tricresyl Phosphate or Tri-Orthocresyl Phosphate*, *Journal of the American College of Toxicology,* 12(4), pp. 409-416 Available at: 10.1177/109158189301200410.

German Federal Bureau of Aircraft Accident Investigation *Study of Reported Occurrences in Conjunction with Cabin Air Quality in Transport Aircraft* (2010) Bundesstell Fur Flugunfalluntersuchung

Global Cabin Air Quality Executive (GCAQE) (online) Last accessed 20/12/2019 at 11

Goldberg, A. (1976) *Biology of Cholinergic Function* Raven Press

Guan, B., Pochopien, B.A. and Wright, D.S. (2016) *The chemistry, mechanism and function of tricresyl phosphate (TCP) as an anti-wear lubricant additive*, Lubrication science, 28(5), pp. 257-265. doi: 10.1002/ls.1327.

Gupta, R. (2006) *Toxicology of Organophosphate and Carbamate Compounds* Elsevier

Guo, Q., Wang, J., Estill, J., Lan, H., Zhang, J., Wu, S., Yao, J., Yan, X. and Chen, Y. (2022) 'Risk of COVID-19 *Transmission Aboard Aircraft: An Epidemiological Analysis Based on the National Health Information Platform*, International journal of infectious diseases, 118, pp. 270-276 Available at: 10.1016/j.ijid.2022.03.024.

Hanel, P.J., Kibby, J., DeNola, G., and Mazurek, W. (2005) *Organophosphate and Amine Contamination of Cockpit Air in Hawk, F-II And Hercules C-130 Aircraft* Australian Government Department of Defence

Hausherr, V., Schöbel, N., Liebing, J. and van Thriel, C. (2017) *Assessment of neurotoxic effects of tri-cresyl phosphates (TCPs) and cresyl saligenin phosphate (CBDP) using a combination of in vitro techniques*, Neurotoxicology, 59, pp. 210-221. doi: 10.1016/j.neuro.2016.06.005.

Hiltz, J. and Haggett, R, D. (2016) *Pyrolysis gas chromatography/mass spectrometry identification of poly(butadiene-acrylonitrile) rubbers* Elsevier BV.

Hoffman R, Wiener S *Nerve Agents: A Comprehensive Review* Journal of Intensive Care Medicine Sage, 2004. - 1 : Vol. 19.

Houtzager, M., Havermans, J., Noort, D., Joosen, M. Bos, J., Jongeneel, R., van Kesteren, P., Heusinkveld, H., van Kamp, I., Brandsma, S., and Westerink R (2015) *Characterisation of the toxicity of aviation turbine engine oils after pyrolysis. EASA* Available at: file://lha-112/pers-J/00031FA8/Downloads/EASA%20AVOIL_final%20report_final%20version_160217%20(1).pdf (Accessed: Jun 8, 2023).

Hunt, E., and Space, D. (1994) *The Airplane Cabin Environment: Issues pertaining to Flight Attendant Comfort* Boeing Company

IATA. (2022) Available at: Air Passenger Market Analysis (Accessed: Jun 6, 2023).

International Air Transport Association (IATA) Annual Review 2019. Accessed on-line 19/11/2019 https://www.iata.org/publications/Documents/iata-annual-review-2019.pdf

International Air Transport Association (IATA) Press Release. Accessed on-line 19/11/2019 https://www.iata.org/pressroom/pr/Pages/2018-10-24-02.aspx

Kamanyire, R., and Karalliedde, L., (2004) *Organophosphate Toxicity and Occupational Exposure* Occupational Medicine; 54:69-75

Katz, K. D., (2023) *Organophosphate Toxicity: Practice Essentials, Background, Pathophysiology.* Available at: https://emedicine.medscape.com/article/167726-overview (Accessed: Jun 1, 2023).

Kenneth, D. Katz, M.D., FAAEM, A.B.M.T., (2010) *Toxicity, Organophosphate* (online) University of Pittsburgh Medical Center; Updated: Mar 16, 2010 Last accessed October 2010 at http://emedicine.medscape.com/article/167726-overview

Kim, J., Stevens, R., MacCoss, M., Goodlett, D., Scherl, A., Richter, R., Suzuki, S., and Furlong, C. (2010) *Identification and Characterization of Biomarkers of Organophosphorus (OP) Exposures in Humans* Paraoxonases in Inflammation, Infection and Toxicology Humana Press;660:61-71

Lakies, M. (2019) *Dynamic Cabin Air Contamination Calculation Theory.* Aircraft Design and Systems Group (AERO), Department of Automotive and Aeronautical Engineering, Hamburg University of Applied Sciences.

Latendresse, J.R., Brooks, C.L. and Capen, C.C. (1994) *Pathologic effects of butylated triphenyl phosphate based hydraulic fluid and tricresyl phosphate on the adrenal gland, ovary and testis in the Fischer-344 rat*. Toxicological Pathology; 22: 314-352

Leder, K., Newman, D., (2005) *Respiratory infections during air travel*. Intern Med J. Jan;35(1):50-5. doi: 10.1111/j.1445-5994.2004.00696.x. PMID: 15667469; PMCID: PMC7165774.

Marklund, A. (2005). *Levels and sources of organophosphorus flame retardants and plasticizers in indoor and outdoor environments* (Doctoral dissertation, Kemi).

Mann, G.W., Eckels, S.J. and W. Jones, B. (2014) *Analysis of particulate size distribution and concentrations from simulated jet engine bleed air incidents*, HVAC&R Research, 20(7), pp. 780-789. doi: 10.1080/10789669.2014.950922.

May, P. (2018) *Novickok – The Notorious Nerve Agent 07*/12/2018]; Available from: a

McGrattan, K., Hostikka, S., McDermott, R., Floyd, J., Vanella, M., (2022) *Fire Dynamics Simulator User's Guide,* NIST Special Publication 1019, Sixth Edition

McGrattan, K., Hostikka, S., McDermott, R., Floyd, J., Vanella, M., (2022) *Fire Dynamics Simulator Technical Reference Guide Volume 3: Validation*, NIST Special Publication 1018, Sixth Edition

Michaelis, S. (2007) *Aviation Contaminated Air Reference Manual* CPI Antony Rowe

Michaelis, S. (2008) *Critique of the UK Committee on Toxicity Report on Exposure to Oil Contaminated Air on Commercial Aircraft and Pilot Ill Health* Committee on Toxicology

Morgan, J. and Tulloss, T. (1976) *The Jake Walk Blues A Toxicologic Tragedy Mirrored in American Popular Music*; Rochester, New York; and College Park, Maryland

Mott, J., *Application of Differential Equations: Inflow – Outflow Mixing Problems* Student Revision Series Texas Instruments available on-line
2020_StudSpec_InOutEqns_WSCAS.pdf

Muir, H. and Wren, C. (2009) *Investigating contaminated air incidents* ICE International Aviation Conference

Muir, H. Walton, C. and McKeown, R. (2008) *Cabin Air Sampling Study Functionality Test.* Cranfield University School of Engineering, January 2008 National, Research

National Research Council, Division on Earth and Life Studies, Commission on Life Sciences and Committee on Toxicology (1997) *Review of Acute Human-Toxicity Estimates for Selected Chemical-Warfare Agents.* Washington, D.C.: National Academies Press.

National Research Council, (2002) *The Airliner Cabin Environment and the Health of Passengers and Crew*, National Academies Press, *ProQuest Ebook Central*, https://ebookcentral.proquest.com/lib/uclan-ebooks/detail.action?docID=3377249.

New Jersey Department for Health (2015) *Right to Know Hazardous Substance Fact Sheet*. Available from https://nj.gov/health/eoh/rtkweb/documents/fs/3130.pdf

Nielsen, P.V., (1974) *Flow in air-conditioned rooms* Ph.D. thesis Technical Univertisy Denmark

Olsen, S.J., Chang, H., Cheung, T.Y., Tang, A.F., Fisk, T.L., Ooi, S.P., Kuo, H., Jiang, D.D., Chen, K., Lando, J., Hsu, K., Chen, T. and Dowell, S.F. (2003) *Transmission of the Severe Acute Respiratory Syndrome on Aircraft*, The New England Journal of Medicine, 349(25), pp. 2416-2422 Available at: 10.1056/NEJMoa031349.

Organophosphate Poisoning: Symptoms, Treatment, and More. (2017) Available at: https://www.healthline.com/health/organophosphate-poisoning (Accessed: Jun 6, 2023).

Paediatric Environmental Health Specialty Unit *Organophosphate Pesticides and Child Health: A Primer for Health Care Providers* (online) Last accessed 14/10/2010
Parliamentary advisory council for transport safety (online) Last accessed 10/10/2010 at http://www.pacts.org.uk/index.php

Pall Corporation (2020) *How Cabin Air Filters Work* - Commercial Fixed Wing | Pall Corporation', Available on-line: How Cabin Air Filters Work - Commercial Fixed Wing | Pall Corporation
Perkin Elmer (2023) Website *www.perkinelmer.com/uk* (accessed: June 16, 2023)

Ramsden, J.J. (2013) *Jet engine oil consumption as a surrogate for measuring chemical contamination in aircraft cabin air*, Journal Of Biological Physics And Chemistry, Vol.13, Nr. 4 (2013) TOC*,* 13(4), pp. 114-118.

Rayman, R. B., and McNaughton, G. B. (1983) *Smoke/ Fumes in the Cockpit* Aviation Space and Environmental Medicine 1983; 67: 738-740

Rehm, R.G., Baum, H.R., (1978) *The Equations of Motion for Thermally Driven, Buoyant Flows* Journal of Research of the NBS, 83:297–308, 1978. 2, 9, 15, 133

Rep. Garamendi, J. [. (2022). *H.R.7267 - 117th congress (2021-2022): Cabin air safety act of 2022.* http://www.congress.gov/bill/117th-congress/house-bill/7267

Robb, E.L., and Baker, M.B., (2023) *Organophosphate Toxicity*. [Updated 2022 May 1]. In: StatPearls [Internet]. Treasure Island (FL): StatPearls Publishing; Available from: https://www.ncbi.nlm.nih.gov/books/NBK470430/

Schopfer, L., Furlong, C. and Lockridge, O. (2010) *Development of Diagnostics In The Search For An Explanation Of Aerotoxic Syndrome* Analytical Biochemistry 2010;404:64-74 Elsevier

Scholz, D. (2017) *Aircraft Cabin Air and Engine Oil - A Systems Engineering View* Zenodo.

Schuchardt, S; Bitsch, A; Koch, W; Rosenberger, W; (2104) European Aviation Safety Agency *Final Report EASA_REP_RESEA*_2014_4 Research Project: CAQ Preliminary cabin air quality measurement campaign

Senate Rural and Regional Affairs and Transport References Committee (2000) Air *Safety and Cabin Air Quality in the BAe 146 Aircraft*

Shang, Y., Tao, Y., Dong, J., He, F. and Tu, J. (2021) *Deposition features of inhaled viral droplets may lead to rapid secondary transmission of COVID-19*, Journal of Aerosol Science, 154, pp. 105745. doi: 10.1016/j.jaerosci.2021.105745.

Sinnett, M., (2007) 787 *No-Bleed Systems: Saving Fuel and Enhancing Operational Efficiencies* Aero 28(04) pp6-11 www.boeing.com/commercial/aeromagazine

Sjogren, B., Iregren, A., and Jamberg, J. (2009) *Phosphate trimesters with flame retardant properties* The Nordic Expert Group for Criteria Documentationof Health Risks from Chemicals University of Gothenburg

Somani, S., and Husain, K. (2000). *Low-Level Nerve Agent Toxicity under Normal and Stressful Conditions* 10.1201/9781420041576.ch3.

Solbu, K., Daae, H.L., Olsen, R., Thorud, S., Ellingsen, D.G., Lindgren, T., Bakke, B., Lundanes, E. and Molander, P. (2011) *Organophosphates in aircraft cabin and cockpit air—method development and measurements of contaminants*, Journal of Environmental Monitoring, 13(5), pp. 1393-1403. doi: 10.1039/C0EM00763C.

Sparks, P. S., Simon, G.E., Katon, W.J., Altman, L.C., Ayars, G.H., and Johnson, R.L., (1990) *An Outbreak of Illness Among Aerospace Workers* Western Journal of Medicine 1990; 158:28-33

Spila, E., Sechi, G. and Bernabei, M. (1999) *Determination of organophosphate contaminants in jet fuel*, Journal of Chromatography A, 847(1), pp. 331-337. doi: 10.1016/S0021-9673(99)00033-3

Stein, S., Mirokhin, Y., Tchekhovskoi, D., and Mallard, D., (2005) NIST *Mass Spectral Search Programme* Version 2.0 The NIST Mass Spectrometry Data Center

Stephens, R., Spurgeon, A., Calvert, I.A., Beach, J., Levy, L.S., Harrington, J.M. and Berry, H. (1995) *Neuropsychological effects of long-term exposure to organophosphates in sheep dip*, The Lancet, 345(8958), pp. 1135-1139 Available at: 10.1016/S0140-6736(95)90976-1

Traumagency: Organophosphate Poisoning, (2015) *Traumagency,* Tuesday, September 29. Available at: http://traumagency.blogspot.com/2015/09/organophosphate-poisoning.html (Accessed: Jun 6, 2023).

Trump, R. A., (2012) An *In-Depth Review of Organophosphate Poisoning.* 07/12/2012]; Available from: http://www.emsvillage.com/articles/article.cfm?id=801

Turner, D. (2022) *GC-MS Principle, Instrument and Analyses and GC-MS/MS.* Available at: http://www.technologynetworks.com/analysis/articles/gc-ms-principle-instrument-and-analyses-and-gc-msms-362513 (Accessed: Jun 8, 2023).

Tsuda, A., Henry, F.S. and Butler, J.P. (2013) *Particle transport and deposition: basic physics of particle kinetics*, Comprehensive Physiology, 3(4), pp. 1437-1471. doi: 10.1002/cphy.c100085.

US EPA, O. (2019) *What is a HEPA filter*? Available at: https://www.epa.gov/indoor-air-quality-iaq/what-hepa-filter (Accessed: Jun 20, 2023).

US Military Dictionary Nerve Agent (online) Last accessed August 2010 at http://www.answers.com/topic/nerve-agent

van Netten, C. (1999) *Multi-elemental analysis of jet engine lubricating oils and hydraulic fluids and their implication in aircraft air quality incidents* Science of The Total Environment, Elsevier

Van Netten, C. (2009) *Design of Small Personal Air Monitor and its Application in Aircraft* Science of the Total Environment; 407: 1206-1210

Wiener, S.W., and Hoffman, R., (2004) *Nerve Agents: A Comprehensive Review,* Journal of Intensive Care Medicine, 19(1), pp. 22-37. doi: 10.1177/0885066603258659.

Winder, C. and Balouet, J. (2001). *Aerotoxic Sydrome: Adverse Health Effects Following Exposure To Jet Oil Mist During Commercial Flights*. Toxicology. 164.

Winder, C. and Balouet, J., (2002) *The Toxicity of Commercial Jet Oils* Environmental Research 2002; 89:146-164

Winder, C., (2005) Proceedings of the BALPA *Air Safety and Cabin Air Quality International Aero Industry Conference* Imperial College London 2005

Winder, C., (2006) *Hazardous chemicals on jet aircraft: case study – jet engine oils and aerotoxic syndrome* School of Safety Science, Current Topics in Toxicology

World Health Organisation (WHO) (1990) *Environmental Health Criteria 110 Tricresyl phosphate.* WHO Library Cataloguing in Publication Data ISBN 92 4 157110 1

Yan, W., Zhang, Y., Sun, Y. and Li, D. (2009) *Experimental and CFD study of unsteady airborne pollutant transport within an aircraft cabin mock-up*, Building and Environment, 44(1), pp. 34-43. doi: 10.1016/j.buildenv.2008.01.010.

Yan, Y., Li, X., Fang, X., Yan, P. and Tu, J. (2021) *Transmission of COVID-19 virus by cough-induced particles in an airliner cabin section*, Engineering Applications of Computational Fluid Mechanics, 15(1), pp. 934-950. doi: 10.1080/19942060.2021.1922124.

Yimaer, A., Chen, G., Zhang, M., Zhou, L., Fang, X., & Jiang, W. (2017). *Childhood pesticide poisoning in zhejiang, China: A retrospective analysis from 2006 to 2015*. *BMC Public Health, 17*(1), 602. doi:10.1186/s12889-017-4505-3

You, R., Chen, J., Shi, Z., Liu, W., Lin, C., Wei, D. and Chen, Q. (2016) *Experimental and numerical study of airflow distribution in an aircraft cabin mock-up with a gasper on* Informa UK Limited.

Zee, M., Davis, A.C., Clark, A.D., Wu, T., Jones, S.P., Waite, L.L., Cummins, J.J. and Olson, N.A. (2021) *Computational fluid dynamics modelling of cough transport in an aircraft cabin*, *Scientific reports,* 11(1), pp. 23329 Available at: 10.1038/s41598-021-02663-8.

Zhang, C., and Yu, J., (Sep 2011) *Real-time aircraft cabin channel modelling*. IEEE, pp. 141.

Zhang, T., Yin, S. and Wang, S. (2010) *An under-aisle air distribution system facilitating humidification of commercial aircraft cabins*, Building and environment, 45(4), pp. 907-915. doi: 10.1016/j.buildenv.2009.09.010.

Zhang, W., and Li, D., (2009) *Experimental and CFD study of unsteady airbourne pollutant transport within an aircraft cabin mock up* Building and Environment 44 (34-43) Elsevier

Appendix 1 – Mathematical solutions - Eigenvalues

$$\frac{dm_{out}}{dt} = 0.1 * m\ kg/min \quad \text{(A2 - 1)}$$

Combining the rate flowing out with the rate flowing in :

$$\frac{dm}{dt} = 0.1 - 0.1m \quad \text{(A2 - 2)}$$

Each side is multiplied by dt to give

$$dm = (0.1 - 0.1m\ )dt \quad \text{(A2 - 3)}$$

Each side is multiplied by 1/(m-1)

$$\frac{dm}{m-1} = -0.1dt \quad \text{(A2 - 4)}$$

Integrate both sides of the equation:

$$ln|m-1| = -0.1t + K \quad \text{(A2 - 5)}$$

Rearrange to obtain m, assuming m>1

$$m = 1 + e^{-0.1t+K} \quad \text{(A2 - 6)}$$

Expand this to be:

$$m - 1 = e^{k}e^{-0.1t} \quad \text{(A2 - 7)}$$

$$m = 1 + De^{-0.1t}, \qquad D = e^{K} \quad \text{(A2 - 8)}$$

$$m = De^{-0.1t} + 1 \quad \text{(A2 – 9)}$$